

AN EQUIVALENT LINEARIZATION PROCEDURE FOR SEISMIC  
RESPONSE PREDICTION OF MDOF SYSTEMS

A THESIS SUBMITTED TO  
THE GRADUATE SCHOOL OF NATURAL AND APPLIED SCIENCES  
OF  
MIDDLE EAST TECHNICAL UNIVERSITY

BY

MEHMET SELİM GÜNAY

IN PARTIAL FULFILLMENT OF THE REQUIREMENTS  
FOR  
THE DEGREE OF DOCTOR OF PHILOSOPHY  
IN  
CIVIL ENGINEERING

MARCH 2008

Approval of the thesis:

**AN EQUIVALENT LINEARIZATION PROCEDURE FOR SEISMIC  
RESPONSE PREDICTION OF MDOF SYSTEMS**

submitted by **MEHMET SELİM GÜNAY** in partial fulfillment of the requirements for the degree of **Doctor of Philosophy in Civil Engineering Department, Middle East Technical University** by,

Prof. Dr. Canan Özgen \_\_\_\_\_  
Dean, Graduate School of **Natural and Applied Sciences**

Prof. Dr. Güney Özcebe \_\_\_\_\_  
Head of Department, **Civil Engineering**

Prof. Dr. Haluk Sucuoğlu \_\_\_\_\_  
Supervisor, **Civil Engineering Dept., METU**

**Examining Committee Members:**

Prof. Dr. Polat Gülkan \_\_\_\_\_  
Civil Engineering Dept., METU

Prof. Dr. Haluk Sucuoğlu \_\_\_\_\_  
Civil Engineering Dept., METU

Prof. Dr. Yalçın Mengi \_\_\_\_\_  
Department of Engineering Sciences, METU

Prof. Dr. Michael Fardis \_\_\_\_\_  
Dept. of Civil Engineering, University of Patras, Greece

Assoc. Prof. Dr. Sinan Akkar \_\_\_\_\_  
Civil Engineering Dept., METU

**Date:** \_\_\_\_\_ 28.03.2008

**I hereby declare that all information in this document has been obtained and presented in accordance with academic rules and ethical conduct. I also declare that, as required by these rules and conduct, I have fully cited and referenced all material and results that are not original to this work.**

Name, Last Name : Mehmet Selim GÜNAY

Signature :

## **ABSTRACT**

### **AN EQUIVALENT LINEARIZATION PROCEDURE FOR SEISMIC RESPONSE PREDICTION OF MDOF SYSTEMS**

Günay, Mehmet Selim

Ph.D., Department of Civil Engineering

Supervisor: Prof. Dr. Haluk Sucuoğlu

March 2008, 200 pages

Nonlinear response history analysis is accepted as the most accurate analytical tool for seismic response determination. However, accurate estimation of displacement responses using conceptually simple, approximate analysis procedures is preferable, since there are shortcomings in the application of nonlinear response history analysis resulting from its complexity.

An equivalent linearization procedure, which utilizes the familiar response spectrum analysis as the analysis tool and benefits from the capacity principles, is developed in this thesis study as an approximate method for predicting the inelastic seismic displacement response of MDOF systems under earthquake excitations. The procedure mainly consists of the construction of an equivalent linear system by reducing the stiffness of structural members which are expected to respond in the inelastic range. Different from similar studies in literature, equivalent damping is not explicitly employed in this study. Instead, predetermined spectral displacement

demands are utilized in each mode of the equivalent linear system for the determination of global displacement demands.

Response predictions of the equivalent linearization procedure are comparatively evaluated by using the benchmark nonlinear response history analysis results and other approximate methods including conventional pushover analysis and modal pushover analysis (MPA). It is observed that the proposed procedure results in similar accuracy with approximate methods which employ nonlinear analysis. Considering the conceptual simplicity of the procedure and the conventional analysis tools used in its application, presented equivalent linearization procedure can be suggested as a practically applicable method for the prediction of inelastic seismic displacement response parameters with sufficient accuracy.

Keywords: Equivalent Linearization, Capacity Principles, Nonlinear Response History Analysis, Conventional Pushover Analysis, Modal Pushover Analysis (MPA)

## ÖZ

### ÇOK DERECELİ SİSTEMLERİN DEPREM TEPKİLERİNİN EŞDEĞER DOĞRUSAL BİR YÖNTEM İLE TAHMİNİ

Günay, Mehmet Selim

Doktora, İnşaat Mühendisliği Bölümü

Tez Yöneticisi: Prof. Dr. Haluk Sucuoğlu

Mart 2008, 200 sayfa

Zaman tanım alanında doğrusal olmayan analiz, deprem davranışının belirlenmesi için kullanılan en kesin analitik yöntem olarak kabul edilmektedir. Ancak, bu yöntemin karmaşıklığı nedeni ile uygulanmasında oluşabilecek eksikliklerden dolayı, deplasman tepkilerinin kavramsal basitliğe sahip, yaklaşık analiz yöntemleri kullanılarak yeterli doğrulukta tahmin edilmesi pratikte tercih edilmektedir.

Bu tez çalışmasında çok dereceli sistemlerin deprem hareketi sırasındaki elastik ötesi deplasman tepkilerinin tahmin edilmesi için, mod birleştirme yöntemini kullanan ve kapasite prensiplerinden yararlanan bir eşdeğer doğrusal yöntem geliştirilmiştir. Bu yöntem esas olarak elastik ötesi davranış göstermesi beklenen yapısal elemanların rijitliklerinin azaltılması ile eşdeğer doğrusal bir sistemin oluşturulmasından ibarettir. Bu çalışmada, literatürdeki benzer çalışmalardan farklı olarak, eşdeğer sönümlenme değeri kullanılmamaktadır. Onun yerine eşdeğer

sistemin tüm modları için önceden ayrıca belirlenen spektral deplasmanlar, global deplasman talebinin belirlenmesinde kullanılmaktadır.

Eşdeğer doğrusal yöntem ile bulunan tepki tahminleri, referans olarak kabul edilen zaman tanım alanında doğrusal olmayan analiz ve klasik statik itme analizi ve modal statik itme analizinin de aralarında bulunduğu diğer yaklaşık yöntemlerle karşılaştırmalı olarak değerlendirilmiştir. Önerilen yöntemin, doğrusal olmayan analiz kullanan yaklaşık yöntemlerle benzer doğrulukta sonuçlar verdiği gözlemlenmiştir. Yöntemin kavramsal basitliği ve uygulanmasında kullanılan geleneksel araçlar da gözönüne alınarak, sunulan eşdeğer doğrusal yöntemin elastik ötesi deprem deplasman davranış parametrelerini yeterli doğrulukta hesaplamak için pratik bir araç olarak kullanılması önerilebilir.

**Anahtar Kelimeler:** Eşdeğer Doğrusallık, Kapasite Prensipleri, Zaman Tanım Alanında Doğrusal Olmayan Analiz, Klasik Statik İtme Analizi, Modal Statik İtme Analizi

To my family for their endless love and support

## ACKNOWLEDGEMENTS

This study was performed under the supervision of Prof. Dr. Haluk Sucuođlu. I would like to express my sincere appreciation for his support, guidance and insights throughout the study.

I would like to thank Professors Yalçın Mengi and Polat Gülkan who provided valuable comments during the course of the study.

I am thankful to Altuđ Erberik for his guidance, support and friendship that he has provided throughout my graduate life.

Many thanks to my friends Burcu Erdođan and Yasemin Didem Aktaş for all those precious moments of close friendship shared together.

I would like to extend my thanks to Ayşegöl Askan, Ufuk Yazgan, Ali Şengöz, Beyhan Bayhan, Koray Kadaş, Nazan Yılmaz Öztürk, Sinan Akarsu, İlker Kazaz and Bora Acun who supported me with their friendship and collaboration during different stages of this “long and windy road” which I started traveling in 1996 with my university education and stopped in 2008 with a PhD degree probably for another road.

My dear parents and my brother deserve the greatest thanks for their endless love, support, friendship, understanding and endurance.

## TABLE OF CONTENTS

ABSTRACT.....	iv
ÖZ.....	vi
ACKNOWLEDGEMENTS.....	ix
TABLE OF CONTENTS.....	x
LIST OF TABLES.....	xiii
LIST OF FIGURES.....	xiv
LIST OF SYMBOLS AND ABBREVIATIONS.....	xxii
CHAPTER	
1 INTRODUCTION.....	1
1.1 Statement of the Problem.....	1
1.2 Review of Past Studies.....	2
1.2.1 Equivalent Linearization Methods.....	2
1.2.2 Nonlinear Static (Pushover) Analysis.....	19
1.2.3 Seismic Analysis of Unsymmetrical Plan Buildings.....	28
1.3 Objective and Scope.....	30
2 METHODS EMPLOYED FOR INELASTIC SEISMIC RESPONSE	
PREDICTION.....	32
2.1 Nonlinear Response History Analysis.....	32
2.2 Conventional Pushover Analysis with Coefficient Method of	
FEMA-356.....	34
2.3 Modal Pushover Analysis (MPA).....	38
2.4 A General Comment on the Evaluation of Approximate Methods	
in Comparison with Nonlinear Response History Analysis.....	41

3	EQUIVALENT LINEARIZATION PROCEDURE.....	44
3.1	Demand Analysis.....	45
3.2	Capacity Analysis.....	46
3.2.1	Calculation of Beam Moment Capacities (Step 1).....	46
3.2.2	Calculation of Column Axial Forces and Moment Capacities (Steps 2 and 3).....	47
3.2.3	Calculation of Column-to-Beam Capacity Ratios (CBCR) at the Joints (Step 4).....	49
3.2.4	Identification of Potential Yielding Member-Ends (Step 5).....	50
3.2.5	Estimation of Base Shear Capacity.....	50
3.3	Determination of Final Yielding Distribution.....	52
3.4	Stiffness Reduction.....	53
3.5	Spectral Displacement Demands for the Equivalent Linear System....	56
3.5.1	Nonlinear Response History Analysis of the Equivalent SDOF System.....	57
3.5.2	Equal Displacement Assumption.....	58
3.6	Response Spectrum Analysis of the Equivalent Linear System.....	59
3.7	Determination of Response Parameters.....	60
3.8	Basic Assumptions of the Equivalent Linearization Procedure.....	61
4	GROUND MOTIONS EMPLOYED IN CASE STUDIES.....	64
5	CASE STUDY I: TWELVE STORY RC PLANE FRAME.....	76
5.1	Description of the Building.....	76
5.2	Modeling.....	78
5.3	Free Vibration Properties.....	79
5.4	Presentation of Results.....	80
5.4.1	Description of Statistical Error Parameters.....	81
5.4.2	Roof (Top Story) Displacement Demands .....	83
5.4.3	Local Response Parameters.....	87
5.4.4	Response Prediction Under a Pulse Type Ground Motion.....	105
5.4.5	Response Prediction Under an Ordinary Ground Motion.....	111

6 CASE STUDY II: SIX STORY UNSYMMETRICAL-PLAN	
RC SPACE FRAME.....	116
6.1 Description of the Building.....	116
6.2 Modeling.....	118
6.3 Free Vibration Properties.....	122
6.4 Presentation of Results.....	124
6.4.1 Roof (Top Story) Displacement Demands at the Center of Mass...	
.....	124
6.4.2 Local Response Parameters.....	128
6.4.2.1 Torsional Effects Observed in Nonlinear	
Response History Analyses.....	132
6.4.2.2 Roof Displacements of the Frames.....	134
6.4.2.3 Interstory Drift Ratios and Beam Chord Rotations.....	139
6.4.3 Response Prediction Under a Pulse Type Ground Motion.....	160
6.4.4 Response Prediction Under an Ordinary Ground Motion.....	170
7 SUMMARY AND CONCLUSIONS.....	179
7.1 Summary.....	179
7.2 Conclusions.....	180
REFERENCES.....	184
APPENDICES	
A STIFFNESS FORMULATION of DRAIN-2DX for “PLASTIC HINGE	
BEAM-COLUMN ELEMENT”.....	195
CURRICULUM VITAE.....	199

## LIST OF TABLES

### TABLES

Table 1.1	Equivalent period $T_{eq}$ , and equivalent viscous damping $\zeta_{eq}$ , used in different equivalent linearization based methods (Miranda and Ruiz-Garcia, 2002).....	10
Table 3.1	$R_M$ corresponding to different yielding situations.....	56
Table 4.1	Pulse type ground motion properties.....	65
Table 4.2	Ordinary ground motion properties.....	68
Table 5.1	Free vibration properties of the twelve story frame model.....	79
Table 5.2	Roof displacement statistics for pulse type ground motions.....	83
Table 5.3	Roof displacement statistics for ordinary ground motions.....	83
Table 6.1	Free vibration properties of the six story building.....	123
Table 6.2	Roof displacement statistics for pulse type ground motions.....	127
Table 6.3	Roof displacement statistics for ordinary ground motions.....	127

## LIST OF FIGURES

### FIGURES

Figure 1.1	Hysteresis loop of an elastoplastic system and equivalent stiffness....	3
Figure 1.2	Hysteresis loop for Takeda stiffness degrading model for an unloading stiffness factor of 0.5 and zero strain hardening.....	9
Figure 1.3	Comparison of equivalent damping ratios for different equivalent linearization methods (Miranda and Ruiz-Garcia, 2002).....	11
Figure 2.1	Bilinearization of pushover curve according to FEMA-356.....	36
Figure 2.2	Corner period ( $T_c$ ) for a design spectrum.....	37
Figure 2.3	Acceleration response spectrum of a particular ground motion.....	38
Figure 2.4	Top story displacement history examples a) displacement is mainly in the positive direction b) displacement is mainly in the negative direction.....	42
Figure 2.5	Top story displacement history examples; the structure is displaced similarly in the positive and negative directions.....	42
Figure 2.6	Algorithm for the determination of analysis direction for the approximate methods.....	43
Figure 3.1	Outline of the equivalent linearization procedure.....	45
Figure 3.2	Outline of capacity analysis.....	46
Figure 3.3	Beam-end forces due to gravity and earthquake loadings.....	48
Figure 3.4	Calculation of axial forces of columns due to earthquake loading....	48
Figure 3.5	Biaxial bending for a rectangular column.....	49
Figure 3.6	Column-to-Beam Capacity Ratio (CBCR) at a joint.....	50
Figure 3.7	Calculation of base shear capacity for 2D models.....	51

Figure 3.8	Calculation of base shear capacity for 3D models.....	51
Figure 3.9	Demonstration of moment directions at the ends of a beam due to earthquake loading and gravity loading.....	52
Figure 3.10	Definition of chord rotation at the i and j ends of a frame member .....	53
Figure 3.11	The variation of the sum of moments with the sum of chord rotations at member-ends in the linear elastic and inelastic ranges.....	55
Figure 3.12	Calculation of pseudo acceleration corresponding to the target spectral displacement at the n <sup>th</sup> mode.....	60
Figure 3.13	Schematical demonstration of the application of equivalent linearization procedure.....	62
Figure 3.14	Flowchart of the equivalent linearization procedure for a 3D model with reference to Figure 3.13.....	63
Figure 4.1	Moment magnitude plotted against the closest distance to fault rupture for the utilized ground motions.....	71
Figure 4.2	Ground acceleration, velocity and displacement traces of a pulse type ground motion (TCU052-W).....	72
Figure 4.3	Pulse period plotted against moment magnitude for the utilized pulse type ground motions .....	73
Figure 4.4	Ground acceleration, velocity and displacement traces of an “ordinary” ground motion (LOB000).....	74
Figure 4.5	a) PGA, b) PGV, c) PGV/PGA ratios of the considered ground motions.....	75
Figure 5.1	Story plan of the twelve story building.....	77
Figure 5.2	Plane model of the twelve story building.....	77
Figure 5.3	Bilinear moment-curvature relation utilized in Drain-2DX.....	78
Figure 5.4	Modal static force distributions $s_n$ for the first three modes.....	80
Figure 5.5	Comparison of the roof displacement demand predictions of approximate methods with the benchmark method (NRHA) for pulse type ground motions.....	84

Figure 5.6	Comparison of the roof displacement demand predictions of approximate methods with the benchmark method (NRHA) for ordinary ground motions.....	85
Figure 5.7	Roof displacement demands obtained from a) pulse type ground motions, b) ordinary ground motions marked on the first mode pushover curve.....	88
Figure 5.8	5% damped pseudo acceleration response spectra for a) pulse type, b) ordinary ground motions.....	89
Figure 5.9	5% damped displacement response spectra for a) pulse type, b) ordinary ground motions.....	90
Figure 5.10	a) Median, b) RMSE of story displacements for pulse type ground motions.....	93
Figure 5.11	a) Median, b) RMSE of interstory drift ratios for pulse type ground motions.....	94
Figure 5.12	a) Median, b) RMSE of beam chord rotations for pulse type ground motions.....	95
Figure 5.13	a) Median, b) RMSE of column bottom end chord rotations for pulse type ground motions.....	96
Figure 5.14	Interstory drift ratios of the approximate methods normalized with those of NRHA for pulse type ground motions.....	97
Figure 5.15	a) Median, b) RMSE of story displacements for ordinary ground motions.....	100
Figure 5.16	a) Median, b) RMSE of interstory drift ratios for ordinary ground motions.....	101
Figure 5.17	a) Median, b) RMSE of beam chord rotations for ordinary ground motions.....	102
Figure 5.18	a) Median, b) RMSE of column bottom end chord rotations for ordinary ground motions.....	103
Figure 5.19	Interstory drift ratios of the approximate methods normalized with those of NRHA for ordinary ground motions.....	104

Figure 5.20	Maximum roof displacement and maximum base shear pair resulting from the ground motion CHY080-N plotted against the first mode capacity curve.....	106
Figure 5.21	Ground acceleration, velocity and displacement traces for the ground motion CHY080-N.....	107
Figure 5.22	5% damped pseudo acceleration and displacement response spectra for the ground motion CHY080-N.....	108
Figure 5.23	Comparison of maximum a) story displacements, b) interstory drift ratios, c) beam chord rotations, d) column bottom end chord rotations for the ground motion CHY080-N.....	109
Figure 5.24	Maximum roof displacement and maximum base shear pair resulting from the ground motion IZT090 plotted against the first mode capacity curve.....	112
Figure 5.25	Ground acceleration, velocity and displacement traces for the ground motion IZT090.....	113
Figure 5.26	5% damped pseudo acceleration and displacement response spectra for the ground motion IZT090.....	114
Figure 5.27	Comparison of maximum a) story displacements, b) interstory drift ratios, c) beam chord rotations, d) column bottom end chord rotations for the ground motion IZT090.....	115
Figure 6.1	Story plan and 3D view of the six story building.....	117
Figure 6.2	Modeling features of OpenSees employed in Case Study II.....	118
Figure 6.3	Moment-curvature relation recorded in the section at the base of one of the ground story columns during nonlinear response history analysis .....	119
Figure 6.4	Effect of utilizing fiber sections for the beam sections on the pushover curve of the case study building.....	121
Figure 6.5	Moment-curvature relation recorded in a section at the end of one of the first story beams during nonlinear response history analysis.....	121
Figure 6.6	Modal static forces and torques for the first two pairs of modes.....	123

Figure 6.7	Comparison of the roof center of mass displacement demand predictions of approximate methods with the benchmark method (NRHA) for pulse type ground motions.....	125
Figure 6.8	Comparison of the roof center of mass displacement demand predictions of approximate methods with the benchmark method (NRHA) for ordinary ground motions.....	126
Figure 6.9	Center of mass roof displacement demands obtained from a) pulse type ground motions, b) ordinary ground motions marked on the first mode pushover curve.....	129
Figure 6.10	5% damped pseudo acceleration response spectra for a) pulse type, b) ordinary ground motions.....	130
Figure 6.11	5% damped displacement response spectra for a) pulse type, b) ordinary ground motions.....	131
Figure 6.12	Median interstory drift ratios obtained from NRHA for a) pulse type, b) ordinary ground motions.....	133
Figure 6.13	a) Median, b) RMSE of roof displacements of the four individual frames for pulse type ground motions.....	137
Figure 6.14	a) Median, b) RMSE of roof displacements of the four individual frames for ordinary ground motions.....	138
Figure 6.15	Equivalent lateral first modal static forces for the linear elastic system acting at the stiff and flexible edge frames with and without the torques at the center of mass.....	139
Figure 6.16	Median of a) interstory drift ratios, b) beam chord rotations at the stiff edge frame for pulse type ground motions.....	142
Figure 6.17	Median of a) interstory drift ratios, b) beam chord rotations at the inner frame close to stiff edge for pulse type ground motions.....	143
Figure 6.18	Median of a) interstory drift ratios, b) beam chord rotations at the inner frame close to flexible edge for pulse type ground motions...	144
Figure 6.19	Median of a) interstory drift ratios, b) beam chord rotations at the flexible edge frame for pulse type ground motions.....	145

Figure 6.20	Beam chord rotations obtained from the approximate methods normalized with those obtained from NRHA at the stiff edge frame under pulse type ground motions.....	146
Figure 6.21	Beam chord rotations obtained from the approximate methods normalized with those obtained from NRHA at the inner frame close to the stiff edge under pulse type ground motions.....	147
Figure 6.22	Beam chord rotations obtained from the approximate methods normalized with those obtained from NRHA at the inner frame close to the flexible edge under pulse type ground motions.....	148
Figure 6.23	Beam chord rotations obtained from the approximate methods normalized with those obtained from NRHA at the flexible edge frame under pulse type ground motions.....	149
Figure 6.24	Median of a) interstory drift ratios, b) beam chord rotations at the stiff edge frame for ordinary ground motions.....	152
Figure 6.25	Median of a) interstory drift ratios, b) beam chord rotations at the inner frame close to the stiff edge for ordinary ground motions.....	153
Figure 6.26	Median of a) interstory drift ratios, b) beam chord rotations at the inner frame close to the flexible edge for ordinary ground motions.....	154
Figure 6.27	Median of a) interstory drift ratios, b) beam chord rotations at the flexible edge frame for ordinary ground motions.....	155
Figure 6.28	Beam chord rotations obtained from the approximate methods normalized with those obtained from NRHA at the stiff edge frame under ordinary ground motions.....	156
Figure 6.29	Beam chord rotations obtained from the approximate methods normalized with those obtained from NRHA at the inner frame close to stiff edge under ordinary ground motions.....	157
Figure 6.30	Beam chord rotations obtained from the approximate methods normalized with those obtained from NRHA at the inner frame close to flexible edge under ordinary ground motions.....	158

Figure 6.31	Beam chord rotations obtained from the approximate methods normalized with those obtained from NRHA at the flexible edge frame under ordinary ground motions.....	159
Figure 6.32	Ground acceleration, velocity and displacement traces for the ground motion SYL360.....	162
Figure 6.33	5% damped pseudo acceleration and displacement response spectra for the ground motion SYL360.....	163
Figure 6.34	Comparison of maximum story displacements a) at the stiff edge frame, b) at the inner frame close to the stiff edge for the ground motion SYL360.....	164
Figure 6.35	Comparison of maximum story displacements a) at the inner frame close to the flexible edge, b) at the flexible edge frame for the ground motion SYL360.....	165
Figure 6.36	Comparison of maximum interstory drift ratios a) at the stiff edge frame, b) at the inner frame close to the stiff edge for the ground motion SYL360.....	166
Figure 6.37	Comparison of maximum interstory drift ratios a) at the inner frame close to the flexible edge, b) at the flexible edge frame for the ground motion SYL360.....	167
Figure 6.38	Comparison of maximum beam chord rotations a) at the stiff edge frame, b) at the inner frame close to the stiff edge for the ground motion SYL360.....	168
Figure 6.39	Comparison of maximum beam chord rotations a) at the inner frame close to flexible edge, b) at the flexible edge frame for the ground motion SYL360.....	169
Figure 6.40	Ground acceleration, velocity and displacement traces for the ground motion ELC180.....	171
Figure 6.41	5% damped pseudo acceleration and displacement response spectra for the ground motion ELC180.....	172

Figure 6.42	Comparison of maximum story displacements a) at the stiff edge frame, b) at the inner frame close to the stiff edge for the ground motion ELC180.....	173
Figure 6.43	Comparison of maximum story displacements a) at the inner frame close to flexible edge, b) at the flexible edge frame for the ground motion ELC180.....	174
Figure 6.44	Comparison of maximum interstory drift ratios a) at the stiff edge frame, b) at the inner frame close to the stiff edge for the ground motion ELC180.....	175
Figure 6.45	Comparison of maximum interstory drift ratios a) at the inner frame close to flexible edge, b) at the flexible edge frame for the ground motion ELC180.....	176
Figure 6.46	Comparison of maximum beam chord rotations a) at the stiff edge frame, b) at the inner frame close to the stiff edge for the ground motion ELC180.....	177
Figure 6.47	Comparison of maximum beam chord rotations a) at the inner frame close to flexible edge, b) at the flexible edge frame for the ground motion ELC180.....	178
Figure A.1	Local degrees of freedom for a prismatic beam-column element....	195
Figure A.2	Local stiffness matrix for a prismatic beam-column element with the degrees of freedom shown in Figure A.1.....	196
Figure A.3	Bilinear moment curvature relationship and decomposition into components.....	196
Figure A.4	Stiffness matrices for component EP of a “Plastic Hinge Beam-Column Element” for which yielding occurs a) at end i, b) at end j.....	198
Figure A.5	Stiffness matrix for component EP of a “Plastic Hinge Beam-Column Element” both ends of which yield.....	198

## LIST OF SYMBOLS AND ABBREVIATIONS

CBCR	: Column-to-Beam Capacity Ratio
DCR	: Demand-to-Capacity Ratio
EQL-NL	: Nonlinear version of the equivalent linearization procedure
EQL-ED	: Equal displacement version of the equivalent linearization procedure
$\mathbf{f}_n'$	: Modal force vector for the $n^{\text{th}}$ mode of the equivalent linear system
$h^*$	: Distance of the centroid of the lateral force vector to the base of the structure
$I$	: Original (unreduced) moment of inertia
$I'$	: Reduced moment of inertia
LRHA	: Linear Elastic Response History Analysis
$M_{ci}$	: Moment capacity of the section at “i” end of a beam
$M_{cj}$	: Moment capacity of the section at “j” end of a beam
$M_{cx}$	: Moment capacity of the section at a column end about x axis
$M_{cy}$	: Moment capacity of the section at a column end about y axis
$M_E$	: Moment at a member end obtained from response spectrum analysis
$M_{Ex}$	: Moment obtained from response spectrum analysis at a column end about x axis
$M_{Ey}$	: Moment obtained from response spectrum analysis at a column end about y axis
$M_{Gi}$	: Moment at “i” end of a beam due to gravity loading
$M_{Gj}$	: Moment at “j” end of a beam due to gravity loading
MPA	: Modal Pushover Analysis
MPA-1	: Modal Pushover Analysis conducted by considering the response due to only the first mode

$M_{rc}$	: Residual moment capacity (gravity moment excluded from moment capacity)
NRHA	: Nonlinear Response History Analysis
PO-FEMA	: Conventional Pushover Analysis with Coefficient Method of FEMA-356
$PSa_n^*$	: Pseudo acceleration at the $n^{\text{th}}$ mode of the equivalent linear system corresponding to $Sd_n^*$
$q$	: Distributed gravity load on the beam
$R_M$	: Reduction factor used for moment of inertia reduction
RMSE	: Root mean square error
RSA	: Response Spectrum Analysis
$Sd_n^*$	: Target spectral displacement at the $n^{\text{th}}$ mode of the equivalent linear system
$Sd_{nc}^*$	: Target spectral displacement at the $n^{\text{th}}$ mode of the equivalent linear system calculated from equal displacement assumption
$Sd_{ni}^*$	: Target spectral displacement at the $n^{\text{th}}$ mode of the equivalent linear system calculated by conducting single-degree-of-freedom NRHA
$s_n$	: Modal static force vector for the $n^{\text{th}}$ mode
$T_n$	: Period of the $n^{\text{th}}$ mode of the original (unreduced stiffness) system
$T_n'$	: Period of the $n^{\text{th}}$ mode of the equivalent linear system
$V_{Ei}$	: Maximum shear force due to earthquake loading that can be transmitted from “i” end of a beam
$V_{Ej}$	: Maximum shear force due to earthquake loading that can be transmitted from “j” end of a beam
$V_{Gi}$	: Shear force at “i” end of a beam due to gravity loading
$V_{Gj}$	: Shear force at “j” end of a beam due to gravity loading
$V_y$	: Base shear capacity
$\Gamma_n'$	: Participation factor of the $n^{\text{th}}$ mode of the equivalent linear system
$\eta_{ny}$	: Yield base shear at the $n^{\text{th}}$ mode divided by the effective modal weight
$\phi_n'$	: $n^{\text{th}}$ modal vector of the equivalent linear system

# CHAPTER 1

## INTRODUCTION

### 1.1 Statement of the Problem

The analysis procedures employed for determining the earthquake performance of buildings can be grouped as linear static, linear dynamic, nonlinear static and nonlinear dynamic. Among these, nonlinear dynamic (nonlinear response history) analysis is accepted as the most accurate simulation of dynamic response. However, there are several shortcomings in the application of nonlinear response history analysis. First, the developed analysis tools are not as standard as the linear elastic analysis methods. Second, most of the structural engineering professionals are not familiar with inelastic and nonlinear analysis concepts. Third, nonlinear response history analysis may suffer from stability or convergence problems. Finally, it may require considerable amount of run time and post processing efforts. On the other hand, linear elastic dynamic (time history or response spectrum) analysis has limited capacity in simulating inelastic seismic behavior. However, linear elastic procedures are simple, conventional, stable, theoretically sound and they are well accepted by the practicing engineers.

Hence, in this transition period from linear to nonlinear analysis, and from force-based to deformation-based assessment and design, an equivalent linearization procedure which utilizes the familiar response spectrum analysis as the

analysis tool and benefits from the capacity principles may serve as an appropriate and efficient approach for seismic assessment.

## **1.2 Review of Past Studies**

Review of past studies is presented in three sections. In the first section, studies on the application of equivalent linearization methods to single-degree-of-freedom (SDOF) and multi-degree-of-freedom (MDOF) systems are presented. In the second section, studies on conventional, adaptive and modal pushover analyses are presented. Finally, past studies on the seismic analysis of unsymmetrical plan buildings are reviewed.

### **1.2.1 Equivalent Linearization Methods**

#### **a) SDOF Systems**

Equivalent linearization methods developed for SDOF systems mainly comprises of the determination of an equivalent stiffness (period) and equivalent damping. Equivalent period is employed to reflect the elongation of the linear elastic period due to inelasticity. Equivalent damping represents the actual hysteretic energy dissipation of the inelastic system.

Studies on the equivalent linear analysis of SDOF systems started in 1930's. The concept of equivalent viscous damping was originally proposed by Jacobsen (1930) to obtain approximate solutions for the steady state vibration of SDOF systems with linear restoring force-deformation and nonlinear damping force-velocity relationships under harmonic loading. In this method, equivalent damping was determined by equating the energy per cycle of the nonlinearly damped oscillator to the energy per cycle of a linearly damped oscillator having the same period with the original system.

In 1960, Jacobsen extended the concept of equivalent damping to SDOF systems with nonlinear restoring force-deformation relationships. In his approach, the geometry of the skeleton curve and the geometry of the hysteresis loop determine the amount of equivalent viscous damping (Equation 1.1). No corresponding stiffness value was presented for predicting nonlinear response.

$$\zeta_{eq} = \frac{1}{2\pi} \frac{\text{work done in a half cycle of the hysteresis loop}}{\text{work area under skeleton curve}} \quad (1.1)$$

Rosenblueth and Herrera (1964) introduced an equivalent linearization method in order to obtain approximate solutions for the steady state vibration of elastoplastic SDOF systems under harmonic loading. In this method, the equivalent stiffness was chosen to be the slope of the line joining the ends of the hysteresis loop (Equation 1.2, Figure 1.1). In addition, the resonant amplitudes of the yielding and the associated linear system were assumed to be the same and equivalent damping was determined by equating the energy dissipated per cycle at resonance (Equation 1.3).

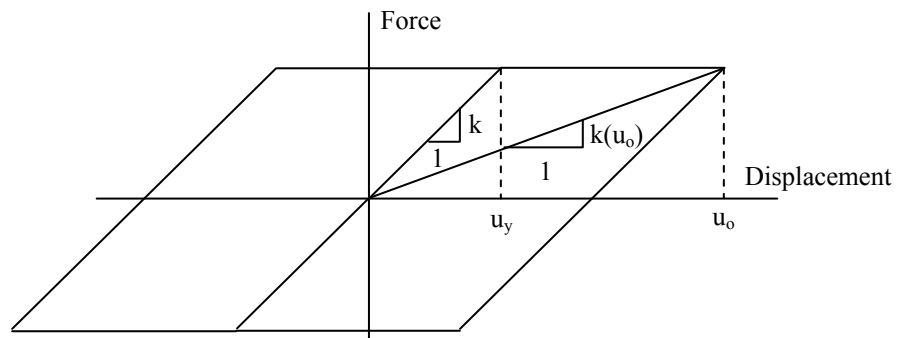


Figure 1.1 Hysteresis loop of an elastoplastic system and equivalent stiffness

$$k(u_o) = k \frac{u_y}{u_o} \quad (1.2)$$

$$2\pi\beta(u_o)k(u_o)u_o^2 = 4k u_y(u_o - u_y) \quad (1.3)$$

In Equation 1.3, left hand side represents the dissipated energy per cycle at resonance by a linear SDOF system with damping equal to  $\beta(u_o)$  and stiffness equal to  $k(u_o)$  in response to a sinusoidal force  $p_o \sin \omega t$ . Right hand side represents the energy dissipated per cycle by the elastoplastic system. Substituting Equation 1.2 in Equation 1.3, equivalent damping  $\beta(u_o)$  can be represented with Equation 1.4.

$$\beta(u_o) = \frac{2}{\pi} \left( 1 - \frac{1}{\mu} \right) \quad (1.4)$$

where  $\mu$  is the ductility ratio which is equal to  $u_o / u_y$ .

In the Capacity Spectrum Method of ATC-40 (ATC, 1996), a similar approach is used. Energy dissipated by the bilinear system in the cycle where the maximum displacement occurs is equated to the energy per cycle dissipated at resonance by a linear SDOF system possessing equivalent viscous damping and equivalent stiffness (slope of the line joining the ends of the hysteresis loop) under harmonic loading. Further, equivalent damping is multiplied with a factor  $\kappa$ , in order to take into account the effect of imperfections in the hysteresis loop such as pinching or degradation and the maximum value of equivalent damping is limited to 0.45. Capacity spectrum method was originally developed as a rapid evaluation procedure for a pilot seismic risk project of the Puget Sound Naval Shipyard of the U.S. Navy (Freeman et al., 1975).

This method has two important deficiencies when used with ground motions.

- 1) Dissipated energy in the cycle of maximum displacement of a yielding system results in overestimated equivalent damping, since displacement is significantly smaller than the maximum displacement most of the time during a ground motion. Chopra and Goel (2000) compared the displacement demand predictions of the ATC-40 Procedure B with the exact nonlinear response history analysis of SDOF systems and demonstrated that the approximate procedure

underestimated the displacements significantly for a wide range of period values with errors approaching 50%.

2) Dissipated energy per cycle of the linear system is calculated by considering the response to a harmonic force at resonance, which is not the case during a ground motion. It can be justifiable if there is a dominant pulse with frequency close to the equivalent natural frequency, however it is misleading for ground motions containing significant components from a broad range of frequencies.

Jennings (1968) examined six different methods in which equivalent viscous damping can be defined for the steady state response of SDOF elasto-plastic oscillators to sinusoidal excitation. The methods of Jacobsen (1960) and Rosenblueth and Herrera (1964) were among the investigated methods. In all considered methods except the method of Jacobsen, equivalent damping was calculated by equating the energy per cycle dissipated by the equivalent linear system at resonance to that dissipated by the yielding system. Different equivalent damping ratios were obtained in each method due to the differences in the consideration of stiffness and mass employed in describing the equivalent linear systems. Jennings stated that any of the considered methods might be appropriate under certain circumstances; however the method which uses equivalent damping and the initial stiffness was preferable because of its clarity, simplicity and conservative results.

Gülkan and Sozen (1974) stated that the response of reinforced concrete structures to strong earthquake motions was influenced by two basic phenomena, which were reduction in stiffness and increase in energy dissipation capacity. They also stated that the maximum dynamic response of reinforced concrete structures, which can be represented by SDOF systems, can be approximated by linear response analysis using a reduced stiffness and a substitute damping. Substitute damping represents the increase in energy dissipation capacity through the use of Equation 1.5.

$$\beta_o \left[ 2m\omega_o \int_0^t (\dot{u})^2 dt \right] = - \int_0^t m \ddot{u}_g \dot{u} dt \quad (1.5)$$

Equation 1.5 is based on the fact that the energy input from a ground motion is entirely dissipated by a viscous damper which has a damping ratio equal to substitute damping,  $\beta_o$ .  $\omega_o$  is equal to the natural frequency of the system with reduced stiffness, calculated as the square root of the ratio of maximum absolute acceleration to maximum absolute displacement.

Gülkan and Sözen conducted dynamic experiments with one story, one bay frames. They calculated  $\beta_o$  values through Equation 1.5 using the test results. In doing so, they assumed that the velocity of the equivalent linear system is equal to the velocity obtained from the test frames. In addition, they calculated ductility ratio ( $\mu$ ) as the ratio of maximum absolute displacement to calculated yield displacement using the test results. Utilizing the  $\beta_o$  and  $\mu$  pairs that they have obtained, they ended up with a relation between  $\beta_o$  and  $\mu$  (Equation 1.6).

$$\beta_o = 0.02 + 0.2 \left( 1 - \frac{1}{\sqrt{\mu}} \right) \quad (1.6)$$

It can be observed from Equation 1.6 that 0.02 is the value of damping ratio corresponding to no inelasticity.

Gülkan and Sözen expressed that the equivalent viscous damping approach had considerable potential as a vehicle to interpret the response of RC systems from the design point of view, and used the equivalent damping approach to estimate the design base shear corresponding to an assumed displacement limit.

Iwan and Gates (1979) have conducted a statistical study in order to estimate the effective period and effective damping by using nonlinear SDOF systems possessing force-deformation relations with nondegrading and degrading properties. They used twelve ground motions representing a variety of different types of earthquake excitation. They calculated the spectral displacements corresponding to

different ductility levels considering nine period values. Then they tried to minimize the differences between these displacements and the displacements obtained by conducting elastic analyses of SDOF systems with shifted periods and effective damping values. They observed that the period shift is always less than an order of two even for very large ductility and the optimum effective damping never exceeds 14% for all the systems that they have analyzed. They also observed that the primary effect of deterioration or stiffness degradation is to increase the effective period but they do not have a significant effect on effective damping.

Using the optimum effective period and damping values of Iwan and Gates, Iwan (1980) developed the empirical relations represented by Equations 1.7 and 1.8 for effective period and effective damping in the period range of 0.4 -4.0 s and for ductility ratios in the range of 2 to 8.

$$T_e/T_o = 1 + 0.121(\mu - 1)^{0.939} \quad (1.7)$$

$$\zeta_e - \zeta_o = 0.0587(\mu - 1)^{0.371} \quad (1.8)$$

In Equations 1.7 and 1.8,  $T_e$  is the effective period,  $\zeta_e$  is the effective damping ratio,  $T_o$  is the initial period,  $\zeta_o$  is the damping ratio corresponding to no inelasticity, and  $\mu$  is the ductility ratio.

Iwan observed that the differences in hysteretic behavior have a secondary effect on the accuracy of results predicted by his empirical equations. He compared the response predictions of the empirical equations, with the predictions of Newmark-Hall method (1973), substitute structure method (Shibata and Sozen, 1976) and ATC-3 (1978) design guidelines, and concluded that his empirical equations seem to produce more accurate predictions than those produced by the other considered methods.

A more comprehensive version of the optimization study of Iwan (1980) was conducted by Guyader (2003) to obtain equations for the effective damping and effective period values of bilinear, stiffness degrading and strength degrading SDOF systems for use in an improved equivalent linearization procedure in

FEMA-440 (ATC, 2005). Akkar and Metin (2007) evaluated the improved equivalent linearization method together with the improved displacement coefficient method (DCM) presented in FEMA-440 by using 24 nondegrading, three- to nine-story RC moment resisting frames and 78 stiff soil near-fault records. They compared the maximum roof and interstory drift predictions obtained from the approximate methods with the reference nonlinear response history analysis results. They stated that the improved methods result in good deformation demand estimations on the median for near-fault records without pulse whereas they tend to underestimate the peak roof and interstory drifts for increasing fundamental periods in the case of near-fault records with pulse. They observed that the improved displacement coefficient method led to more conservative estimations with higher dispersion relative to the improved equivalent linearization method.

Kowalsky (1994) used an equivalent linear method similar to the substitute structure method to estimate the target deformation as a key step of his proposed displacement based design methodology. He used the secant stiffness at maximum deformation as the equivalent stiffness and derived an equation for equivalent damping by equating the energy dissipated by an inelastic system with Takeda hysteretic model at the cycle of maximum deformation, to the energy per cycle dissipated at resonance by an equivalent SDOF system under harmonic loading. This approach is similar to the one employed by Rosenblueth and Herrera (1964). Difference comes from employing Takeda hysteresis model instead of the elastoplastic model used by Rosenblueth and Herrera. For an unloading stiffness factor of 0.5 and zero post yield stiffness (Figure 1.2), the relation between equivalent damping and ductility, proposed by Kowalsky is expressed with Equation 1.9.

$$\zeta_e = \zeta_o + \frac{1}{\pi} \left( 1 - \frac{1}{\sqrt{\mu}} \right) \quad (1.9)$$

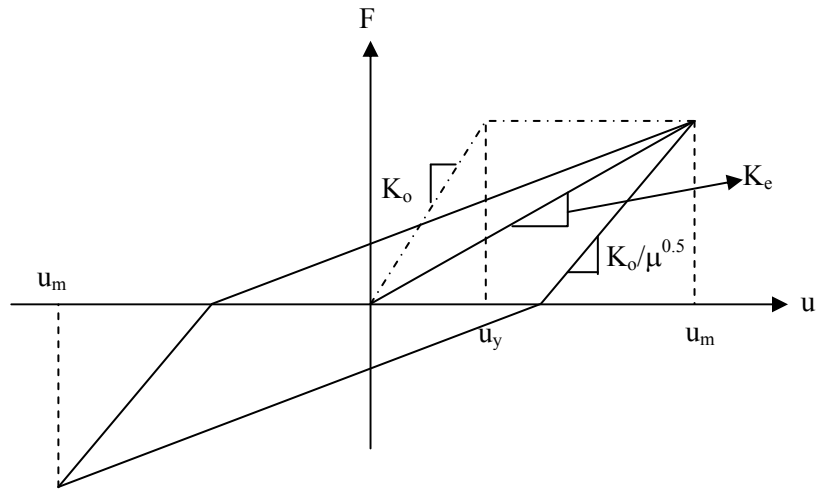


Figure 1.2 Hysteresis loop for Takeda stiffness degrading model for an unloading stiffness factor of 0.5 and zero strain hardening

Judi et al. (2000) compared the use of equivalent viscous damping and substitute damping in the direct displacement based design methodology of Kowalsky et al. (1994). They obtained the substitute damping values via Equation 1.5, for a series of oscillators with different ductility levels using the original records of El Centro NS 1940, Taft N21E 1952, Matahina Dam Base 1987, Hachinohe NS 1968 and the scaled versions of the records such that their 5% damped spectra matches the New Zealand code spectrum for intermediate soils. They used two types of oscillators, which were elastoplastic and stiffness degrading. They observed that substitute damping depends on ductility, not much on period, and substitute damping values are similar for different earthquake motions for the same ductility, period and hysteretic form. They obtained a linear relationship between substitute damping and ductility for bilinear and stiffness degrading systems. They concluded that substitute damping is the most suitable form of damping for calculating displacement or ductility demands in the direct displacement based design procedure.

Miranda and Ruiz-Garcia (2002) evaluated six approximate methods to estimate the maximum inelastic displacements of SDOF systems. Four of the

approximate methods were based on equivalent linearization. They evaluated the equivalent linearization methods by Rosenblueth and Herrera (1964), Gülkan and Sözen (1974), Iwan (1980) and Kowalsky (1994). Equivalent period and equivalent viscous damping values used in different methods are summarized in Table 1.1. A comparison of equivalent damping ratios of the various methods, with  $\zeta_0$  set to zero is shown in Figure 1.3.

Miranda and Ruiz-Garcia used the approximate methods to estimate the maximum response of SDOF systems with elastoplastic, modified Clough, and Takeda hysteretic load–deformation models possessing periods between 0.05 and 3.0 sec. Six different levels of maximum displacement ductility demands were aimed when the SDOF systems were subjected to 264 ground motions recorded on firm sites in 12 California earthquakes. For each method, they calculated the mean ratios of approximate to exact maximum displacement (relative error) and dispersion of relative errors as a function of the period of vibration and the displacement ductility ratio. Their conclusions are as follows:

Table 1.1 Equivalent period  $T_{eq}$ , and equivalent viscous damping  $\zeta_{eq}$ , used in different equivalent linearization based methods (Miranda and Ruiz-Garcia, 2002)

Author	$T_{eq}$	$\zeta_{eq}$
Rosenblueth and Herrera (1964)	$T\sqrt{\mu}$	$\zeta_0 + \frac{2}{\pi} \left( 1 - \frac{1}{\mu} \right)$
Gülkan and Sözen (1974)	$T\sqrt{\mu}$	$\zeta_0 + 0.2 \left( 1 - \frac{1}{\sqrt{\mu}} \right)$
Iwan (1980)	$T \left( 1 + 0.121(\mu - 1)^{0.939} \right)$	$\zeta_0 + 0.0587(\mu - 1)^{0.371}$
Kowalsky (1994)	$T\sqrt{\mu}$	$\zeta_0 + \frac{1}{\pi} \left( 1 - \frac{1}{\sqrt{\mu}} \right)$

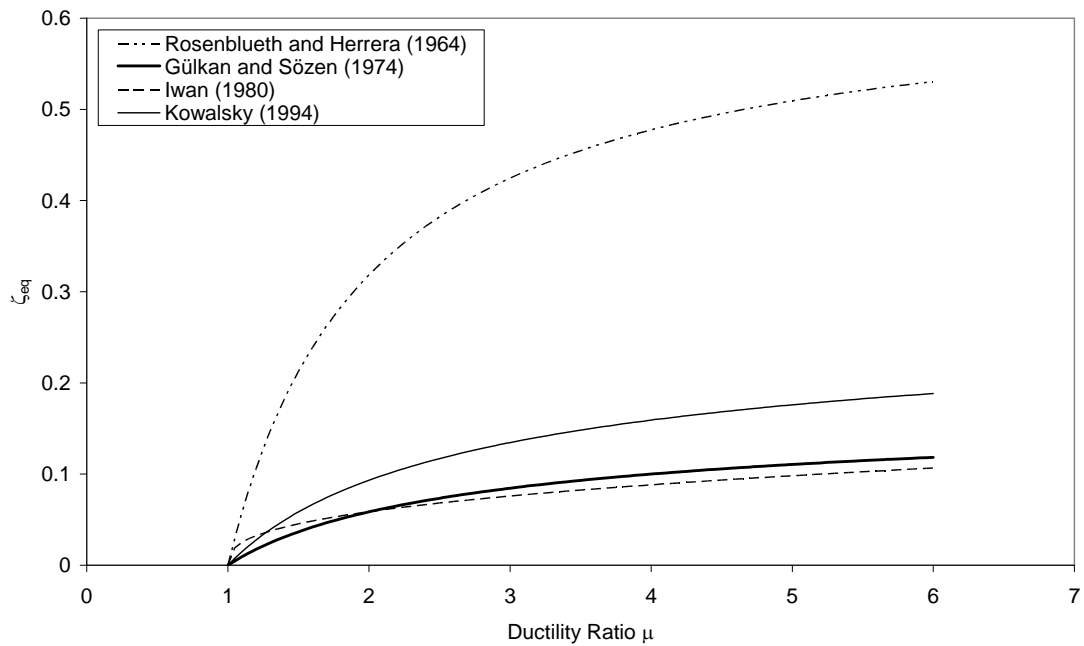


Figure 1.3 Comparison of equivalent damping ratios for different equivalent linearization methods (Miranda and Ruiz-Garcia, 2002)

1) Rosenblueth and Herrera method produces significant underestimations of the maximum inelastic displacement for all three types of hysteretic models (This is an expected result as explained in the previous paragraphs).

2) Other methods based on equivalent linearization produce much better results. Mean relative errors in these methods, in general, increase with increasing ductility and with decreasing period. In general, these methods produce more accurate results in the intermediate and long-period regions than in the short-period region. In the short-period spectral region, the methods of Gülkan and Sözen and Kowalsky tend to significantly overestimate the maximum displacement while the overestimations of Kowalsky's method are lower than Gülkan and Sözen method. Iwan and Gates method produce on the average very accurate estimations with the exception of the short period range. This method underestimates the maximum displacement, particularly for periods smaller than 0.4 s.

3) Despite having relatively small mean errors, dispersion of the results in some cases is substantial, particularly for large levels of inelastic behavior. Hence, when applied to individual earthquake ground motion records, any of these methods can lead to significant errors in the estimation of maximum displacement.

One probable reason of obtaining more accurate results using the procedure of Iwan (1980) is that the equations are obtained through a statistical study by direct consideration of displacements, whereas the equations in the Gülkan-Sözen and Kowalsky methods are obtained by considering energy equilibrium.

Although some of the approximate methods like the methods of Gülkan and Sözen (1974) and Kowalsky (1994) are originally developed for design purposes, an iterative approach should be employed while using these equivalent linearization methods for displacement prediction. If it is intended to determine the maximum displacement of an existing structure under a ground motion by using equivalent linearization methods, ductility is not known prior to analysis but the base shear capacity of the structure is known. For a SDOF system with known base shear capacity coefficient ( $\eta_y = F_y/W$ ) and period  $T$ , the yield displacement can be calculated by using Equation 1.10.

$$u_y = \frac{\eta_y T^2 g}{4\pi^2} \quad (1.10)$$

Then a maximum displacement is assumed and the ductility ratio ( $\mu$ ) is calculated by dividing the assumed maximum displacement by the yield displacement  $u_y$ . With this ductility ratio, equivalent period and damping ( $T_{eq}$  and  $\zeta_{eq}$ ) are calculated using the expressions for the considered approximate equivalent linearization procedure. Maximum displacement is obtained from the linear time history analysis of the equivalent SDOF system with  $T_{eq}$  and  $\zeta_{eq}$ . If the calculated maximum displacement is close to the assumed maximum displacement within a specified error bound, analysis is terminated. If not, another displacement is assumed, and the process is repeated until the difference between the calculated and

the assumed displacements is smaller than the specified error bound. Through such an analysis, equivalent damping and equivalent period are calculated automatically at the end of iterations.

In fact, this iterative method is the basis of the procedure presented in the capacity spectrum method of ATC-40 (ATC, 1996) and the improved equivalent linearization method developed in FEMA-440 (ATC, 2005), in case that these methods are employed for use with individual ground motions.

In order to prevent iterations for the calculation of maximum displacements in the equivalent linearization methods, Miranda and Lin (2004) developed simplified expressions for equivalent period and equivalent damping ratio as a function of strength ratio,  $R$  and the period of vibration,  $T$  (Equations 1.11 and 1.12). In the derivation of these expressions, they tried to minimize the error between the exact maximum nonlinear displacement and the approximate displacement obtained by using equivalent damping and period. They conducted analyses for 72 ground motions, seven levels of force reduction factors and 48 periods of vibration. They used an initial viscous damping ratio of 5% in their analyses.

$$\frac{T_{eq}}{T} = 1 + (R^{1.8} - 1) \left( 0.027 + \frac{0.01}{T^{1.6}} \right) \quad (1.11)$$

$$\zeta_{eq} = \zeta_o + (R - 1) \left( 0.02 + \frac{0.002}{T^{2.4}} \right) \quad (1.12)$$

Akkar and Miranda (2005) evaluated the accuracy of five approximate methods in estimating the maximum displacement demand of single degree of freedom systems possessing elastoplastic force-deformation relations by utilizing 216 ground motions recorded in firm sites during 12 California earthquakes. Three of the evaluated methods were based on equivalent linearization. They evaluated the equivalent linearization methods of Iwan (1980), Kowalsky (1994) and Guyader (2003). With regard to the above discussion about the application of equivalent linearization methods based on ductility ratios ( $\mu$ ), they used the single degree of

freedom systems with known lateral strengths instead of ductility ratios. They observed that all of the considered equivalent linearization methods have a tendency to overestimate the deformation demands for systems in the short period range ( $T < 0.5$  sec). The method of Kowalsky overestimated the response for periods longer than 1.0 sec. According to the results of their study, they concluded that the users of nonlinear static procedures where target displacements are calculated using equivalent linear methods or displacement modification factors should be aware of the limited accuracy provided by these methods, especially for stiff systems with low lateral strengths in the period range smaller than 0.6 sec.

## **b) MDOF Systems**

In literature, the number of studies related to the application of equivalent linearization methods to MDOF systems is much less than the number of studies related to the application of equivalent linearization methods to SDOF systems.

Schnabel et al. (1972) developed the computer program SHAKE for seismic response analysis of soil layers based on one-dimensional wave propagation. The nonlinearity of the shear modulus and damping were accounted for by employing equivalent linear soil properties (Idriss and Seed, 1968; Seed and Idriss, 1970). An iterative procedure was implemented in order to obtain the equivalent linear values for shear modulus and damping compatible with the effective strains in each layer. Outline of the method is as follows.

1. Initial estimates of  $G$  (shear modulus) and damping ( $\zeta$ ) are made for each layer.
2. Using the estimated  $G$  and  $\zeta$  values, linear analysis is conducted to compute the ground response and maximum shear strain for each layer. The effective shear strain is determined as a percentage of the maximum shear strain.
3. New equivalent linear values of  $G$  and  $\zeta$  corresponding to the calculated effective shear strain values are determined.

4. Steps 2 and 3 are repeated until differences between the computed shear modulus and damping ratios in two successive iterations fall below a predetermined value in all layers.

Mengi et al. (1992) employed a similar approach for the equivalent linear earthquake analysis of brick masonry buildings.

Shibata and Sözen (1976) used the idea of employing equivalent stiffness and damping in their substitute structure method. The substitute structure method is a design method which is used to determine the minimum strengths of the elements of a structure such that a tolerable response displacement is not likely to be exceeded. They indicated that the structure should satisfy the following conditions in order to apply the substitute structure method.

- The system can be analyzed in a single vertical plane.
- There exists no abrupt change in geometry and mass along the height of the structure.
- Beams, columns and walls may be designed for different limits of inelastic response, but all beams in the same bay or all columns in the same axis should have the same limit.
- Elements and joints are designed and reinforced to avoid significant strength decay as a result of inelastic response.
- Non-structural elements do not interfere with response.

In addition to the assumptions stated above, it is observed that the method is applicable when the failure mode of the members is bending and brittle shear failures do not exist. Since the substitute structure method is a design method, it is obvious that shear failures should be prevented.

In the substitute structure method, stiffness of the structure is reduced by reducing the stiffness of elements. Stiffness of element  $i$  of the substitute structure is obtained from Equation 1.13.

$$(EI)_{si} = \frac{(EI)_{ai}}{\mu_i} \quad (1.13)$$

In Equation 1.13,  $(EI)_{si}$  is the flexural stiffness of element  $i$  of the substitute structure,  $(EI)_{ai}$  is the flexural stiffness of element  $i$  of the actual structure and,  $\mu_i$  is the acceptable damage ratio for element  $i$ . The damage ratio  $\mu$  roughly corresponds to the ductility ratio. In order to give an idea,  $\mu$  is chosen as 1.0 for columns and 6.0 for beams.

The substitute damping factor for each element is calculated with Equation 1.14 (Gülkan and Sözen, 1974) in the substitute structure method.

$$\beta_s = 0.02 + 0.2 \left( 1 - \frac{1}{\sqrt{\mu}} \right) \quad (1.14)$$

where  $\beta_s$  is the substitute damping factor and  $\mu$  is the damage ratio. Then the substitute damping factors of the elements are combined according to the elements' relative flexural strain energy in each mode to calculate the damping coefficient of a mode. The damping coefficient in a vibration mode of the substitute structure is used to simulate the observed effect of hysteretic damping in reinforced concrete structures.

Response spectrum analysis is conducted using the substitute structure's periods and the response spectra corresponding to the calculated damping coefficients. Design forces are calculated as a result of response spectrum analysis.

Shibata and Sözen stated that the substitute structure method is reasonable for situations where the force response decreases as the structure becomes more flexible. In other cases, it should be utilized iteratively. Equivalent linearization approach of the substitute structure method and its design implication, which is to determine the minimum strengths of elements in a structure such that a tolerable response displacement is not likely to be exceeded, is now commonly used within the context of the Direct Displacement Based Design approach (Priestley, 2000; Priestley, 2003; NZSEE, 2003; Grant et al., 2005; Priestley et al., 2007).

Panagiotakos and Fardis (1999) developed a simple linear-elastic analysis procedure for the estimation of mean and 95 percent characteristic values of

inelastic chord rotation demands in the individual members of multistory RC frame buildings which are symmetric in plan. They benefited from the equal displacement rule, since the cracked fundamental periods of the considered elastic structures are usually beyond the corner periods of the ground motions. They stated that the fundamental periods of even low-rise bare RC structures are normally longer than the predominant or corner period of the ground motions which cause full cracking and bring several members to incipient yielding, as evidenced by full-scale pseudodynamic or shake table tests. They employed the chord rotation demands, which they regarded as the most meaningful deformation measure for the assessment or proportioning of RC members, as the deformation demand parameter.

In linear elastic analysis, they used a flexural stiffness ( $EI$ ) value calculated from the secant stiffness to yielding assuming that the inflection point is at mid-length under anti-symmetric bending (Equation 1.15).

$$EI = \frac{M_y}{\theta_y} \cdot \frac{L}{6} \quad (1.15)$$

Here,  $EI$  represents the effective elastic stiffness,  $M_y$  is the yield moment computed at first yielding of tension steel,  $\theta_y$  is the chord rotation at yielding (composed of a flexural component, a component due to shear deformations and a component due to the pull-out of the tension steel) and  $L$  is the length of the member.

Panagiotakos and Fardis have conducted 1008 non-linear dynamic analyses and corresponding linear analyses (response spectrum and equivalent lateral load analyses) on 42 bare frame structures, and 576 nonlinear dynamic analyses and corresponding linear analyses on 36 open ground storey infilled structures that they have designed. In both the nonlinear and linear models, they utilized the stiffness values calculated from Equation 1.15. According to the analysis results, they have concluded that the mean of the normalized chord rotation ratios (ratio of average of the chord rotations of columns or beams at a story obtained from nonlinear analyses to that obtained from linear analyses) are close to 1.0 at the lower stories, but they

increase at the upper stories where the inelastic deformations are not as important as the lower stories. They also concluded that the use of multimodal response spectrum analysis estimated the inelastic chord rotations better than the equivalent static lateral load analysis.

Kosmopoulos and Fardis (2007) tested the approach of Panagiotakos and Fardis for asymmetric RC buildings. For this purpose, they utilized four real buildings with three to six stories, strong irregularities in plan and little engineered earthquake resistance and 56 bidirectional smooth-spectra-compatible ground motions. They observed that for multistorey RC buildings which typically have fundamental periods in the velocity-sensitive part of the spectrum, 5% damped linear elastic response spectrum analysis gives unbiased and fairly accurate estimates of member inelastic chord rotations on average.

According to Part 3 of Eurocode 8 (2005), linear elastic analysis with secant stiffness is applicable, if the inelasticity distribution over the entire structure is fairly uniform. For this purpose, flexural demand-to-capacity ratios (analysis moment/capacity moment) are used. Linear elastic analysis with secant stiffness is applicable if the maximum DCR value in all primary elements is smaller than 2.5 times the minimum DCR over all primary elements having DCR greater than 1.0. Kosmopoulos and Fardis applied linear elastic analysis to buildings in which this criterion was not satisfied. They obtained accurate chord rotation estimations in comparison with nonlinear response history analyses. They concluded that these criteria should be reexamined and possibly relaxed to allow wider use of linear elastic analysis for the estimation of member deformation demands.

Fardis and Kosmopoulos (2007) validated the nonlinear response history analysis according to Eurocode-8 by comparing its predictions with the pseudodynamic test results of the SPEAR frame (Kosmopoulos and Fardis, 2004; Negro et al., 2004). They found good agreement for the floor displacement histories and member damage. By doing so, they have also showed the validity of the nonlinear response history analysis as the reference analysis in comparison with linear elastic analysis.

### 1.2.2 Nonlinear Static (Pushover) Analysis

Saiidi and Sözen (1981) pioneered the idea of nonlinear static analysis (or pushover) in order to determine the force-deformation characteristics of the SDOF oscillator in the so called Q-model. In this model, force-deformation characteristics of a SDOF model is obtained from the variation of the top story displacement with the overturning moment under monotonically increasing forces with a triangular shape. The variation of the top story displacement with the overturning moment is established by considering the moment-curvature relationship of the individual elements. Saiidi and Hudson (1982), Moehle (1984), Moehle and Alarcon (1986) modified the Q-model and applied it to the analysis of vertically irregular buildings.

In 1987, Fajfar and Fischinger introduced the N2 method as an extension of the Q-model. The method mainly consists of four steps. In the first step, capacity curve representing the stiffness, strength and supplied ductility characteristics of the considered MDOF system is determined by nonlinear static analysis under a monotonically increasing lateral load vector. In the second step, the capacity curve is converted to an equivalent SDOF system. In the third step, maximum displacement demand of the equivalent SDOF system is calculated by carrying out nonlinear response history analysis of the equivalent SDOF system. In the last step, the maximum SDOF displacement is converted to the top story displacement of the MDOF system and details of the structural response (formation of plastic hinges, inelastic behavior of different structural elements, etc.) at the pushover step corresponding to this top story displacement are obtained. It is stated that N2 method is applicable for structures oscillating predominantly in a single mode.

The four steps that comprise the N2 method are the main steps involved in the seismic assessment methods which employ nonlinear static analysis (designated as the Nonlinear Static Procedure, NSP, FEMA-356, 2000). Different versions of the first step may be due to the differences in the shape of the lateral load force vector, examples of which are triangular distribution, uniform distribution or a distribution proportional to the multiplication of the mass matrix and the first mode shape (ATC-40, 1996). Fajfar and Gaspersic (1996) used a force distribution proportional

to the mass matrix multiplied with an assumed displacement shape. This displacement shape may be estimated by considering the post yield mechanism of the structure.

Different approaches are also proposed to convert the capacity curve to the equivalent SDOF system. The first modal mass and participation factor are utilized for this purpose in ATC-40, whereas an assumed displacement shape is used for the conversion by Fajfar and Gaspersic (1996) and Krawinkler and Seneviratna (1998). Properties of the SDOF systems obtained from ATC-40 and Fajfar and Gaspersic or Krawinkler and Seneviratna are equivalent to each other if the first mode shape is utilized as the displacement shape.

In order to calculate the maximum displacement demand of the SDOF system, the capacity spectrum method (Freeman et al., 1975; ATC-40, 1996), the coefficient method (FEMA-356, 2000) or the modified versions of these methods (FEMA-440, 2005) may be utilized. Capacity spectrum method is based on equivalent linearization as explained in the above paragraphs whereas the coefficient method calculates the inelastic displacement by multiplying the displacement of a linear elastic SDOF system with several coefficients. Both the capacity spectrum method and the coefficient method are approximate methods utilized for the determination of maximum displacements and possess drawbacks (Chopra and Goel, 2000; Miranda and Akkar, 2002) when used with individual ground motions. Another method utilized for the determination of maximum displacement of a SDOF system is the nonlinear response history analysis of the equivalent SDOF system under a ground motion. In fact, nonlinear response history analysis of a SDOF system is a simpler task when compared with the nonlinear static analysis of a MDOF system. Therefore, the basic motivation of the approximate displacement calculation methods of ATC-40 (1996) and FEMA-356 (2000) and their variants in FEMA-440 (2005) is not developing easily applicable methods, but to develop displacement demand prediction methods when the ground excitation is expressed by an elastic design spectrum. Inelastic response spectra developed in the form of  $R-\mu-T$  relations (such as Newmark and Hall, 1982, Krawinkler and Nassar, 1992, Miranda and Bertero, 1994, Vidic et al., 1994) are also employed for the determination of

maximum displacements of the equivalent SDOF systems (Fajfar and Gaspercic, 1996, Fajfar, 2000).

Krawinkler and Seneviratna (1998) discussed the applicability of nonlinear static analysis (pushover) as a seismic performance evaluation tool. According to Krawinkler and Seneviratna, pushover can be used qualitatively for the determination of the consequences of strength deterioration of individual elements on the behavior of structural system, identification of the critical regions in which the deformation demands are expected to be high, identification of the strength discontinuities in plan or elevation, and verification of the completeness and adequacy of load path. It can be used quantitatively to determine the force demands on potentially brittle elements, estimates of the deformation demands for elements which deform inelastically, and the interstory drifts.

Krawinkler and Seneviratna stated that the invariant load pattern utilized in the pushover analysis is valid if the structural response is not severely affected by higher modes, and if the structure has only a single yielding mechanism. They also stated that the most critical concern is that the pushover analysis may detect only the first local mechanism which forms under a ground motion and may not capture other weaknesses which will form after the dynamic characteristics change with the formation of the first local mechanism. By comparing the results of nonlinear response history and pushover analyses for a four story steel frame, they concluded that pushover analysis provides very good predictions of seismic demands for regular low-rise structures for which higher mode effects are not of concern and for which inelasticity is distributed uniformly over the height.

Mwafy and Elnashai (2001) claimed that nonlinear response history analysis is complex and therefore unsuitable for practical design applications despite the improvement of the accuracy and efficiency of the computational tools. They stated that the calculated inelastic dynamic response is quite sensitive to the ground motion characteristics and accordingly the computational effort increases since a number of representative ground motions should be selected. They employed different invariant load patterns for pushover analysis (the code design lateral pattern, uniform distribution and the force distribution obtained by combining the

external modal forces with SRSS). They compared the obtained capacity curves with those obtained by applying the ground motions with incrementally increased intensities. They also compared the local responses at the global limit state. They commented that conventional pushover analysis (with invariant lateral forces) is more appropriate for low rise and short period frame structures and the discrepancies between nonlinear static analyses and nonlinear response history analyses for long period buildings can be overcome by utilizing more than one load pattern.

The studies which are conducted to improve the conventional (single mode) pushover analysis may be classified as the studies which utilize the adaptive force distributions, which consider the higher mode effects and those which employ both of the above considerations.

Bracci et al. (1997) stated that a predetermined lateral load distribution and a base shear-top story displacement format is not suitable for structures failing from midstory mechanisms, and extended the capacity spectrum method to include the effects of potential midstory mechanisms and a story-by-story performance evaluation using modal superposition. In this method, the lateral forces at each step are updated by considering the story shear forces at the previous step along with Equation 1.16. As a result of pushover analysis, shear force versus drift response at each story is determined and used to capture potential soft story mechanisms.

$$\Delta F_i^{j+1} = V^j \left( \frac{F_i^j}{V^j} - \frac{F_i^{j-1}}{V^{j-1}} \right) + \Delta P^{j+1} \left( \frac{F_i^j}{V^j} \right) \quad (1.16)$$

In Equation 1.16,  $i$  is the story number,  $j$  is the analysis step,  $\Delta F_i^{j+1}$  is the incremental  $i^{\text{th}}$  story force at step  $j+1$ ,  $V^j$  is the base shear at step  $j$ ,  $\Delta P^{j+1}$  is the incremental base shear applied at step  $j+1$  and  $F_i^j$  is the  $i^{\text{th}}$  story force at step  $j$ .

Bracci et al. mentioned that dynamic strain rate effects and system degradation or deterioration are not captured in pushover analysis, since it is based on the static application of lateral story forces. They commented that these effects

could be accounted for by adjusting the moment-curvature properties of the members. However, they did not present an explicit method on this issue.

Gupta and Kunnath (2000) developed a procedure which considers the adaptive nature of lateral forces as well as the higher mode effects. They showed the limitations of conventional static procedures, by utilizing the response of instrumented buildings which experienced strong ground motions during 1994 Northridge earthquake. For this purpose, they observed the vertical distribution of inertia forces at the times of maximum displacement, maximum drift, maximum base shear and maximum overturning moment. They concluded that higher mode effects significantly affect the response of buildings during ground shaking with the exception of low rise buildings, and stated that higher mode effects are better understood by analyzing the inertial force and story drift profiles rather than the displacement profile. In the light of these observations, they developed a method for pushover analysis of structures which considers the higher mode effects and accounts for the force distribution following yielding. In this formulation, response spectrum analysis is conducted at each step of pushover analysis instead of a static analysis of the conventional pushover. Required modal properties are obtained from the eigenvalue analysis of the structure at the considered pushover step. Associated pseudo accelerations are calculated from the elastic response spectrum as the pseudo accelerations corresponding to the instantaneous period values. They applied the method on 4, 8, 12, 16 and 20 story 2D reinforced concrete frames by utilizing 15 ground motions which do not contain significant pulses. They considered both code designed frames and the versions of these frames with strength and stiffness irregularities. They incorporated story drifts and plastic hinge locations as the response parameters. They showed that uniform and FEMA-273 (ATC, 1997) modal load patterns were inadequate in capturing the response for high-rise frames where higher mode effects are important, whereas the proposed method performed reasonably well and resulted in close responses to nonlinear response history analyses. In the application of this method, they did not state explicitly the calculation of a global displacement demand at which the response

parameters are obtained. They only commented that FEMA-273 coefficient method could be used for this purpose.

Aydinoğlu (2003) observed that elastic pseudo accelerations corresponding to the instantaneous periods in Gupta and Kunnath's method are not compatible with the inelastic instantaneous response, and modified Gupta and Kunnath's incremental response spectrum analysis procedure by considering inelastic spectral displacements corresponding to the instantaneous state of the system instead of the elastic pseudo accelerations. He stated that utilization of inelastic spectral displacements permitted consistent estimation of the peak response quantities at the last step of pushover analysis, where the analysis ends upon a control process. Therefore, the top story displacement at the last step is the global displacement demand. The results obtained for a presented case study were sufficiently close to the nonlinear response history analysis results, at the expense of considerable computational work. Aydinoğlu also developed a practical version of his method for smooth elastic response spectrum by employing the equal displacement rule.

Antoniou and Pinho (2004a) also developed a procedure similar to that of Gupta and Kunnath (2000) in order to take into consideration the higher mode effects and variant force distributions. They stated that equilibrium can not be satisfied at each step of pushover analysis due to the combination rules (such as SRSS or CQC) utilized for the combination of modal responses in the method of Gupta and Kunnath. Instead, Antoniou and Pinho combined the external modal forces using modal combination rules at each step of pushover analysis in order to determine the lateral forces to be applied at the corresponding step. As an alternative, they combined the external modal static forces (defined as the external modal forces divided by the pseudo acceleration, Chopra, 2001). They called the former and latter methods as the methods "with spectral amplification" and "without spectral amplification" respectively. They commented that the combination of the external modal forces should be done by adding them vectorially for the purpose of a better match with nonlinear dynamic response. However, they did not investigate the applicability of such an option. In addition to the "with spectral amplification" and "without spectral amplification" cases, they also

employed “total updating” and “incremental updating” alternatives for the lateral forces to be applied at each step. In the “total updating” alternative, the lateral force calculated as explained above is applied as the external force, whereas it is added with proper scaling to the external force at the previous step in the “incremental updating” alternative. They stated that the method “with spectral amplification” and “incremental updating” is the most suitable when numerical stability and the accuracy of the results are observed. They evaluated the proposed method in comparison with conventional pushover analyses (employing uniform and triangular distributions) with reference to nonlinear response history analyses, by conducting a parametric study with regular, irregular and dual systems using 2D models and four ground motions. They concluded that the proposed adaptive pushover method features a relatively minor advantage over the conventional pushover analysis.

In a companion paper, Antoniou and Pinho (2004b) developed a displacement-based adaptive pushover procedure, in which a displacement vector updated according to the instantaneous stiffness of the structure is imposed at each step of the analysis. The displacement vector combines the contributions from all modes by employing a combination rule. Similar to the companion paper, “with spectral amplification”, “without spectral amplification”, “incremental updating” and “total updating” alternatives are utilized. Similar to the force-based case, a global displacement demand is not calculated in this method. They used the same frames and ground motions with the companion paper for the validation part. They concluded that the proposed method provides greatly improved predictions in comparison to the conventional pushover analysis throughout the entire deformation range.

Main disadvantage of the methods in which adaptive nature of lateral forces (or displacements) are taken into consideration (Gupta and Kunnath, 2000; Aydinoglu, 2003; Antoniou and Pinho, 2004a, 2004b) is that they are conceptually complicated and computationally demanding for routine application in structural engineering practice (Chopra and Goel, 2002). They can not be applied directly by using the software developed for conventional pushover analysis. Instead, these

methods should be implemented in the source codes of the available software. The methods in which higher mode effects are considered and the adaptive nature of lateral forces is not taken into consideration are conceptually less complicated and they can be directly applied by utilizing the available software for conventional pushover analysis through post-processing.

Paret et al., (1996) introduced the idea of conducting several pushover analyses with force distributions proportional to the multiplication of the mass matrix and the elastic mode shapes corresponding to different modes of the structure. As a result of these analyses, a pushover curve is obtained for each of the considered modes. Then, the pushover curves are converted into ADRS format (Mahaney et al., 1993). Pseudo acceleration corresponding to yielding is obtained from the pushover curves in ADRS format. Then the elastic pseudo acceleration corresponding to the period of the considered mode is obtained from the utilized elastic spectrum. Elastic pseudo acceleration is divided by the pseudo acceleration corresponding to yielding in order to calculate the Modal Criticality Index (MCI) for each mode and the critical mode is determined as the mode with highest MCI. The procedure is applied graphically in order to preserve the graphical attractiveness of the capacity spectrum method.

Sasaki et al. (1998) extended the idea of MCI to identify the failure modes in the Multi-Mode Pushover (MMP) procedure. They did not specify a combination procedure for modal responses.

Chopra and Goel (2002) improved the MMP procedure to develop Modal Pushover Analysis (MPA). A pushover analysis is conducted under an invariant load pattern for each mode independently, and then inelastic modal demands are calculated by independent nonlinear response history analysis of the equivalent inelastic SDOF systems which are represented by the associated modal capacity curves. Finally, modal response quantities are combined with SRSS or CQC as in response spectrum analysis (RSA). MPA fully reduces to RSA in case of linear elastic response. Implementation of MPA is simple and requires only a post-processing effort. Its major drawback is the assumption of independent inelastic response at each mode, which is not theoretically correct. While this assumption

leads to acceptable results for lower order response quantities (displacement, drift), it usually leads to errors for higher order response quantities (plastic rotations, curvatures, etc.). Chintanapakdee and Chopra (2003) evaluated the accuracy of MPA by utilizing height-wise regular generic frames. Goel and Chopra (2004) improved MPA, especially in its treatment of P- $\Delta$  effects due to gravity loads and calculation of plastic hinge rotations. Chintanapakdee and Chopra (2004) evaluated the accuracy of MPA by using vertically irregular generic frames. Chopra et al. (2004) proposed a modified version of MPA (MMPA) in which the inelastic response obtained from first-mode pushover analysis has been combined with the elastic contribution of higher modes. Chopra and Goel (2004) presented the application of MPA to buildings with unsymmetrical plan.

Kalkan and Kunnath (2006) proposed a pushover analysis procedure which is derived through adaptive modal combinations (AMC). This method attempts to integrate concepts built into the capacity spectrum method (ATC-40, 1996), the adaptive method proposed by Gupta and Kunnath (2000) and the modal pushover analysis of Chopra and Goel (2002).

Relying on nonlinear response history analyses, Vamvatsikos and Cornell (2002) developed the (single-record) incremental dynamic analysis procedure (IDA) for generating intensity-demand diagrams similar to pushover capacity curves, where variations in structural response under a specific ground motion record is fully accounted for. Generation of a single IDA curve requires several nonlinear response history analysis of the structural system under scaled ground motions. Recently, Aschheim et al. (2007) proposed a scaled nonlinear dynamic procedure (NDP) for improving nonlinear static procedures (NSP). Several nonlinear response history analyses of the investigated structural system are carried out under scaled ground motions to match the target demand determined from NSP. The obtained results are then evaluated statistically in order to establish levels of confidence for the considered response parameters. IDA and scaled NDP may bring new sights into NSP; however they completely remove its physical and computational simplicity.

### 1.2.3 Seismic Analysis of Unsymmetrical Plan Buildings

A review of the studies on the seismic response of asymmetric structures conducted before 1994, between 1994 and 1998 and between 1998 and 2002 were summarized by Rutenberg et al. (1995), Rutenberg (1998) and Rutenberg (2002), respectively. Most of the reviewed studies were conducted using simple single-storey asymmetric models. Summary of the research between the years 2002 and 2007 can be found in De Stefano and Pintucchi (2007). Some of these studies are also reviewed here.

In the first applications of nonlinear static analysis on 3D unsymmetrical plan buildings, exact 3D formulations were not utilized. Approximate analysis procedures were developed. Kilar and Fajfar (1997) described an application of pushover analysis to asymmetric buildings by modeling the structure as a collection of planar macro-elements. An approximate relation between the global base shear of the building and its top displacement is obtained at the end of pushover analysis.

Moghadam and Tso (1998) developed a pushover analysis procedure for asymmetrical multistory buildings which take into account the higher modal and three dimensional effects induced by torsion. In this procedure, pushover analysis is conducted separately for each frame using lateral force distributions obtained from the elastic response spectrum analysis. Target displacement for each frame is also obtained from elastic response spectrum analysis. They applied the procedure on a seven-storey symmetrical plan reinforced concrete building and mass and stiffness eccentric versions of this building. They conducted reference nonlinear response history analyses by applying ten artificial ground motions unidirectionally. By comparison of the floor displacements, interstory drifts and column and beam ductility demands, they have stated that the proposed method led to good estimates at the stiff and flexible edge frames of both mass and stiffness eccentric buildings.

Chopra and Goel (2004) extended the application of MPA (Chopra and Goel, 2002) to buildings with unsymmetrical plan. Essentially the procedure is the same as the 2D case where the torques and the lateral forces in both orthogonal directions are considered in the external modal force vectors for the 3D case. In the presence

of asymmetry about both of the orthogonal axes, there exist two pushover curves. The authors suggested that the pushover curve in the dominant direction of the mode should be utilized in such cases. When there is asymmetry about only one of the axes; such a problem does not occur since there exists a pushover curve only in one direction. They modified a 9-story symmetric plan steel frame to create a mass eccentric system. The eccentricity between the center of mass and center of stiffness was set as 10% of the plan dimension. They further created three versions of the mass eccentric system by changing the moment of inertia values, which were a ‘torsionally stiff’ system, a ‘torsionally flexible’ system and a ‘torsionally-similarly-stiff’ system. Periods corresponding to the torsional modes of vibration are significantly smaller than, significantly greater than and similar to those corresponding to the translational modes in the torsionally stiff, torsionally flexible and torsionally-similarly-stiff systems respectively. They applied the method on the considered buildings by utilizing one ground motion in comparison with nonlinear response history analysis, and obtained accurate results at the center of mass for torsionally stiff and torsionally flexible systems. However, erroneous results were obtained for the torsionally-similarly-stiff system because of the strong coupling of modes and the underestimation of the roof displacement because of the CQC rule. They concluded that the application of MPA on unsymmetrical-plan buildings should be investigated by utilizing an ensemble of ground motions.

Fajfar et al. (2005) performed parametric studies on single and multistory buildings with bi-axial eccentricity subjected to bi-directional ground motion to investigate the effect of torsion in the elastic and inelastic ranges of deformation. They utilized the ratio of the roof displacements at the edge frames to the roof displacement at the center of mass as the investigated parameter for observing the effect of torsion. They observed that the torsional effects generally decrease with increasing inelasticity and stated that the linear elastic response spectrum analysis results in an upper bound for the torsional effects. Based on these observations, they extended the N2 method for use in asymmetric buildings. According to this extension, N2 method applicable to the symmetric systems is employed first. Then the responses are amplified using the response spectrum analysis results for the

consideration of torsion effects. As the amplification factor, the ratio between normalized roof displacement (roof displacement at an arbitrary location to the roof displacement at the center of mass) obtained from elastic modal analysis to that obtained from pushover analysis is used. Minimum value of the amplification factor is taken as 1.

It can be concluded that the improved pushover methods summarized in the previous section are generally validated by using 2D frames, but none of them has been totally validated for 3D unsymmetrical plan buildings.

### **1.3 Objective and Scope**

An equivalent linearization procedure which utilizes the familiar response spectrum analysis as the analysis tool and benefits from the capacity principles is presented for the inelastic seismic displacement response prediction of MDOF systems. The procedure is applied on a twelve story reinforced concrete plane frame for which higher mode effects are important, and a six story unsymmetrical-plan reinforced concrete space frame where torsion significantly effects the response. The predictions of the equivalent linearization procedure are compared with the nonlinear response history analysis results by utilizing 162 ground motions. Response predictions from two other approximate procedures, which are conventional pushover analysis according to FEMA-356 (ASCE, 2000) and modal pushover analysis (MPA, Chopra and Goel, 2002) are also presented. In addition, results of response spectrum analyses and linear response history analyses are used for comparison purposes. Roof displacement demands and several local response parameters; namely story displacements, interstory drift ratios and chord rotations are used in the comparative evaluations.

Main objective of the study is to develop an equivalent linearization procedure for inelastic seismic response prediction of MDOF systems. A subsequent objective is to test the accuracy of the proposed procedure in predicting

the global displacement demands (roof displacements) and local response parameters.

This thesis is composed of seven main chapters and an appendix. Brief contents are given as follows:

- Chapter 1 Statement of the problem and literature survey on equivalent linearization methods, pushover analysis and seismic analysis of unsymmetrical plan buildings.
- Chapter 2 Brief information on the inelastic analysis methods employed for comparing the results obtained from the proposed equivalent linearization procedure.
- Chapter 3 Explanation of the equivalent linearization procedure.
- Chapter 4 Information about the employed ground motions.
- Chapter 5 Case study I: Twelve story reinforced concrete plane frame. Application of the equivalent linearization procedure and comparison of results with those of nonlinear response history analysis and other approximate methods.
- Chapter 6 Case study II: Six story unsymmetrical-plan reinforced concrete space frame. Application of the equivalent linearization procedure and comparison of results with those of nonlinear response history analysis and other approximate methods.
- Chapter 7 A brief summary and conclusions.
- Appendix A Stiffness formulation of Drain-2DX for “Plastic Hinge Beam-Column Element”.

## **CHAPTER 2**

### **METHODS EMPLOYED FOR INELASTIC SEISMIC RESPONSE PREDICTION**

The response parameters obtained from the implementation of the proposed equivalent linearization procedure are compared with those of nonlinear response history analyses. Moreover, two other approximate methods are also employed in order to observe the relative accuracy of the predictions of the equivalent linearization procedure with respect to other approximate methods. One of these approximate methods is the conventional pushover analysis with the coefficient method (FEMA-356, ASCE, 2000). The second approximate method is the Modal Pushover Analysis (MPA) developed by Chopra and Goel (2002). Nonlinear response history analysis (NRHA), pushover analysis with coefficient method (PO-FEMA) and MPA are described briefly in the following sections.

#### **2.1 Nonlinear Response History Analysis**

Nonlinear response history analysis is accepted as the most accurate simulation of dynamic response under a ground excitation. In this analysis, the equation of motion defined with Equation 2.1 is solved in the range of the requested time interval.

$$\begin{aligned} \mathbf{m}\ddot{\mathbf{u}} + \mathbf{c}\dot{\mathbf{u}} + \mathbf{f} &= -\mathbf{m}\mathbf{1}\ddot{u}_g \\ \mathbf{u}_0 &= \mathbf{u}(0) \text{ and } \dot{\mathbf{u}}_0 = \dot{\mathbf{u}}(0) \end{aligned} \quad (2.1)$$

In Equation 2.1,  $\mathbf{m}$  is the mass matrix,  $\mathbf{c}$  is the damping matrix,  $\mathbf{1}$  is the influence vector which describes the degrees of freedom exposed to the ground acceleration history  $\ddot{u}_g$ ,  $\ddot{\mathbf{u}}$  and  $\dot{\mathbf{u}}$  are the acceleration and velocity vectors of the considered degrees of freedom,  $\mathbf{u}_0$  and  $\dot{\mathbf{u}}_0$  are the initial displacement and velocity vectors and  $\mathbf{f}$  represents the resisting forces, which are generally idealized mathematically as a function of displacement (or space derivatives of displacement) and velocity, defined as hysteresis rules. Hysteresis rules can be defined at the material level in the form of stress-strain relationships, in the section level such as moment-curvature relationships or in the member level such as moment-rotation or force-displacement relationships. Regardless of the level at which these rules are defined, these functions are usually nonlinear (or piecewise linear), from which the name of the analysis method originates. Due to the complexity of the ground motion acceleration history  $\ddot{u}_g$  and the nonlinearity in the hysteresis rules, equation of motion can not be solved analytically in closed form. For the numerical solution on the other hand, time stepping methods such as the Newmark integration methods (Newmark, 1959) examples of which are average acceleration or linear acceleration methods, or Hilber-Hughes-Taylor (HHT, 1977) integration scheme are generally employed in the civil engineering applications. In order to handle the nonlinearity resulting from the hysteresis rules, numerical solution methods like Newton-Raphson or modified Newton-Raphson are utilized within a time step.

Since the involved process is highly numerical, it may result in significantly long run-time depending on the complexity of the problem. In addition, sometimes convergence problems may occur since equilibrium should be satisfied within a desired accuracy and the numerical methods are generally iterative.

## 2.2 Conventional Pushover Analysis with Coefficient Method of FEMA-356

It has long been recognized that damage control should be achieved through the control of displacements (Shibata and Sözen, 1976). It has also been recognized that nonlinear analysis should be used for the determination of displacements (Saiidi and Sözen, 1981; Fajfar and Fishinger, 1987). After the destructive earthquakes in the last two decades, it has been accepted that nonlinear analysis should be more explicitly considered for design purposes (Fajfar, 2000). Due to the above mentioned complexities and difficulties of nonlinear response history analyses, it would be an impractical decision to enforce the application of nonlinear response history analyses. Therefore, research has been focused on the simpler approximate nonlinear analysis methods. Nonlinear static (pushover) analysis has gained considerable acceptance and popularity as a fairly simple approximate method.

In conventional pushover analysis, the structure is loaded under gravity forces, then the lateral forces described by a predetermined distribution is increased until a specified displacement is achieved, or the structure reaches a collapse state. The response parameters are recorded in every pushover step. Pushover analysis is generally represented by a pushover or capacity curve, which is the base shear plotted against the lateral displacement of a control node. Different lateral load patterns such as triangular distribution, uniform distribution or a distribution proportional to the multiplication of the first mode shape and the mass matrix can be utilized. Latter distribution is used in this study.

Pushover analysis is useful in observing the critical locations where the deformation demands are expected to be high, identification of the possible strength discontinuities in plan or elevation and determination of the adequacy of the load path (Krawinkler and Seneviratna, 1998). It can also be used as a method for the approximate determination of seismic demands. Such an application of pushover analysis is presented in FEMA-356 (ASCE, 2000). In this application, a “Target Displacement” is determined by multiplying the spectral displacement of a linear elastic single degree of freedom system possessing the effective fundamental period

of the building with some modification factors (Equation 2.2). This procedure is called the coefficient method.

$$\delta_t = C_0 \cdot C_1 \cdot C_2 \cdot C_3 \cdot S_d(T_e) \quad (2.2)$$

In Equation 2.2,  $\delta_t$  is the target displacement,  $S_d$  is the elastic spectral displacement corresponding to the effective fundamental period in the direction under consideration ( $T_e$ ), which is calculated with Equation 2.3.

$$T_e = T_i \cdot \sqrt{\frac{K_i}{K_e}} \quad (2.3)$$

In Equation 2.3,  $T_i$  is the fundamental period in the direction under consideration, obtained from eigenvalue analysis,  $K_i$  is the initial slope of the original pushover curve, and  $K_e$  is the slope of the initial line segment of the bilinearized pushover curve. In the bilinerization process, two criteria are employed. First criterion is that the areas under the original and the bilinearized pushover curves are approximately equal, and the second criterion is that the initial line segment of the bilinearized pushover curve intersects the original pushover curve at the point with coordinates  $0.6u_y$  and  $0.6V_y$  where  $u_y$  and  $V_y$  are the yield displacement and yield base shear, respectively (Figure 2.1).

An iterative strategy is used for the bilinerization process in this study. First, a trial target displacement, which corresponds to 2% of the building height, is selected, then the pushover curve is bilinearized according to the above two criteria. Then the target displacement is calculated by using Equation 2.2 and compared with the trial target displacement. If the two displacements are sufficiently close, bilinerization process is terminated, else the calculated displacement becomes the trial displacement and iterations continue until sufficiently close displacements are obtained.

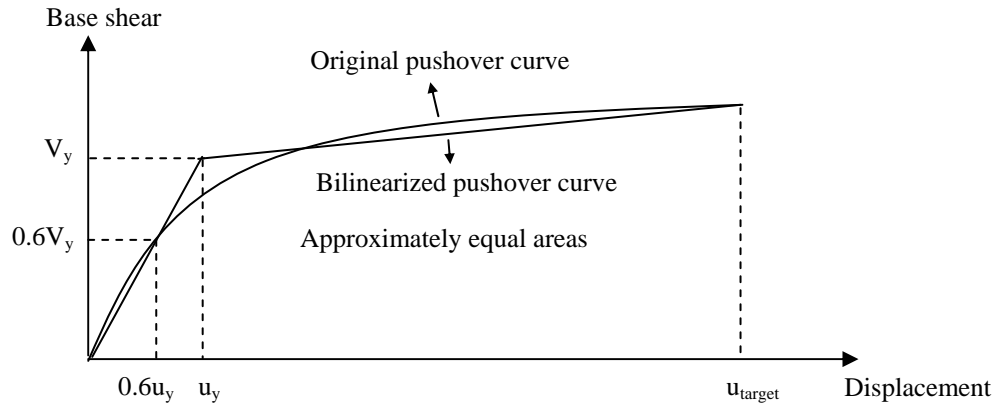


Figure 2.1 Bilinearization of pushover curve according to FEMA-356

In Equation 2.2,  $C_0$ ,  $C_1$ ,  $C_2$  and  $C_3$  are the coefficients that modify the elastic spectral displacement, which are defined below.

$C_0$ : Modification factor that relates the SDOF spectral displacement coordinate to the MDOF system control node displacement.

$C_1$ : Modification factor that relates the expected maximum inelastic displacements to the linear elastic displacements.

$C_2$ : Modification factor to represent the effect of pinched hysteretic shape, stiffness degradation and strength degradation on maximum displacement response.

$C_3$ : Modification factor to represent increased displacements due to P- $\Delta$  effects.

In this study,  $C_0$  is defined by the multiplication of first mode participation factor with the amplitude of the first mode vector at the top story.  $C_1$  is calculated from Equation 2.4, which is presented in FEMA-356. Since stiffness and strength degradation and P- $\Delta$  effects are not considered,  $C_2$  and  $C_3$  are accepted to be equal to 1.0.

$$C_1 = \begin{cases} 1 & \text{for } T_e \geq T_s \\ 1 + (R - 1)T_s / T_e & \text{for } T_e < T_s \end{cases} \quad (2.4)$$

where

$$R = \frac{S_a \cdot M_1^*}{V_y} \quad (2.5)$$

In Equations 2.4 and 2.5,  $T_e$  is the effective fundamental period in the direction under consideration,  $S_a$  is the pseudo acceleration corresponding to  $T_e$ ,  $M_1^*$  is the effective first modal mass,  $V_y$  is the yield base shear and  $R$  is the force reduction factor for the first mode.  $T_s$  is the characteristic period of the response spectrum, defined as the period associated with the transition from the constant acceleration segment of the spectrum to the constant velocity segment of the spectrum.  $T_s$  is clearly observable for a design spectrum, since it is smooth (Figure 2.2). However,  $T_s$  may not be clearly distinguishable for the jagged response spectrum of a particular ground motion (Figure 2.3). It can be calculated approximately with Equation 2.6 for particular ground motions.

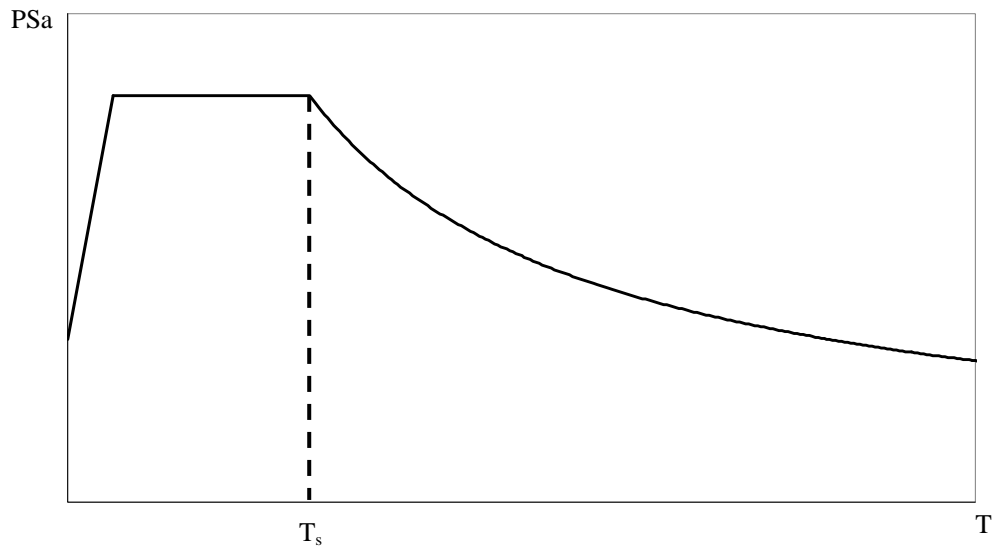


Figure 2.2 Corner period ( $T_s$ ) for a design spectrum

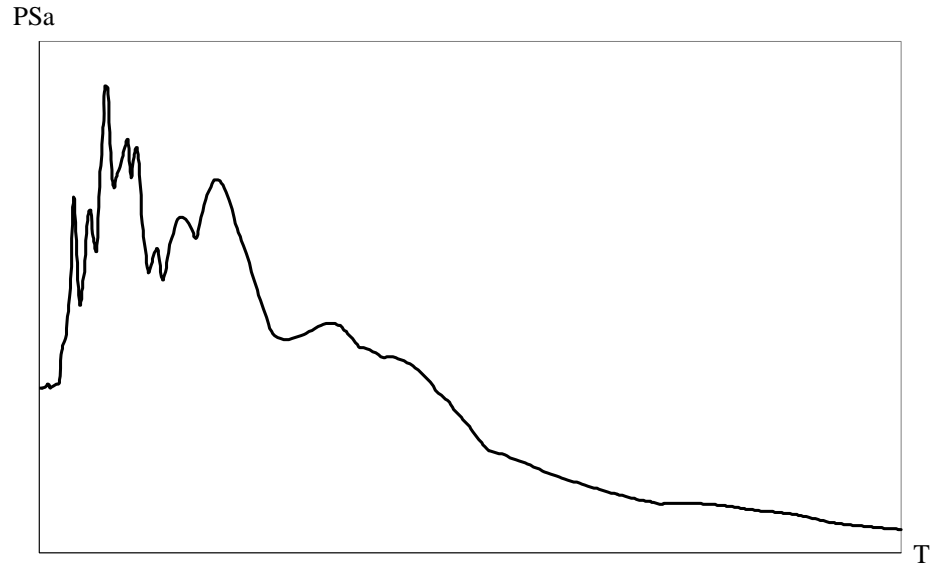


Figure 2.3 Acceleration response spectrum of a particular ground motion

$$T_s = 2\pi \frac{PSv_{\max}}{PSa_{\max}} \quad (2.6)$$

where  $PSv_{\max}$  and  $PSa_{\max}$  are the maximum values of the 5% damped pseudo-velocity and pseudo-acceleration spectra, respectively, as described by Cuesta and Aschheim (2001).

According to FEMA-356, the requested response parameters, such as interstory drifts, chord rotations, plastic rotations, member forces etc. are obtained at the pushover step corresponding to the calculated target displacement.

### 2.3 Modal Pushover Analysis (MPA)

Conventional pushover analysis has been an important development serving the purposes of performance based analysis and design. However, pushover analysis possesses some drawbacks. One of these drawbacks is the inability of the method in considering the response originating from the higher modes of vibration (Sasaki et

al., 1998; Gupta and Kunnath, 2000). In order to improve pushover analysis to consider the higher mode effects, Chopra and Goel (2002) developed a modal pushover analysis method (MPA) based on the structural dynamics theory. Chintanapakdee and Chopra (2003) evaluated the accuracy of MPA by utilizing height-wise regular generic frames. Goel and Chopra (2004) improved MPA, especially in its treatment of P- $\Delta$  effects due to gravity loads and calculation of plastic hinge rotations. Chintanapakdee and Chopra (2004) evaluated the accuracy of MPA by using vertically irregular generic frames.

Basic idea behind MPA originates from linear elastic analysis and the structural dynamics theory. For linear elastic analysis, maximum value of any response quantity in the  $n^{\text{th}}$  mode can be obtained by increasing the lateral force vector which is proportional to the multiplication of mass matrix and the  $n^{\text{th}}$  mode vector up to the value when the roof displacement is equal to  $u_{rno}$ , defined by Equation 2.7.

$$u_{rno} = \Gamma_n \phi_{rn} D_n \quad (2.7)$$

In Equation 2.7,  $D_n$  is the spectral displacement in the  $n^{\text{th}}$  mode, obtained from the solution of  $n^{\text{th}}$  mode SDOF equation, and transformed to the top story displacement by multiplying with  $\Gamma_n \phi_{rn}$ .  $\Gamma_n \phi_{rn}$  is the  $n^{\text{th}}$  mode participation factor multiplied with the amplitude of the  $n^{\text{th}}$  mode vector at the top story level. Maximum responses in each mode are combined by using combination rules such as SRSS or CQC, resulting in the same values with the well known response spectrum analysis method for linear elastic systems.

Extending the same approach to inelastic systems; with the assumption that the response in each mode is not significantly affected from the other modes (therefore independent of the other modes), maximum responses in each mode can be estimated by conducting pushover analysis with the lateral force vector proportional to the multiplication of the mass matrix and the  $n^{\text{th}}$  mode vector at a calculated peak displacement. Lateral force vector shape is kept invariant during

pushover analysis. Similar to the linear elastic case, peak displacement is calculated by multiplying the maximum value of  $n^{\text{th}}$  mode SDOF displacement ( $D_n$ ) with  $\Gamma_n \phi_{rn}$ , where  $\Gamma_n$  and  $\phi_{rn}$  are obtained from the eigenvalue analysis of the system at the beginning of pushover analysis.

For the calculation of  $D_n$ , pushover curve of the corresponding mode is utilized. For this purpose, an iterative strategy is followed. First, a trial displacement is chosen for  $D_n$  and multiplied with the  $\Gamma_n \phi_{rn}$  value. Then, the pushover curve with this displacement as the end point is bilinearized using the approach explained for the Coefficient Method of FEMA-356. Period,  $T_n$  (Equation 2.8), yield base shear coefficient,  $\eta_{ny}$  (Equation 2.9) and strain hardening slope,  $\alpha_n$  of the corresponding inelastic SDOF system are obtained from the bilinearized pushover curve.

$$T_n = 2\pi \left( \frac{V_{bny} / M_n^*}{u_{my} / \Gamma_n \phi_{rn}} \right)^{0.5} \quad (2.8)$$

$$\eta_{ny} = \frac{V_{bny}}{M_n^*} \quad (2.9)$$

In Equations 2.8 and 2.9,  $V_{bny}$  and  $u_{my}$  are the yield base shear and yield displacement values,  $M_n^*$  is the  $n^{\text{th}}$  mode effective modal mass,  $\Gamma_n$  is the  $n^{\text{th}}$  mode participation factor, and  $\phi_{rn}$  is the amplitude of the  $n^{\text{th}}$  mode vector at the roof level.  $T_n$  calculated from Equation 2.8 is always longer than or equal to the period calculated from eigenvalue analysis. The difference depends on the shape of the pushover curve.

Maximum displacement of the inelastic SDOF system with period  $T_n$ , yield base shear coefficient  $\eta_{ny}$  and strain hardening slope  $\alpha_n$  is obtained under the considered ground motion excitation, and compared with the trial displacement. If these two displacements are sufficiently close,  $D_n$  is equal to the trial displacement,

else calculated displacement becomes the trial displacement and iterations continue until sufficiently close displacements are obtained.

Requested response parameters at each mode are obtained from the pushover database at the peak displacement of the corresponding mode, and the responses due to gravity loading are extracted from these values. Then these response quantities are combined by using a combination rule such as SRSS or CQC and superposed with the responses due to gravity loading.

Chopra and Goel (2004) presented the application of Modal Pushover Analysis to buildings with unsymmetrical plan. Essentially the procedure is the same as the 2D case where the torques and the lateral forces in both orthogonal directions are considered in the external modal force vectors for the 3D case. In the presence of asymmetry about both of the orthogonal axes, there exist two pushover curves; the authors stated that the pushover curve in the dominant direction of the mode should be utilized in such cases. When there is asymmetry about only one of the axes; such a problem does not occur since there exists a pushover curve only in one direction, and the algorithm explained above can be utilized.

#### **2.4 A General Comment on the Evaluation of Approximate Methods in Comparison with Nonlinear Response History Analysis**

In nonlinear response history analysis, the building may be mainly displaced either in the positive or in the negative directions (Figure 2.4). This is especially true for pulse-type ground motions when non-degrading force deformation relations are utilized and the analysis is based on lumped plasticity approach. In such cases, direction should be taken into consideration in the comparison of local response parameters, such as plastic rotations or chord rotations. If the structure is mainly displaced in the positive direction in nonlinear response history analysis, then the results of pushover analysis or MPA conducted in the positive direction should be used for comparison purposes. Same is also true for the equivalent linearization method developed in this study.

However, some ground motions may displace the structure similarly in the positive and negative directions (Figure 2.5). Accordingly, envelope of the responses obtained from the application of the approximate method in both of the directions should be used for comparison purposes for these ground motions.

In order to conduct automated analyses, directions to be utilized for the approximate methods are determined with the algorithm in Figure 2.6. In this figure,  $\delta_p$  is the maximum value of top story displacement in the positive sense obtained from nonlinear response history analysis,  $\delta_n$  is the maximum value of top story displacement in the negative sense obtained from nonlinear response history analysis, and  $\delta_{cut}$  is a displacement value for which slight to moderate amount of inelasticity occurs.

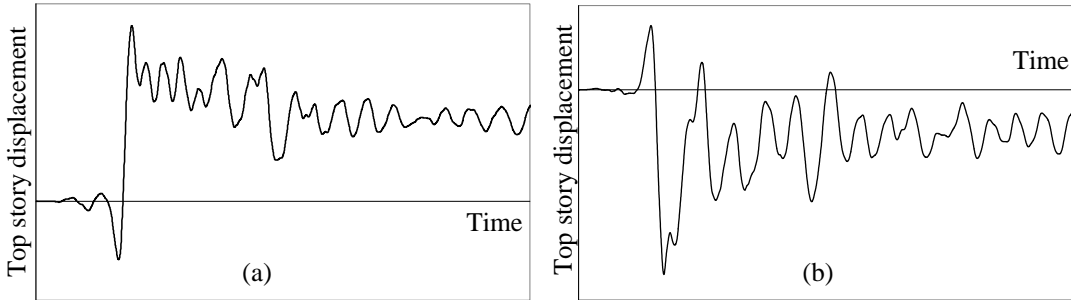


Figure 2.4 Top story displacement history examples a) displacement is mainly in the positive direction b) displacement is mainly in the negative direction

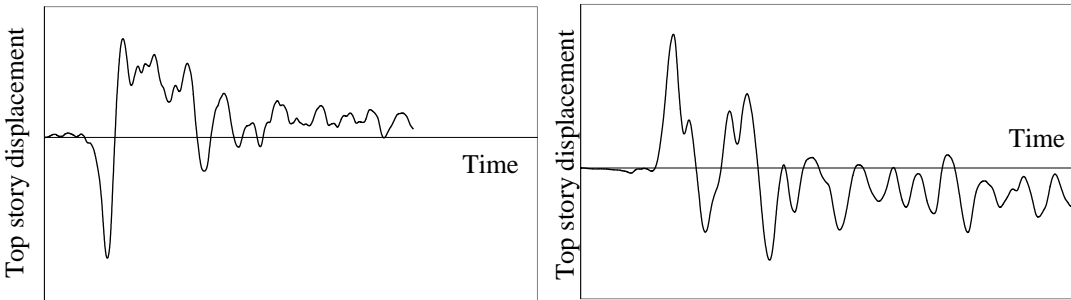


Figure 2.5 Top story displacement history examples; the structure is displaced similarly in the positive and negative directions

```
If  $\delta_p > \delta_n$ 
  If  $\delta_n > 0.75 \delta_p$  or  $\delta_n > \delta_{cut}$ 
    Analysis directions= Both positive and negative directions
  Else
    Analysis directions= Only positive direction
Elseif  $\delta_n > \delta_p$ 
  If  $\delta_p > 0.75 \delta_n$  or  $\delta_p > \delta_{cut}$ 
    Analysis directions= Both positive and negative directions
  Else
    Analysis directions= Only negative direction
End
```

Figure 2.6 Algorithm for the determination of analysis direction for the approximate methods

## **CHAPTER 3**

### **EQUIVALENT LINEARIZATION PROCEDURE**

An equivalent linearization procedure is developed in this thesis study as an approximate method for predicting the inelastic seismic displacement response of MDOF systems under earthquake excitations. The procedure mainly consists of reducing the stiffness of the structural members that are expected to respond in the inelastic range. Combined results of demand and capacity analyses are employed for the construction of equivalent linear system with reduced stiffness.

Estimation of equivalent damping was one of the main tasks of the equivalent linearization methods employed in the past for predicting the seismic demands of MDOF systems (Schnabel et al., 1972; Shibata and Sözen, 1976; Mengi et al., 1992). Different from such previous studies, there is no need for the determination of equivalent damping in this study. Instead, predetermined spectral displacement demands are utilized in each mode of the equivalent linear system for the determination of global displacement demands. Hence, response spectrum analysis is utilized as the analysis tool in the implementation of the proposed equivalent linearization procedure.

Outline of the procedure is presented in Figure 3.1 and further details are explained in the following paragraphs.

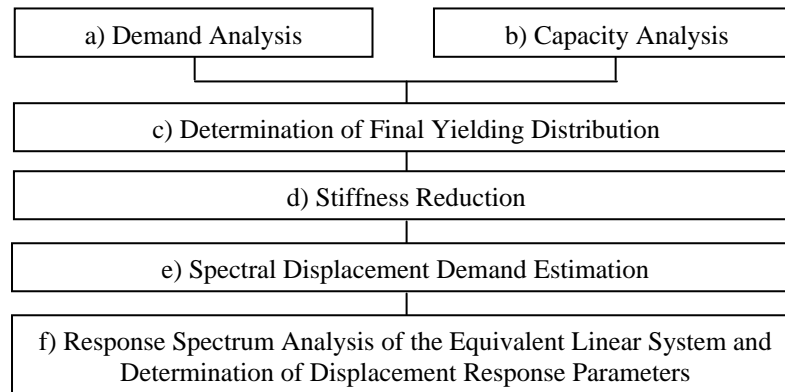


Figure 3.1 Outline of the equivalent linearization procedure

### 3.1 Demand Analysis

Gravity analysis and response spectrum analysis are conducted as the demand analysis. In response spectrum analysis, earthquake ground excitation is expressed by its 5% damped linear elastic pseudo acceleration response spectrum. Axial forces in the columns and other members obtained from gravity analysis are employed in the capacity analysis. Moment demands obtained from gravity analysis and response spectrum analysis are employed for the determination of final yielding distribution and accordingly in stiffness reduction as described in the following sections.

In three dimensional (3D) models, moment demands obtained from response spectrum analysis at the column ends are utilized in capacity analysis for estimating the ratio of flexural capacities about the two orthogonal bending axes. Therefore, gravity analysis and response spectrum analysis should be carried out before the capacity analysis for 3D models. For two dimensional (2D) models, response spectrum analysis and capacity analysis are independent. On the other hand, it is practical to conduct response spectrum analysis together with gravity analysis for 2D models also.

## 3.2 Capacity Analysis

Capacity analysis is conducted in order to determine the member capacities first, and then to identify those member-ends which have a yielding potential. In addition, base shear capacity of the building at the fundamental mode is obtained as a by-product. Capacity analysis is composed of five basic steps (Figure 3.2), which are explained in detail below.

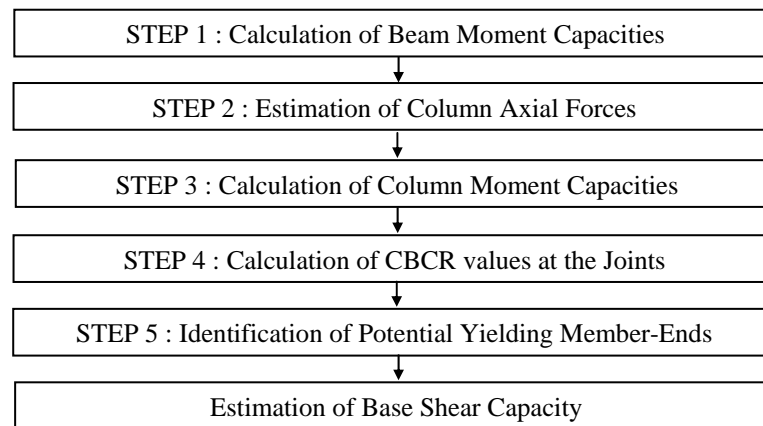


Figure 3.2 Outline of capacity analysis

### 3.2.1 Calculation of Beam Moment Capacities (Step 1)

Positive and negative flexural capacities of beam end sections are calculated by using nominal material strengths.

### 3.2.2 Calculation of Column Axial Forces and Moment Capacities (Steps 2 and 3)

Axial forces are required for calculating the moment capacities of columns and walls. The total axial force in a column is equal to the sum of the axial forces due to gravity loading ( $N_G$ ) and due to earthquake loading ( $N_E$ ). Axial forces due to gravity loading can be obtained by conducting linear elastic analysis, by assuming that no inelasticity develops under the presence of gravity loads alone. However it is misleading to calculate the axial forces due to earthquake loading by conducting linear elastic analysis, because they are bounded by the maximum shear forces that can be transmitted from the spanning beams. Hence it is adequate to calculate the axial forces due to gravity loading ( $N_G$ ) by conducting linear elastic analysis, and axial forces due to earthquake loading ( $N_E$ ) by conducting limit analysis. Limit analysis leads to axial force values at the limit state of the structure when it reaches its lateral load capacity. This is acceptable, since most of the structures reach their base shear force capacities under a strong earthquake excitation for which they are seismically assessed or designed.

In the calculation of  $N_E$  by limit analysis, both ends of the beams located parallel to the considered earthquake direction are accepted to yield in flexure, compatible with the lateral load direction. Since  $N_G$  is available from linear elastic gravity analysis, beam end moments due to gravity loading should be eliminated from the beam end moment capacities. The remaining “residual capacity” moment at a beam end is equal to the difference between the moment capacity and the moment due to gravity loading. Beam-end shear forces are then calculated by dividing the sum of the residual capacity moments at the beam ends by the clear length of the beam ( $V_E$  in Figure 3.3). Axial force of a column due to earthquake loading is calculated by using vertical equilibrium, from the free body diagram of the considered column axis (Figure 3.4). It is assumed that there is no shear force due to earthquake, transferred from the beams which are located in the orthogonal direction to the considered earthquake direction. When masonry infill walls are modeled as struts, vertical components of the strut forces should also be considered

in the calculation of column axial forces. Axial force capacities of the struts can be used as the strut forces.

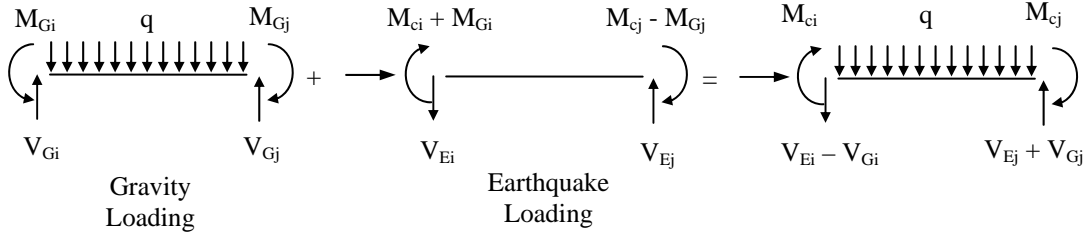


Figure 3.3 Beam-end forces due to gravity and earthquake loadings

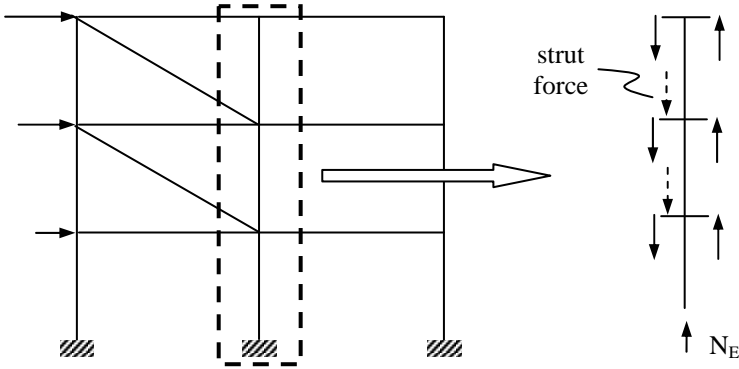


Figure 3.4 Calculation of axial forces of columns due to earthquake loading

After calculation of  $N_E$ , the total axial force on a column ( $N$ ) is calculated as the sum of  $N_G$  and  $N_E$ . The moment capacity is then calculated under the total axial force  $N$  by using the interaction diagram of the associated column. In a 3D model, moment capacities of the columns are calculated under biaxial bending since there exists moments about both axes of a column (Figure 3.5). For the calculation of the ratio of the moments about the two orthogonal axes of a column ( $M_{cx} / M_{cy}$  with reference to Figure 3.5), moments obtained from response spectrum analysis are utilized (Equation 3.1).

$$\frac{M_{cx}}{M_{cy}} = \frac{M_{Ex}}{M_{Ey}} \quad (3.1)$$

In Equation 3.1,  $M_{cx}$  and  $M_{cy}$  are the capacity moments about x and y axes of the column respectively, whereas  $M_{Ex}$  and  $M_{Ey}$  are the moments about x and y axes of the column obtained from response spectrum analysis, respectively. In a 2D model, moment capacity of a column is obtained under uniaxial bending. Therefore, moments obtained from response spectrum analysis are not required. Accordingly, response spectrum analysis and capacity analysis become two separate independent analyses for 2D models.

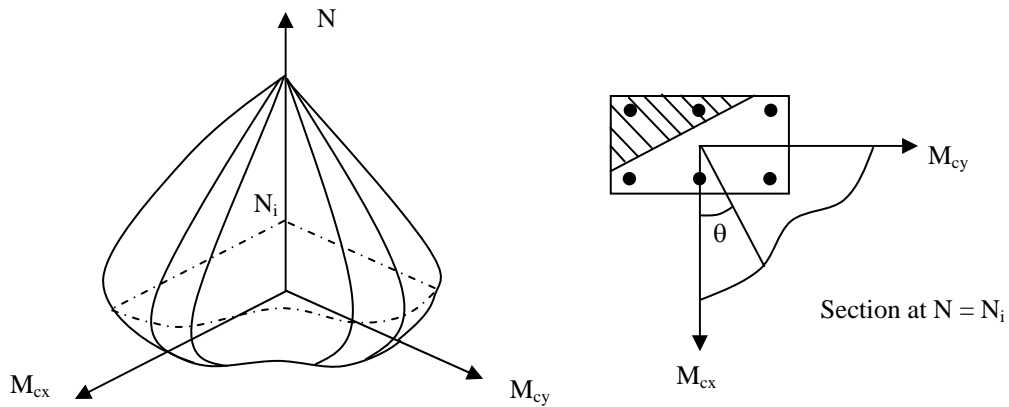


Figure 3.5 Biaxial bending for a rectangular column

### 3.2.3 Calculation of Column-to-Beam Capacity Ratios (CBCR) at the Joints (Step 4)

Column-to-Beam Capacity Ratios (CBCR) are calculated at all joints by dividing the total moment capacity of the column-ends, by the total moment capacity of the beam-ends connecting to the joint (Figure 3.6). Only those beams located parallel to the excitation direction are considered in the CBCR calculation.

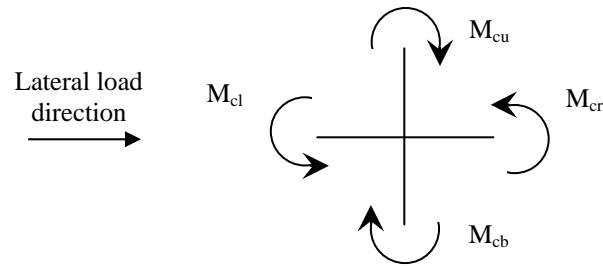


Figure 3.6 Column-to-Beam Capacity Ratio (CBCR) at a joint

### 3.2.4 Identification of Potential Yielding Member-Ends (Step 5)

If CBCR at a joint is smaller than 0.8, column-ends are considered as the potential yielding member-ends. If CBCR is greater than 1.2, beam-ends (beams located both parallel and orthogonal to earthquake direction) are considered as the potential yielding member-ends. Finally, if CBCR is between 0.8 and 1.2, all member ends connecting to the joint are considered to have yielding potential. There are two reasons for using the values 0.8 and 1.2. First reason is the possible errors due to the approximate calculation of axial forces and moment capacities of the columns. Second reason is the effect of shear forces at the ends of the rigid end zones on the equilibrium of the joint, which is not taken into account in the calculation of CBCR values. Bottom ends of ground story columns are accepted to have yielding potential inherently.

### 3.2.5 Estimation of Base Shear Capacity

Base shear capacity is obtained as a by-product of capacity analysis. As explained previously, axial forces of the ground story columns due to earthquake loading and the moment capacities of these columns are calculated as a result of capacity analysis. Assuming that all of the ground story column bases yield, base shear capacity of a structure can be estimated by considering the global moment equilibrium of the structure (Figure 3.7).

In 3D models, moment capacities of the ground story columns about the sectional axes perpendicular to the direction of the lateral force are considered in the moment equilibrium, and moments of the forces are calculated about an axis perpendicular to the lateral force direction (for example, yy axis in Figure 3.8).

The base shear capacity estimated accordingly corresponds to the base shear capacity calculated under the first mode lateral force for 2D models. It corresponds to the base shear capacity for the fundamental translational mode in the considered earthquake direction in 3D models. Estimated base shear capacity is employed for the calculation of spectral displacement demand for the fundamental mode.

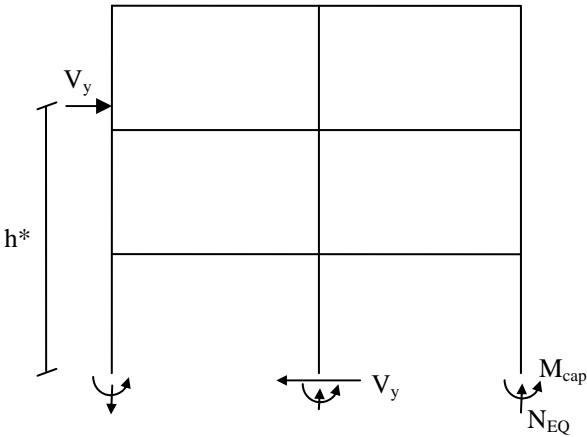


Figure 3.7 Calculation of base shear capacity for 2D models

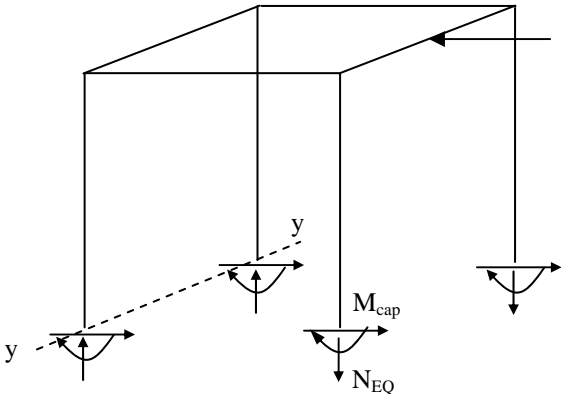


Figure 3.8 Calculation of base shear capacity for 3D models

### 3.3 Determination of Final Yielding Distribution

Potential yielding member ends were identified as a result of capacity analysis. Final yielding distribution is determined by involving the demand analysis results. Member-ends which do not have yielding potential are inherently non-yielding member ends. A potentially yielding member end is considered as a yielding member-end if the Demand-to-Capacity Ratio (DCR, Equation 3.2) at that end is greater than unity. Otherwise, it is considered as a non-yielding member-end.

$$DCR = \frac{M_E}{M_{rc}} \quad (3.2)$$

In Equation 3.2,  $M_E$  is the earthquake moment obtained from response spectrum analysis and  $M_{rc}$  is the residual capacity moment at the considered member end. Residual capacity moment at a member end is calculated by excluding the gravity moment from the capacity moment, by considering the directions consistently. If the earthquake moment and the gravity moment are in opposite directions (i end of the beam in Figure 3.9), gravity moment is added to the capacity moment in order to calculate the residual capacity moment. Gravity moment is subtracted from the capacity moment in the reverse case (j end of the beam in Figure 3.9). As stated previously, it is assumed that the directions of the earthquake moments at member ends are controlled by the fundamental vibration mode in the considered earthquake direction.

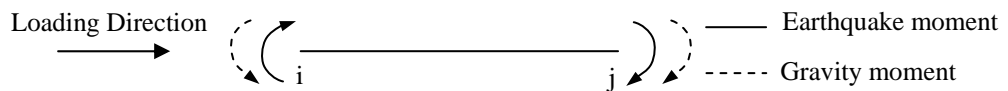


Figure 3.9 Demonstration of moment directions at the ends of a beam due to earthquake loading and gravity loading

### 3.4 Stiffness Reduction

Stiffness of the structure is reduced by reducing the stiffness of the structural members. Member stiffness reduction is achieved by reducing the moment of inertia.

Considering that beams and columns of the structural frames are prismatic members, it can be accepted that moment of inertia 'I' along the member length is constant. Reduced moment of inertia of a member is calculated by considering the relation between the sum of moments and the sum of chord rotations at the member ends. Chord rotation at a member end is defined as the angle between the chord which connects the two ends of a member and the tangent to the deflected shape at the considered member end (Figure 3.10).

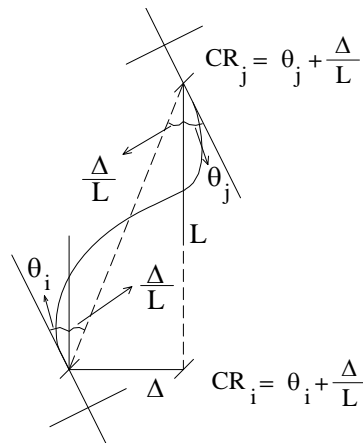


Figure 3.10 Definition of chord rotation at the i and j ends of a frame member

The relation between the chord rotations and moments at the ends of a linear elastic prismatic member is expressed as

$$\begin{bmatrix} M_i \\ M_j \end{bmatrix} = \frac{2EI}{L} \begin{bmatrix} 2 & 1 \\ 1 & 2 \end{bmatrix} \begin{bmatrix} \theta_i \\ \theta_j \end{bmatrix} \quad (3.3)$$

In Equation 3.3,  $M_i$  and  $M_j$  are the moments and  $\theta_i$  and  $\theta_j$  are the chord rotations at the  $i$  and  $j$  ends of a member, respectively.  $E$  is the modulus of elasticity,  $L$  is the clear span length and  $I$  is the moment of inertia.

Summation of the first and second rows of the matrix equality in Equation 3.3 gives

$$M_i + M_j = \frac{6EI}{L}(\theta_i + \theta_j) \quad (3.4)$$

Equation 3.4 can then be used in order to relate the sum of moments and sum of chord rotations at the member-ends obtained from response spectrum analysis.

$$\Sigma M_E = \frac{6EI}{L} \Sigma \theta_E \quad (3.5)$$

“ $\Sigma$ ” in Equation 3.5 designates the sum of the moments or chord rotations at both ends of the member.  $M_E$  and  $\theta_E$  denote the earthquake moment and earthquake chord rotation obtained from response spectrum analysis respectively.

The relation between the sum of residual capacity moments and the sum of chord rotations calculated from response spectrum analysis can be expressed similarly, by employing the equal displacement rule (Figure 3.11).

$$\Sigma M_{rc} = \frac{6EI'}{L} \Sigma \theta_E \quad (3.6)$$

In Equation 3.6,  $I'$  is the reduced moment of inertia and  $\Sigma M_{rc}$  is the sum of residual capacity moments at both ends of the member.

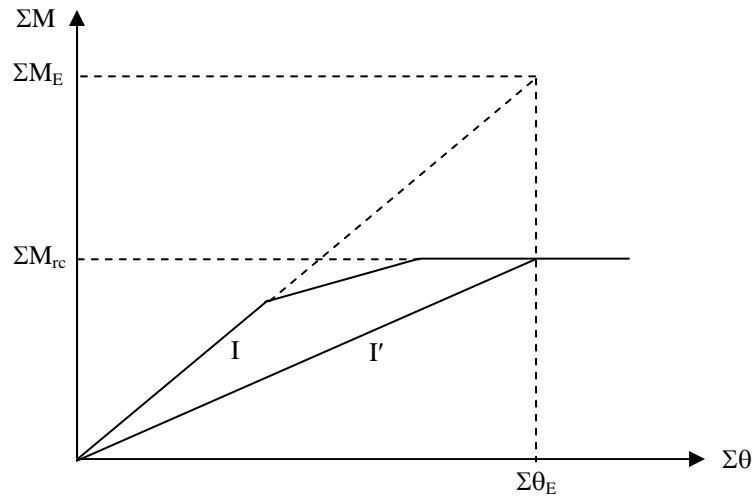


Figure 3.11 The variation of the sum of moments with the sum of chord rotations at member-ends in the linear elastic and inelastic ranges

Dividing Equation 3.5 by Equation 3.6 and rearranging, Equation 3.7 is obtained.

$$I' = \frac{I}{\frac{\sum M_E}{\sum M_{rc}}} \quad (3.7)$$

The denominator in Equation 3.7 can be defined as the reduction factor  $R_M$ .

$$R_M = \frac{\sum M_E}{\sum M_{rc}} \quad (3.8)$$

Substituting Equation 3.8 in Equation 3.7, Equation 3.9 is obtained for the moment of inertia reduction.

$$I' = \frac{I}{R_M} \quad (3.9)$$

$R_M$  expressions that correspond to different yielding situations are presented in Table 3.1. It can be observed that moment of inertia is not reduced when both ends of a member are non-yielding. Sum of the residual capacity moments is used for the reduction when both ends are yielding. When one end is yielding, sum of the residual capacity moment at the yielding end and a moment smaller than the residual capacity moment at the non-yielding end is used for the reduction. Moment at the non-yielding end is calculated approximately by dividing the capacity moment by the CBCR value (of the joint to which the non-yielding end connects) if CBCR is greater than 1.0 or by multiplying the capacity moment with CBCR if CBCR is smaller than 1.0.

As a note, it is worth to mention that stiffness reduction is also applied to the beams located orthogonal to the earthquake direction in 3D models.

Table 3.1  $R_M$  corresponding to different yielding situations

Yielding Situation	$R_M$
Both ends non-yielding	1
One end yielding	$R_M = \frac{\sum M_E}{M_{rc,i} + \alpha M_{rc,j}} \quad \alpha = \begin{cases} \text{CBCR} & \text{if CBCR} < 1 \\ 1/\text{CBCR} & \text{if CBCR} > 1 \end{cases} *$
Both ends yielding	$R_M = \frac{\sum M_E}{M_{rc,i} + M_{rc,j}}$

\* i denotes yielding end, j denotes non-yielding end, CBCR is the column-to-beam capacity ratio around the joint to which the non-yielding end connects

### 3.5 Spectral Displacement Demands for the Equivalent Linear System

Stiffness reduction results in an equivalent linear system with reduced stiffness. Stiffness distribution of this system is different from the original system. New stiffness distribution reflects the expected distribution of inelasticity in the system under the considered ground excitation. Stiffness of members which are

subjected to larger inelastic action are reduced more. On the other hand, stiffness of those members which are anticipated to behave elastic according to capacity analysis or demand-to-capacity ratios are not reduced. Therefore, stiffness reduction determines the relative displacement distribution within the structure. In order to calculate the actual deformations, global displacement demands should be determined in addition to the relative displacement distribution.

The global displacement demand of the reduced equivalent linear system can not be determined by conducting linear response history or response spectrum analysis under a ground motion unless an increased (equivalent) damping is imposed for reflecting the hysteretic energy dissipation of the actual system. Although there are established methods for estimating increased damping in an equivalent linear SDOF system (Gülkan and Sözen, 1974; Iwan, 1980; Kowalsky, 1994), these methods are more suitable for design purposes since they require the prior knowledge of ductility ratios ( $\mu$ ) as stated in Chapter 1. In addition, it was previously stated that equivalent linearization procedures should be employed with care for the estimation of maximum inelastic displacement demands for systems with known lateral strength (Akkar and Miranda, 2005). Therefore increased damping is not employed in this study. Global displacement demands are directly obtained from the spectral displacement demands in each mode of the equivalent linear system. These spectral displacement demands are called the target spectral displacements  $Sd_n^*$ .

Two alternative methods are utilized for the calculation of target spectral displacements, explained below.

### **3.5.1 Nonlinear Response History Analysis of the Equivalent SDOF System**

Target spectral displacement in the first mode (or the fundamental mode in the considered earthquake direction in a 3D model) is calculated via nonlinear response history analysis (NRHA) of the equivalent SDOF system representing this mode ( $Sd_{ni}^*$ ).

When the hysteresis behavior of the SDOF system is elastoplastic, three parameters are required in each mode for conducting nonlinear response history analysis. These parameters are the period ( $T_n$ ), the base shear capacity coefficient ( $\eta_{ny}$ ), which is the ratio of base shear capacity to effective modal weight, and the damping ratio (5% damping ratio is assumed).  $T_n$  is obtained from the eigenvalue analysis of the original structure whereas the base shear capacity in the first mode is estimated as a result of capacity analysis.

Target spectral displacements of the higher modes are assumed to be equal to the elastic spectral displacements corresponding to the periods of the original structure ( $Sd_{ne}^*$ ). In fact, the base shear capacity coefficients of the higher modes are much higher when compared with the first mode base shear capacity coefficient in structures that do not possess significant irregularity, since the modal masses of the higher modes are small. Spectral displacements corresponding to the higher modes usually remain in the elastic range under most ground excitations.

This alternative is referred to as EQL-NL in the following chapters.

### **3.5.2 Equal Displacement Assumption**

In the second alternative, target spectral displacements of all modes are calculated as the elastic spectral displacements corresponding to the modal vibration periods of the original (unreduced-stiffness) structure according to the equal displacement rule (Veletsos and Newmark, 1960). Equal displacement assumption is valid for the average of many ground motions in the medium and long period ranges (Miranda, 2000; Miranda, 2001). Therefore it may result in misleading values for short periods and for individual ground motions. However, target spectral displacement determination using the equal displacement assumption is employed as an alternative in this study, because the implementation of equal displacement rule is much practical with respect to the NRHA of inelastic SDOF systems. The trade-off between the increase in errors due to equal displacement assumption and the simplicity of its application is investigated in the case studies.

This alternative is referred to as EQL-ED in the following chapters.

### 3.6 Response Spectrum Analysis of the Equivalent Linear System

Response spectrum analysis of the equivalent linear system is conducted after the determination of the target spectral displacements. In the application of response spectrum analysis, modal force vector at any mode ( $\mathbf{f}'_n$ ) should be determined such that the  $n^{\text{th}}$  mode SDOF system is subjected to a maximum displacement that is equal to the target spectral displacement calculated for that mode. For this purpose, pseudo acceleration ( $\text{PSa}_n^*$ ) corresponding to the  $n^{\text{th}}$  mode target spectral displacement ( $\text{Sd}_n^*$ ) at the  $n^{\text{th}}$  mode period of the equivalent linear system ( $T'_n$ ) is calculated from Equation 3.10 as explained in Figure 3.12.

$$\text{PSa}_n^* = \text{Sd}_n^* \left( \frac{2\pi}{T'_n} \right)^2 \quad (3.10)$$

The  $n^{\text{th}}$  modal force vector ( $\mathbf{f}'_n$ ) is calculated from Equation 3.11.

$$\mathbf{f}'_n = \Gamma'_n \mathbf{m} \boldsymbol{\phi}'_n \text{PSa}_n^* \quad (3.11)$$

In Equation 3.11,  $\boldsymbol{\phi}'_n$  and  $\Gamma'_n$  are the  $n^{\text{th}}$  modal vector and  $n^{\text{th}}$  modal participation factor for the equivalent linear system, respectively and  $\mathbf{m}$  is the mass matrix.

Maximum responses in each mode are calculated by applying the modal force vector in Equation 3.11 to the equivalent linear structure. Then, the modal responses are combined by using statistical combination rules. SRSS (square root of sum of squares, Rosenblueth, 1951) and CQC (complete quadratic combination, Der

Kiureghian, 1981) are the two widely applied combination rules. SRSS is used for structures with well separated frequencies, like planar frame structures. However CQC is preferred for systems with close periods of vibration, like the case of unsymmetrical plan buildings, since it accounts for cross-correlations between the modes (Chopra, 2001).

At this point, it is beneficial to state that the equivalent linearization procedure is equivalent to standard response spectrum analysis when it is applied to elastic systems.

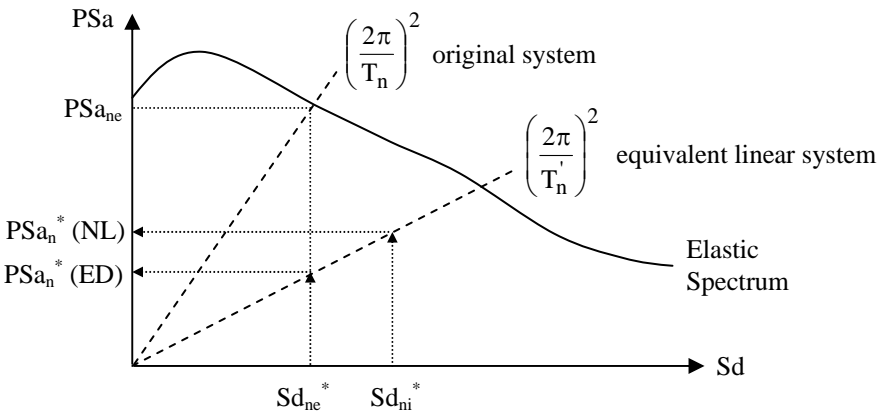


Figure 3.12 Calculation of pseudo acceleration corresponding to the target spectral displacement at the  $n^{\text{th}}$  mode

**3.7 Determination of Response Parameters**

As a result of the gravity analysis and response spectrum analysis conducted for the equivalent linear system, displacement response parameters including story displacements, interstory drift ratios and chord rotations are calculated.

### 3.8 Basic Assumptions of the Equivalent Linearization Procedure

The following assumptions have been made in developing the equivalent linearization procedure.

- Stiffness reduction equations are based on the assumption that inelasticity develops at the member ends.
- Strength or stiffness degradation or pinching is not considered in the derivation of stiffness reduction equations. It is worth to mention that such behavior is not also considered in the conventional pushover analysis or the alternative pushover procedures which consider higher mode effects and adaptive nature of inertia forces. Strength or stiffness degradation or pinching develop under load reversals, which is not observed in pushover analysis.
- The method is mainly applicable for structures with members which are expected to possess flexural mode of failure. Shear force capacity is compared with the shear force corresponding to the moment capacities at the member ends, to determine if the failure mode of a member is flexure or shear.

Implementation of the equivalent linearization method is demonstrated schematically in Figure 3.13 and an algorithmic step by step application of the equivalent linearization method for 3D models is presented in Figure 3.14.

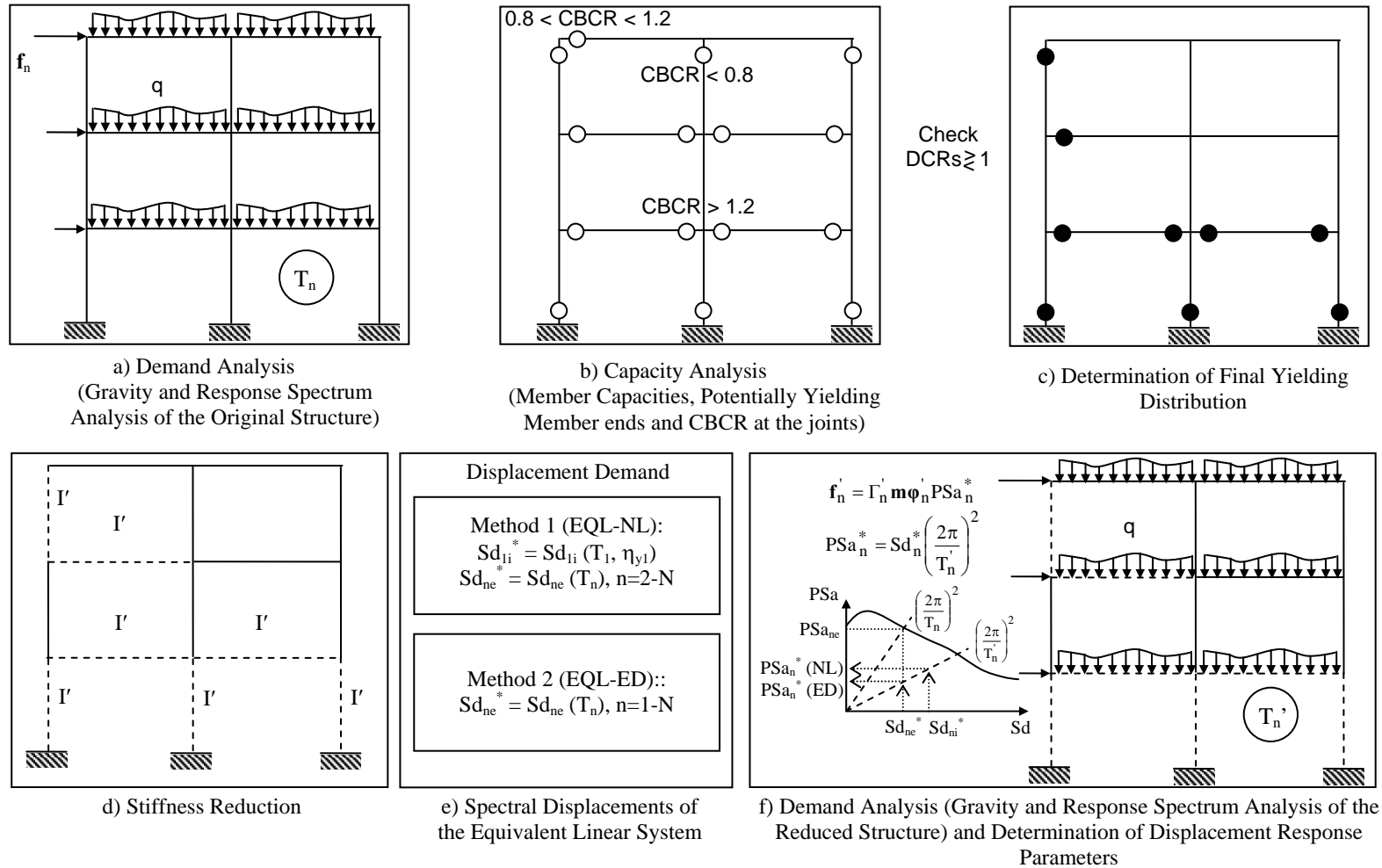


Figure 3.13 Schematical demonstration of the application of equivalent linearization procedure

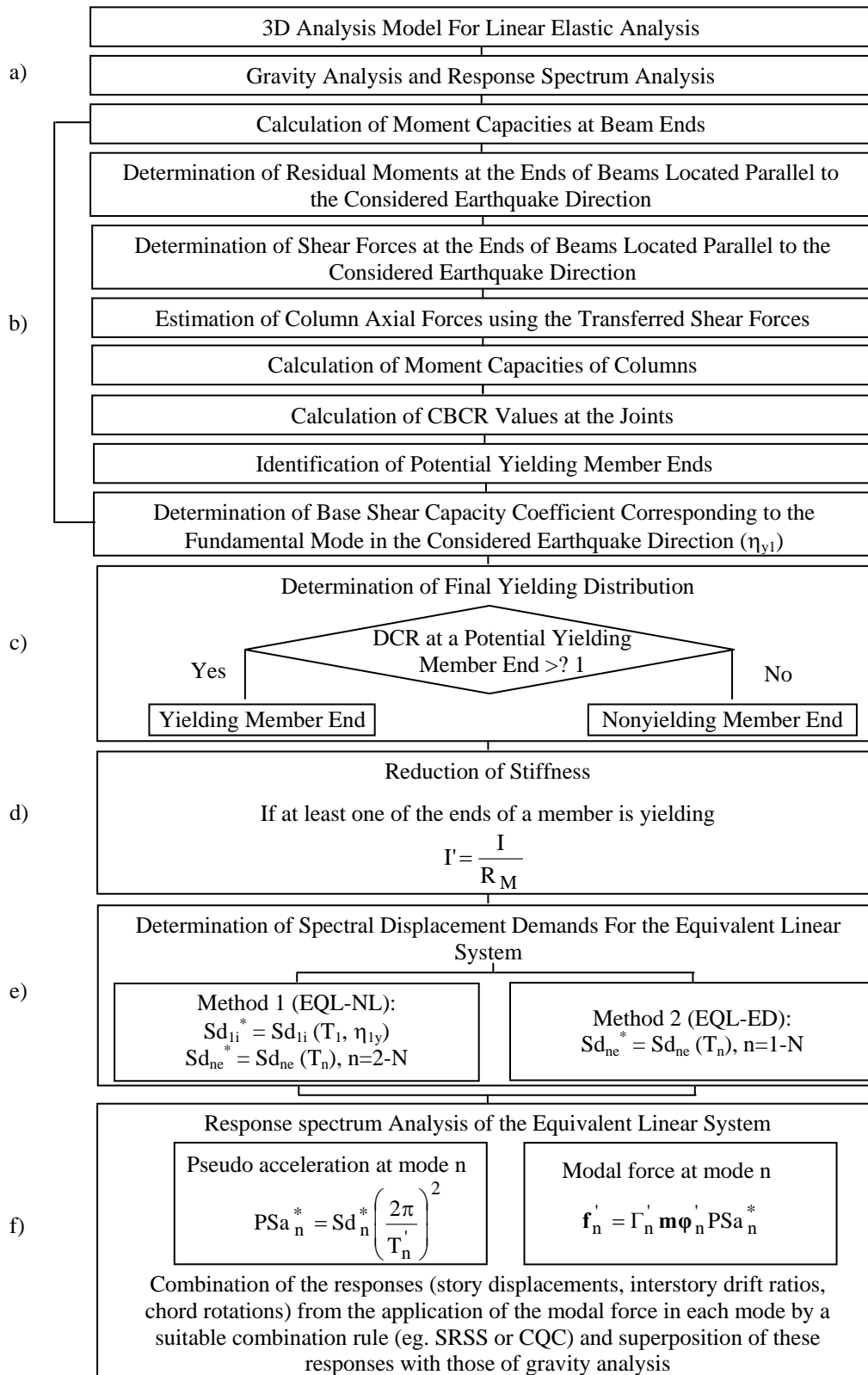


Figure 3.14 Flowchart of the equivalent linearization procedure for a 3D model with reference to Figure 3.13

## **CHAPTER 4**

### **GROUND MOTIONS EMPLOYED IN CASE STUDIES**

Ground motions which contain pulses especially in their velocity and displacement traces impose larger demands on structures than ordinary ground motions. These ground motions are usually near-fault ground motions with forward directivity effects (Alavi and Krawinkler, 2001; 2004). Therefore, ground motions utilized in this study are divided into two sets, designated as pulse type ground motion set (96 ground motions) and ordinary ground motion set (66 ground motions). Pulse type ground motion set consists of ground motions possessing significant velocity pulses with PGV greater than 35 cm/s. Ordinary ground motion set consists of ground motions which do not satisfy the above criterion. A grouping based on the existence of pulse signals was previously employed by Akkar et al. (2005).

All of the utilized ground motions are downloaded from PEER strong motion database. Important features of these ground motions are listed in Tables 4.1 and 4.2.

Table 4.1 Pulse type ground motion properties

#	G-M Code	Earthquake	Mw	Station	Component	CD <sup>1</sup> (km)	Site <sup>2</sup> Geology	PGA (g)	PGV (cm/sec)	PGV/PGA (sec)	PGD (cm)	Scale	T <sub>p</sub> <sup>3</sup> (sec)
1	PET000	Cape Mendocino, 04/25/92	7.0	Petrolia	000	8.2	B	0.590	48.1	0.08	21.9	1.0	0.75
2	RIO270	Cape Mendocino, 04/25/92	7.0	Rio Dell Overpass - FF	270	14.3	C	0.385	43.8	0.12	21.6	1.0	1.18
3	CHY006-E	Chi-Chi, 09/20/99	7.6	CHY006	E	9.8	B	0.364	55.4	0.16	25.6	1.0	2.05
4	CHY028-N	Chi-Chi, 09/20/99	7.6	CHY028	N	3.1	A	0.822	67.0	0.08	23.3	1.0	0.81
5	CHY035-W	Chi-Chi, 09/20/99	7.6	CHY035	W	18.1	A	0.252	45.6	0.18	12.0	1.0	1.42
6	CHY080-N	Chi-Chi, 09/20/99	7.6	CHY080	N	2.7	A	0.902	102.5	0.12	34.0	1.0	1.04
7	CHY080-W	Chi-Chi, 09/20/99	7.6	CHY080	W	2.7	A	0.968	107.6	0.11	18.6	1.0	0.91
8	CHY101-N	Chi-Chi, 09/20/99	7.6	CHY101	N	10.0	D	0.440	115.0	0.27	68.8	1.0	4.68
9	CHY101-W	Chi-Chi, 09/20/99	7.6	CHY101	W	10.0	D	0.353	70.7	0.20	45.3	1.0	3.37
10	NSY-E	Chi-Chi, 09/20/99	7.6	NSY	E	13.2	B	0.145	47.5	0.33	50.7	1.0	8.12
11	NSY-N	Chi-Chi, 09/20/99	7.6	NSY	N	13.2	B	0.128	41.9	0.33	28.7	1.0	4.55
12	TCU036-W	Chi-Chi, 09/20/99	7.6	TCU036	W	16.7	A	0.139	59.7	0.44	63.6	1.0	5.35
13	TCU052-N	Chi-Chi, 09/20/99	7.6	TCU052	N	0.7	A	0.419	118.5	0.29	246.3	1.0	11.62
14	TCU052-W	Chi-Chi, 09/20/99	7.6	TCU052	W	0.7	A	0.348	159.0	0.47	184.5	1.0	5.95
15	TCU053-N	Chi-Chi, 09/20/99	7.6	TCU053	N	6.0	D	0.140	41.1	0.30	48.1	1.0	6.62
16	TCU057-N	Chi-Chi, 09/20/99	7.6	TCU057	N	11.8	B	0.093	42.6	0.47	56.3	1.0	8.59
17	TCU059-W	Chi-Chi, 09/20/99	7.6	TCU059	W	17.8	C	0.165	59.4	0.37	63.7	1.0	6.80
18	TCU060-W	Chi-Chi, 09/20/99	7.6	TCU060	W	9.5	B	0.201	36.3	0.18	51.9	1.0	11.73
19	TCU063-N	Chi-Chi, 09/20/99	7.6	TCU063	N	9.8	D	0.134	73.2	0.56	59.3	1.0	3.98
20	TCU064-N	Chi-Chi, 09/20/99	7.6	TCU064	N	16.6	D	0.117	54.1	0.47	59.1	1.0	7.10
21	TCU068-N	Chi-Chi, 09/20/99	7.6	TCU068	N	0.3	A	0.462	263.2	0.58	430.2	1.0	10.96
22	TCU068-W	Chi-Chi, 09/20/99	7.6	TCU068	W	0.3	A	0.566	176.7	0.32	324.3	1.0	9.35
23	TCU084-W	Chi-Chi, 09/20/99	7.6	TCU084	W	11.2	A	1.157	114.8	0.10	31.4	1.0	1.82
24	TCU087-N	Chi-Chi, 09/20/99	7.6	TCU087	N	3.2	A	0.122	37.1	0.31	25.6	1.0	4.18
25	TCU087-W	Chi-Chi, 09/20/99	7.6	TCU087	W	3.2	A	0.128	40.8	0.32	62.7	1.0	8.89
26	TCU101-W	Chi-Chi, 09/20/99	7.6	TCU101	W	2.9	B	0.202	67.9	0.34	75.4	1.0	7.58
27	TCU102-N	Chi-Chi, 09/20/99	7.6	TCU102	N	1.5	A	0.169	77.2	0.47	44.9	1.0	2.82
28	TCU103-W	Chi-Chi, 09/20/99	7.6	TCU103	W	4.0	A	0.134	61.9	0.47	87.6	1.0	7.97
29	TCU104-N	Chi-Chi, 09/20/99	7.6	TCU104	N	12.9	B	0.085	47.2	0.57	52.7	1.0	6.51
30	TCU122-W	Chi-Chi, 09/20/99	7.6	TCU122	W	9.4	D	0.220	42.5	0.20	43.0	1.0	4.25
31	TCU128-N	Chi-Chi, 09/20/99	7.6	TCU128	N	13.2	B	0.170	68.8	0.41	41.9	1.0	4.78
32	TCU128-W	Chi-Chi, 09/20/99	7.6	TCU128	W	13.2	B	0.159	73.1	0.53	90.7	1.0	7.47
33	WGK-E	Chi-Chi, 09/20/99	7.6	WGK	E	10.0	D	0.334	69.0	0.21	35.7	1.0	3.35
34	WGK-N	Chi-Chi, 09/20/99	7.6	WGK	N	10.0	D	0.484	74.5	0.16	67.0	1.0	4.09
35	BOL090	Duzce, 11/12/99	7.1	Bolu	090	12.0	D	0.822	62.1	0.08	13.6	1.0	0.92

Table 4.1 Pulse type ground motion properties (continued)

#	G-M Code	Earthquake	Mw	Station	Component	CD <sup>1</sup> (km)	Site <sup>2</sup> Geology	PGA (g)	PGV (cm/sec)	PGV/PGA (sec)	PGD (cm)	Scale	T <sub>p</sub> <sup>3</sup> (sec)
36	DZC180dzc	Duzce, 11/12/99	7.1	Duzce	180	8.2	D	0.348	60.0	0.18	42.1	1.0	5.58
37	DZC270dzc	Duzce, 11/12/99	7.1	Duzce	270	8.2	D	0.535	83.5	0.16	51.6	1.0	4.10
38	ERZ-Ewa	Erzincan, 03/13/92	6.9	Erzincan	EW	4.4	D	0.496	64.3	0.13	21.9	1.5	1.99
39	ERZ-Ewb	Erzincan, 03/13/92	6.9	Erzincan	EW	4.4	D	0.496	64.3	0.13	21.9	1.0	1.99
40	EMO270	Imperial Valley, 10/15/79	6.5	EC Meloland Overpass FF	270	0.5	D	0.296	90.4	0.31	31.7	1.0	3.18
41	H-BRA225	Imperial Valley, 10/15/79	6.5	Brawley Airport	225	10.4	D	0.160	35.9	0.23	22.4	1.0	3.21
42	H-E04140	Imperial Valley, 10/15/79	6.5	El Centro Array #4	140	7.1	D	0.485	37.4	0.08	20.1	1.0	1.20
43	H-E04230	Imperial Valley, 10/15/79	6.5	El Centro Array #4	230	7.1	D	0.360	76.5	0.22	59.1	1.0	4.35
44	H-E05140	Imperial Valley, 10/15/79	6.5	El Centro Array #5	140	4.0	D	0.519	46.9	0.09	35.4	1.0	3.39
45	H-E05230	Imperial Valley, 10/15/79	6.5	El Centro Array #5	230	4.0	D	0.379	90.5	0.24	63.1	1.0	3.76
46	H-E06140	Imperial Valley, 10/15/79	6.5	El Centro Array #6	140	1.4	D	0.411	64.9	0.16	27.6	1.0	2.83
47	H-E06230	Imperial Valley, 10/15/79	6.5	El Centro Array #6	230	1.4	D	0.439	109.8	0.26	65.8	1.0	3.77
48	H-E07230	Imperial Valley, 10/15/79	6.5	El Centro Array #7	230	0.6	D	0.463	109.3	0.24	44.7	1.0	3.37
49	H-E08230	Imperial Valley, 10/15/79	6.5	El Centro Array #8	230	3.9	D	0.454	49.1	0.11	35.6	1.0	4.02
50	H-E10050	Imperial Valley, 10/15/79	6.5	El Centro Array #10	050	6.2	D	0.171	47.5	0.28	31.1	1.0	4.37
51	H-E10320	Imperial Valley, 10/15/79	6.5	El Centro Array #10	320	6.2	D	0.224	41.0	0.19	19.5	1.0	1.96
52	H-ECC092	Imperial Valley, 10/15/79	6.5	EC County Center FF	092	7.3	D	0.235	68.8	0.30	39.4	1.0	3.51
53	H-EDA270	Imperial Valley, 10/15/79	6.5	El Centro Differential Array	270	5.1	D	0.352	71.2	0.21	45.8	1.0	4.04
54	H-EDA360	Imperial Valley, 10/15/79	6.5	El Centro Differential Array	360	5.1	D	0.480	40.8	0.09	14.0	1.0	1.55
55	H-EMO000	Imperial Valley, 10/15/79	6.5	EC Meloland Overpass FF	000	0.5	D	0.314	71.8	0.23	25.6	1.0	3.24
56	H-HVP225	Imperial Valley, 10/15/79	6.5	Holtville Post Office	225	7.7	D	0.253	48.8	0.20	31.6	1.0	5.09
57	H-HVP315	Imperial Valley, 10/15/79	6.5	Holtville Post Office	315	7.7	D	0.221	49.8	0.23	31.9	1.0	3.69
58	KBU000	Kobe, 01/16/95	6.9	Kobe University	000	0.9	A	0.290	54.8	0.19	13.5	1.0	1.42
59	KJM000	Kobe, 01/16/95	6.9	KJMA	000	1.0	B	0.821	81.3	0.10	17.7	1.0	0.92
60	KJM090	Kobe, 01/16/95	6.9	KJMA	090	1.0	B	0.599	74.4	0.13	20.0	1.0	1.26
61	PRI000	Kobe, 01/16/95	6.9	Port Island (0 m)	000	3.3	E	0.315	74.9	0.24	38.3	1.0	2.29
62	PRI090	Kobe, 01/16/95	6.9	Port Island (0 m)	090	3.3	E	0.278	54.2	0.20	24.9	1.0	1.97
63	TAK000	Kobe, 01/16/95	6.9	Takatori	000	1.5	E	0.611	127.2	0.21	35.8	1.0	1.44
64	TAK090	Kobe, 01/16/95	6.9	Takatori	090	1.5	E	0.616	120.7	0.20	32.7	1.0	1.46
65	DZC180	Kocaeli, 08/17/99	7.4	Duzce	180	15.4	D	0.312	58.9	0.19	44.1	1.0	4.32
66	DZC270	Kocaeli, 08/17/99	7.4	Duzce	270	15.4	D	0.358	46.4	0.13	17.6	1.0	1.45
67	GBZ000	Kocaeli, 08/17/99	7.4	Gebeze	000	10.9	A	0.244	50.3	0.21	42.8	1.0	4.37
68	YPT060	Kocaeli, 08/17/99	7.4	Yarimca	060	4.8	D	0.268	65.7	0.25	57.0	1.0	4.67
69	YPT330	Kocaeli, 08/17/99	7.4	Yarimca	330	4.8	D	0.349	62.2	0.18	51.0	1.0	4.16
70	LCN275	Landers, 06/28/92	7.3	Lucerne	275	1.1	A	0.721	97.7	0.14	70.3	1.0	4.60

Table 4.1 Pulse type ground motion properties (continued)

#	GM Code	Earthquake	Mw	Station	Component	CD <sup>1</sup> (km)	Site <sup>2</sup> Geology	PGA (g)	PGV (cm/sec)	PGV / PGA (sec)	PGD (cm)	Scale	T <sub>p</sub> <sup>3</sup> (sec)
71	CLS090	Loma Prieta, 10/18/89	7.0	Corralitos	090	3.9	A	0.479	45.2	0.10	11.3	1.0	0.70
72	G02090	Loma Prieta, 10/18/89	7.0	Gilroy Array #2	090	13.7	D	0.322	39.1	0.12	12.1	1.0	1.34
73	G03090	Loma Prieta, 10/18/89	7.0	Gilroy Array #3	090	13.0	D	0.367	44.7	0.12	19.3	1.0	2.08
74	LEX000	Loma Prieta, 10/18/89	7.0	Los Gatos - Lexington Dam	000	5.0	A	0.420	73.5	0.18	20.0	1.0	1.31
75	LEX090	Loma Prieta, 10/18/89	7.0	Los Gatos - Lexington Dam	090	5.0	A	0.433	86.3	0.20	30.1	1.0	1.50
76	STG090	Loma Prieta, 10/18/89	7.0	Saratoga - Aloha Ave	090	8.5	D	0.324	42.6	0.13	27.6	1.0	3.09
77	WVC000	Loma Prieta, 10/18/89	7.0	Saratoga - W Valley Coll.	000	9.3	D	0.255	42.4	0.17	19.5	1.0	1.74
78	CYC285	Morgan Hill, 04/24/84	6.1	Coyote Lake Dam (SW A but)	285	0.5	A	1.298	80.8	0.06	9.6	1.0	0.86
79	NPS210	N. Palm Springs, 07/08/86	6.2	North Palm Springs	210	4.0	D	0.594	73.2	0.13	11.5	1.0	1.23
80	CNP196	Northridge, 01/17/94	6.7	Canoga Park - Topanga Can	196	14.7	D	0.420	60.7	0.15	20.3	1.0	1.42
81	LOS270	Northridge, 01/17/94	6.7	Canyon Country - W Lost Cany	270	12.4	C	0.482	44.9	0.09	12.5	1.0	0.69
82	NWH360	Northridge, 01/17/94	6.7	Newhall - Fire Sta	360	5.9	D	0.590	96.9	0.17	38.1	1.0	1.34
83	RIN228	Northridge, 01/17/94	6.7	Rinaldi Receiving Sta	228	7.1	C	0.838	166.0	0.20	28.1	1.0	1.16
84	SCS052	Northridge, 01/17/94	6.7	Sylmar - Converter Sta	052	5.4	D	0.613	117.4	0.20	54.3	1.0	2.50
85	SCS142	Northridge, 01/17/94	6.7	Sylmar - Converter Sta	142	5.4	D	0.897	102.2	0.12	45.1	1.0	1.21
86	SPV270	Northridge, 01/17/94	6.7	Sepulveda VA	270	8.9	D	0.753	84.5	0.11	18.7	1.0	1.06
87	SYL090	Northridge, 01/17/94	6.7	Sylmar - Olive View Med FF	090	5.3	D	0.605	78.1	0.13	16.8	1.0	2.08
88	SYL360	Northridge, 01/17/94	6.7	Sylmar - Olive View Med FF	360	5.3	D	0.843	129.4	0.16	31.9	1.0	1.94
89	TAR090	Northridge, 01/17/94	6.7	Tarzana - Cedar Hill A	090	15.6	B	1.779	109.6	0.06	32.9	1.0	0.78
90	WPI046	Northridge, 01/17/94	6.7	Newhall - W Pico Canyon Rd.	046	5.5	B	0.455	92.8	0.21	56.6	1.0	2.55
91	WPI316	Northridge, 01/17/94	6.7	Newhall - W Pico Canyon Rd.	316	5.5	B	0.325	67.4	0.21	16.1	1.0	1.91
92	PCD164	San Fernando, 02/09/71	6.6	Pacoima Dam	164	2.8	B	1.226	112.5	0.09	35.4	1.0	1.32
93	PCD254	San Fernando, 02/09/71	6.6	Pacoima Dam	254	2.8	B	1.160	54.1	0.05	11.8	1.0	0.47
94	B-ICC090	Supersition Hills, 11/24/87	6.6	El Centro Imp. Co. Cent	090	18.2	D	0.258	40.9	0.16	20.1	1.0	2.41
95	B-PTS225	Supersition Hills, 11/24/87	6.6	Parachute Test Site	225	1.0	D	0.455	112.0	0.25	52.8	1.0	2.22
96	TAB-LN	Tabas-Iran, 09/16/78	7.5	Tabas	LN	2.1	A	0.836	97.8	0.12	38.7	1.0	1.54

<sup>1</sup> CD: Closest distance to fault rupture

<sup>2</sup> Site Geology based on the third letter of Geomatrix's classification

A = Rock. Instrument on rock ( $V_s > 600$  m/sec) or < 5m of soil over rock, B = Shallow (stiff) soil. Instrument on/in soil profile up to 20m thick overlying rock.

C = Deep narrow soil. Instrument on/in soil profile at least 20m thick overlying rock, in a narrow canyon or valley no more than several km wide.

D = Deep broad soil. Instrument on/in soil profile at least 20m thick overlying rock, in a broad valley, E = Soft deep soil. Instrument on/in deep soil profile with

average  $V_s < 150$  m/sec.

<sup>3</sup> T<sub>p</sub>: Pulse period

Table 4.2 Ordinary ground motion properties

#	G-M Code	Earthquake	Mw	Station	Component	CD <sup>1</sup> (km)	Site <sup>2</sup> Geology	PGA (g)	PGV (cm/sec)	PGV / PGA (sec)	PGD (cm)	Scale
1	RI0360	Cape Mendocino, 04/25/92	7.0	Rio Dell Overpass - FF	360	14.3	C	0.549	41.9	0.08	19.5	1.0
2	CHY006-N	Chi-Chi, 09/20/99	7.6	CHY006	N	9.8	B	0.345	42.8	0.13	15.2	1.0
3	CHY028-W	Chi-Chi, 09/20/99	7.6	CHY028	W	3.1	A	0.653	72.8	0.11	14.7	1.0
4	TCU084-N	Chi-Chi, 09/20/99	7.6	TCU084	N	11.2	A	0.417	45.6	0.11	21.3	1.0
5	TCU122-N	Chi-Chi, 09/20/99	7.6	TCU122	N	9.4	D	0.261	34.1	0.13	36.1	1.0
6	WNT-E	Chi-Chi, 09/20/99	7.6	WNT	E	1.8	D	0.958	68.8	0.07	31.1	1.0
7	WNT-N	Chi-Chi, 09/20/99	7.6	WNT	N	1.8	D	0.626	42.0	0.07	18.8	1.0
8	BOL000	Duzce, 11/12/99	7.1	Bolu	000	12.0	D	0.728	56.4	0.08	23.1	1.0
9	ELC180	Imperial Valley 05/19/40	6.9	117 El Centro Array #9	180	8.3	D	0.313	29.8	0.10	13.3	2.0
10	H-BCR140	Imperial Valley, 10/15/79	6.5	Bonds Corner	140	2.7	D	0.588	45.2	0.08	16.8	1.0
11	H-BCR230	Imperial Valley, 10/15/79	6.5	Bonds Corner	230	2.7	D	0.775	45.9	0.06	15.0	1.0
12	H-BRA315	Imperial Valley, 10/15/79	6.5	Brawley Airport	315	10.4	D	0.220	38.9	0.18	13.5	1.0
13	H-CXO225	Imperial Valley, 10/15/79	6.5	Calixto Fire Station	225	10.5	D	0.275	21.2	0.08	9.0	1.0
14	H-CXO315	Imperial Valley, 10/15/79	6.5	Calixto Fire Station	315	10.5	D	0.202	16.0	0.08	9.2	1.0
15	H-E02140	Imperial Valley, 10/15/79	6.5	El Centro Array #2	140	15.3	D	0.315	31.5	0.10	14.3	1.0
16	H-E07140	Imperial Valley, 10/15/79	6.5	El Centro Array #7	140	0.6	D	0.338	47.6	0.14	24.7	1.0
17	H-E08140	Imperial Valley, 10/15/79	6.5	El Centro Array #8	140	3.9	D	0.602	54.2	0.09	32.3	1.0
18	H-E11140	Imperial Valley, 10/15/79	6.5	El Centro Array #11	140	12.5	D	0.364	34.4	0.10	16.1	1.0
19	H-E11230	Imperial Valley, 10/15/79	6.5	El Centro Array #11	230	12.5	D	0.380	42.1	0.11	18.6	1.0
20	H-ECC002	Imperial Valley, 10/15/79	6.5	EC County Center FF	002	7.3	D	0.213	37.5	0.18	16.0	1.0
21	H-PTS315	Imperial Valley, 10/15/79	6.5	Parachute Test Site	315	12.7	D	0.204	16.1	0.08	10.0	1.0
22	KBU090	Kobe, 01/16/95	6.9	Kobe University	090	0.9	A	0.311	34.2	0.11	7.2	1.0
23	IZT090	Kocaeli, 08/17/99	7.4	Izmit	090	7.2	A	0.220	29.8	0.14	17.1	1.0
24	IZT180	Kocaeli, 08/17/99	7.4	Izmit	180	7.2	A	0.152	22.6	0.15	9.8	1.0
25	LCN000	Landers, 06/28/92	7.3	Lucerne	000	1.1	A	0.785	31.9	0.04	16.4	1.0
26	YER270	Landers, 06/28/92	7.3	Yermo Fire Station	270	23.6	D	0.245	51.4	0.21	43.8	1.0
27	AND270	Loma Prieta, 10/18/89	7.0	Anderson Dam (Downstream)	270	21.4	D	0.244	20.3	0.08	7.7	1.0
28	AND360	Loma Prieta, 10/18/89	7.0	Anderson Dam (Downstream)	360	21.4	D	0.240	18.4	0.08	6.7	1.0
29	CLS000	Loma Prieta, 10/18/89	7.0	Corralitos	000	3.9	A	0.644	55.1	0.09	10.8	1.0
30	G02000	Loma Prieta, 10/18/89	7.0	Gilroy Array #2	000	13.7	D	0.367	32.9	0.09	7.2	1.0

Table 4.2 Ordinary ground motion properties (continued)

#	G/M Code	Earthquake	Mw	Station	Component	CD <sup>1</sup> (km)	Site <sup>2</sup> Geology	PGA (g)	PGV (cm/sec)	PGV / PGA (sec)	PGD (cm)	Scale
31	G03000	Loma Prieta, 10/18/89	7.0	Gilroy Array #3	000	13.0	D	0.555	35.7	0.07	8.3	1.0
32	G04000	Loma Prieta, 10/18/89	7.0	Gilroy Array #4	000	14.3	D	0.417	38.8	0.09	7.1	1.0
33	G04090	Loma Prieta, 10/18/89	7.0	Gilroy Array #4	090	14.3	D	0.212	37.9	0.18	10.1	1.0
34	GGB270	Loma Prieta, 10/18/89	7.0	Golden Gate Bridge	270	79.8	A	0.233	38.1	0.17	11.4	1.0
35	GIL067	Loma Prieta, 10/18/89	7.0	Gilroy - Gavilan Coll.	067	14.8	B	0.357	28.6	0.08	6.4	1.0
36	GIL337	Loma Prieta, 10/18/89	7.0	Gilroy - Gavilan Coll.	337	14.8	B	0.325	22.2	0.07	4.6	1.0
37	LOB000	Loma Prieta, 10/18/89	7.0	UCSC Lick Observatory	000	18.4	A	0.450	18.7	0.04	3.8	1.0
38	LOB090	Loma Prieta, 10/18/89	7.0	UCSC Lick Observatory	090	18.4	A	0.395	17.5	0.05	5.0	1.0
39	STG000	Loma Prieta, 10/18/89	7.0	Saratoga - Aloha Ave	000	8.5	D	0.513	41.2	0.08	16.2	1.0
40	WVC270	Loma Prieta, 10/18/89	7.0	Saratoga - W Valley Coll.	270	9.3	D	0.332	61.5	0.19	36.3	1.0
41	AND250	Morgan Hill, 04/24/84	6.1	Anderson Dam (Downstream)	250	3.3	D	0.423	25.3	0.06	4.6	1.0
42	AND340	Morgan Hill, 04/24/84	6.1	Anderson Dam (Downstream)	340	3.3	D	0.289	27.6	0.10	6.3	1.0
43	CYC195	Morgan Hill, 04/24/84	6.1	Coyote Lake Dam (SW Abut)	195	0.5	A	0.711	51.6	0.07	12.0	1.0
44	G04270	Morgan Hill, 04/24/84	6.1	Gilroy Array #4	270	5.7	D	0.224	19.3	0.09	4.3	1.0
45	G04360	Morgan Hill, 04/24/84	6.1	Gilroy Array #4	360	5.7	D	0.348	17.4	0.05	3.1	1.0
46	G06000	Morgan Hill, 04/24/84	6.1	Gilroy Array #6	000	9.9	A	0.222	11.4	0.05	2.5	1.0
47	G06090	Morgan Hill, 04/24/84	6.1	Gilroy Array #6	090	9.9	A	0.292	36.7	0.13	6.1	1.0
48	NPS300	N. Palm Springs, 07/08/86	6.2	North Palm Springs	300	4.0	D	0.694	33.8	0.05	3.9	1.0
49	CNP106	Northridge, 01/17/94	6.7	Canoga Park - Topanga Can	106	14.7	D	0.356	32.1	0.09	9.1	1.0
50	GRN270	Northridge, 01/17/94	6.7	San Gabriel - E Grand Ave	270	41.7	A	0.256	9.7	0.04	2.8	1.0
51	HOL090	Northridge, 01/17/94	6.7	LA - Hollywood Stor FF	090	25.5	D	0.231	18.2	0.08	4.8	1.0
52	HOL360	Northridge, 01/17/94	6.7	LA - Hollywood Stor FF	360	25.5	D	0.358	27.4	0.08	3.0	1.0
53	LOS000	Northridge, 01/17/94	6.7	Canyon Country - W Lost Cany	000	12.4	C	0.410	43.0	0.11	11.7	1.0
54	MTW000	Northridge, 01/17/94	6.7	Mt Wilson - CIT Seis Sta	000	35.9	A	0.234	7.3	0.03	0.7	1.0
55	NWH090	Northridge, 01/17/94	6.7	Newhall - Fire Sta	090	5.9	D	0.583	74.9	0.13	17.7	1.0
56	ORR090	Northridge, 01/17/94	6.7	Castaic - Old Ridge Route	090	20.7	B	0.568	51.8	0.09	9.0	1.0
57	ORR360	Northridge, 01/17/94	6.7	Castaic - Old Ridge Route	360	20.7	B	0.514	52.0	0.10	15.3	1.0
58	PKC090	Northridge, 01/17/94	6.7	Pacoima Kagel Canyon	090	7.3	B	0.301	31.3	0.11	11.2	1.0
59	PKC360	Northridge, 01/17/94	6.7	Pacoima Kagel Canyon	360	7.3	B	0.433	51.2	0.12	8.0	1.0
60	STM090	Northridge, 01/17/94	6.7	Santa Monica City Hall	090	26.5	D	0.883	41.6	0.05	15.0	1.0

Table 4.2 Ordinary ground motion properties (continued)

#	GM Code	Earthquake	Mw	Station	Component	CD <sup>1</sup> (km)	Site <sup>2</sup> Geology	PGA (g)	PGV (cm/sec)	PGV/PGA (sec)	PGD (cm)	Scale
61	STM360	Northridge, 01/17/94	6.7	Santa Monica City Hall	360	26.5	D	0.370	25.1	0.07	7.2	1.0
62	WST000	Northridge, 01/17/94	6.7	LA - N Westmoreland	000	29.0	D	0.404	20.9	0.05	2.3	1.0
63	WST270	Northridge, 01/17/94	6.7	LA - N Westmoreland	270	29.0	D	0.362	20.9	0.06	4.3	1.0
64	B-ICC000	Superstition Hills, 11/24/87	6.6	El Centro Imp. Co. Cent	000	18.2	D	0.358	46.4	0.13	17.6	1.0
65	B-PTS315	Superstition Hills, 11/24/87	6.6	Parachute Test Site	315	1.0	D	0.377	43.9	0.12	15.3	1.0
66	TAB-TR	Tabas-Iran, 09/16/78	7.5	Tabas	TR	2.1	A	0.852	121.2	0.15	95.0	1.0

<sup>1</sup> CD: Closest distance to fault rupture

<sup>2</sup> Site geology based on the third letter of Geomatrix's classification

A = Rock. Instrument on rock ( $V_s > 600$  m/sec) or  $< 5$  m of soil over rock, B = Shallow (stiff) soil. Instrument on/in soil profile up to 20m thick overlying rock.

C = Deep narrow soil. Instrument on/in soil profile at least 20m thick overlying rock, in a narrow canyon or valley no more than several km wide.

D = Deep broad soil. Instrument on/in soil profile at least 20m thick overlying rock, in a broad valley, E = Soft deep soil. Instrument on/in deep soil profile with average  $V_s < 150$  m/sec.

Moment magnitudes of the earthquakes are plotted against the closest distances to the fault rupture in Figure 4.1. It is observed that the closest distances to fault rupture for the stations of pulse type ground motions are all less than 20 km, therefore they can also be designated as near-fault ground motions. Closest distances to fault rupture for the stations of most of the ordinary ground motions are also less than 20 km, however these ground motions do not contain any pulses. This is the reason why the ground motions are classified as pulse type and ordinary, and not as near-fault and far-fault.

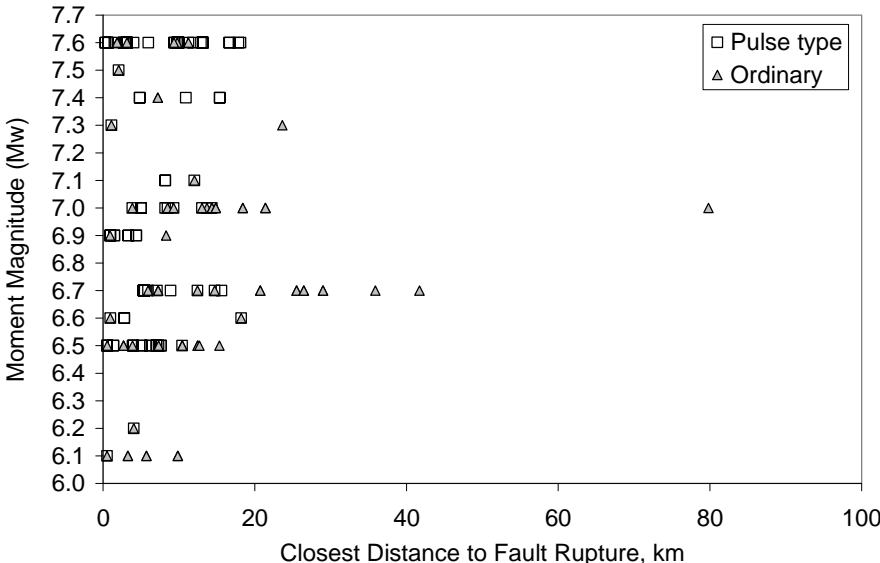


Figure 4.1 Moment magnitude plotted against the closest distance to fault rupture for the utilized ground motions

Acceleration, velocity and displacement traces of a sample ground motion from the pulse type ground motion set are presented in Figure 4.2. The ground motion is from the 1999 Chi-Chi earthquake, during which a lot of pulse type ground motions were recorded. It is labeled as TCU052-W in Table 4.1. Significant pulses can be observed both in the velocity and displacement traces. Pulse period ( $T_p$ ), which is defined as the duration of the largest amplitude pulse in the velocity

trace, is also indicated in this figure. Pulse periods of all the pulse type ground motions are presented in Table 4.1 and plotted against the moment magnitude of the earthquakes in Figure 4.3.

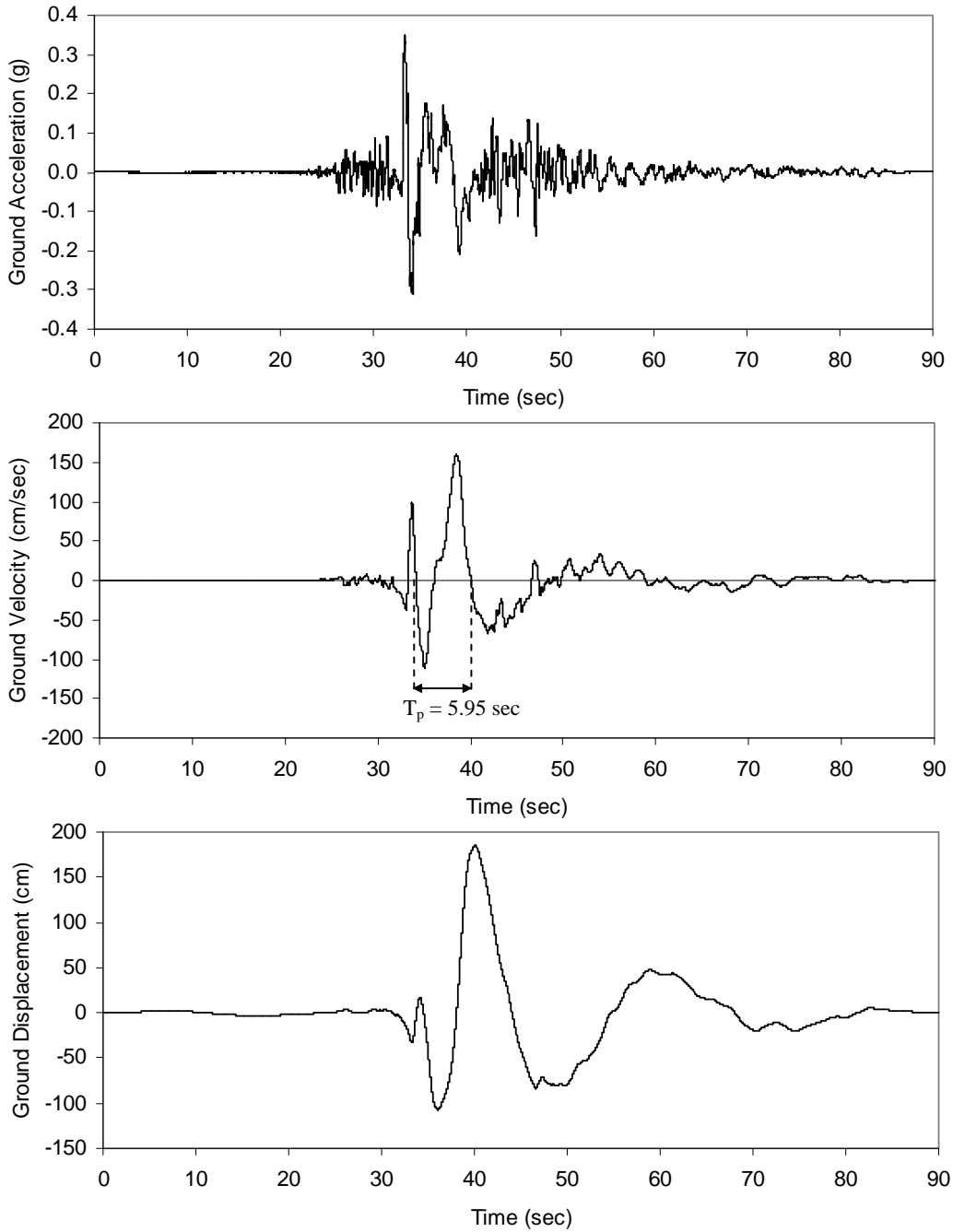


Figure 4.2 Ground acceleration, velocity and displacement traces of a pulse type ground motion (TCU052-W)

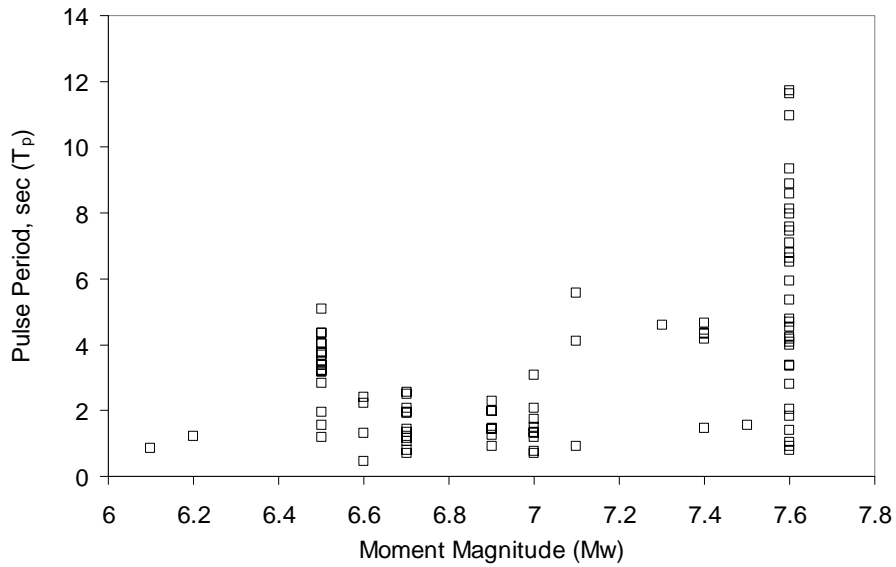


Figure 4.3 Pulse period plotted against moment magnitude for the utilized pulse type ground motions

Investigating Figure 4.3, it is noted that the pulse periods of the utilized pulse type ground motions are generally long. Most of the long pulse period ground motions are from the 1999 Chi-Chi earthquake, which has a moment magnitude of 7.6. The effect of pulses on the structures has been extensively studied in the past, two examples of which are the work of Alavi and Krawinkler (2004) and Kalkan and Kunnath (2006) among others. Investigation of the effect of pulses is beyond the scope of this study, therefore it is not considered in the following case study chapters.

Acceleration, velocity and displacement traces of a sample ground motion from the ordinary ground motion set are presented in Figure 4.4. The ground motion is from the Loma Prieta (1989) earthquake, labeled as LOB000 in Table 4.2.

Peak ground acceleration (PGA), peak ground velocity (PGV) and PGV/PGA ratios of the considered ground motions are plotted in Figure 4.5. Mean values are also indicated in these figures. It can be observed that the differences between the PGA values of pulse type and ordinary ground motions are not significant, however PGV of the pulse type ground motions are greater than those of the ordinary ground

motions. Consequently, PGV/PGA ratios of the pulse-type ground motions are greater than those of the ordinary ground motions.

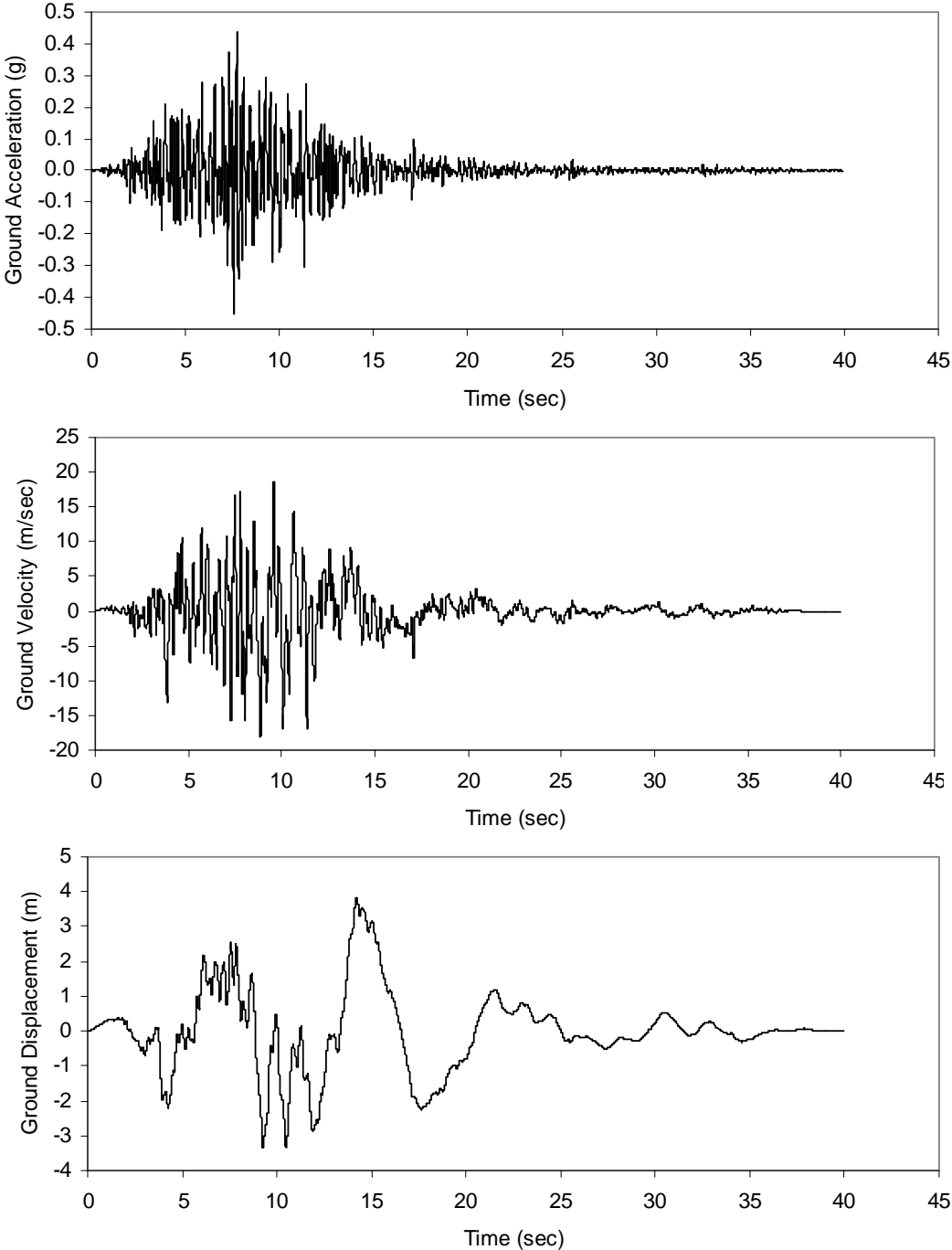


Figure 4.4 Ground acceleration, velocity and displacement traces of an “ordinary” ground motion (LOB000)

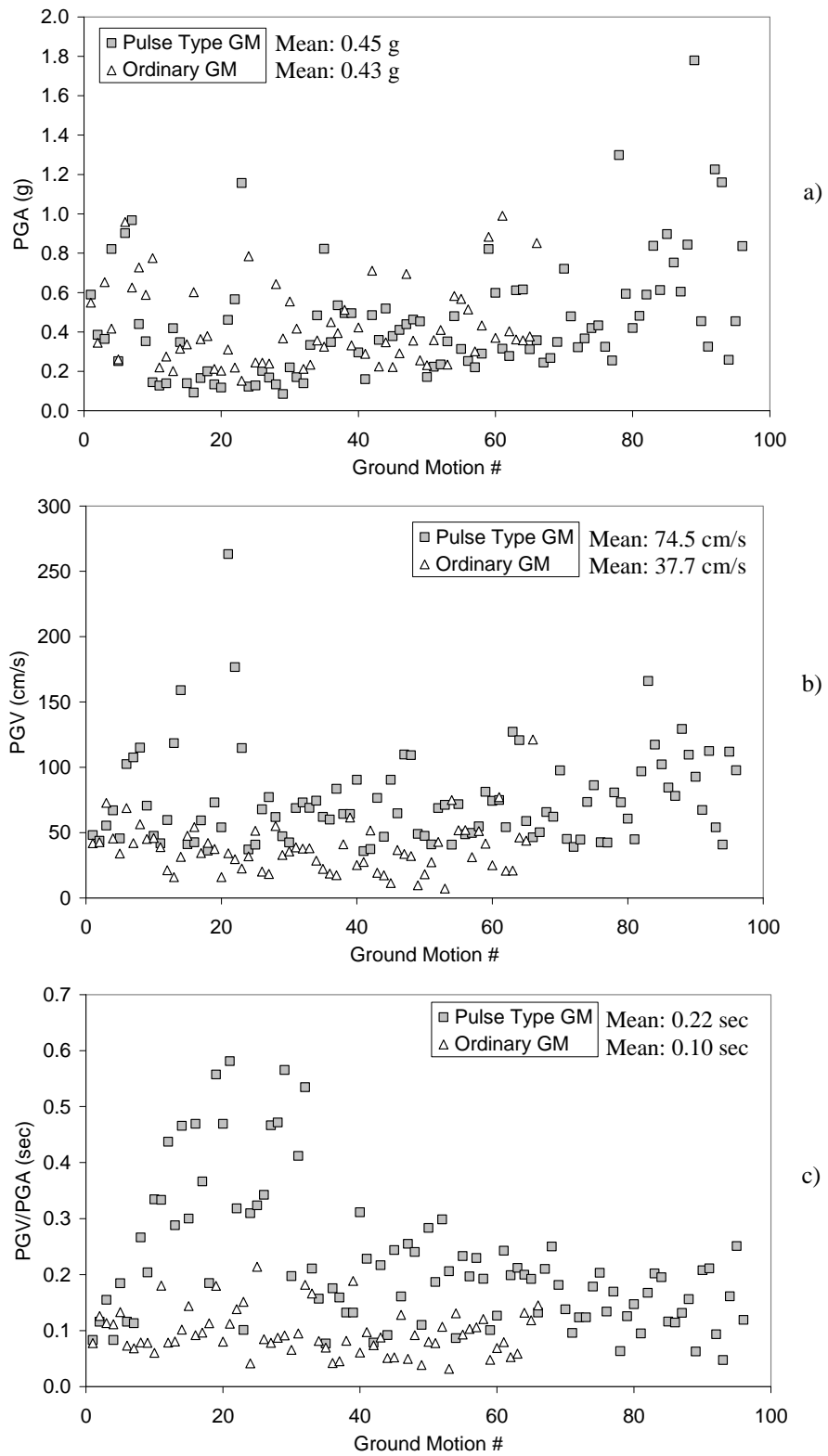


Figure 4.5 a) PGA, b) PGV, c) PGV/PGA ratios of the considered ground motions

## **CHAPTER 5**

### **CASE STUDY I: TWELVE STORY RC PLANE FRAME**

#### **5.1 Description of the Building**

The first case study is a twelve story reinforced concrete building with the floor plan shown in Figure 5.1. The building is designed according to the regulations of TS-500 (2000) and TEC (1998) in accordance with the capacity design principles. An enhanced ductility level ( $R=8$ ) is assumed for the building. It is located in seismic zone 1 and the site class is Z3. Concrete and steel grades are C25 and S420 respectively. Slab thickness for all floors is 14 cm and live load is  $3.5 \text{ kN/m}^2$ . Dimensions of the beams at the first four, the second four and the last four stories are  $30 \times 55$ ,  $30 \times 50$  and  $30 \times 45 \text{ cm}^2$  respectively, whereas dimensions of the columns at the first four, the second four and the last four stories are  $60 \times 60$ ,  $55 \times 55$  and  $50 \times 50 \text{ cm}^2$  respectively. There is no basement, height of the ground story is 4 m while the height of all other stories is 3.2 m. A plane model consisting of Frames A and B is constructed for the analysis of the building (Figure 5.2).

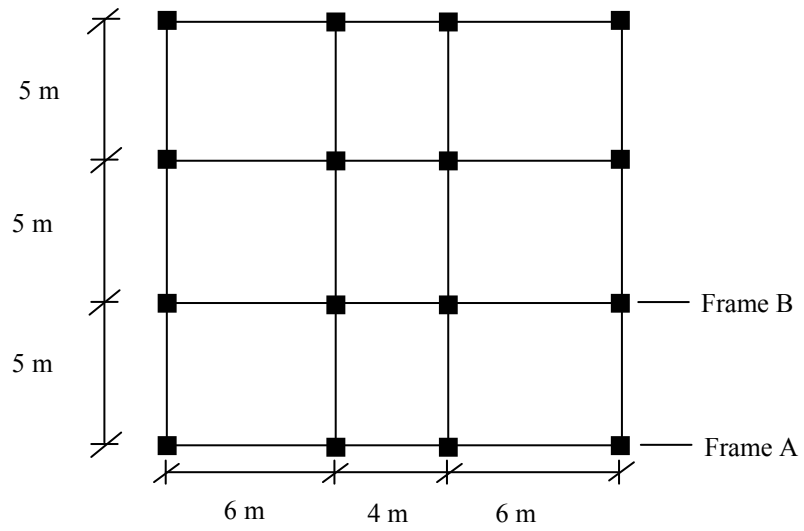


Figure 5.1 Story plan of the twelve story building

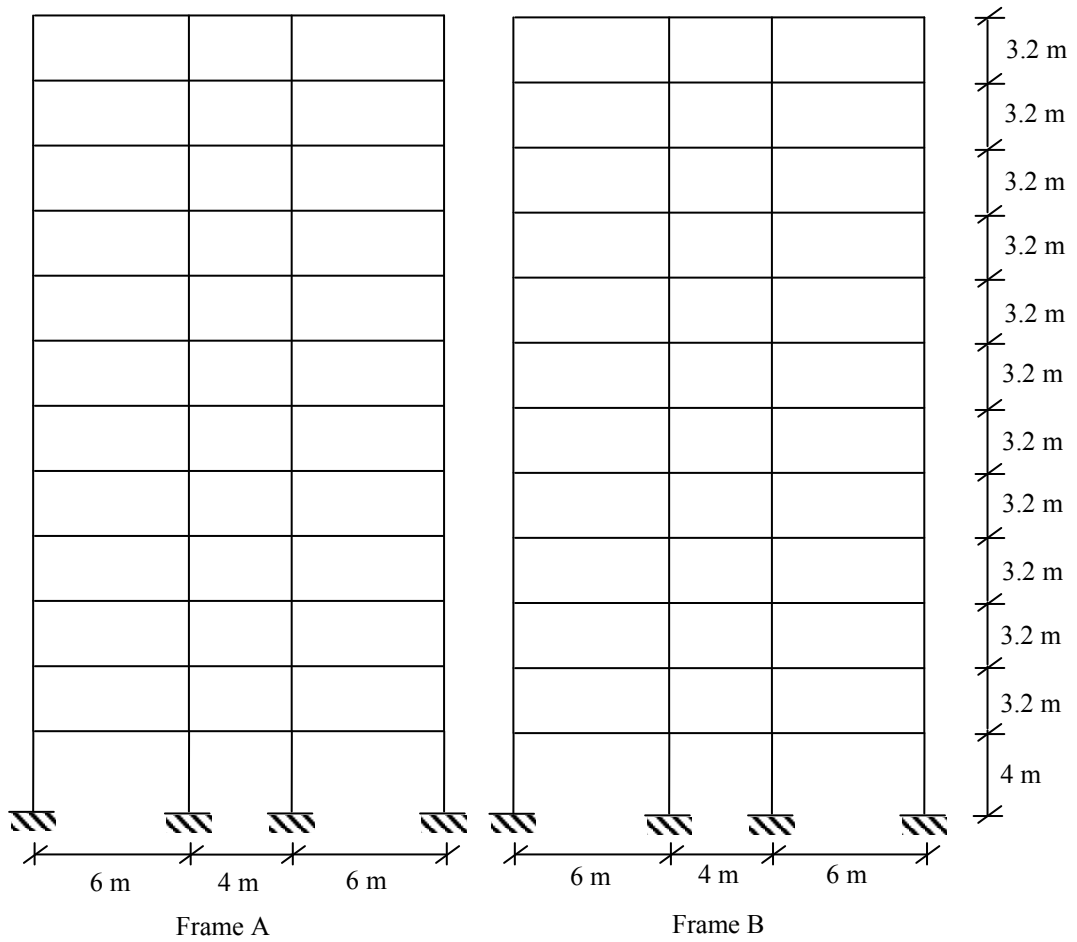


Figure 5.2 Plane model of the twelve story building

## 5.2 Modeling

The plane frame is modeled by using the nonlinear analysis software Drain-2DX (Allahabadi, 1987, Prakash et al., 1993, Powell, 1993). All required nonlinear and linear analyses are conducted with this software.

The frame members are modeled by utilizing the “Plastic Hinge Beam-Column” element. In the formulation of this element, inelasticity is restricted to the lumped flexural plastic hinges at the member ends. Bilinear moment-curvature relationships are utilized to consider the inelasticity at the plastic hinges (Figure 5.3). Drain-2DX software does not define an ultimate curvature value in the moment-curvature relationships. Yield moment - axial force interaction diagrams are employed for the columns. Stiffness formulation of Drain-2DX for the aforementioned element is briefly explained in Appendix A.

In bilinear representation of moment-curvature relationship, it is not possible to consider cracking during the solution process. Hence, cracked section stiffness is employed for the initial line segment of the moment-curvature relations shown in Figure 5.3. In order to employ cracked section stiffness, gross moments of inertia are multiplied with 0.6 and 0.5 for the columns and beams, respectively.

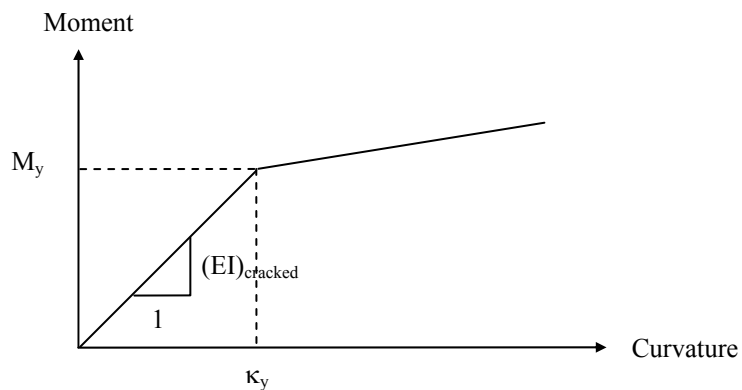


Figure 5.3 Bilinear moment-curvature relation utilized in Drain-2DX

Lateral degrees of freedom are assigned at the story levels in line with the rigid floor diaphragm assumption. P-Δ effects are not considered in the analyses. In both linear and nonlinear response history analyses, Rayleigh damping is assumed with the coefficients obtained from 1<sup>st</sup> and 3<sup>rd</sup> mode periods.

### 5.3 Free Vibration Properties

Free vibration properties for the first three modes of the twelve story frame model are summarized in Table 5.1. Modal static force distributions  $\mathbf{s}_n$  (Chopra, 2001, Equation 5.1) are presented in Figure 5.4 for the first three modes. Although the effect of higher modes may not be apparent when effective modal mass ratios are considered, it can be clearly seen from the force distributions in Figure 5.4 that the second mode and even the third mode have considerable effects on the response in the elastic range, considering that the response accelerations of second and third modes are usually significantly higher than the first mode response acceleration.

Table 5.1 Free vibration properties of the twelve story frame model

Mode	T (sec)	Effective modal mass (tons)	Effective modal mass ratio	$\Gamma_n \phi_{nr}^{(1)}$
1	1.95	1047.72	0.777	1.365
2	0.70	168.55	0.125	0.559
3	0.40	60.68	0.045	0.309

<sup>(1)</sup> Modal participation factor multiplied with the top story modal amplitude

$$\mathbf{s}_n = \Gamma_n \mathbf{m} \boldsymbol{\phi}_n \quad (5.1)$$

In Equation 5.1,  $\Gamma_n$  is the n<sup>th</sup> modal participation factor,  $\mathbf{m}$  is the mass matrix and  $\boldsymbol{\phi}_n$  is the n<sup>th</sup> mode vector.

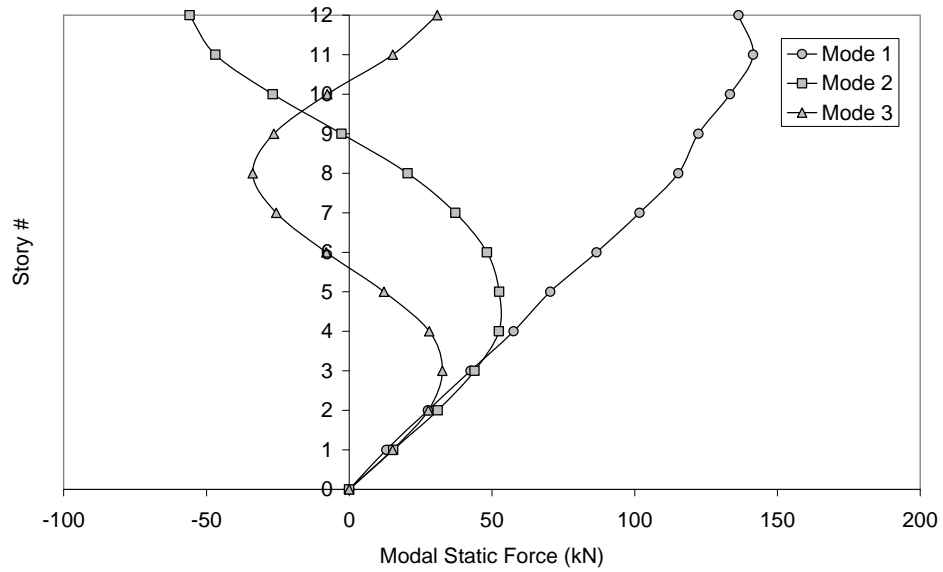


Figure 5.4 Modal static force distributions  $s_n$  for the first three modes

#### 5.4 Presentation of Results

Maximum values of roof displacements, story displacements, interstory drift ratios and chord rotations are obtained for each ground motion included in the two ground motion sets described in Chapter 4. The results from nonlinear response history analysis (NRHA), modal pushover analysis (MPA), modal pushover analysis conducted by considering the response due to only the first mode (MPA-1), conventional pushover analysis according to FEMA-356 (PO-FEMA), two variants of the equivalent linearization procedure described in Chapter 3 (EQL-NL, EQL-ED), linear elastic response spectrum analysis (RSA) and linear elastic response history analysis (LRHA) are presented comparatively. The methods will be referred with the abbreviations in the brackets in the remaining part of the thesis. A force distribution proportional to the multiplication of the first mode shape and the mass matrix is utilized as the lateral load pattern for PO-FEMA; therefore MPA-1 and PO-FEMA are the same for 2D analysis except the difference in the calculation of roof displacement demands. PO-FEMA calculates roof displacement

demand from the elastic spectral displacement of the first mode multiplied by a series of coefficients to account for nonlinearity (Coefficient Method), while MPA-1 calculates the roof displacement demand from the maximum displacement of an equivalent inelastic SDOF system as explained in Chapter 2.

#### 5.4.1 Description of Statistical Error Parameters

Three parameters are utilized in order to summarize the response statistics. The first parameter is the median ( $x_m$ ), defined with Equation 5.2.

$$x_m = \exp\left(\frac{\sum_{i=1}^n \ln x_i}{n}\right) \quad (5.2)$$

In Equation 5.2,  $n$  is the total number of data and  $x_i$  is the  $i^{\text{th}}$  individual data.  $x_i$  can be a response parameter obtained from nonlinear response history analysis or from one of the approximate methods. It can also be a normalized value which is obtained by dividing the considered response parameter found from an approximate method by the one calculated with nonlinear response history analysis.

The second statistical parameter is the standard deviation  $\sigma$  in Equation 5.3.

$$\sigma = \sqrt{\left(e^{\delta^2} - 1\right)} \cdot \mu^2 \quad (5.3)$$

where

$$\mu = x_m \cdot e^{\frac{1}{2} \cdot \delta^2} \quad (5.4)$$

and

$$\delta = \left(\frac{\sum_{i=1}^n (\ln x_i - \ln x_m)^2}{(n-1)}\right)^{0.5} \quad (5.5)$$

$\mu$  in Equation 5.4 is the mean value of a lognormal variable and  $\delta$  in Equation 5.5 is the dispersion (Benjamin and Cornell, 1970).

Median is often used to indicate the central value of a log-normal variable. Standard deviation defined in Equation 5.3 also belongs to a variable sampled from lognormal distribution (Ang and Tang, 1975). Lognormal distribution is suitable for the maximum values of earthquake response parameters since they are always positive.

Median and standard deviation are good indicators for evaluating the accuracy of the approximate methods with respect to the nonlinear response history analysis, which is used as benchmark. However, since these two parameters may result in different combinations (median may be close to 1 whereas dispersion may be high or vice versa), a third parameter, root mean square error (RMSE), is utilized for comparing the relative accuracy of approximate methods (Equation 5.6).

$$\text{RMSE} = \frac{\left( \frac{\sum_{i=1}^n (x'_i - x_i)^2}{n} \right)^{0.5}}{x_m} \quad (5.6)$$

In Equation 5.6,  $x'_i$  is the response parameter obtained from the approximate method,  $x_i$  is the response parameter obtained from nonlinear response history analysis and  $x_m$  is the median for  $x$ . The numerator can be interpreted as the average error. Actually, numerator is sufficient in order to evaluate the accuracy of the approximate methods with respect to each other. It is divided by the median here for normalization. Thus the error is represented as a percentage. It should be noted that RMSE can take values greater than 1.0.

#### 5.4.2 Roof (Top Story) Displacement Demands

Roof displacement demands calculated from the approximate methods are plotted against those obtained from nonlinear response history analyses in Figures 5.5 and 5.6 for the 96 pulse type and 66 ordinary ground motions, respectively. In these figures, displacements are in meters. Calculated statistical parameters are summarized in Tables 5.2 and 5.3.

Table 5.2 Roof displacement statistics for pulse type ground motions

Method	Median (Method, meters)	Median (Method/NRHA)	Standard Deviation (Method/NRHA)	RMSE
LRHA	0.389	1.136	0.412	0.714
RSA	0.381	1.114	0.406	0.703
EQL-ED	0.370	1.080	0.392	0.688
PO-FEMA	0.380	1.111	0.423	0.710
MPA	0.381	1.113	0.150	0.265
MPA-1	0.376	1.099	0.158	0.260
EQL-NL	0.367	1.072	0.175	0.242
NRHA	0.342	-	-	-

Table 5.3 Roof displacement statistics for ordinary ground motions

Method	Median (Method, meters)	Median (Method/NRHA)	Standard Deviation (Method/NRHA)	RMSE
LRHA	0.171	1.146	0.184	0.364
RSA	0.161	1.078	0.193	0.323
EQL-ED	0.159	1.064	0.183	0.306
PO-FEMA	0.155	1.038	0.207	0.314
MPA	0.152	1.022	0.111	0.156
MPA-1	0.147	0.985	0.128	0.150
EQL-NL	0.154	1.036	0.131	0.168
NRHA	0.149	-	-	-

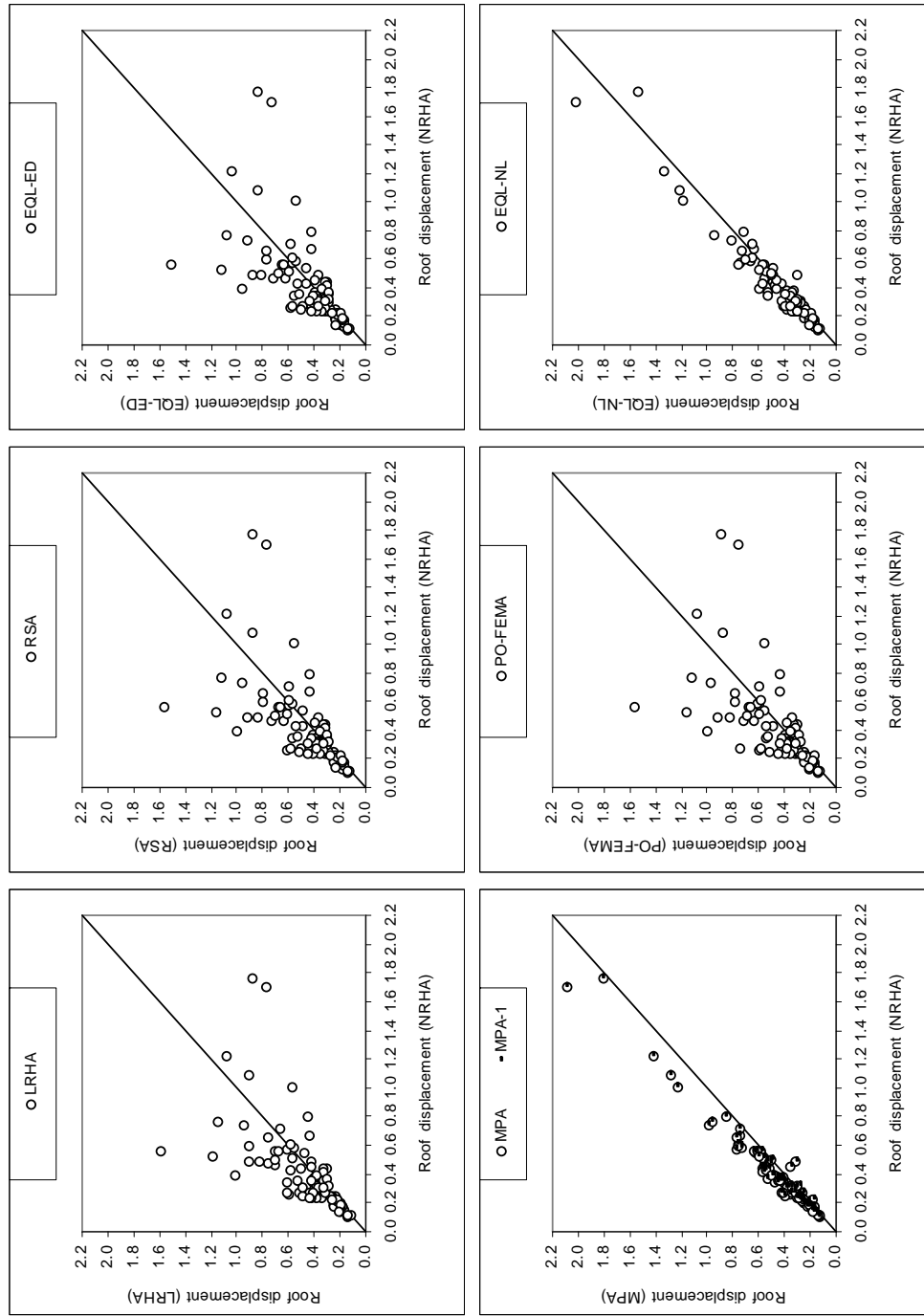


Figure 5.5 Comparison of the roof displacement demand predictions of approximate methods with the benchmark method (NRHA) for pulse type ground motions

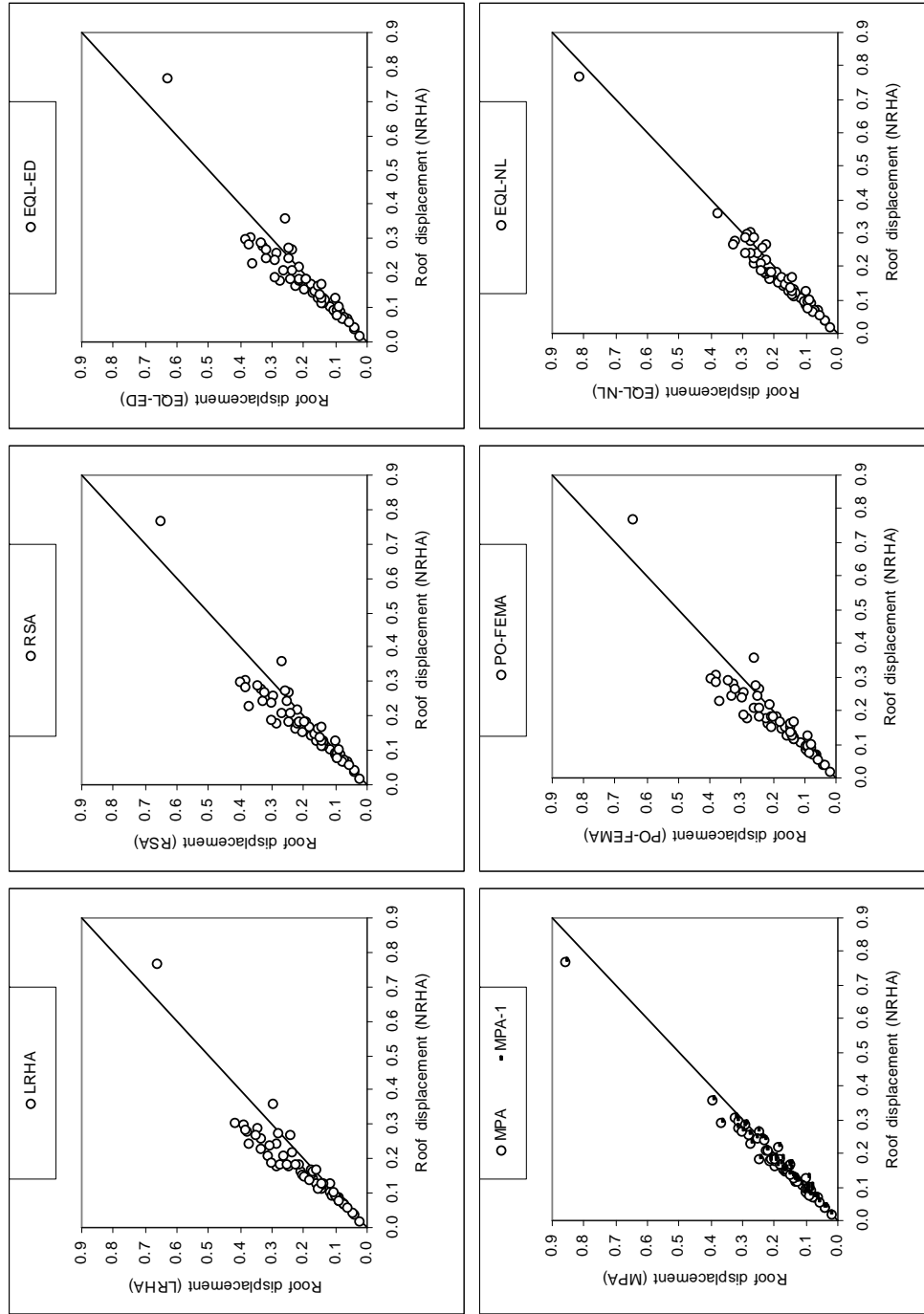


Figure 5.6 Comparison of the roof displacement demand predictions of approximate methods with the benchmark method (NRHA) for ordinary ground motions

When the roof displacement predictions for pulse type ground motions are considered, it can be noted that LRHA and RSA lead to erroneous estimations. EQL-NL is very successful in predicting the roof displacements. It greatly improves the predictions of RSA. Same observation is not valid for EQL-ED. Nonlinear roof displacement predictions of EQL-ED and PO-FEMA are very close to the roof displacement predictions of RSA for the considered case study building by virtue of the equal displacement assumption involved in EQL-ED and PO-FEMA and the dominance of the first mode response on the roof displacement. Roof displacement estimations of MPA and MPA-1 are very similar to each other and they are quite accurate estimations of NRHA.

Observations similar to those gathered from Figure 5.5 can be noted from Table 5.2. It is seen that RMSE of EQL-NL is smallest, those of MPA and MPA-1 are very close to this value whereas the RMSE of other methods are much higher. Regarding the differences in the roof displacement demand predictions of EQL-NL and EQL-ED and the success of MPA in the predictions, it is clear that the improvement in roof displacement prediction is due to considering inelastic response of SDOF systems instead of employing the equal displacement assumption.

Concerning the roof displacement predictions under ordinary ground motions, it is noted that they are much smaller with respect to those under pulse type ground motions. It was previously shown in Chapter 4 that the differences between the PGA values of pulse type and ordinary ground motions are not significant, however PGV of the pulse type ground motions are greater than those of the ordinary ground motions. In addition, pulse type ground motions contain strong velocity pulses. Therefore, it can be concluded that the pulses with high velocity peaks lead to the observed differences between the displacement demands of pulse type and ordinary ground motions. This observation is consistent with the findings of previous research (Alavi and Krawinkler, 2001).

The errors of LRHA and RSA in predicting the roof displacements under ordinary ground motions are not as large as those in the case of pulse type ground motions, which can be observed from Figure 5.6 and Table 5.3. Because the level of

nonlinearity is lower for ordinary ground motions with respect to the pulse type ground motions. EQL-NL improves RSA predictions and reduces the error to the half of RSA for ordinary ground motions. Improvement in the predictions can also be observed from Figure 5.6. Like the case of pulse type ground motions, LRHA, RSA, EQL-ED and PO-FEMA predictions are similar to each other. Estimations of MPA and MPA-1 are very close to each other and accurate as in the case of pulse type ground motions.

### 5.4.3 Local Response Parameters

Comparison of story displacements, interstory drift ratios, beam chord rotations and column chord rotations obtained from the previously mentioned analysis methods are presented in this section. For this purpose, ground motions producing NRHA roof displacements between 0.140 m (0.36 % roof drift) and 1.250 m (3.2 % roof drift) are taken into consideration. Lower bound corresponds to the onset of inelasticity. An upper bound is also set because P- $\Delta$  effects are not considered and ultimate curvature values are not utilized in the moment curvature relations. The number of pulse type and ordinary ground motions remaining in between the aforementioned bounds are 79 and 31, respectively. Roof displacement demands of these ground motions normalized by the building height are marked on the first mode pushover curve of the building in Figure 5.7. Roof displacements obtained from the pulse type ground motions cover a wider range and they are larger than those obtained from ordinary ground motions.

Base shear capacity prediction of the equivalent linearization procedure is also shown with a horizontal line in Figure 5.7. It can be observed that this value is close to the one obtained from pushover analysis. It should be noted that the maximum base shear values obtained from nonlinear response history analyses are different than the values on the pushover curve; therefore ordinates of the marked points in Figure 5.7 are not the actual values.

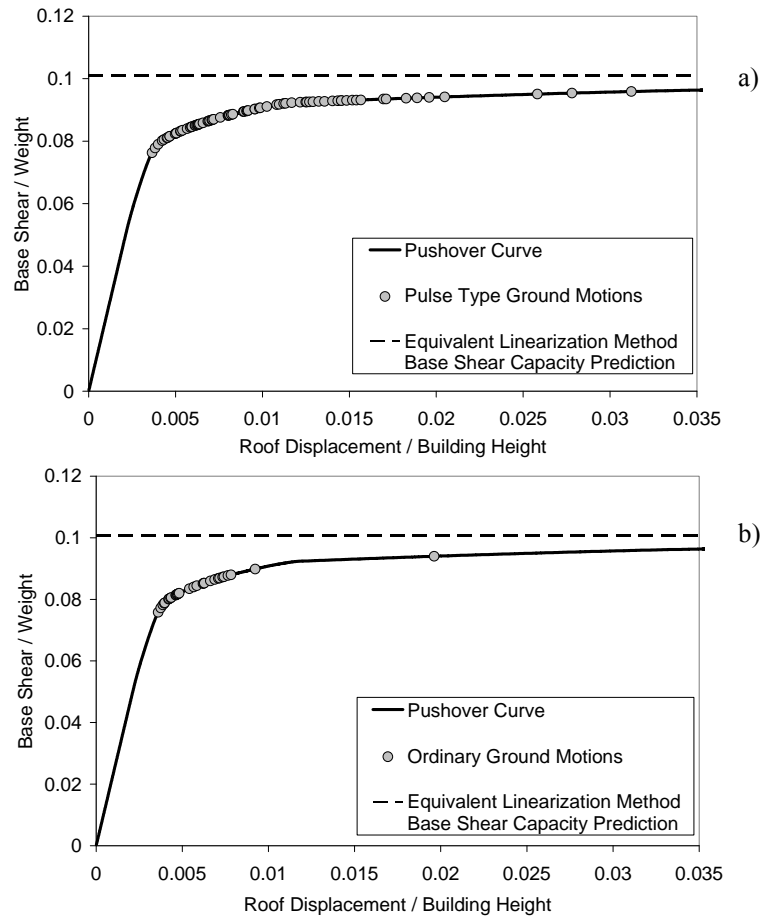


Figure 5.7 Roof displacement demands obtained from a) pulse type ground motions, b) ordinary ground motions marked on the first mode pushover curve

Pseudo acceleration and displacement response spectra of the 79 pulse type and 31 ordinary ground motions are plotted in Figures 5.8 and 5.9, respectively. It can be observed that the displacements and pseudo accelerations corresponding to the second and third mode periods can be regarded as similar for pulse type and ordinary ground motions, whereas those corresponding to the first mode period are much greater for pulse type ground motions with respect to the ordinary ground motions. This observation indicates that higher mode effects are more distinct in the elastic range for ordinary ground motions than the pulse type ground motions.

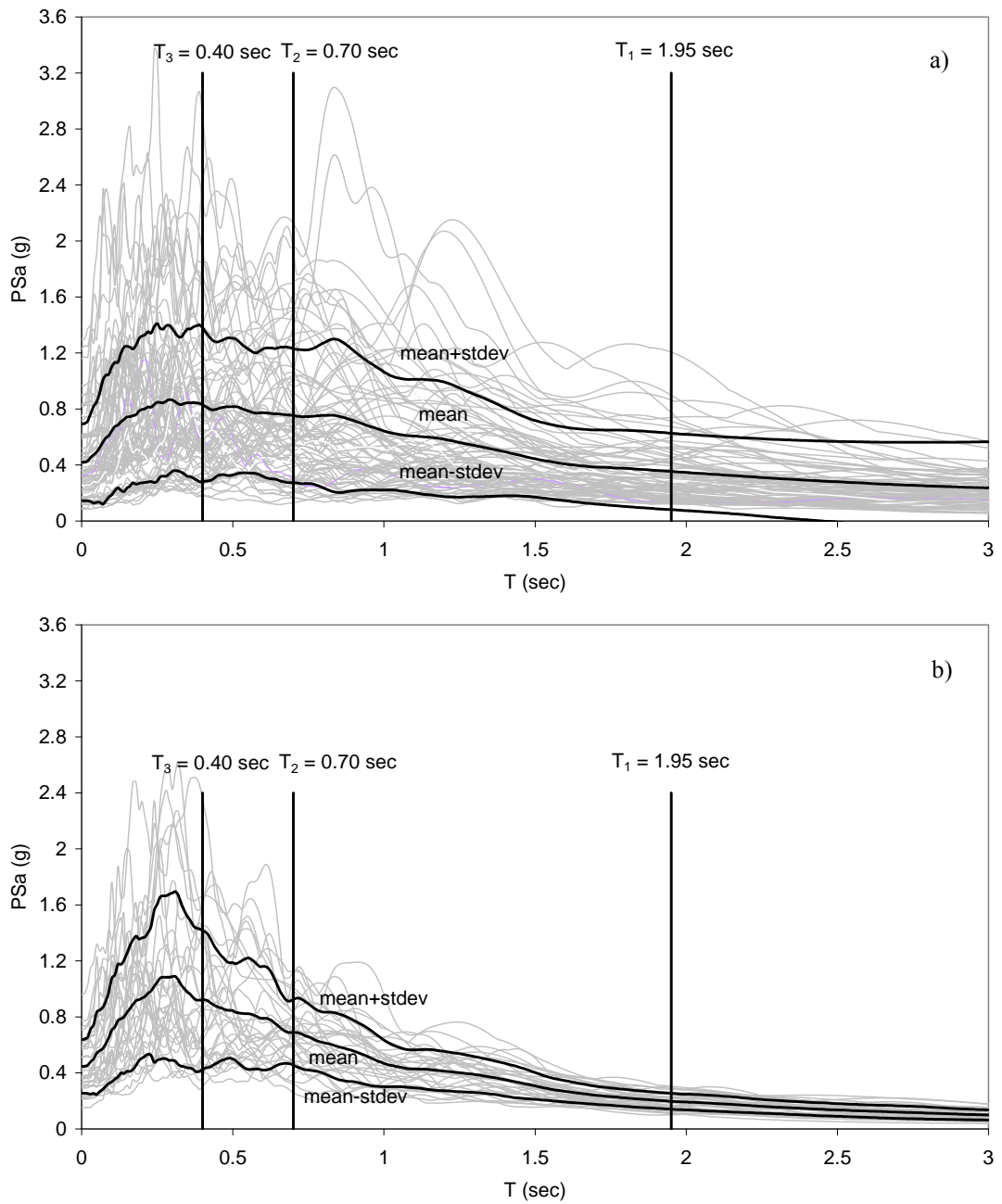


Figure 5.8 5% damped pseudo acceleration response spectra for a) pulse type, b) ordinary ground motions

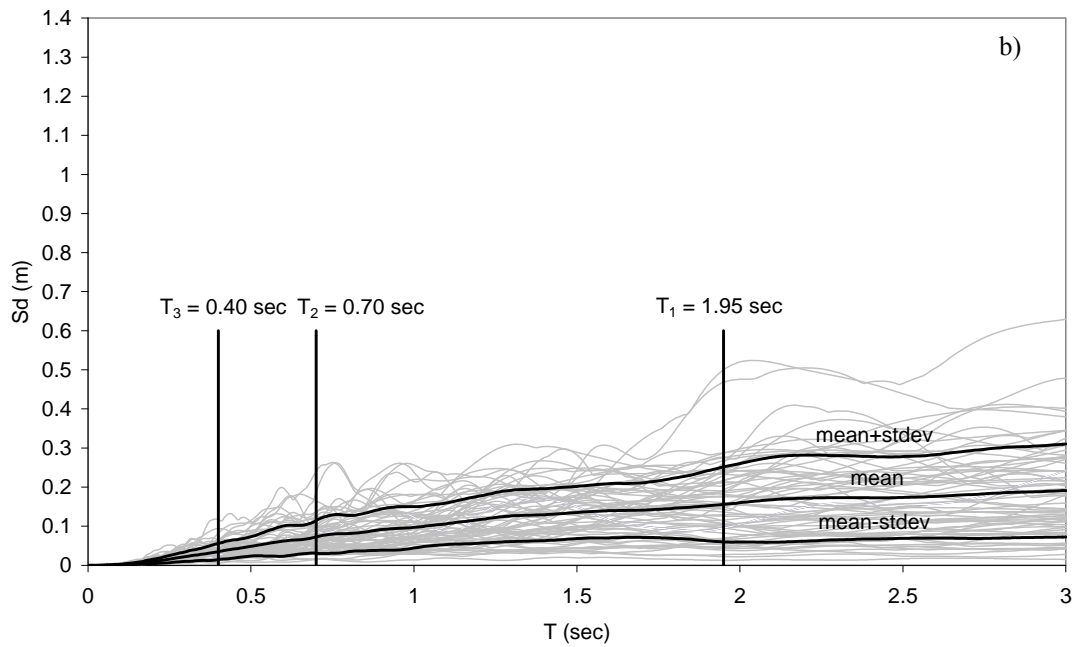
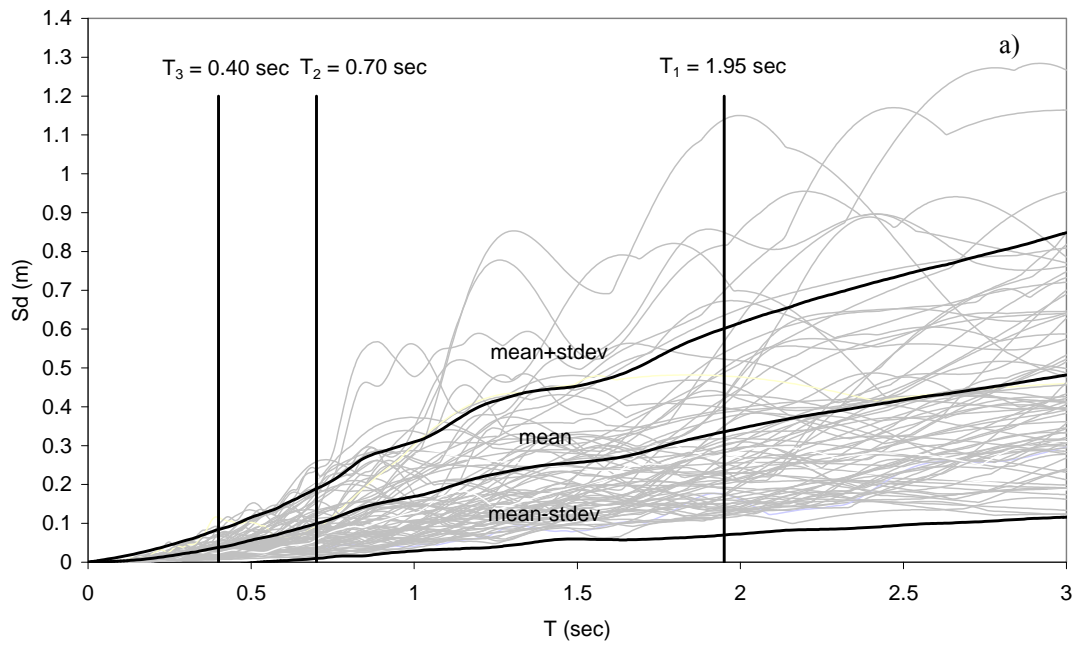


Figure 5.9 5% damped displacement response spectra for a) pulse type, b) ordinary ground motions

Roof displacement comparisons were presented in the previous section and it was observed that the roof displacement predictions of the approximate methods were generally larger than those of the benchmark method (NRHA) by different amounts ranging from 12 to 15 percent at the medial level. Although all of the considered approximate methods have their own ways of calculating a roof displacement demand, comparison of local response parameters is conducted such that each approximate method is assumed to calculate the same roof displacement with NRHA. The purpose for such an adjustment is to observe the accuracy of the approximate methods in estimating the distribution of local response parameters within the structure. Otherwise, as it will be demonstrated later, inaccurate calculation of roof displacements may result in accurate estimations of some local response parameters by coincidence. This comparison strategy was previously employed in FEMA-440 (ATC, 2005). In the case of equating the roof displacements of the approximate methods to that of NRHA, there remains no difference between the methods MPA-1 and PO-FEMA and small difference between EQL-NL and EQL-ED. Therefore, PO-FEMA and EQL-ED results are not presented for further evaluations. For equating the roof displacement to that of NRHA, first mode pushover analysis is conducted with a target displacement equal to the NRHA roof displacement in MPA-1. Modal displacements calculated by MPA, variants of the equivalent linearization procedure and RSA are scaled with the ratio of the NRHA roof displacement to the roof displacement predicted by the approximate method. Response parameters obtained from LRHA are multiplied with the ratio of the roof displacement demand of NRHA to that of LRHA.

Median and RMSE of story displacements, interstory drift ratios, beam chord rotations and column chord rotations obtained from the employed analysis methods are plotted in Figures 5.10-5.13 for pulse type ground motions. For each method and each ground motion, the maximum value of a response parameter is obtained, and then the statistical parameters are calculated for each method by using all the ground motions in the set. It should be noted that, for a ground motion, the maximum values of different response parameters are obtained at different times in response history analyses. Beam chord rotation at a story level indicates the average

of the chord rotations at the beam ends at a story level. Similarly, column bottom end chord rotation indicates the average of the chord rotations at the bottom ends of the columns at a story. Column top end chord rotations are not shown since upper ends of the columns remain in the elastic range and their median chord rotations do not exceed 0.0025 radians.

Interstory drift ratios obtained from the approximate methods divided by those obtained from NRHA are plotted in Figure 5.14 for pulse type ground motions. In this figure, each thin gray line corresponds to a ground motion and the thick gray lines indicate the median minus standard deviation, median and median plus standard deviation values. Beam chord rotations produce almost exactly the same figures, hence they are not presented herein. Following observations can be made from Figures 5.10-5.14.

- Equivalent linearization procedure significantly improves the response predictions of RSA. Improvement is substantial for the interstory drift ratios and beam chord rotations, those especially at the upper stories. RSA greatly overestimates the beam chord rotations and interstory drift ratios at the upper stories. Equivalent linearization procedure is successful in bringing these values closer to NRHA results.
- RMSE of column bottom end chord rotations of the first story obtained from RSA is reduced slightly by the equivalent linearization procedure. RMSE of the column bottom end chord rotations of the above stories do not possess a practical importance since they remain in the elastic range.
- Differences in the median and RMSE values of RSA and LRHA are due to the SRSS combination rule. In general, responses obtained from RSA and LRHA are similar (Figure 5.14). Therefore, errors resulting from SRSS combination can be considered to be at an acceptable level.

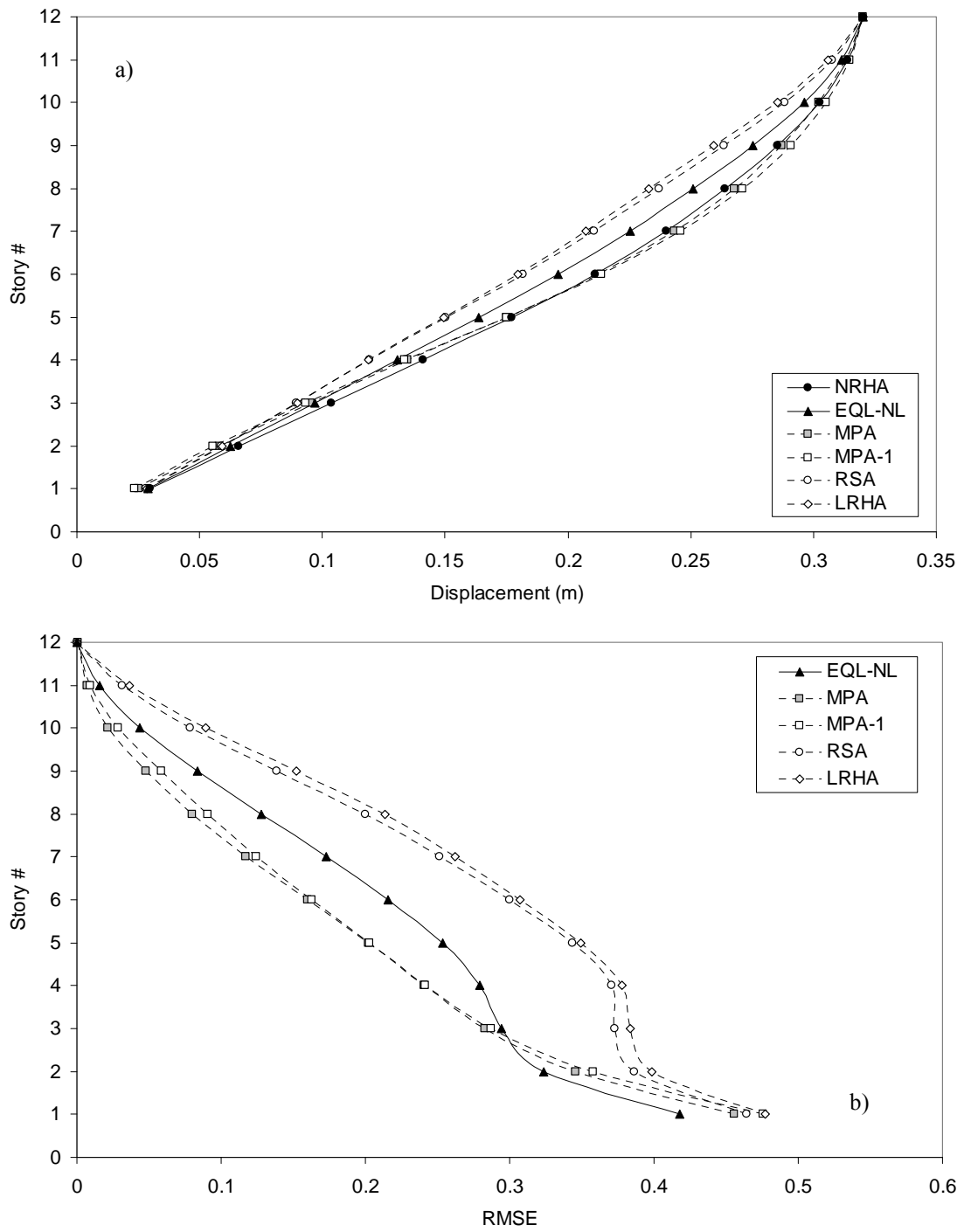


Figure 5.10 a) Median, b) RMSE of story displacements for pulse type ground motions

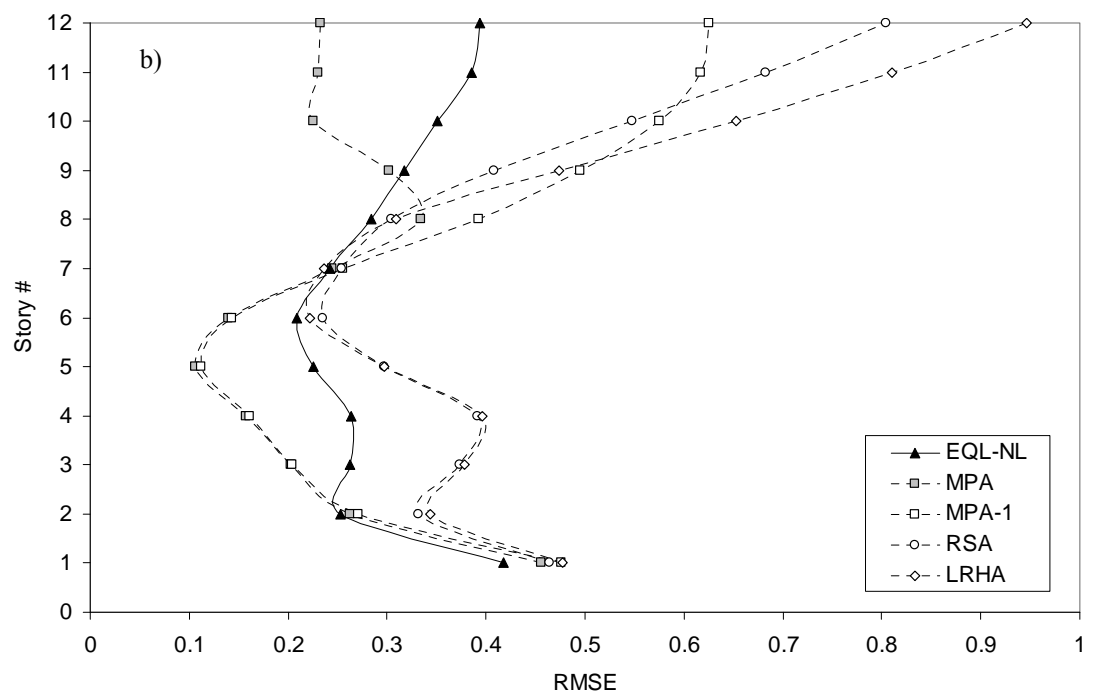
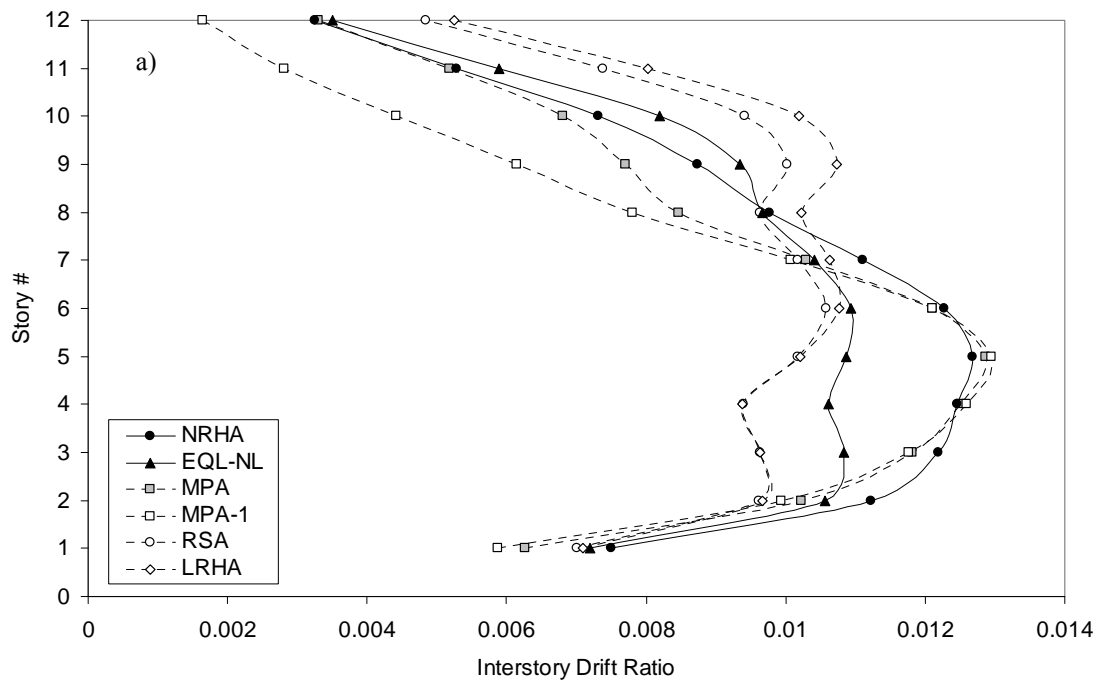


Figure 5.11 a) Median, b) RMSE of interstory drift ratios for pulse type ground motions

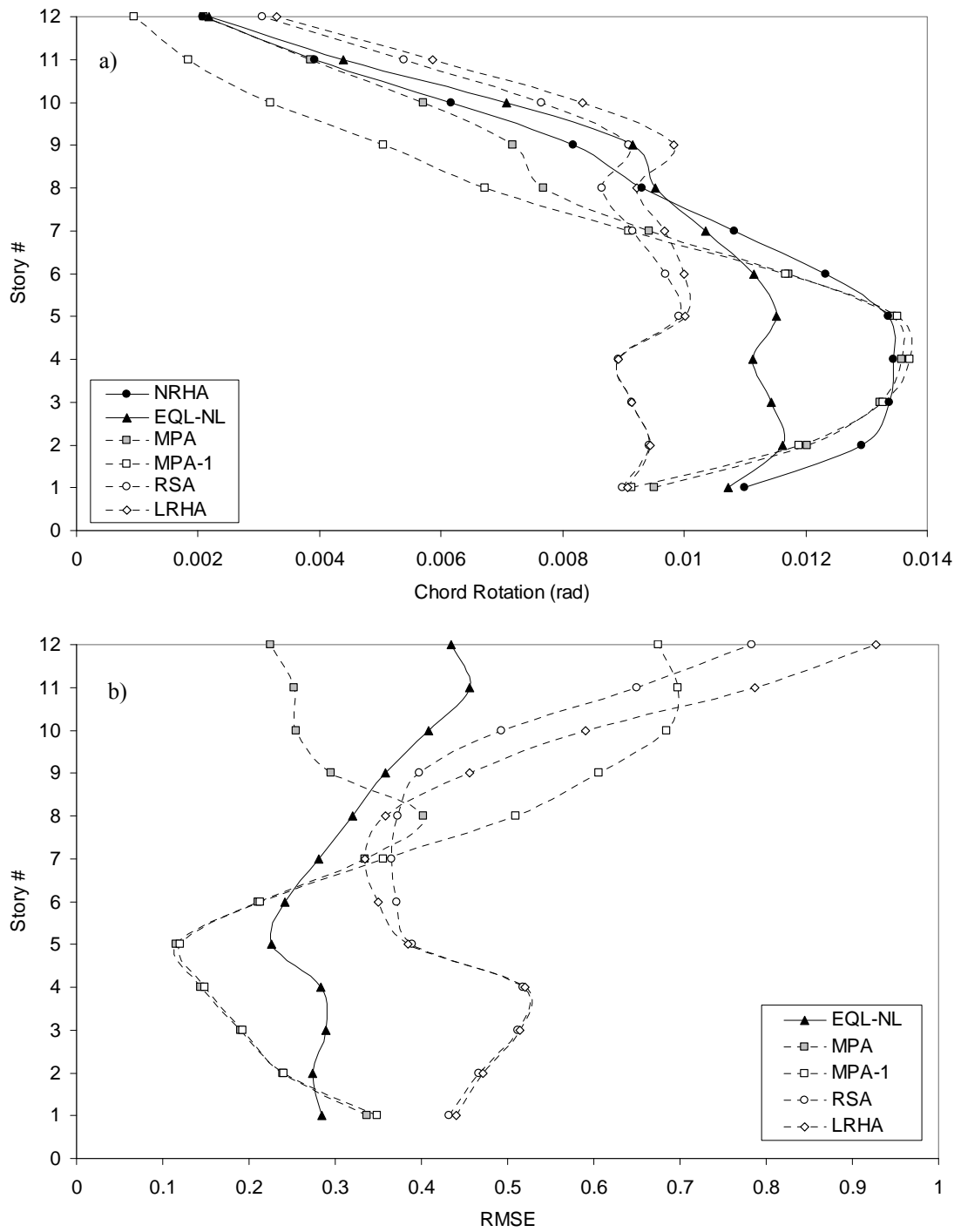


Figure 5.12 a) Median, b) RMSE of beam chord rotations for pulse type ground motions

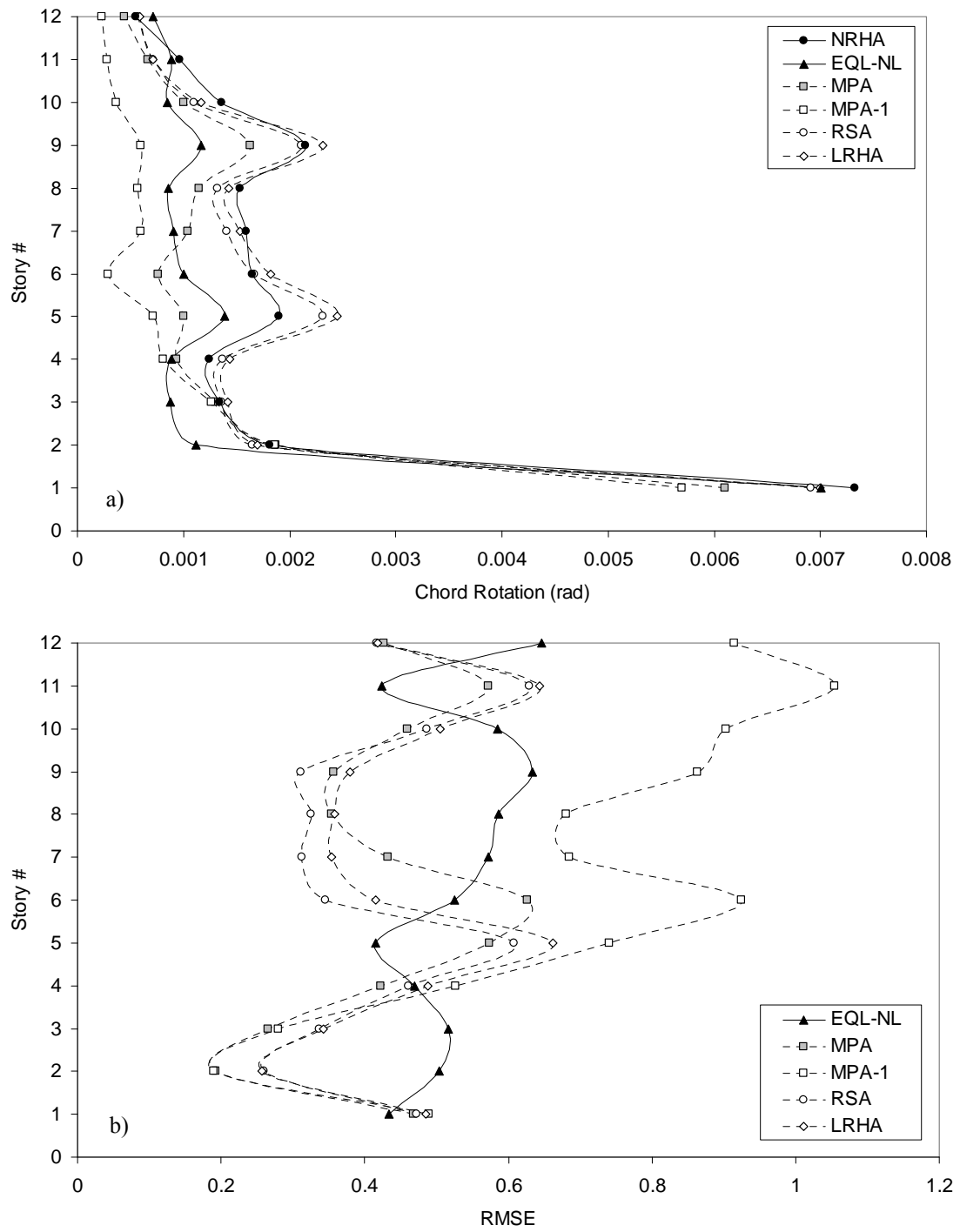


Figure 5.13 a) Median, b) RMSE of column bottom end chord rotations for pulse type ground motions

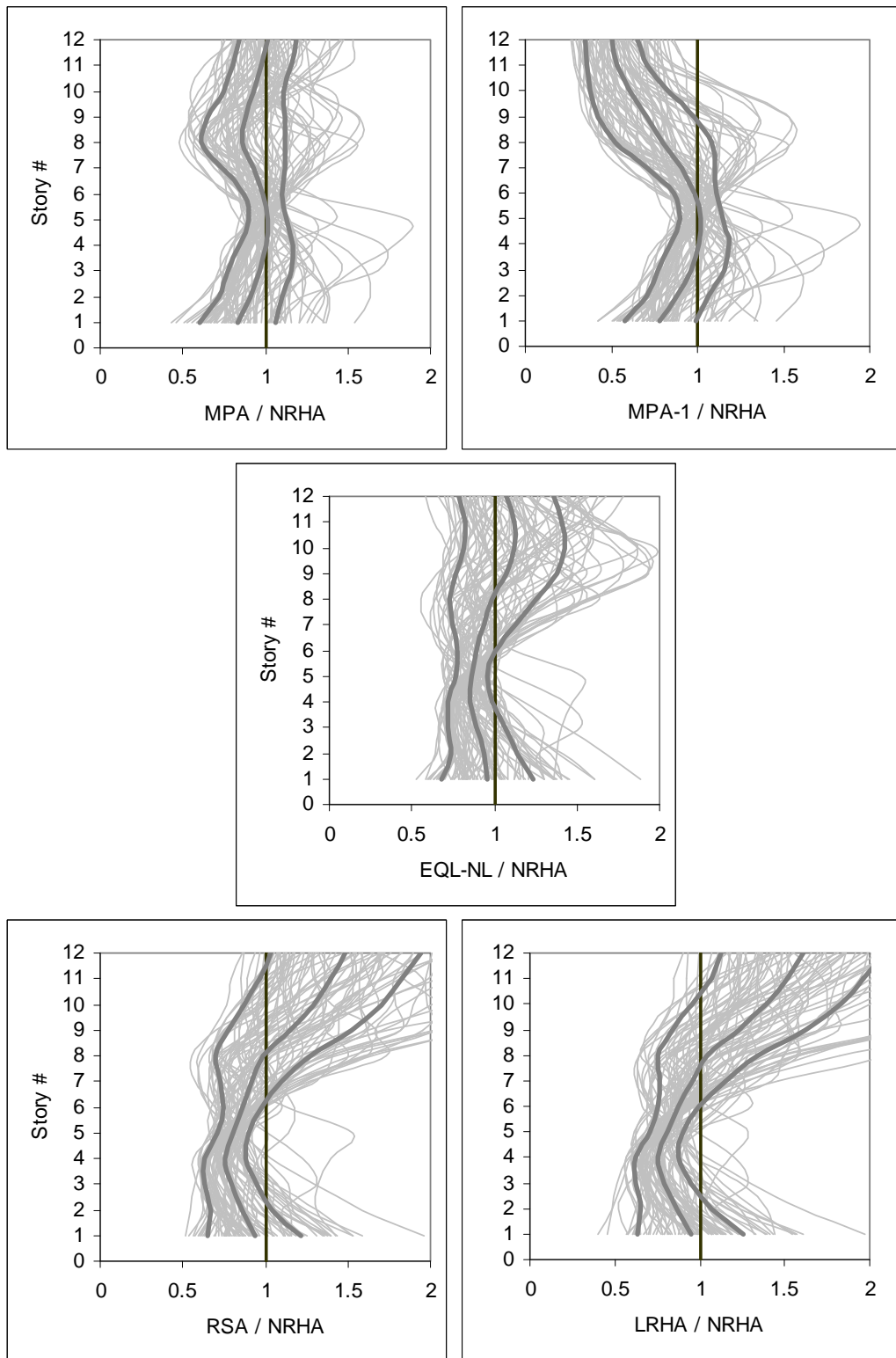


Figure 5.14 Interstory drift ratios of the approximate methods normalized with those of NRHA for pulse type ground motions

- When the distribution of median interstory drift ratios along the building height obtained from LRHA and NRHA are compared (Figure 5.11a), it can be seen that higher mode effects are less apparent in NRHA with respect to LRHA. This situation is due to the fact that; although higher mode forces in the elastic range tend to induce inelasticity at the upper parts, their effects decrease after the onset of yielding at the bottom stories and inelasticity can not increase further at the upper stories as much as at the lower stories.
- The decrease in the effect of higher mode forces in the inelastic range may be explained by inspection of the pseudo acceleration response spectra in Figure 5.8. After the onset of yielding in structural members, natural periods of the structure elongate. Increase in the first mode period does not result in a significant change in pseudo acceleration. However, pseudo accelerations of the second and third modes decrease with respect to the elastic mode periods. Since the second and third mode pseudo accelerations decrease and first mode pseudo acceleration does not change significantly, effect of higher modes decrease in the inelastic range.
- Investigating the distribution of median interstory drift ratios and beam chord rotations along the height (Figures 5.11a and 5.12a), it is observed that reduction in the higher mode effects is captured by the equivalent linearization procedure.
- MPA is successful in correcting the interstory drift ratios and beam chord rotations at the upper stories predicted by the first mode pushover analysis (MPA-1). It possesses much lower RMSE values with respect to MPA-1 and results in very close median response to NRHA median at the upper three stories. However, it is ineffective in reducing the RMSE of first story column bottom end chord rotations. Both MPA and MPA-1 underestimate the median column bottom end chord rotations of the first story.
- In comparison with the approximate nonlinear analysis methods, RMSE of the equivalent linearization procedure is generally larger than RMSE of MPA, however differences are not significant. Error of the equivalent linearization

procedure is smaller than MPA-1 at the upper stories, which is an indication of the ability of the procedure in capturing the higher mode effects.

Median and RMSE of story displacements, interstory drift ratios, beam chord rotations and column chord rotations obtained from the employed analysis methods are plotted in Figures 5.15-5.18 for ordinary ground motions. Column top end chord rotations are not shown in these figures since upper ends of the columns remain in the elastic range and their median chord rotations do not exceed 0.002 radians.

Interstory drift ratios of the approximate methods divided by those of NRHA are plotted in Figure 5.19. In this figure, each thin gray line corresponds to a ground motion and the thick gray lines indicate the median-standard deviation, median and median+standard deviation values. The following observations can be made from Figures 5.15-5.19.

- Similar to the case of pulse type ground motions, it is observed that equivalent linearization procedure improves the response predictions of RSA. RSA overestimates beam chord rotations and interstory drift ratios at the upper stories. Equivalent linearization procedure is successful at bringing these values closer to NRHA results.
- RMSE of column bottom end chord rotations is similar for all of the approximate methods. RMSE of the column bottom end chord rotations of the 2<sup>nd</sup> and upper stories do not possess a practical importance since they remain in the elastic range.
- Observing the distribution of median interstory drift ratios along the height, it is noted that reduction in the higher mode effects between LRHA and NRHA is less pronounced for ordinary ground motions compared to pulse type ground motions. Ordinary ground motions result in lower levels of nonlinearity, which consequently results in smaller amounts of period elongation. Therefore the effect of higher modes does not reduce in the inelastic range for ordinary ground motions as much as the case of pulse type ground motions. In addition, it is also observed that higher mode effect present in NRHA is noticed by the equivalent linearization procedure.

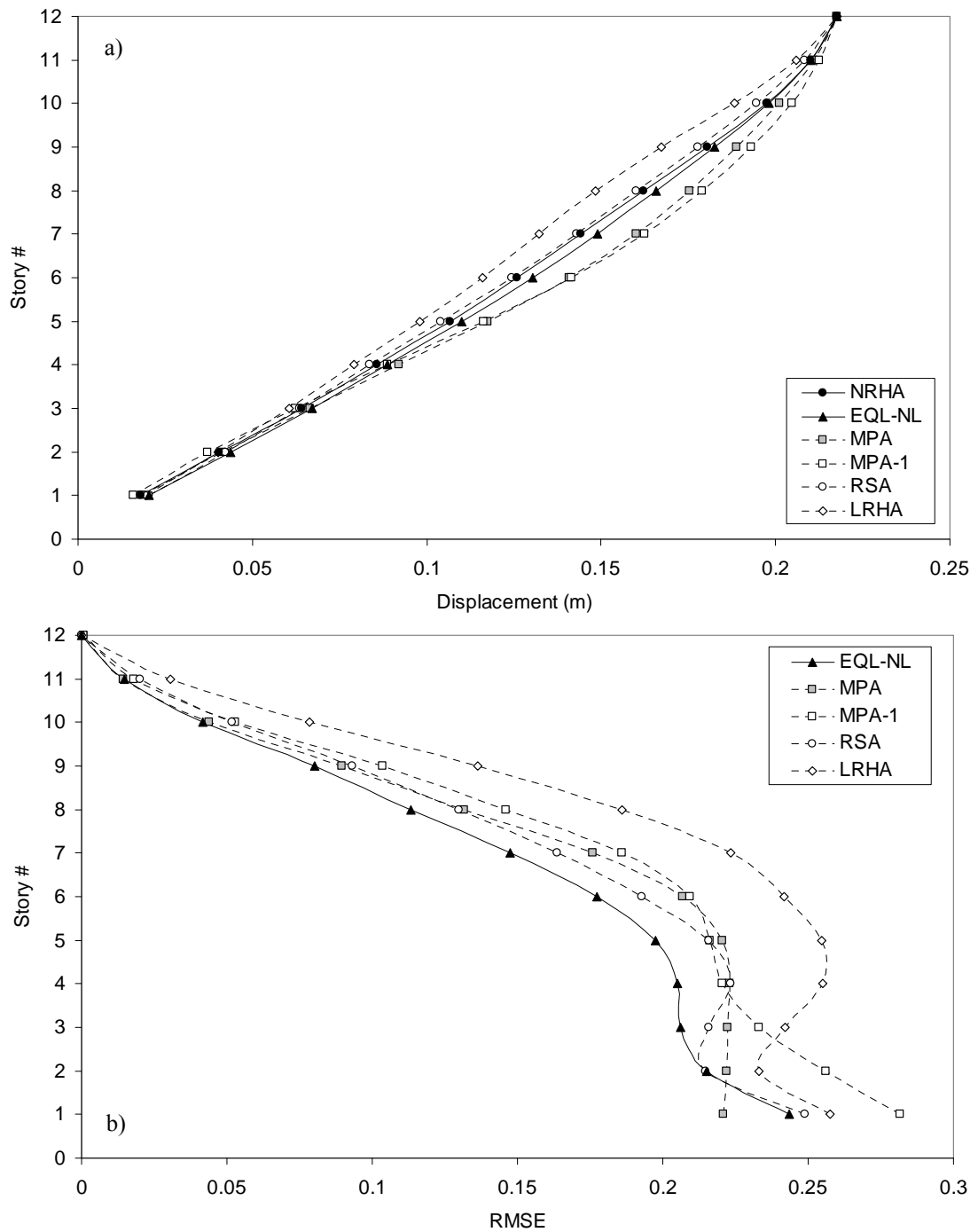


Figure 5.15 a) Median, b) RMSE of story displacements for ordinary ground motions

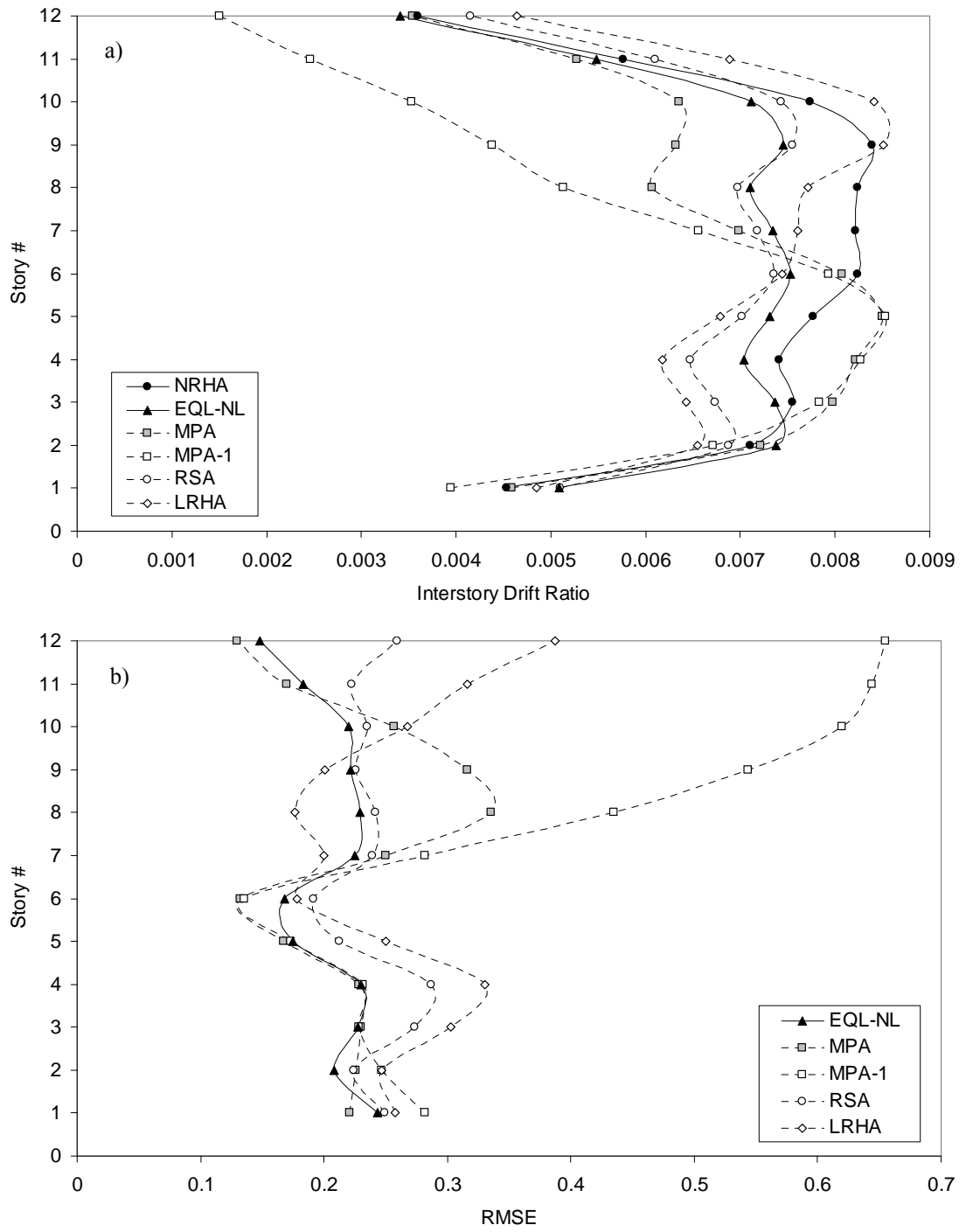


Figure 5.16 a) Median, b) RMSE of interstory drift ratios for ordinary ground motions

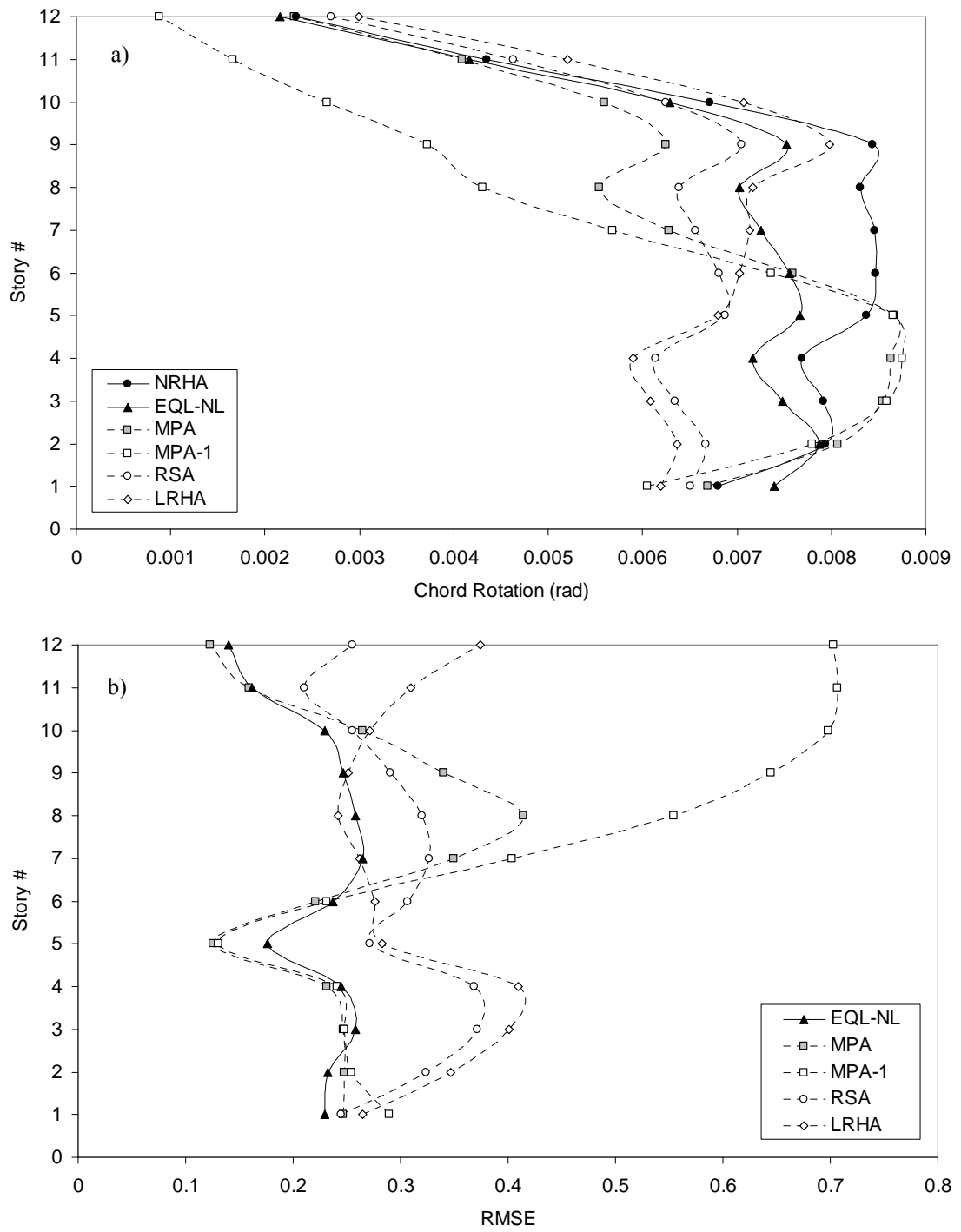


Figure 5.17 a) Median, b) RMSE of beam chord rotations for ordinary ground motions

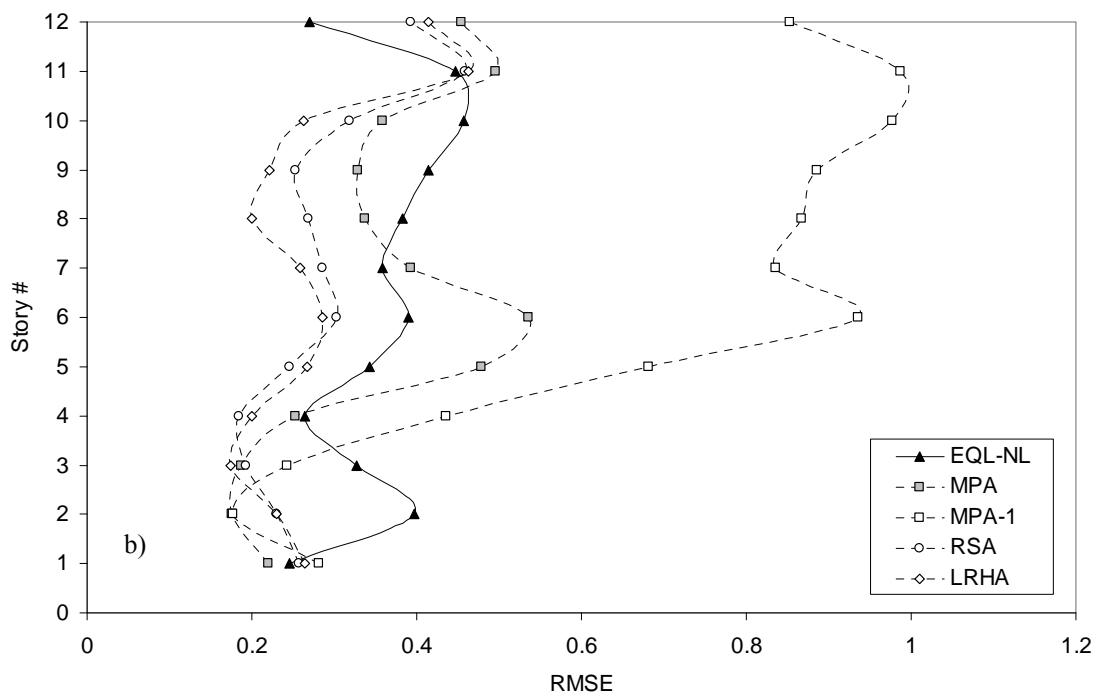
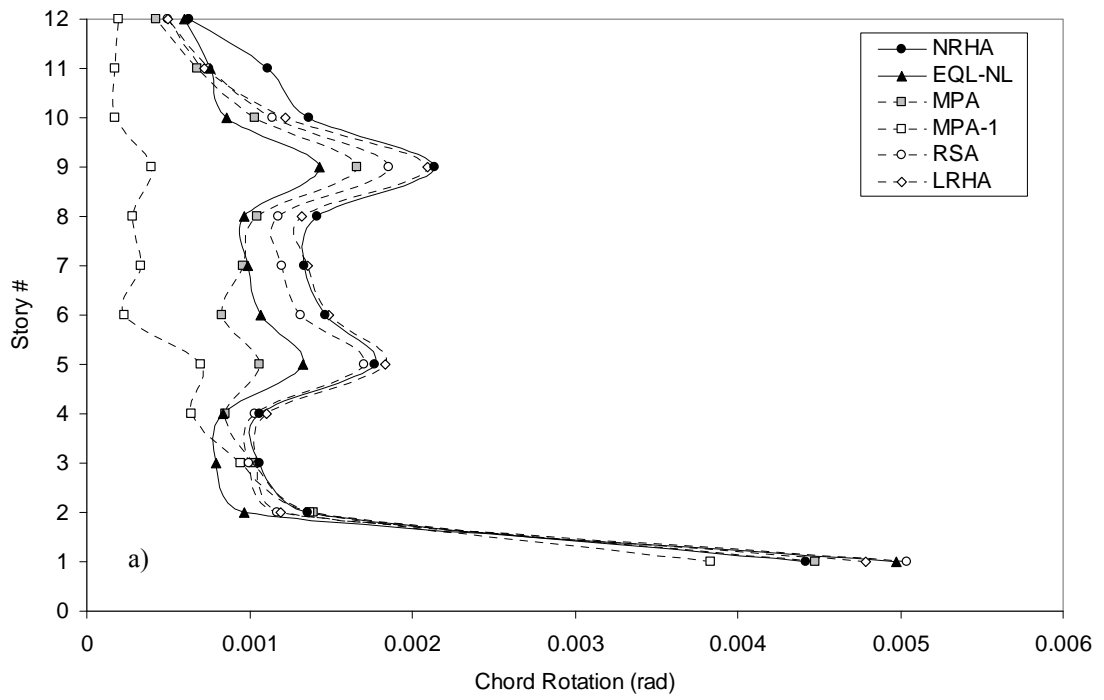


Figure 5.18 a) Median, b) RMSE of column bottom end chord rotations for ordinary ground motions

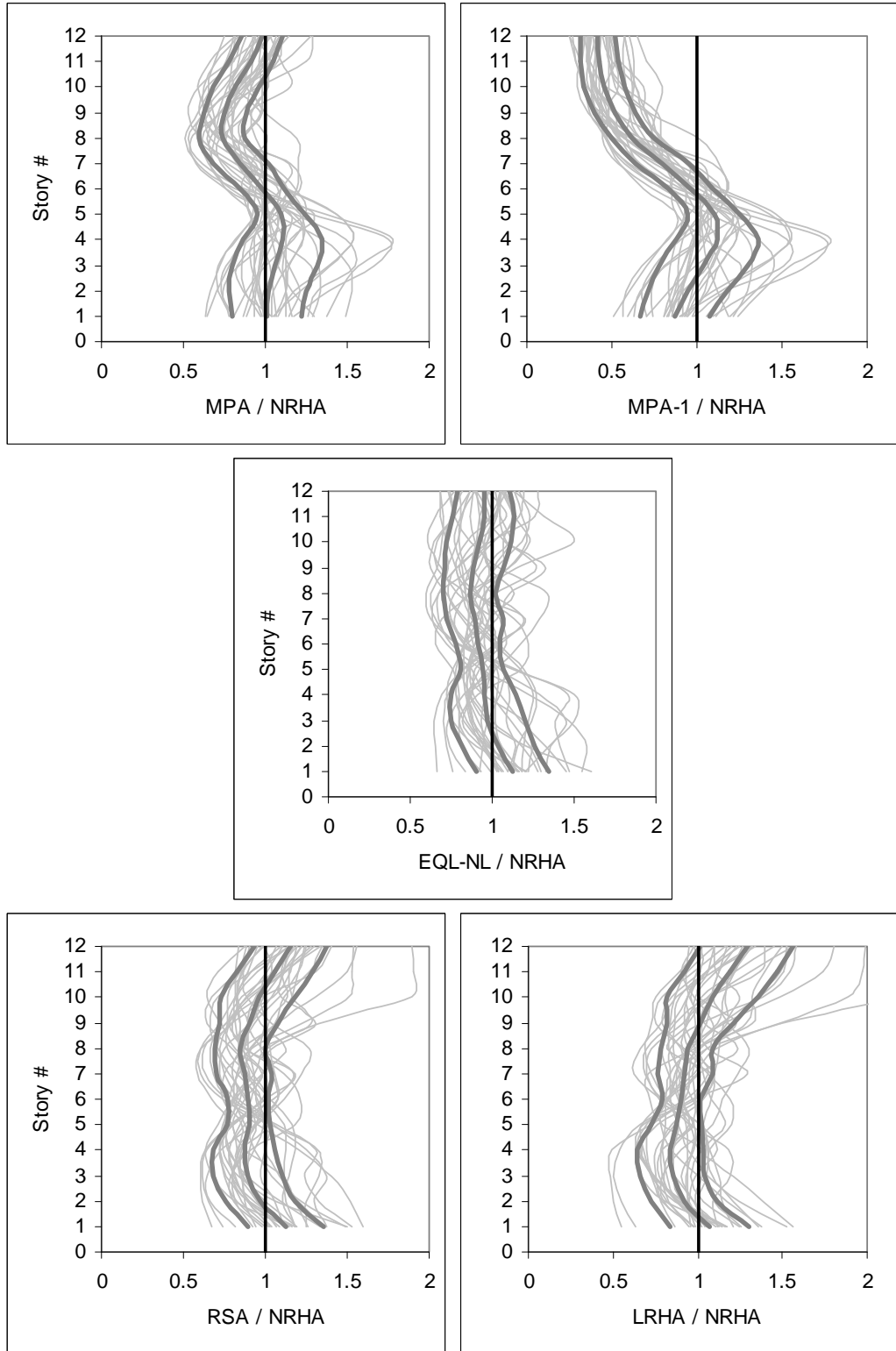


Figure 5.19 Interstory drift ratios of the approximate methods normalized with those of NRHA for ordinary ground motions

- Differences in the median and RMSE values of RSA and LRHA are more pronounced for ordinary ground motions with respect to pulse type ground motions. This observation indicates that the presence of higher mode effects is more distinct in the elastic range for ordinary ground motions.
- Displacement spectra presented in Figure 5.9 show that higher modes contribute more to seismic response under ordinary ground motions for the linear elastic case. It is seen that the spectral displacement corresponding to the first mode period is much greater than the spectral displacements corresponding to the second and third mode periods for pulse type ground motions, whereas differences are less for ordinary ground motions.
- Akin to the pulse type ground motions, MPA is successful in correcting the interstory drift ratios and beam chord rotations predicted by the first mode pushover (MPA-1) at the upper stories. RMSE of the equivalent linearization procedure is similar to or smaller than RMSE of MPA. Observing Figure 5.19, it is seen that equivalent linearization procedure captures the interstory drift distribution along the height better than MPA-1 and MPA for ordinary ground motions.

#### **5.4.4 Response Prediction Under a Pulse Type Ground Motion**

The proposed equivalent linearization procedure is evaluated in comparison with the other analysis methods under a pulse type ground motion in this section. Each method is evaluated at the roof displacement demand pertaining to that method, not at the roof displacement of NRHA.

The ground motion selected as a pulse type example is the one with the code CHY080-N in Table 4.1. The reasons for selecting this ground motion are that it causes considerable nonlinearity and excites higher modes as observed from Figure 5.20. Maximum roof displacement - maximum base shear pair resulting from the selected ground motion and the first mode pushover curve are presented in this figure. It is seen that the maximum base shear resulting from the ground motion is

located much above the first mode pushover curve indicating the contribution of higher modes to base shear.

Considered ground motion was recorded during the 1999 Chi-Chi, Taiwan earthquake. Ground acceleration, velocity and displacement traces of the ground motion are presented in Figure 5.21. Peak ground acceleration, velocity and displacement values are 0.902 g, 102.5 cm/s and 34 cm, respectively. Existence of strong pulses can be identified from Figure 5.21. Pseudo acceleration and displacement response spectra of the ground motion are presented in Figure 5.22. First three mode periods are also marked on these spectra.

Comparison of maximum story displacements, interstory drift ratios, beam chord rotations and column bottom end chord rotations obtained from the employed analysis methods are presented in Figure 5.23.

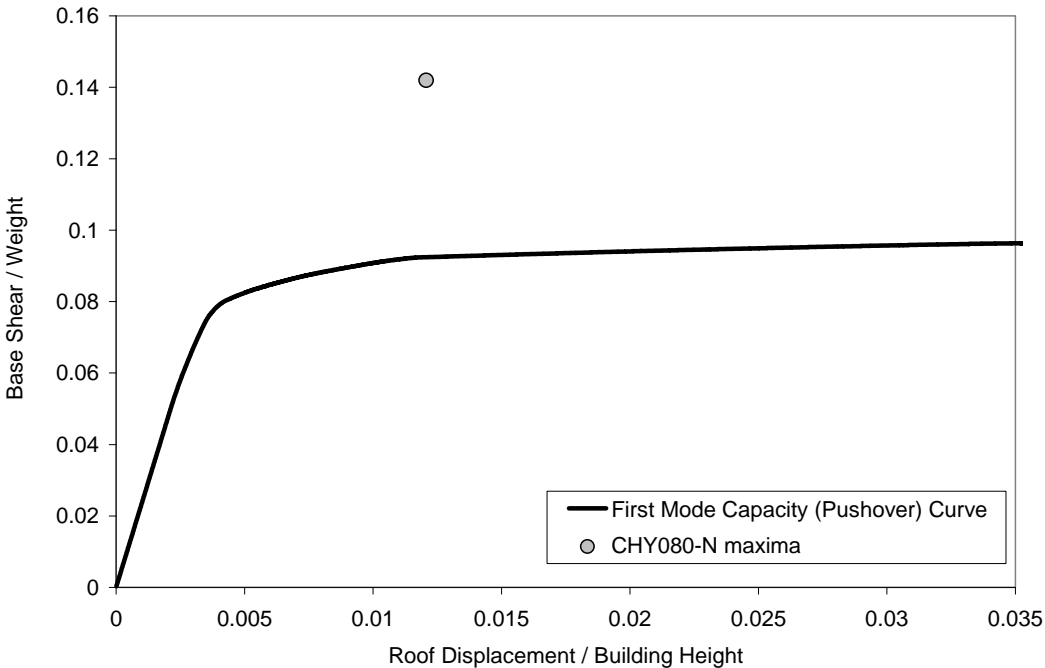


Figure 5.20 Maximum roof displacement and maximum base shear pair resulting from the ground motion CHY080-N plotted against the first mode capacity curve

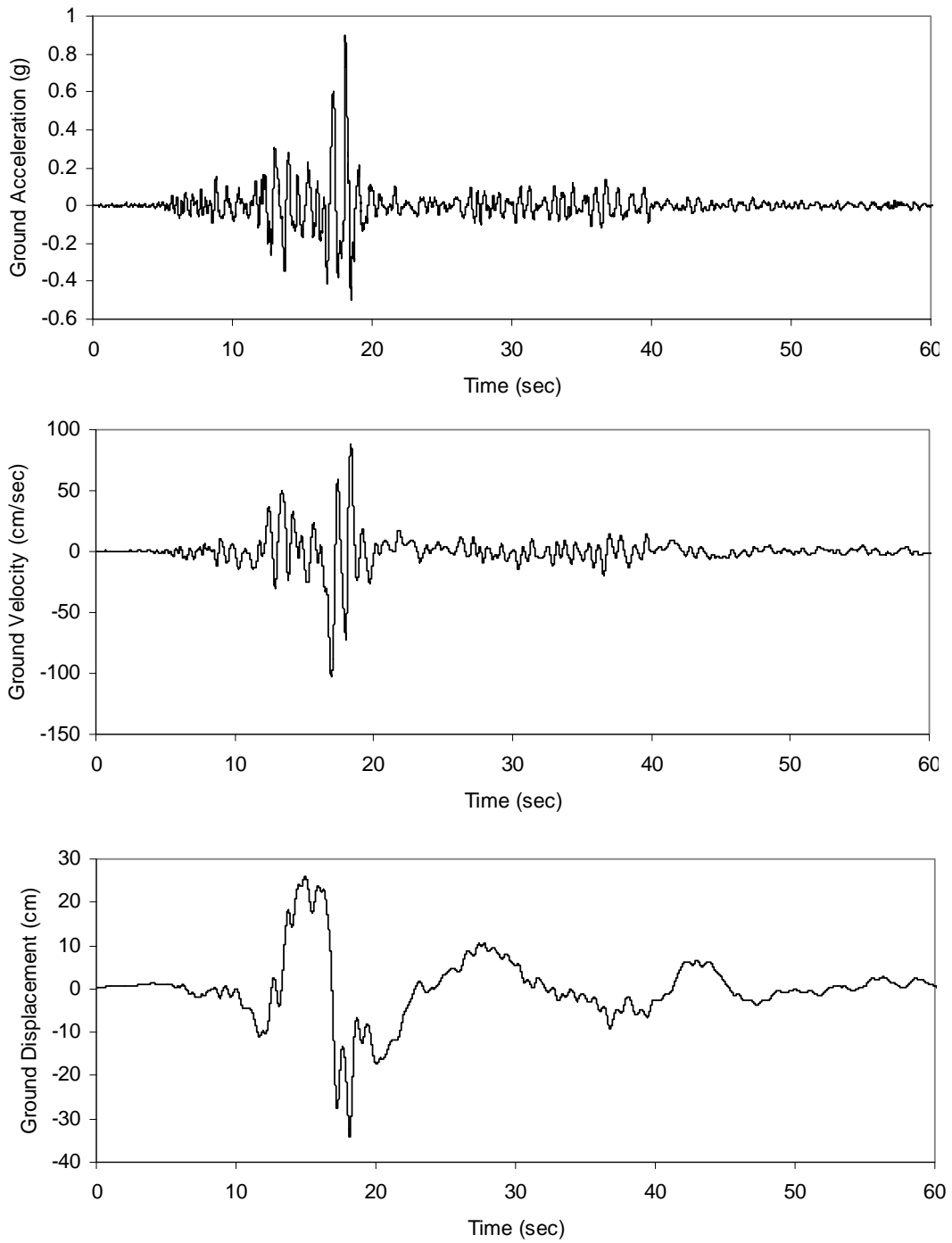


Figure 5.21 Ground acceleration, velocity and displacement traces for the ground motion CHY080-N

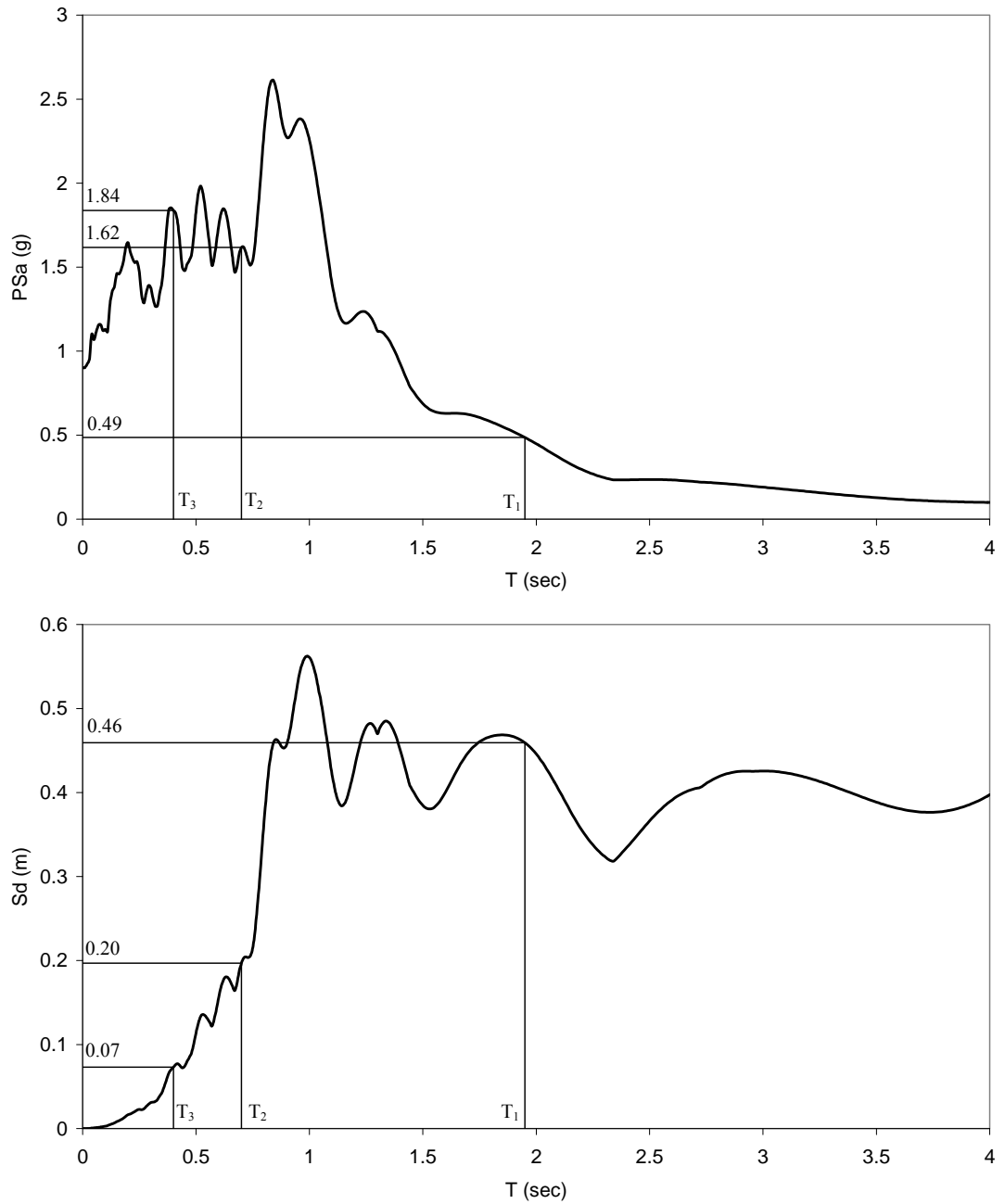


Figure 5.22 5% damped pseudo acceleration and displacement response spectra for the ground motion CHY080-N

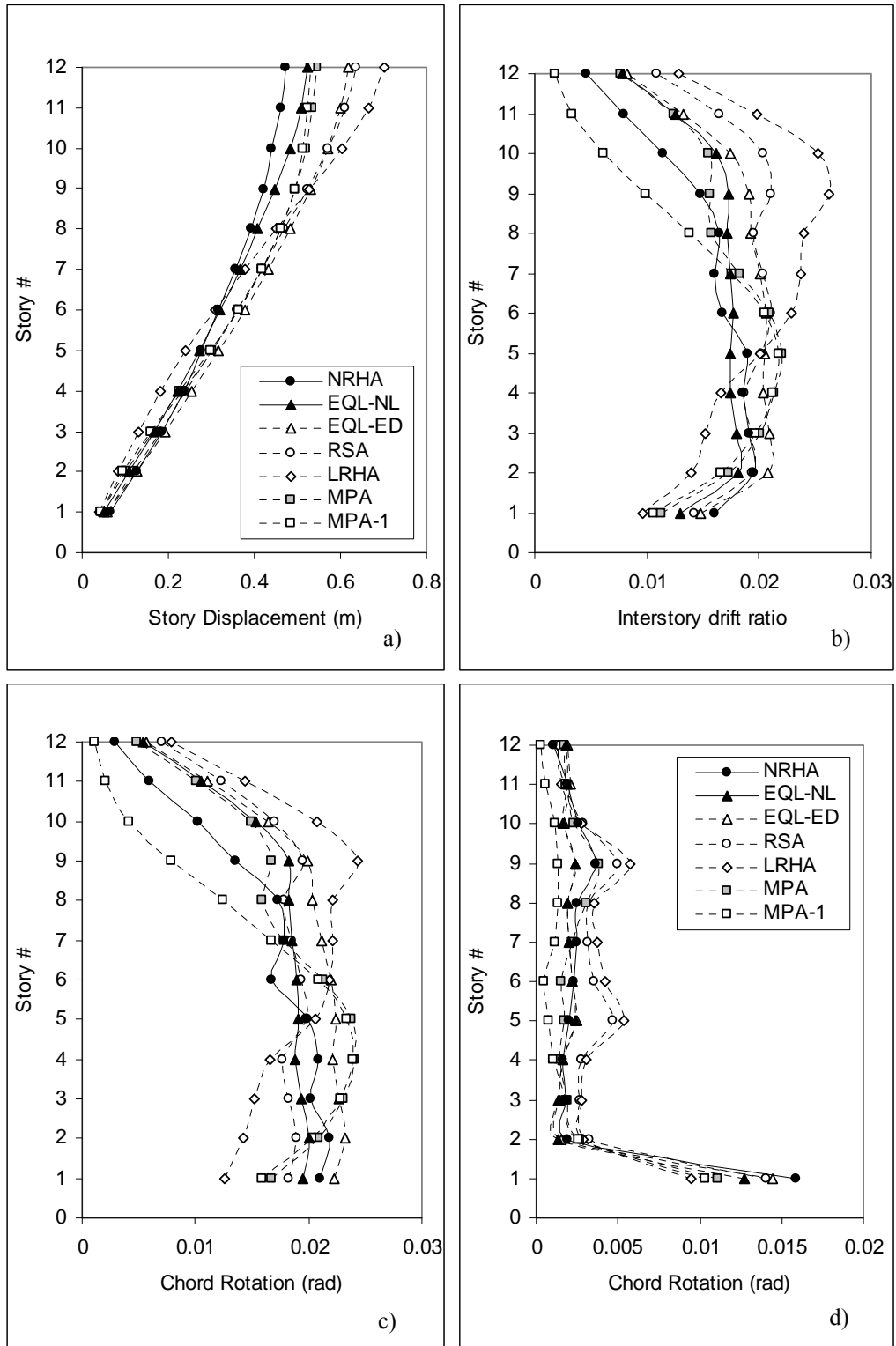


Figure 5.23 Comparison of maximum a) story displacements, b) interstory drift ratios, c) beam chord rotations, d) column bottom end chord rotations for the ground motion CHY080-N

Following observations can be made from Figure 5.23.

- Story displacements predicted by EQL-NL are close to those determined by NRHA. EQL-NL is successful in improving the story displacements predicted by RSA. Same observation is not true for EQL-ED. MPA and MPA-1 result in sufficiently accurate story displacements for the presented ground motion.
- Distribution of interstory drift ratios and beam chord rotations along the height are different for LRHA and NRHA. Presence of higher modes are more pronounced for LRHA, but higher mode effects are also present in NRHA as indicated from the base shear value in Figure 5.20 and the distribution of interstory drift ratios along the height. EQL-NL results in sufficiently accurate estimations of interstory drift ratios and beam chord rotations obtained by NRHA.
- Although RSA and EQL-ED result in inaccurate roof displacement estimations, they are successful in predicting some of the local response parameters like the first story column bottom end chord rotations and beam chord rotations at the intermediate story levels. In order to prevent a misleading evaluation of the approximate methods in such cases, statistical evaluation of the methods were conducted at the roof displacement demands of NRHA as explained previously.
- There are differences between RSA and LRHA results, because higher mode effects are considerable in the elastic range as can be noted from the displacement response spectrum in Figure 5.22.
- MPA is satisfactory in estimating the beam chord rotations and interstory drift ratios for the selected ground motion. It amplifies the predictions of MPA-1 at the upper stories. MPA underestimates the column bottom end chord rotations of the first story, which was previously noted for the median response under the pulse type ground motion set.

#### 5.4.5 Response Prediction Under an Ordinary Ground Motion

The ordinary ground motion for which the results are presented in this section is the one with the code IZT090 in Table 4.2. First mode pushover curve and the maximum roof displacement - maximum base shear pair resulting from the selected ground motion are presented in Figure 5.24. It is seen that the maximum base shear resulting from the ground motion is located much above the first mode capacity curve indicating the presence of higher modes. This ground motion is selected for presentation because higher mode effects are present both in LRHA and NRHA. In addition, distribution of local responses along the height is considerably different in LRHA and NRHA although the ground motion results in a moderate level of inelasticity.

The selected ground motion is the 90 degree component of the ground motion recorded in İzmit station during 1999 Kocaeli earthquake. Ground acceleration, velocity and displacement traces of the ground motion are presented in Figure 5.25. Peak ground acceleration, velocity and displacement values are 0.220 g, 29.8 cm/s and 17.1 cm, respectively. Pseudo acceleration and displacement response spectra of the ground motion are presented in Figure 5.26. First three mode periods are also marked on these spectra.

Comparison of maximum story displacements, interstory drift ratios, beam chord rotations and column bottom end chord rotations obtained from the employed analysis methods are presented in Figure 5.27. Following observations are derived from these figures.

- Story displacements predicted by EQL-NL are very close to those determined by NRHA. EQL-NL is successful at improving the story displacements predicted by RSA. As in the case of the pulse type ground motion example, story displacements determined by EQL-ED and RSA are similar to each other. MPA and MPA-1 overestimate the story displacements.
- Distribution of local responses along the height is considerably different for LRHA and NRHA, although nonlinearity is not significant in the system. Regarding this situation, EQL-NL is successful in predicting the interstory

drift ratios and beam chord rotations determined by NRHA. It improves the predictions of RSA. EQL-NL overestimates the first story column bottom end chord rotation, however since the value determined by NRHA is small, overestimation does not introduce a significant problem.

- MPA improves the beam chord rotation and interstory drift ratio predictions of MPA-1. Both MPA and MPA-1 overestimate the beam chord rotations and interstory drift ratios at the lower stories.

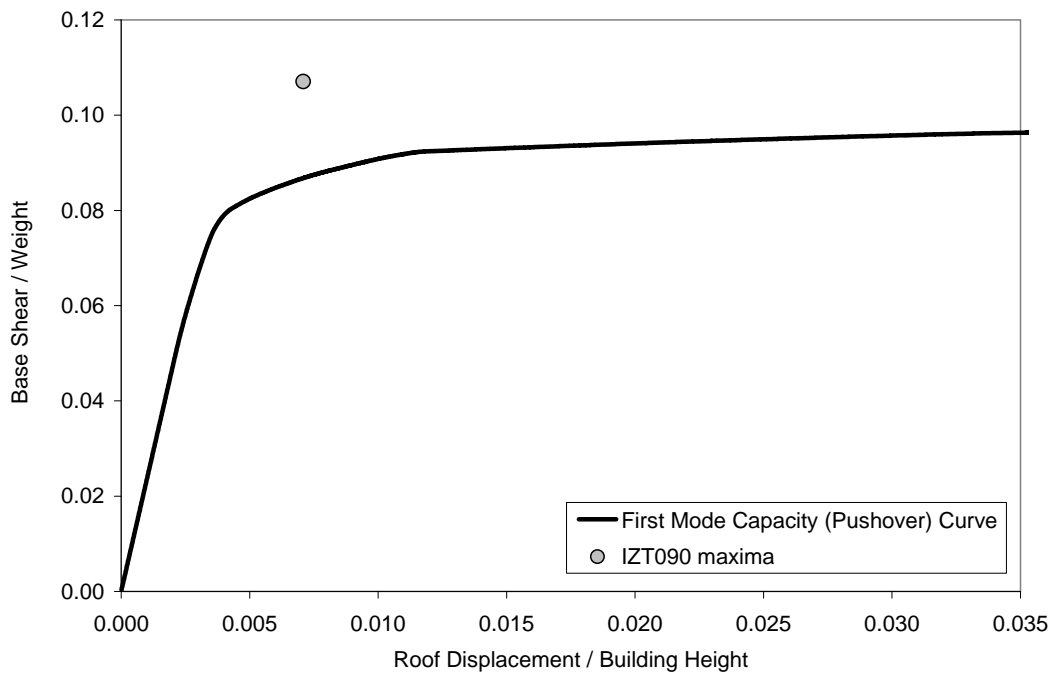


Figure 5.24 Maximum roof displacement and maximum base shear pair resulting from the ground motion IZT090 plotted against the first mode capacity curve

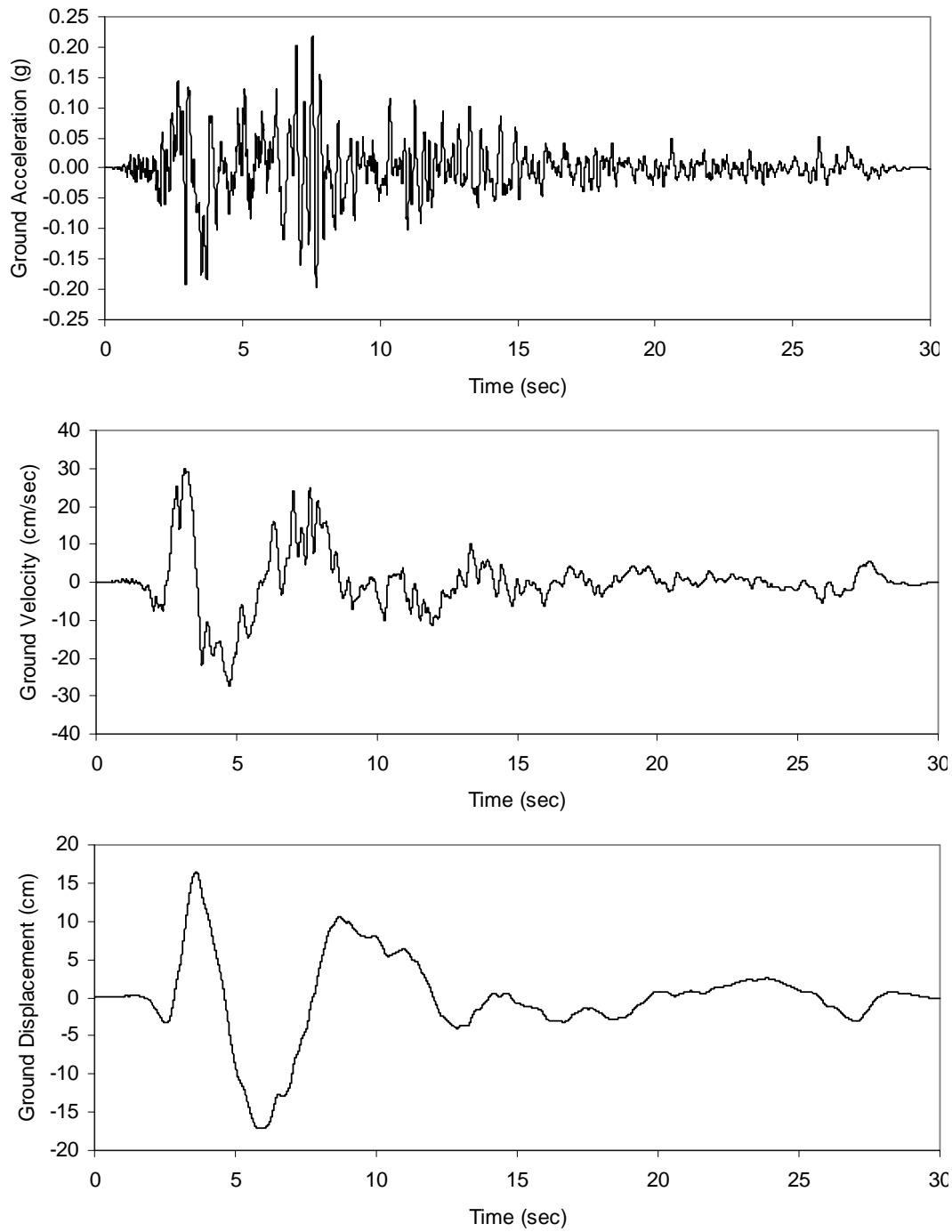


Figure 5.25 Ground acceleration, velocity and displacement traces for the ground motion IZT090

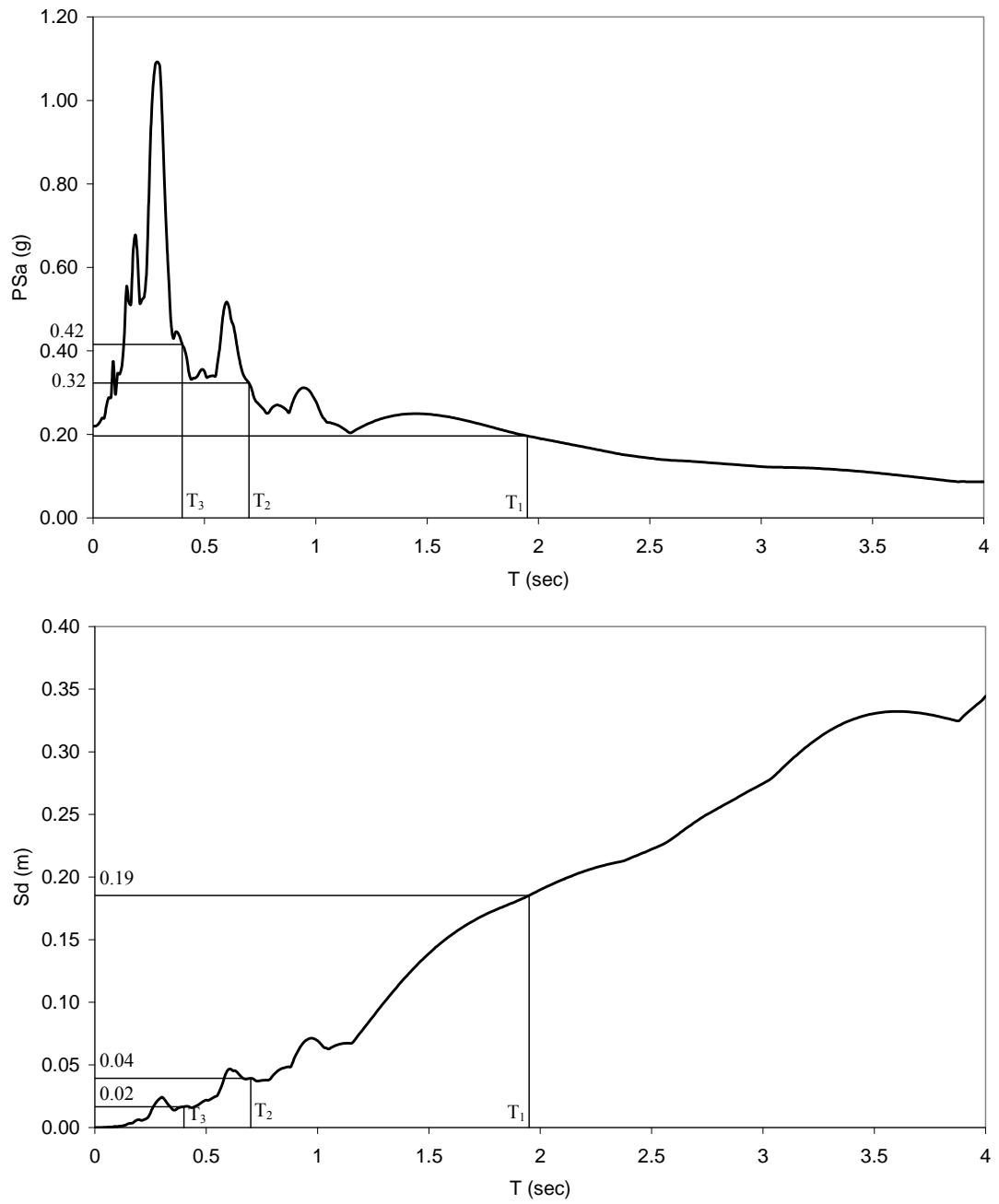


Figure 5.26 5% damped pseudo acceleration and displacement response spectra for the ground motion IZT090

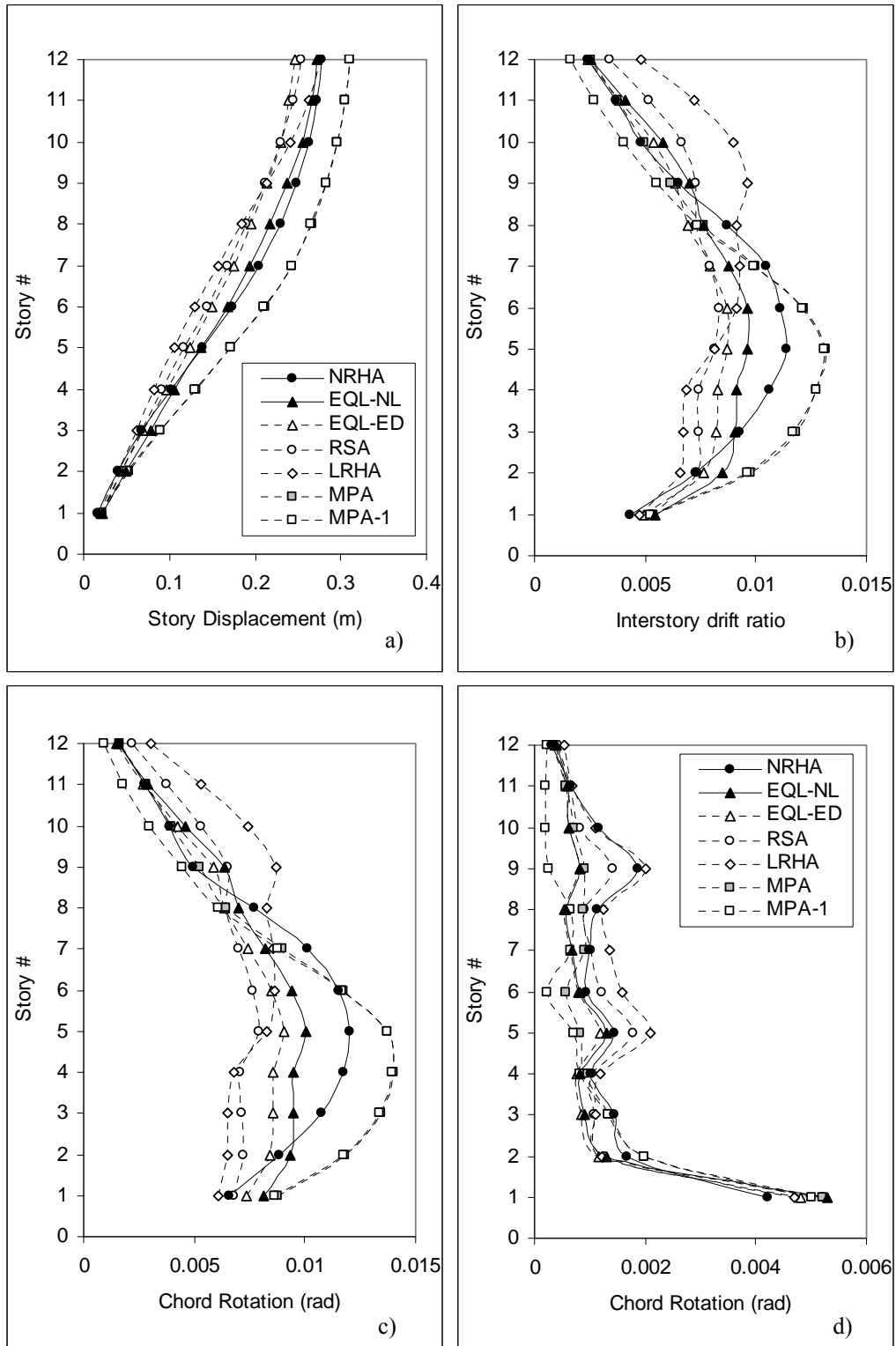


Figure 5.27 Comparison of maximum a) story displacements, b) interstory drift ratios, c) beam chord rotations, d) column bottom end chord rotations for the ground motion IZT090

## **CHAPTER 6**

### **CASE STUDY II: SIX STORY UNSYMMETRICAL-PLAN RC SPACE FRAME**

#### **6.1 Description of the Building**

A six story reinforced concrete building frame is selected as the second case study, for which the story plan and the 3D view are shown in Figure 6.1. The building is designed according to the regulations of TS-500 (2000) and TEC (1998) where capacity design requirements prevail. The building is assumed to be located in seismic zone 1 with local site class Z3. Therefore an enhanced ductility level is employed in design. Utilized concrete and steel grades are C25 and S420 respectively. Slab thickness for all floors is 14 cm and live load is taken as 2 kN/m<sup>2</sup>. Dimensions of all beams are 30x55 cm<sup>2</sup>, whereas dimensions of all columns are 50x50 cm<sup>2</sup>. There is no basement; height of the ground story is 4 m, while the height of other stories is 3 m. For the analysis of the building, eccentricity between the center of stiffness (CS) and center of mass (CM) is increased to 15% of the plan dimension in order to introduce asymmetry about the Y-axis as indicated in Figure 6.1. Labels of the Y-direction frames are also presented in this figure.

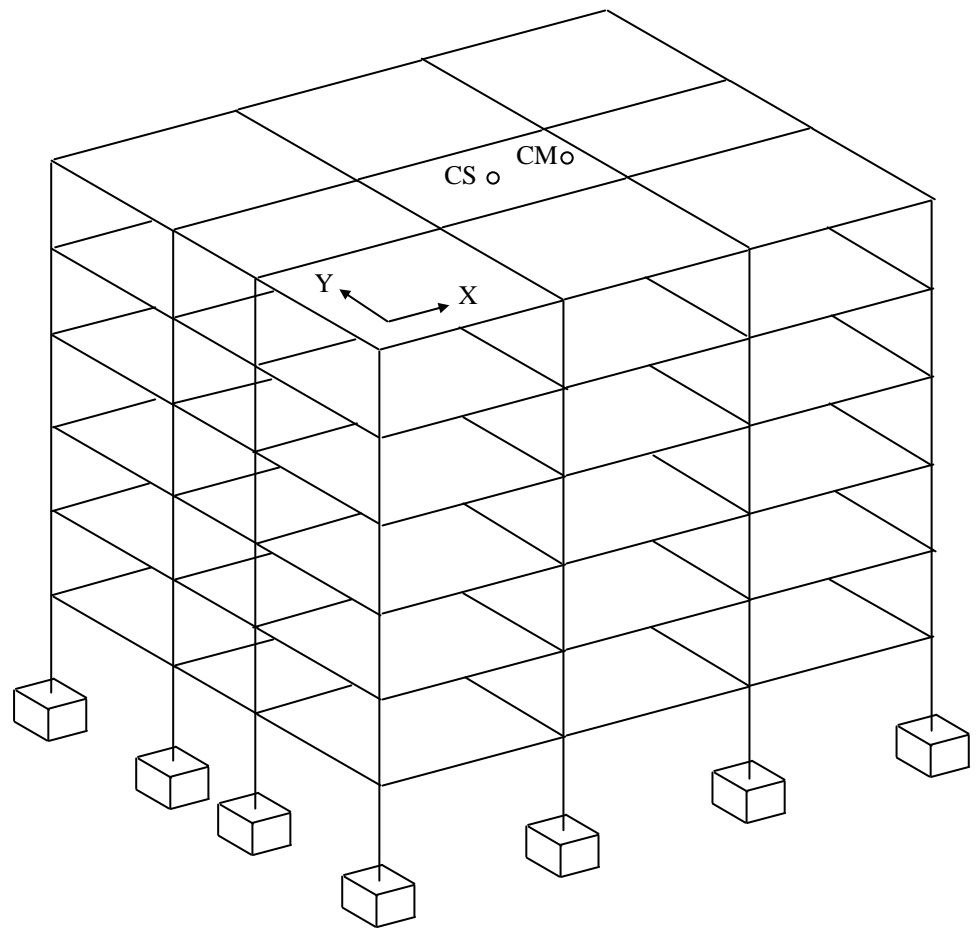
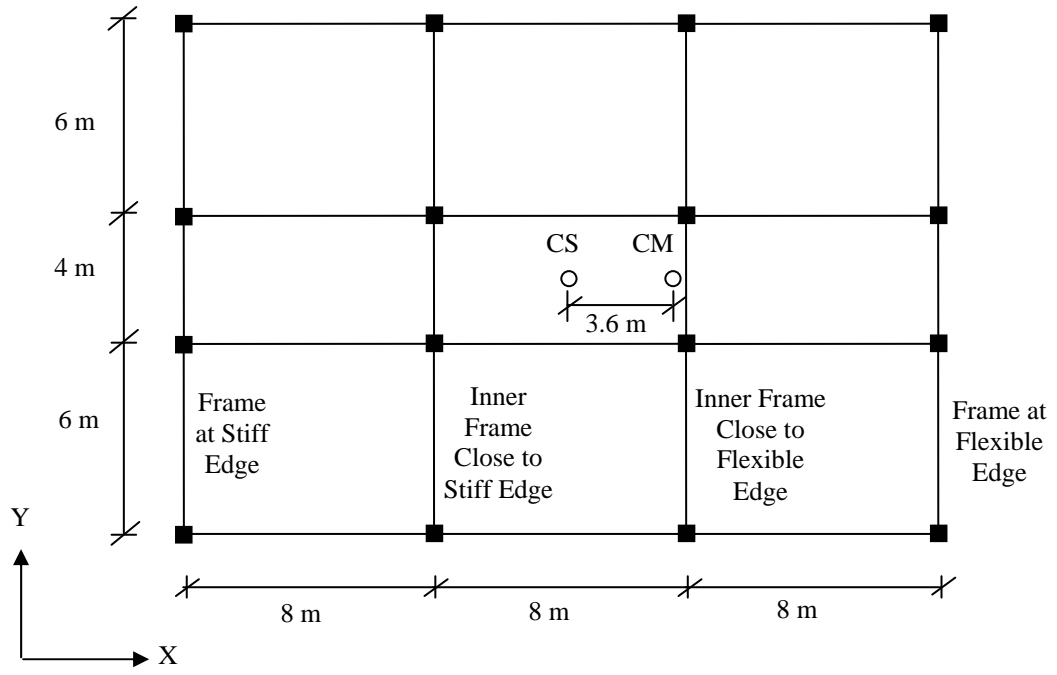


Figure 6.1 Story plan and 3D view of the six story building

## 6.2 Modeling

OpenSees (2005) is utilized for modeling the case study building. Modeling features of OpenSees relevant to this case study are presented in Figure 6.2.

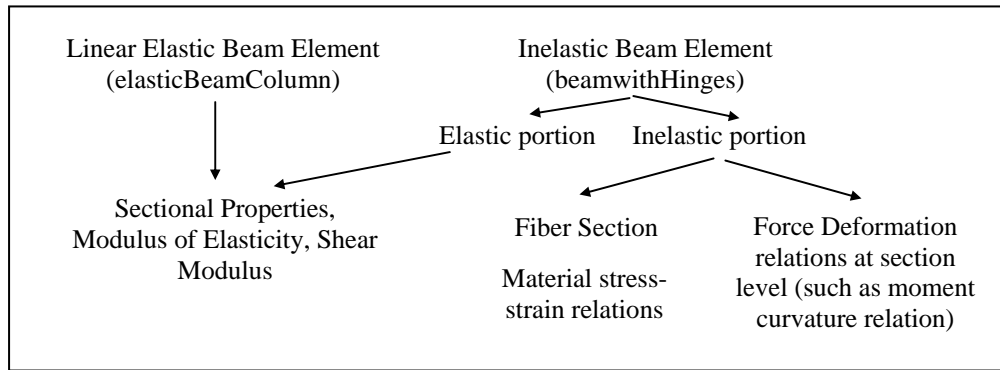


Figure 6.2 Modeling features of OpenSees employed in Case Study II

Linear elastic frame elements, namely “elasticBeamColumn” elements are used for the linear elastic models. Gross moments of inertia reduced with the multipliers 0.6 and 0.5 are employed for the columns and beams respectively, in order to account for the cracked section stiffness.

In the development of the equivalent linearization procedure, inelasticity is assumed to develop at the member ends. Therefore it is consistent to employ such an assumption in the nonlinear analyses for a rational comparison. The “beamwithHinges” element, which is the most suitable element for this purpose is employed in the nonlinear models. In this element formulation, plasticity is considered to be concentrated over specified hinge lengths at the element ends while the interior part is considered as elastic. Hinge lengths are accepted to be equal to half of the cross section depth of the element in this study.

Fiber sections are defined along the hinge lengths of the columns. Stiffness degradation, strength degradation or pinching are not considered in the derivation of the stiffness reduction equations, therefore they are not also considered in the

material models of nonlinear analyses. Non-degrading bilinear models with very small strain-hardening slope are employed for the stress-strain relations of steel and concrete. Reinforcement is modeled with “Steel01” material, and concrete is modeled with “Hysteretic Material” respectively. “Hysteretic Material” is a bilinear hysteretic material model which considers pinching of force and deformation, and degraded unloading stiffness based on ductility. Different yield stress values can be assigned in tension and compression. Parameters of this material are adjusted to result in a non-degrading bilinear relationship. Confined and unconfined concrete are modeled with different compressive strengths. Compressive strength of confined concrete is calculated as 1.175 times of the compressive strength of unconfined concrete according to Modified Kent and Park model (Kent and Park, 1971). Ultimate strain corresponding to failure is not considered in the material models, which reduces the numerical problems encountered in the nonlinear solution algorithm. Slope of the initial segment is chosen to be equal to the modulus of elasticity (E) employed in the linear elastic models. The moment curvature history recorded in the section at the base of one of the ground story columns during nonlinear response history analysis under the ground motion with label ERZ-EWb (Table 4.1) is presented in Figure 6.3.

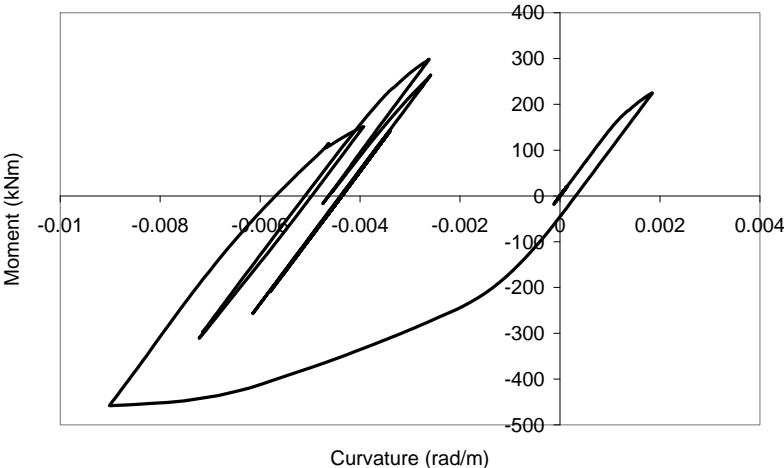


Figure 6.3 Moment-curvature relation recorded in the section at the base of one of the ground story columns during nonlinear response history analysis

Fiber sections are not utilized for the beams, because artificial axial forces develop in the beams when fiber sections are employed despite the imposition of diaphragm constraints. Diaphragm constraints impose the two ends of a beam, located parallel to one of the transverse degrees of freedom of the mass center, deform in equal amounts along the member axis. Since equal axial deformations are imposed at the two ends, it is expected that the axial force in the beam is equal to zero. However, this expectation does not hold in the presence of fiber sections and axial forces develop, which in turn results in an increase in the moment capacities of beams. Accordingly, a building designed for beam yielding may result in a failure formation different than the intended if the design is based on a model without fiber sections. Figure 6.4 shows the effect of utilizing fiber sections for beam sections on the conventional pushover curve of the case study building. It can be seen that fiber sections significantly increase the base shear capacity for the case study building, which is a consequence of the increase in the moment capacities of beams due to axial forces artificially developing in the fiber section model. Existence of axial forces along the beam ends with floors acting as rigid diaphragms should be investigated via experiments. In this study, it is accepted that axial force does not exist along the beam axis in the presence of rigid diaphragms, and accordingly fiber sections are not utilized for beams. Nondegrading bilinear moment-curvature relations with very small strain hardening are utilized along the hinge lengths of beams. Moment-curvature history recorded in a section at the end of one of the first story beams during nonlinear response history analysis under the ground motion with label ERZ-EWb (Table 4.1) is presented in Figure 6.5.

Since fiber sections are employed for the columns, cracking of concrete is explicitly considered during the solution process. However bilinear moment-curvature relations are utilized for the beams, for which it is not possible to consider cracking during the solution process. Therefore, cracked section stiffness is employed for the utilized moment-curvature relations. For this purpose, slope of the initial line segment of the moment curvature relations is set to be  $0.5EI_{gross}$ , where  $E$  is the modulus of elasticity and  $I_{gross}$  is the gross moment of inertia. Moment of

inertia assigned to the elastic portions of the “beamwithHinges” element is also equal to  $0.5I_{gross}$ .

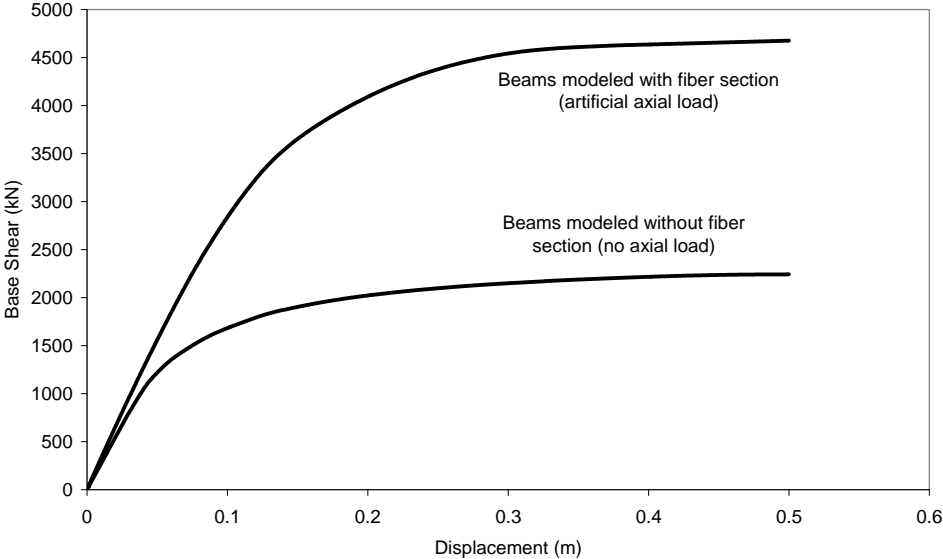


Figure 6.4 Effect of utilizing fiber sections for the beam sections on the pushover curve of the case study building

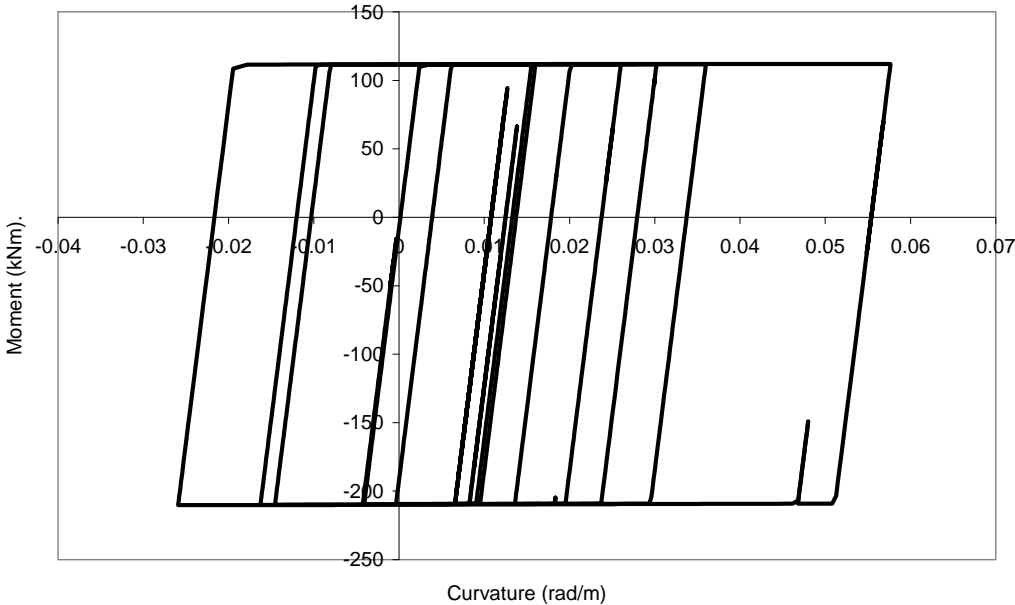


Figure 6.5 Moment-curvature relation recorded in a section at the end of one of the first story beams during nonlinear response history analysis

In both nonlinear and linear response history analyses, Rayleigh damping is used with coefficients obtained from 1<sup>st</sup> and 3<sup>rd</sup> mode periods.

OpenSees is also utilized for conducting nonlinear and linear response history analyses of SDOF systems and the calculation of the moment capacities of columns under biaxial bending.

In order to conduct automated analyses for a variety of ground motions and different analysis methods, special programs have been prepared in MATLAB (2002) in conjunction with OpenSees, which handle the analyses and process the required results.

### **6.3 Free Vibration Properties**

Free vibration properties of the building are summarized in Table 6.1. Only the properties of the first four pairs of coupled modes (Y translation and torsion) are presented in this table, since the analyses are conducted under Y-excitation only. The pure translational response along the X axis under X-excitation is not considered separately, since this exercise was conducted for the 12 story symmetric-plan building in the previous chapter. The modal static forces and torques (Chopra, 2001) corresponding to the first two pairs of coupled modes are plotted in Figure 6.6. It can be observed that the modal static torques belonging to the first pair of modes are equal in magnitude, but opposite in direction. It can also be observed that the modal static force distributions of the first pair of modes are similar. Same observations can be made for the second pair of modes.

Table 6.1 Free vibration properties of the six story building

Mode	T (sec)	Effective modal mass (tons)	Effective modal mass ratio	$\Gamma_n \phi_{nr}^{(1)}$
1Y	1.18	866.16	0.734	1.079
1θ	0.75	155.82	0.132	0.195
2Y	0.37	92.87	0.079	-0.345
2θ	0.24	16.59	0.014	-0.062
3Y	0.2	27.55	0.023	0.168
3θ	0.13	8.20	0.007	-0.076
4Y	0.13	6.37	0.007	0.028
4θ	0.09	3.04	0.007	0.029

<sup>(1)</sup> Modal participation factor multiplied with the top story modal amplitude

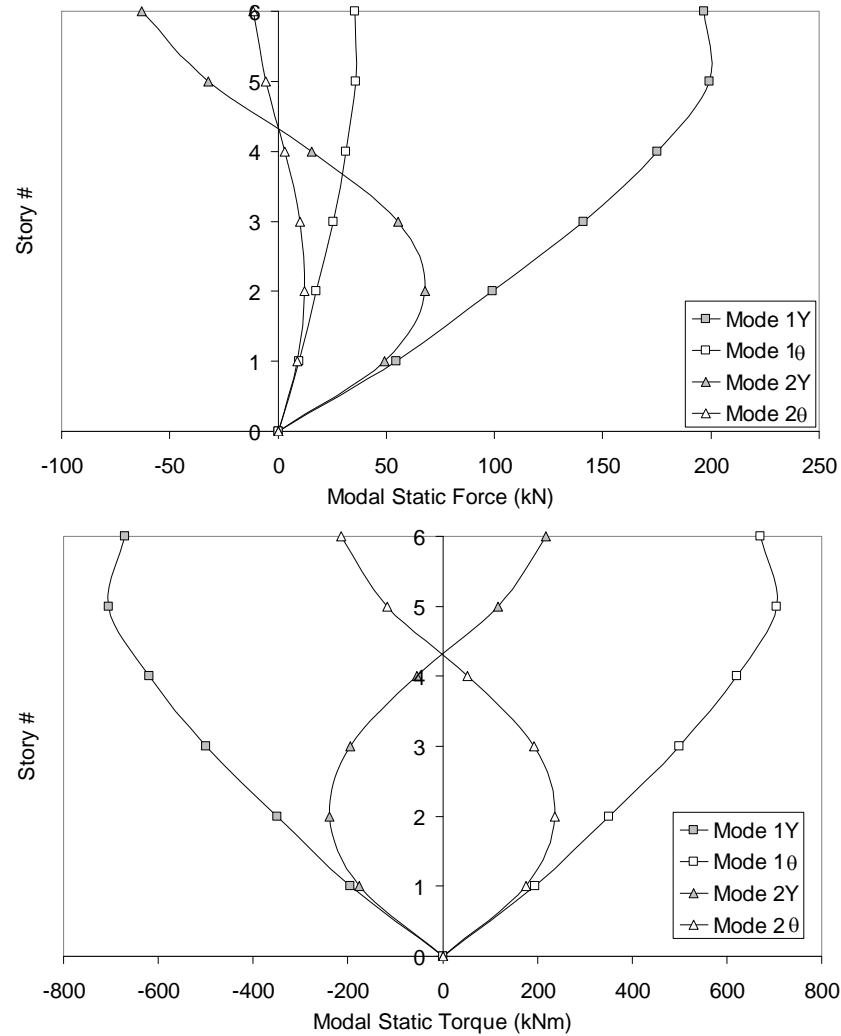


Figure 6.6 Modal static forces and torques for the first two pairs of modes

## **6.4 Presentation of Results**

Maximum values of roof displacements, interstory drift ratios and chord rotations are obtained for each Y direction frame under each ground motion belonging to the two ground motion sets described in Chapter 4. The results from nonlinear response history analysis (NRHA), modal pushover analysis (MPA), conventional pushover analysis according to FEMA-356 (PO-FEMA), two variants of the equivalent linearization procedure described in Chapter 3 (EQL-NL, EQL-ED), linear elastic response spectrum analysis (RSA) and linear elastic response history analysis (LRHA) are presented comparatively. A force distribution proportional to the multiplication of the first mode shape and the mass matrix is utilized as the lateral load pattern for PO-FEMA. Torsional components are not considered and lateral forces are applied at the mass center of each story. However, torsional forces are considered in each modal pushover of MPA as explained in Chapter 2.

### **6.4.1 Roof (Top Story) Displacement Demands at the Center of Mass**

Roof displacement demands at the center of mass calculated from the approximate methods are plotted against those obtained from nonlinear response history analyses (benchmark method) in Figures 6.7 and 6.8 for the 96 pulse type and 66 ordinary ground motions, respectively. In these figures, displacements are in meters. Calculated statistical parameters are summarized in Tables 6.2 and 6.3.

Investigation of Figures 6.7 and 6.8 and Tables 6.2 and 6.3 leads to similar observations to those gathered from the roof displacement estimations of the twelve story frame presented in the first case study.

LRHA and RSA produce erroneous estimations for both pulse type and ordinary ground motions. Predictions of EQL-ED are close to those of RSA, because same spectral displacements are employed in both of the methods, moreover the mode shapes of the resulting equivalent linear systems are not much

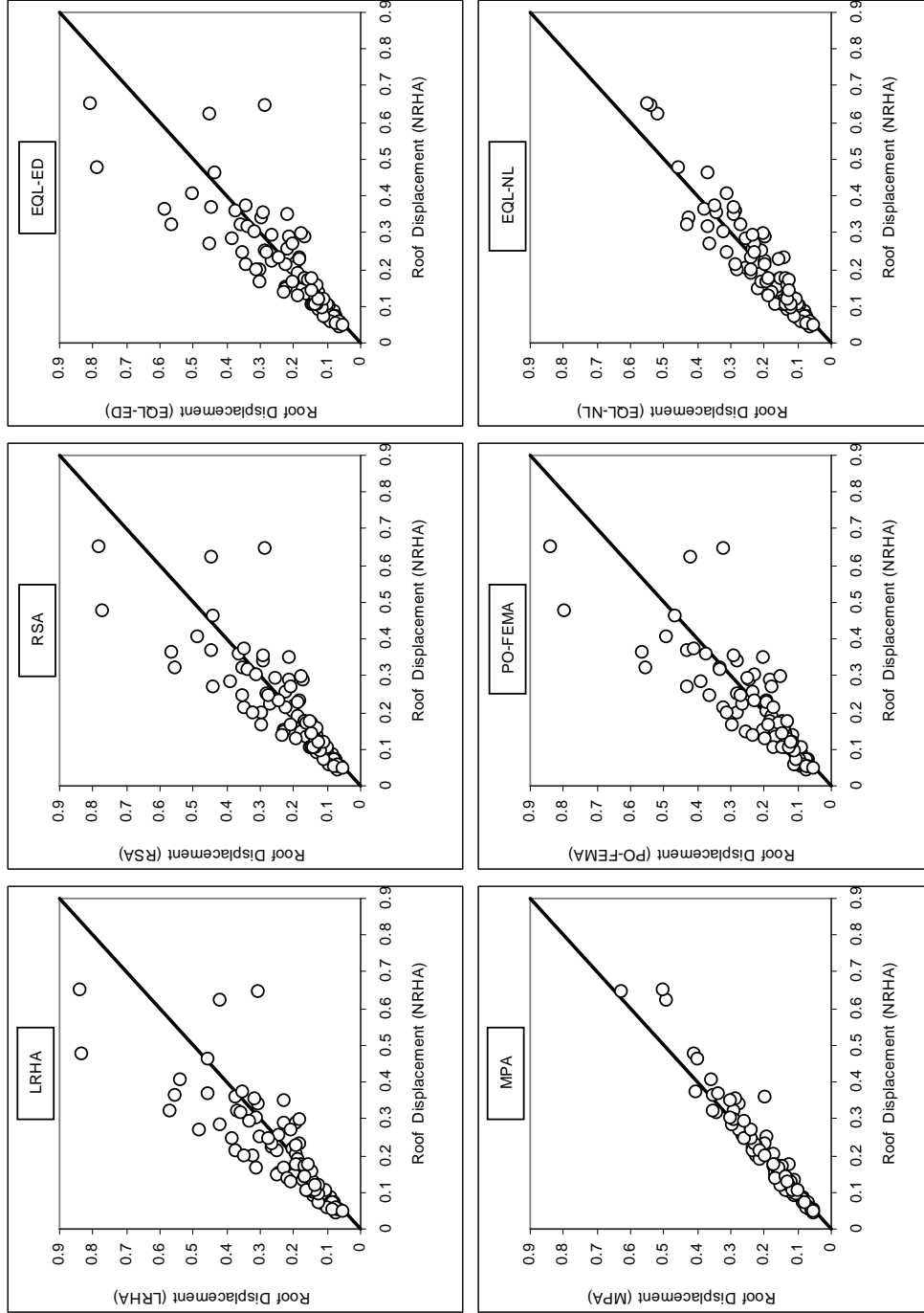


Figure 6.7 Comparison of the roof center of mass displacement demand predictions of approximate methods with the benchmark method (NRHA) for pulse type ground motions

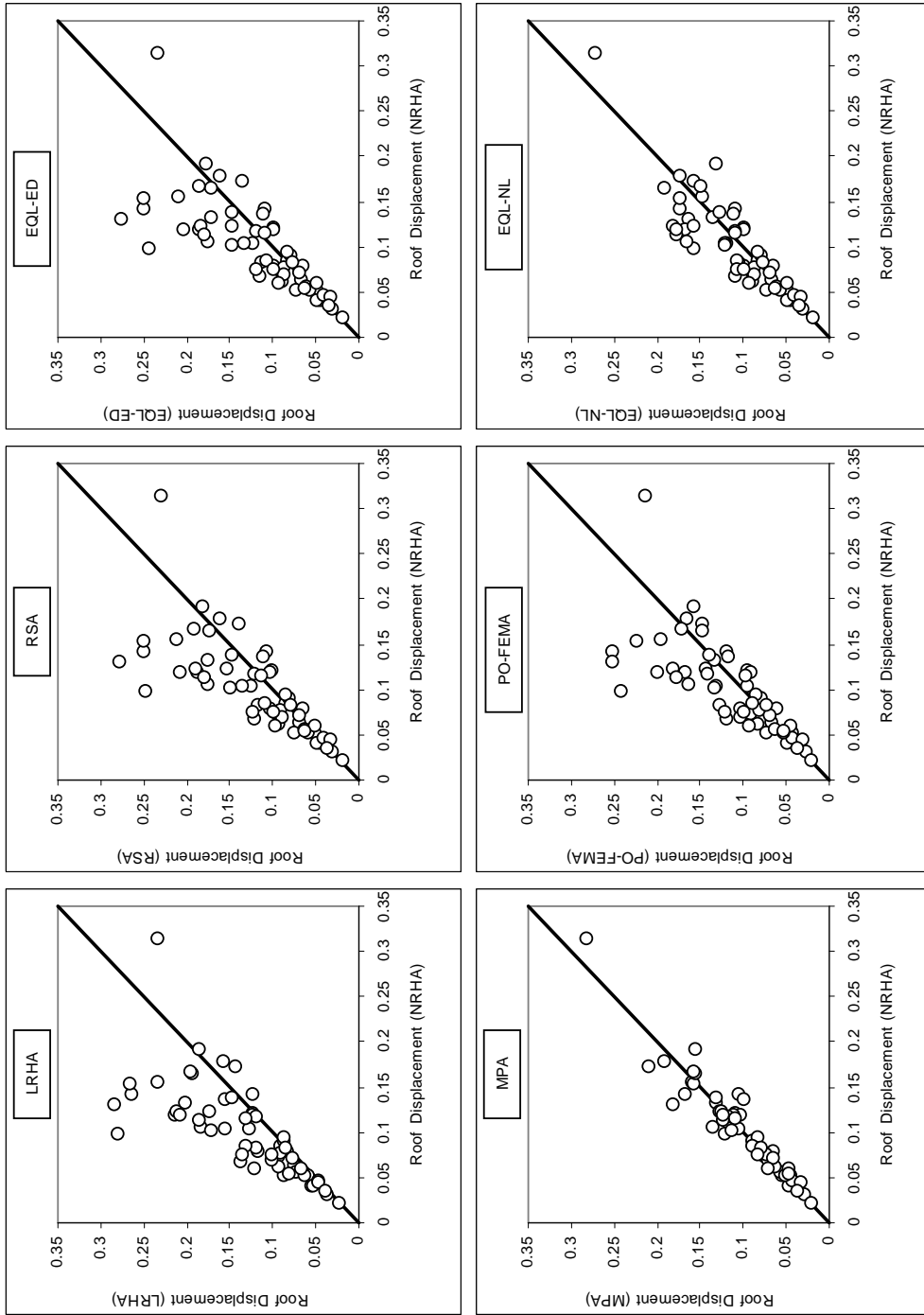


Figure 6.8 Comparison of the roof center of mass displacement demand predictions of approximate methods with the benchmark method (NRHA) for ordinary ground motions

different from those of the linear elastic system. Predictions of PO-FEMA are also close to those of RSA because first mode response is dominant on the roof displacement, and  $C_1$  coefficient which relates the inelastic displacements to elastic displacements is equal to unity for most of the ground motions. EQL-NL greatly improves the predictions of RSA, it reduces the error to about 60% of RSA (Tables 6.2 and 6.3), and therefore it is sufficiently accurate in predicting the roof displacements. MPA is also very accurate in the roof displacement predictions. The observation made for the twelve story frame, stating that the improvement in roof displacement prediction is mainly due to considering inelastic response of SDOF systems instead of employing the equal displacement assumption, also holds for this case study.

Table 6.2 Roof displacement statistics for pulse type ground motions

Method	Median (Method, meters)	Median (Method/NRHA)	Standard Deviation (Method/NRHA)	RMSE
LRHA	0.189	1.145	0.320	0.542
RSA	0.178	1.075	0.294	0.492
EQL-ED	0.175	1.059	0.290	0.505
PO-FEMA	0.176	1.062	0.319	0.505
MPA	0.159	0.961	0.121	0.223
EQL-NL	0.166	1.007	0.224	0.294
NRHA	0.165	-	-	-

Table 6.3 Roof displacement statistics for ordinary ground motions

Method	Median (Method, meters)	Median (Method/NRHA)	Standard Deviation (Method/NRHA)	RMSE
LRHA	0.114	1.273	0.360	0.598
RSA	0.102	1.144	0.341	0.507
EQL-ED	0.101	1.123	0.331	0.492
PO-FEMA	0.097	1.084	0.329	0.462
MPA	0.086	0.965	0.128	0.171
EQL-NL	0.095	1.061	0.243	0.297
NRHA	0.090	-	-	-

Roof displacement demands under ordinary ground motions are smaller than the roof displacement demands under pulse type ground motions. However, RMSE of RSA and LRHA are similarly large for pulse type and ordinary ground motions, which indicates that the nonlinear roof displacements deviate from the linear ones at small to moderate levels of nonlinearity.

#### **6.4.2 Local Response Parameters**

Comparison of roof displacements (for frames), interstory drift ratios and beam chord rotations obtained from the previously mentioned analysis methods are presented in this section. Column chord rotations are not presented, because only the bottom ends of the first story columns exceed yield rotations. According to the definition of chord rotation stated in Chapter 3, bottom end chord rotation of a first story column is equal to the interstory drift ratio of the first story. Since the interstory drift ratios are presented, there remains no need for the presentation of column chord rotations.

For the comparison of local response parameters, ground motions producing NRHA center of mass roof displacements between 0.150 m (0.79 % roof drift) and 0.550 m (2.90 % roof drift) are taken into consideration. Lower bound corresponds to the onset of inelasticity. An upper bound is also set because P- $\Delta$  effects are not considered and ultimate curvature values are not utilized in the moment curvature relations. The number of pulse type and ordinary ground motions remaining in between these bounds are 51 and 11, respectively. Roof displacement demands of these ground motions normalized by the building height are marked on the first mode pushover curve of the building in Figure 6.9. Base shear capacity prediction of the equivalent linearization procedure is also shown with a horizontal line. It is noted that base shear capacity obtained from the equivalent linearization procedure is quite close to the one obtained from pushover analysis.

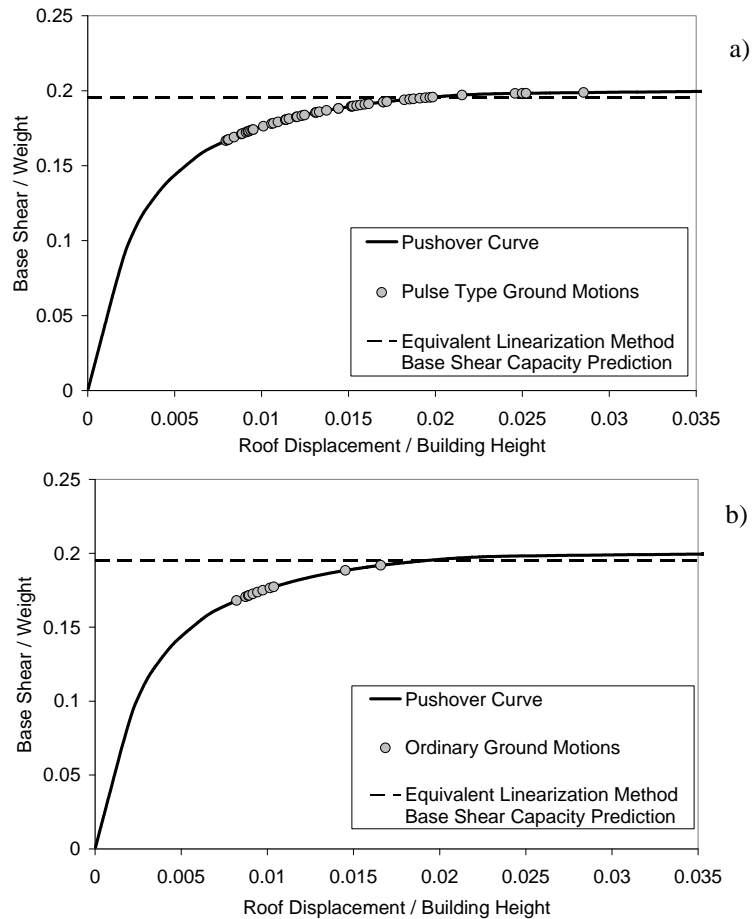


Figure 6.9 Center of mass roof displacement demands obtained from a) pulse type ground motions, b) ordinary ground motions marked on the first mode pushover curve

It can be observed from Figure 6.9 that the roof displacements obtained from pulse type ground motions cover a wider range and they are larger than those obtained from ordinary ground motions. It should be noted that the maximum base shear values obtained from nonlinear response history analyses are different than the values on the pushover curve; therefore ordinates of the marked points are not the actual values.

Pseudo acceleration and displacement response spectra of the 51 pulse type and 11 ordinary ground motions are plotted in Figures 6.10 and 6.11, respectively. It can be observed that the displacements and pseudo accelerations corresponding to

the first and second mode periods are greater for pulse type ground motions with respect to the ordinary ground motions. Differences are larger for the first mode period.

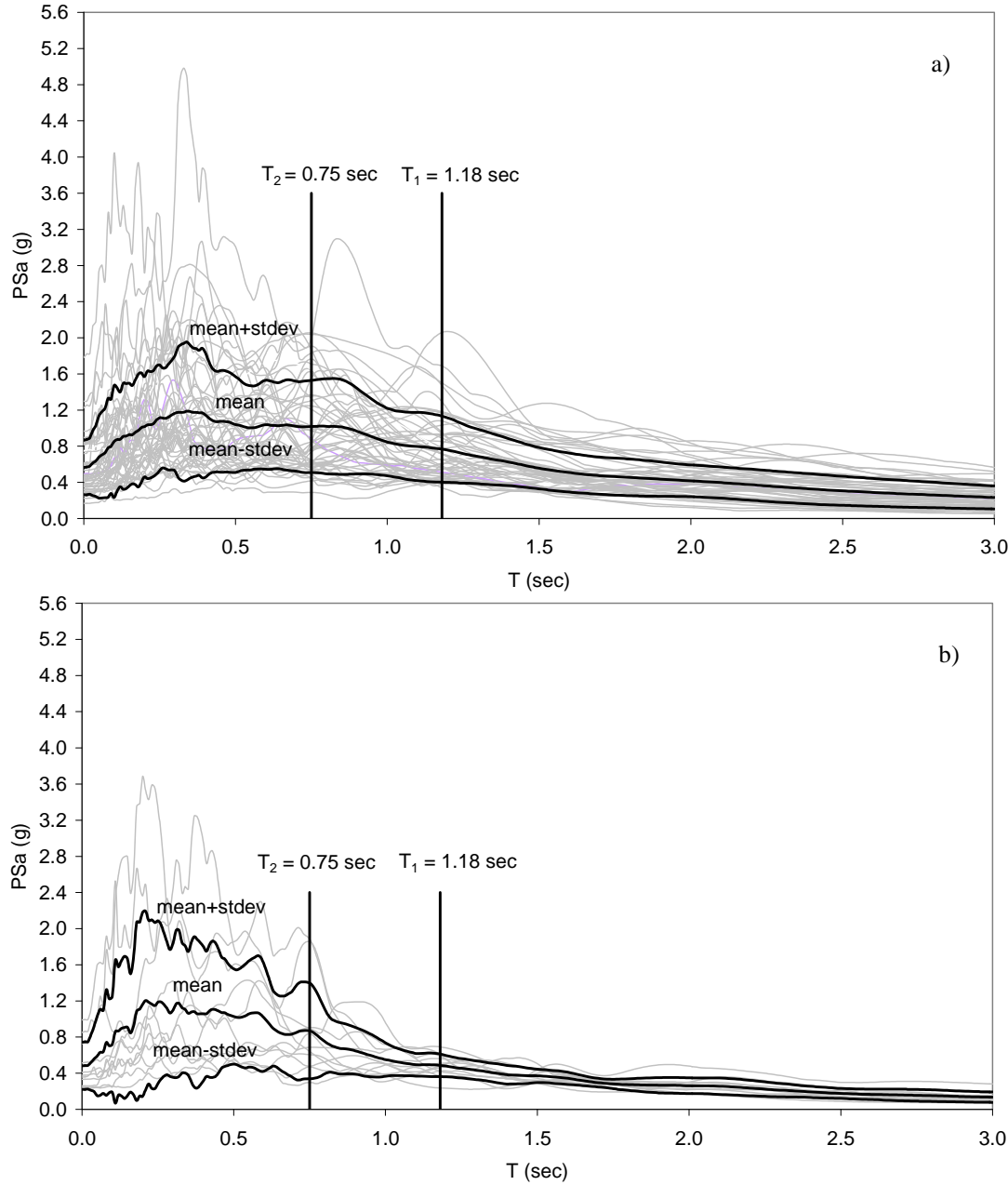


Figure 6.10 5% damped pseudo acceleration response spectra for a) pulse type, b) ordinary ground motions

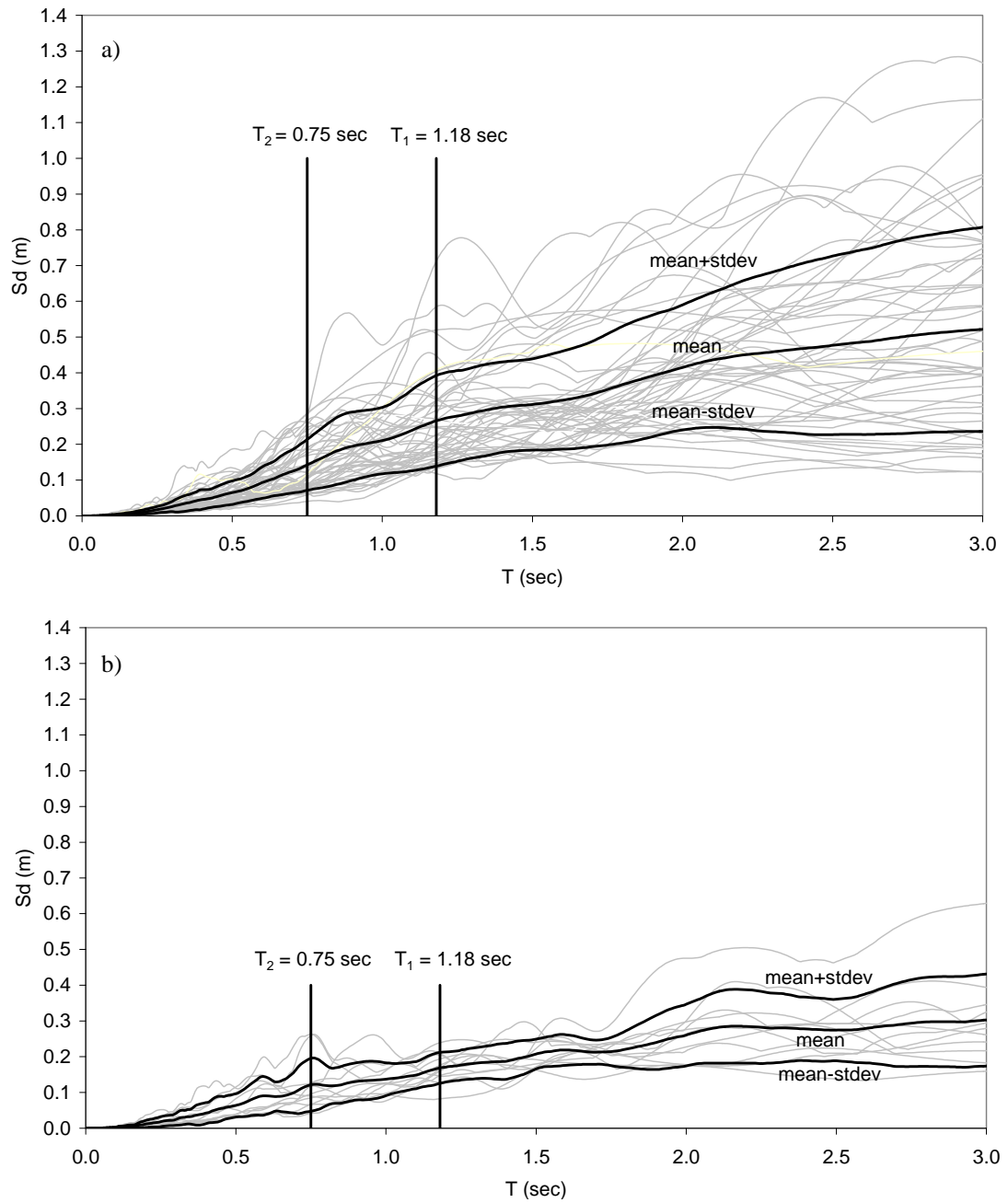


Figure 6.11 5% damped displacement response spectra for a) pulse type, b) ordinary ground motions

Results obtained from the reduced number of ground motions indicated above are presented in the following parts of the chapter.

In order to eliminate the effect of errors due to the differences in the maximum roof displacements at the center of mass, response predictions of the approximate methods are evaluated at roof displacements equal to the maximum roof displacement obtained from NRHA. Such a modification is necessary, because especially the edge frame responses are affected by the magnitude of the lateral displacement at the center of mass and the amount of torsion emanating from the rotation of the center of mass, as presented in the following section. Equating the roof displacements, it is intended to evaluate the approximate methods' accuracy for considering torsion and the inelasticity distribution along the height. Local response parameters determined by EQL-ED are not presented further because they are close to those of EQL-NL at equal roof displacements. In the following part of the chapter, pushover analysis is abbreviated as "PO" instead of "PO-FEMA" since it is evaluated at the roof displacement of NRHA. It should be reminded again that only lateral forces at the center of mass are employed and torques are not considered in the force distribution of PO.

#### **6.4.2.1 Torsional Effects Observed in Nonlinear Response History Analyses**

In order to investigate the amount of torsion arising from asymmetry in plan, median interstory drift ratios obtained from the benchmark method (nonlinear response history analysis) at each frame are plotted in Figure 6.12. Labeling of the frames was presented in Figure 6.1. It can be observed that considerable torsion occurs both for pulse type and ordinary ground motions. It can also be seen that median interstory drift ratios of the pulse type ground motions are greater than those of the ordinary ground motions, similar to the case of roof displacements.

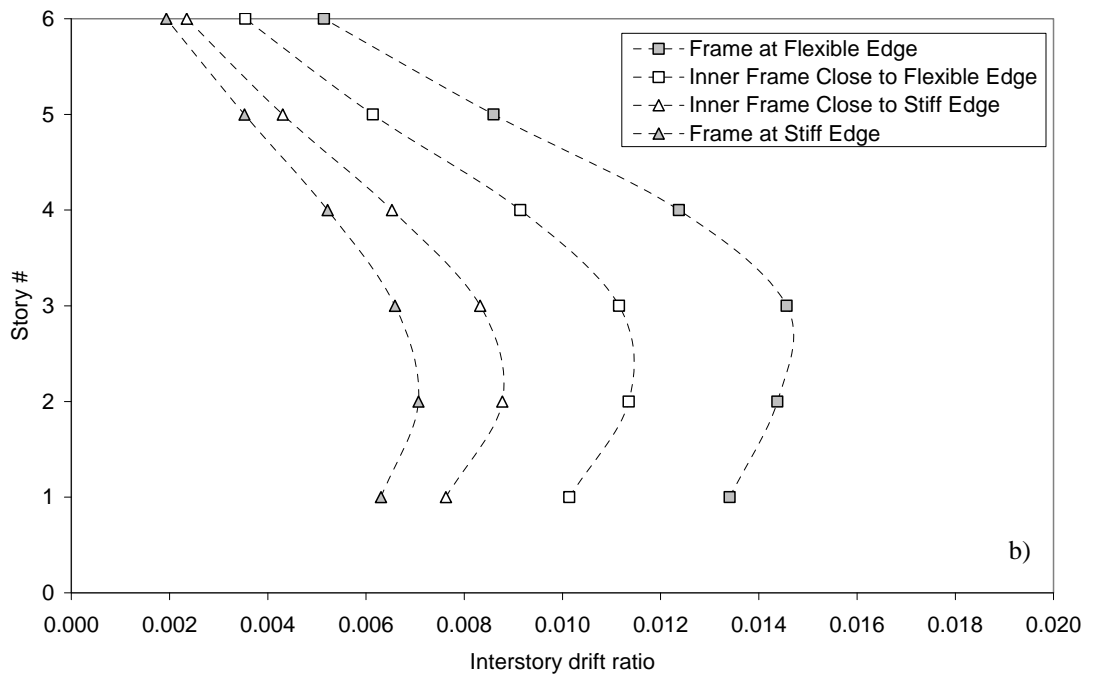
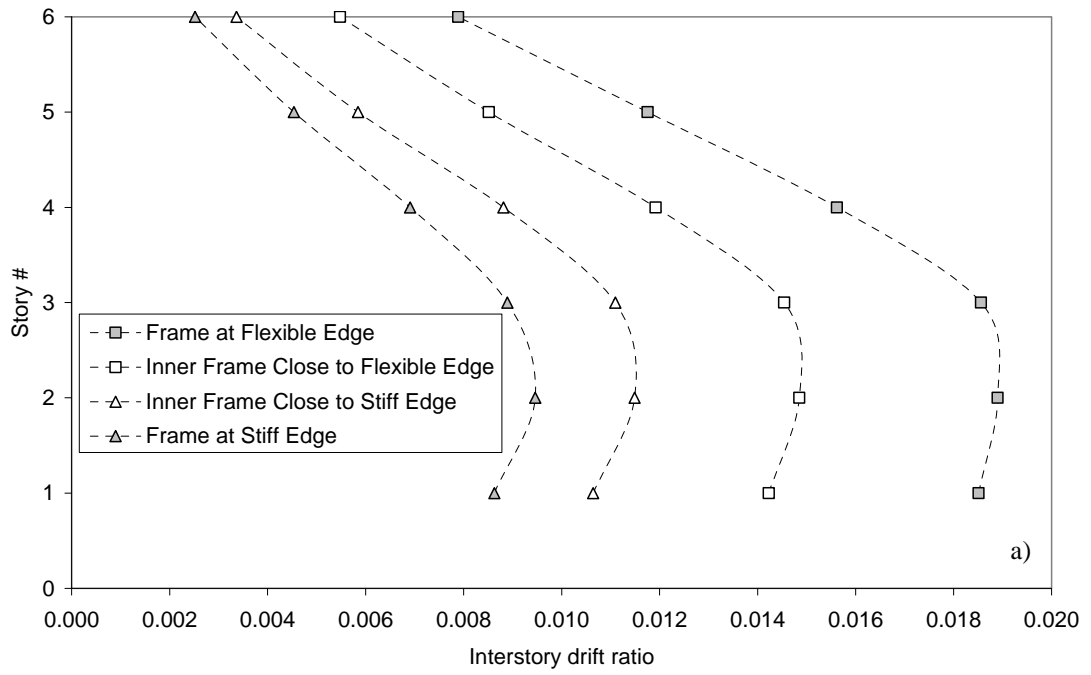


Figure 6.12 Median interstory drift ratios obtained from NRHA for a) pulse type, b) ordinary ground motions

### 6.4.2.2 Roof Displacements of the Frames

Median and RMSE of roof displacements of the four individual frames are presented in the form of bar charts in Figures 6.13 and 6.14 for pulse type and ordinary ground motions respectively. Following observations can be made from the investigation of these figures.

- Median roof displacements of the inner frame close to the flexible edge predicted by the approximate methods are very similar to those determined by NRHA for both types of ground motions. In addition, RMSE of the approximate methods are quite close to zero for this frame since center of mass is located close to this frame (Figure 6.1). Considering that the approximate methods are evaluated at the center of mass roof displacements determined by NRHA, it is evident that the roof displacements predicted by the approximate methods are very close to those of NRHA at the inner frame close to the flexible edge.
- EQL-NL is sufficiently accurate in predicting the roof displacements of frames for both pulse type and ordinary ground motions. It results in predictions close to NRHA at the medial level. It leads to the smallest RMSE among the considered approximate methods for all the frames under pulse type ground motions and for all the frames, except the stiff edge frame, under ordinary ground motions. It greatly reduces RMSE of RSA at the stiff edge frame under ordinary ground motions.
- There are considerable differences between RMSE of RSA and LRHA especially at the edge frames under ordinary ground motions, indicating that these two methods may lead to significantly different responses.
- Main reason of the difference between the response predictions of RSA and LRHA is the torsional components of the modal forces. In Figure 6.6, it can be observed that the modal static torques corresponding to the first pair of modes are equal in magnitude but opposite in direction. The situation is similar for the second pair of modes. Effect of opposite directions is lost in

RSA since the maximum responses in each mode are combined with a combination rule. For this case study building, CQC is employed as the combination rule in which the sign of the responses are taken into consideration. However, the cross correlation coefficients come out to be small since the natural periods are not so close. Therefore, responses from the different modes are additive in RSA. In the case that the maximum elastic SDOF accelerations in the coupling modes possess the same signs, differences between the response predictions of RSA and LRHA deviate from each other. Because, in this case, effect of the torques are counteracting in LRHA and they are additive in RSA.

- PO slightly underestimates the roof displacements at the edge frames for both types of ground motions. It results in median values similar to those of NRHA at the inner frames.
- MPA underestimates the response at the stiff edge and overestimates the response at the flexible edge because of overestimation of torsion. Cause of this overestimation is the torsional component of the first modal force. First mode response is generally dominant in MPA, since the center of mass roof displacement demands of the other modes are small. In the higher modes, base shear capacities are higher, periods are smaller and modal participation factors multiplied with the top story modal amplitudes are smaller than those corresponding to the first mode. Therefore roof displacement demands of these modes are generally quite small when compared to that of the first mode. In the first mode, the torsional component of the first mode vector decreases the equivalent lateral forces acting at the stiff edge frame and increases the equivalent lateral forces acting at the flexible edge frame. Equivalent lateral static first mode forces for the linear elastic system acting at the stiff and flexible edge frames with and without the torques at the center of mass are presented in Figure 6.15. Forces corresponding to the case with torques at the center of mass belong to the MPA first mode distribution and forces corresponding to the case without torques at the center of mass belong to PO force distribution. During NRHA, if the signs of the response

accelerations of the coupled modes are the same, torques of the coupled modes counteract and only lateral forces remain. In such cases, MPA underestimates the response at the stiff edge and overestimates the response at the flexible edge, whereas PO does not result in such an overestimation or underestimation because of the torsion effect since only the lateral forces are considered in the force distribution of PO.

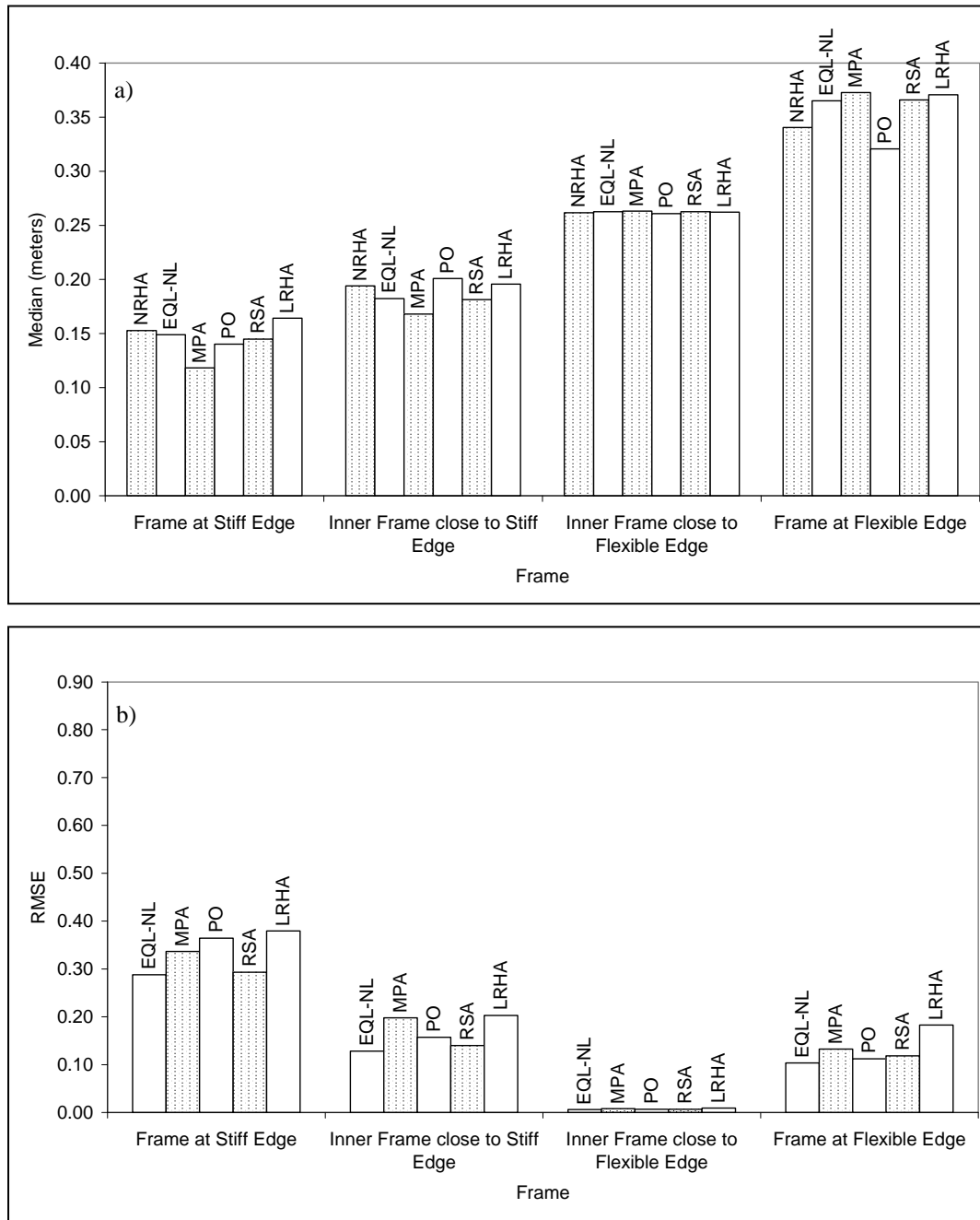


Figure 6.13 a) Median, b) RMSE of roof displacements of the four individual frames for pulse type ground motions

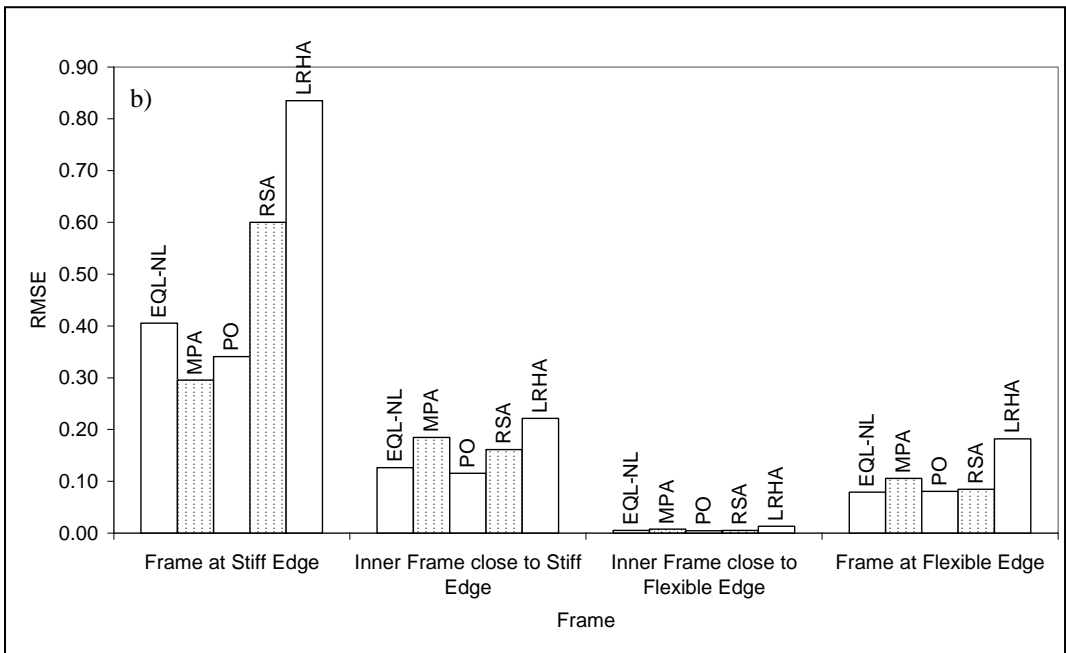
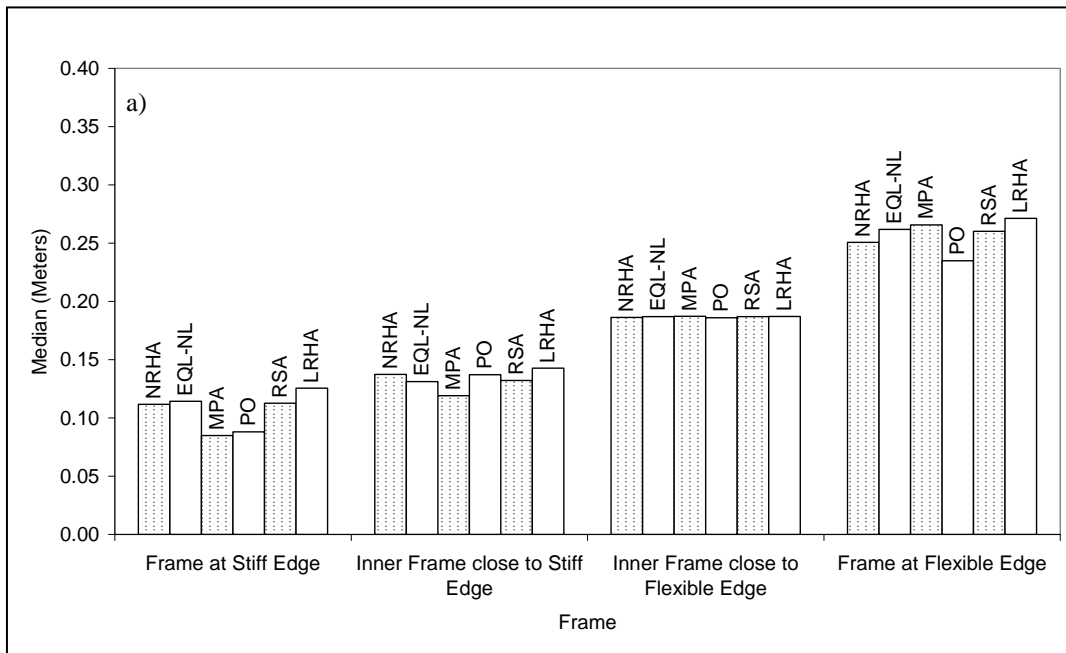


Figure 6.14 a) Median, b) RMSE of roof displacements of the four individual frames for ordinary ground motions

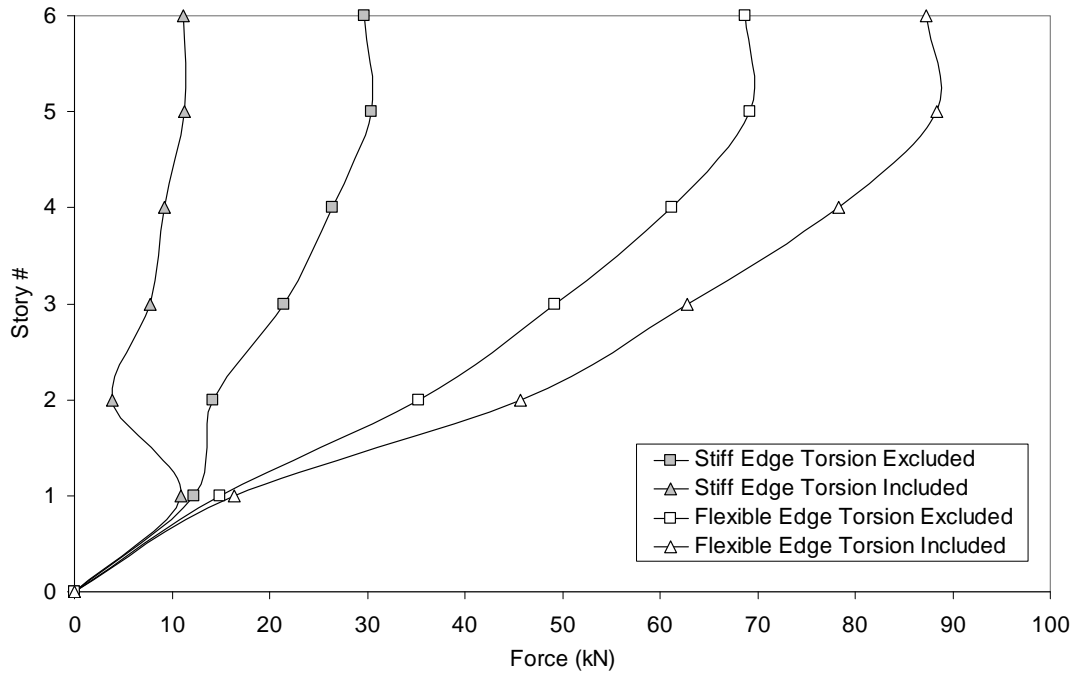


Figure 6.15 Equivalent lateral first modal static forces for the linear elastic system acting at the stiff and flexible edge frames with and without the torques at the center of mass

### 6.4.2.3 Interstory Drift Ratios and Beam Chord Rotations

#### a) Pulse type Ground Motions

Median of interstory drift ratios and beam chord rotations obtained from different analysis methods are plotted in Figures 6.16-6.19 for all frames of the case study building under pulse type ground motions. Beam chord rotation at a story level indicates the average of maximum chord rotations at the beam ends in a story. Beam chord rotations obtained from the approximate methods divided by those obtained from NRHA are plotted in Figures 6.20-6.23. In these figures, each thin gray line corresponds to one ground motion and the thick gray lines indicate the median-standard deviation, median and median+standard deviation values. The

black line belongs to the ground motion selected for presentation in the following sections. Following observations can be deduced from Figures 6.16-6.23.

- Equivalent linearization procedure is successful in improving the median predictions of RSA for all frames, with reference to NRHA. Improvement in the beam chord rotation estimations is more pronounced than the improvement in interstory drift ratios. There is considerable improvement in the beam chord rotations at the flexible edge frame and at the inner frame close to the flexible edge where inelasticity is larger.
- Observing the dispersion in the beam chord rotations in Figures 6.20-6.23, it can be stated that the equivalent linearization procedure reduces the scatter present in RSA or results in similar amounts of scatter with RSA. For both situations, errors are reduced since the equivalent linearization procedure improves the median predictions.
- Generally, RSA and LRHA underestimate the beam chord rotations and interstory drift ratios with large amounts of dispersion. LRHA overestimates the top two story responses. As can be seen from Figures 6.20-6.23, there are substantial differences between the beam chord rotation predictions of RSA and LRHA because of the differences in the consideration of torsional components of modal forces as explained previously.
- PO seems to be very successful in the median predictions except in the top two stories for all frames. However, concerning the dispersion, it is seen that there is large amount of scatter at the stiff edge frame and the inner frame close to the stiff edge. Scatter is small at the lower stories of the flexible edge frame and the inner frame close to the flexible edge. Therefore, PO can be regarded as satisfactory in estimating the responses at the flexible edge except the top stories. It underestimates the responses at the top two stories of all frames. EQL-NL is more successful at the top two stories with respect to PO. EQL-NL also underestimates the response at the top two stories; however the amount of underestimation is smaller. Dispersion in the normalized beam chord rotations of EQL-NL is much smaller than that of PO at the stiff edge

(Figures 6.20 and 6.21). Errors of EQL-NL and PO are similar at the flexible edge frame, PO being more accurate at the first story and EQL-NL being more accurate at the top two stories. Overall, it can be stated that response predictions of the equivalent linearization procedure are as accurate as the response predictions of the conventional pushover analysis, they are more accurate at the top stories at which conventional pushover possesses a drawback in considering the higher mode effects.

- MPA underestimates the response at the stiff edge frame and overestimates the response at the lower three stories of the flexible edge frame because of the overestimated torsion as explained in Section 6.4.2.2. Underestimations at the stiff edge frame are clearly observed in Figure 6.20. In this figure, it is seen that MPA underestimates the beam chord rotations at all of the stories under nearly all of the ground motions. It overestimates the beam chord rotations at the lower two stories of the flexible edge frame under nearly all of the ground motions (Figure 6.23). Response predictions of MPA are accurate at the inner frame close to the flexible edge where the torsion effect is smallest. It can be stated that consideration of torques in the modal force vectors is a drawback of MPA for 3D buildings with unsymmetrical plans.
- MPA slightly reduces the amount of underestimation in the response predictions of PO at the top two stories. However, it introduces additional errors because of the overestimated torques. It can be stated that the proposed equivalent linearization procedure results in more accurate response predictions with respect to MPA for the six story building with unsymmetrical-plan.

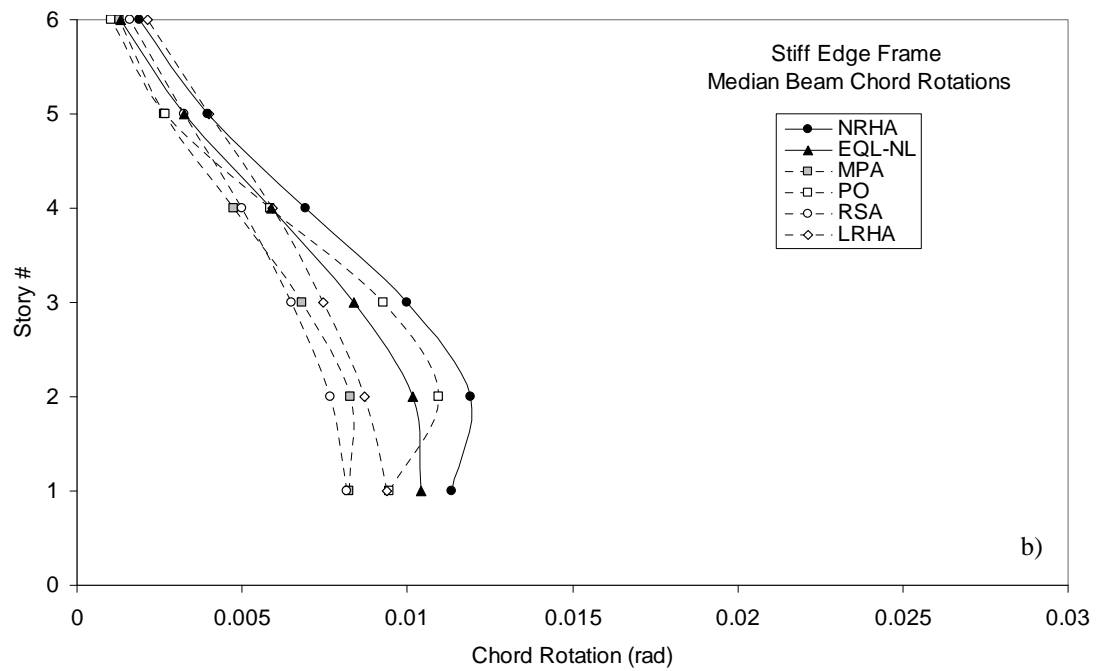
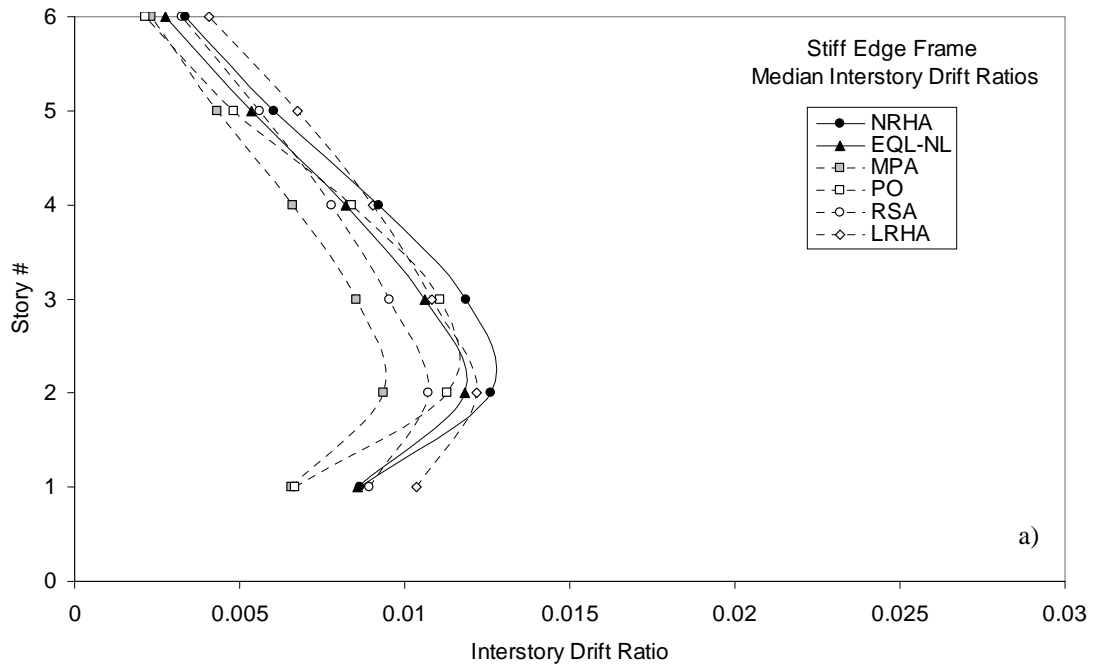


Figure 6.16 Median of a) interstory drift ratios, b) beam chord rotations at the stiff edge frame for pulse type ground motions

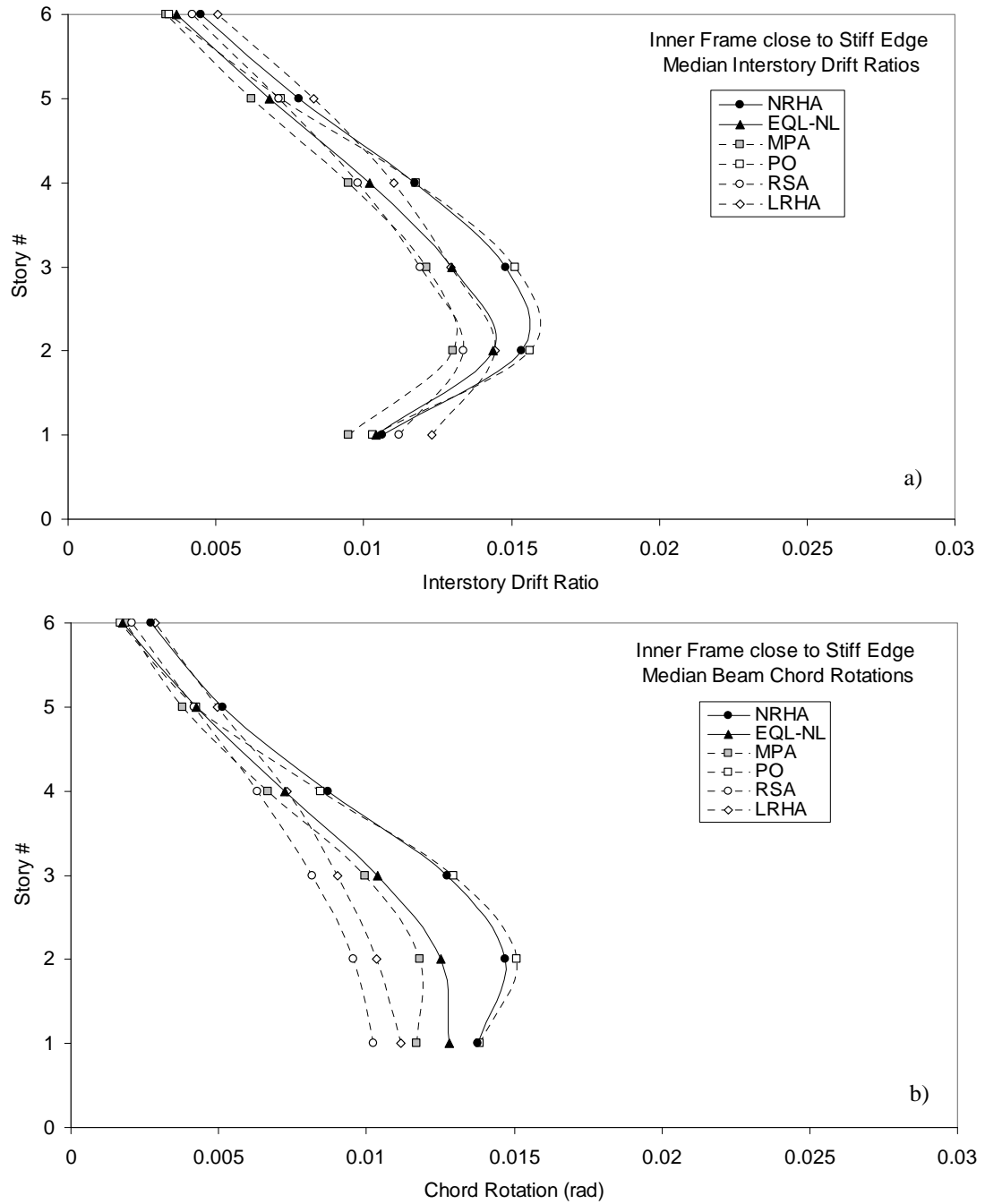


Figure 6.17 Median of a) interstory drift ratios, b) beam chord rotations at the inner frame close to stiff edge for pulse type ground motions

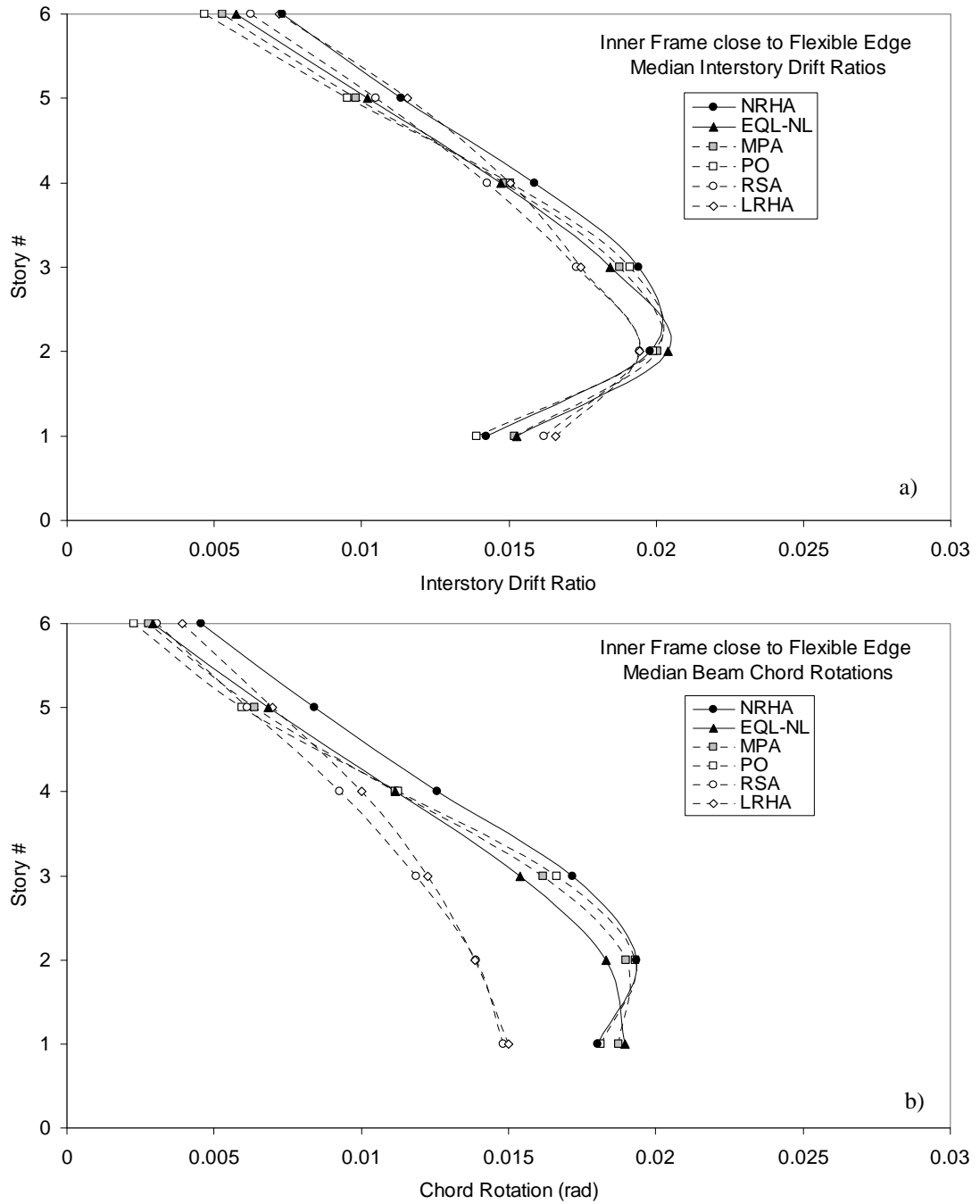


Figure 6.18 Median of a) interstory drift ratios, b) beam chord rotations at the inner frame close to flexible edge for pulse type ground motions

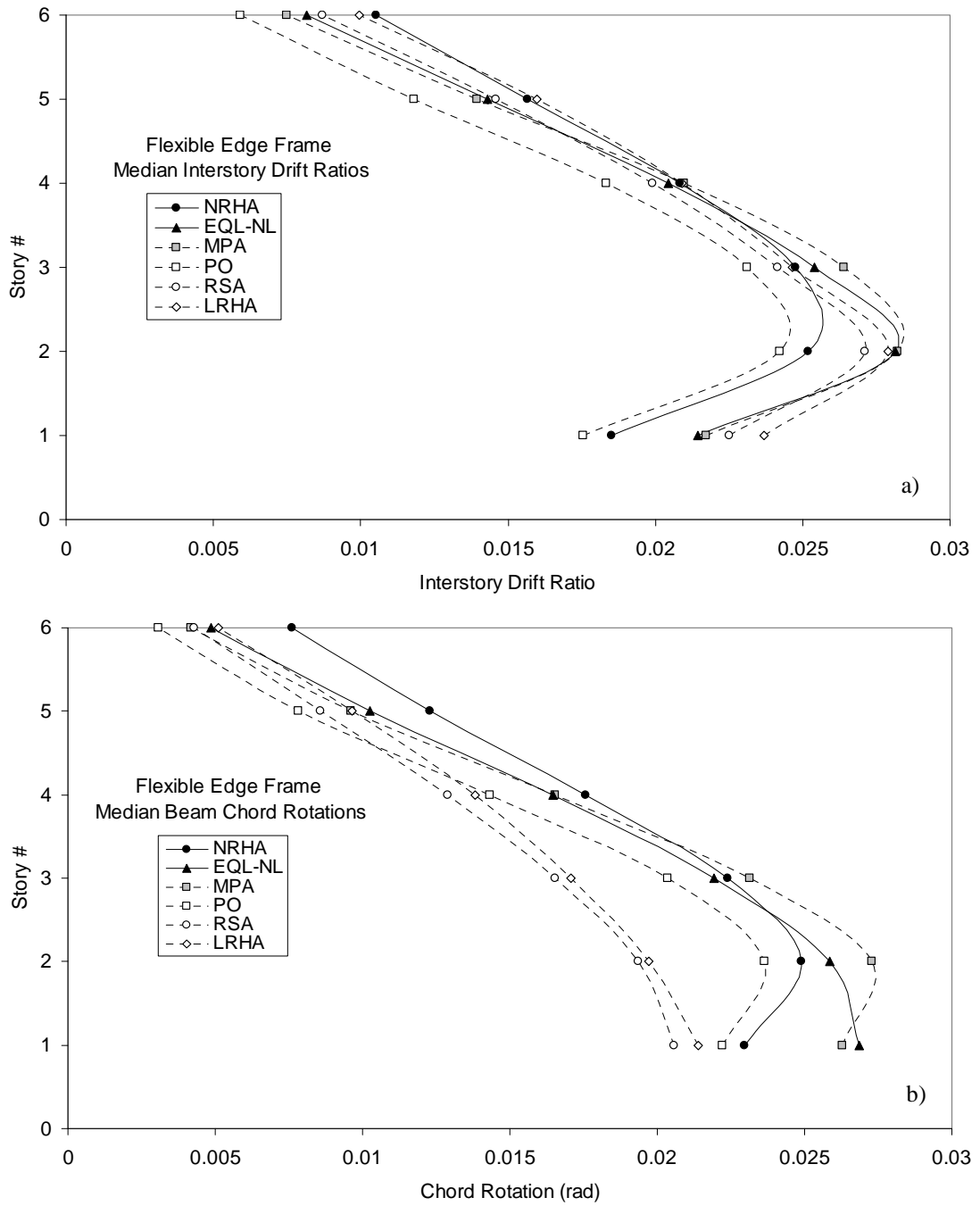


Figure 6.19 Median of a) interstory drift ratios, b) beam chord rotations at the flexible edge frame for pulse type ground motions

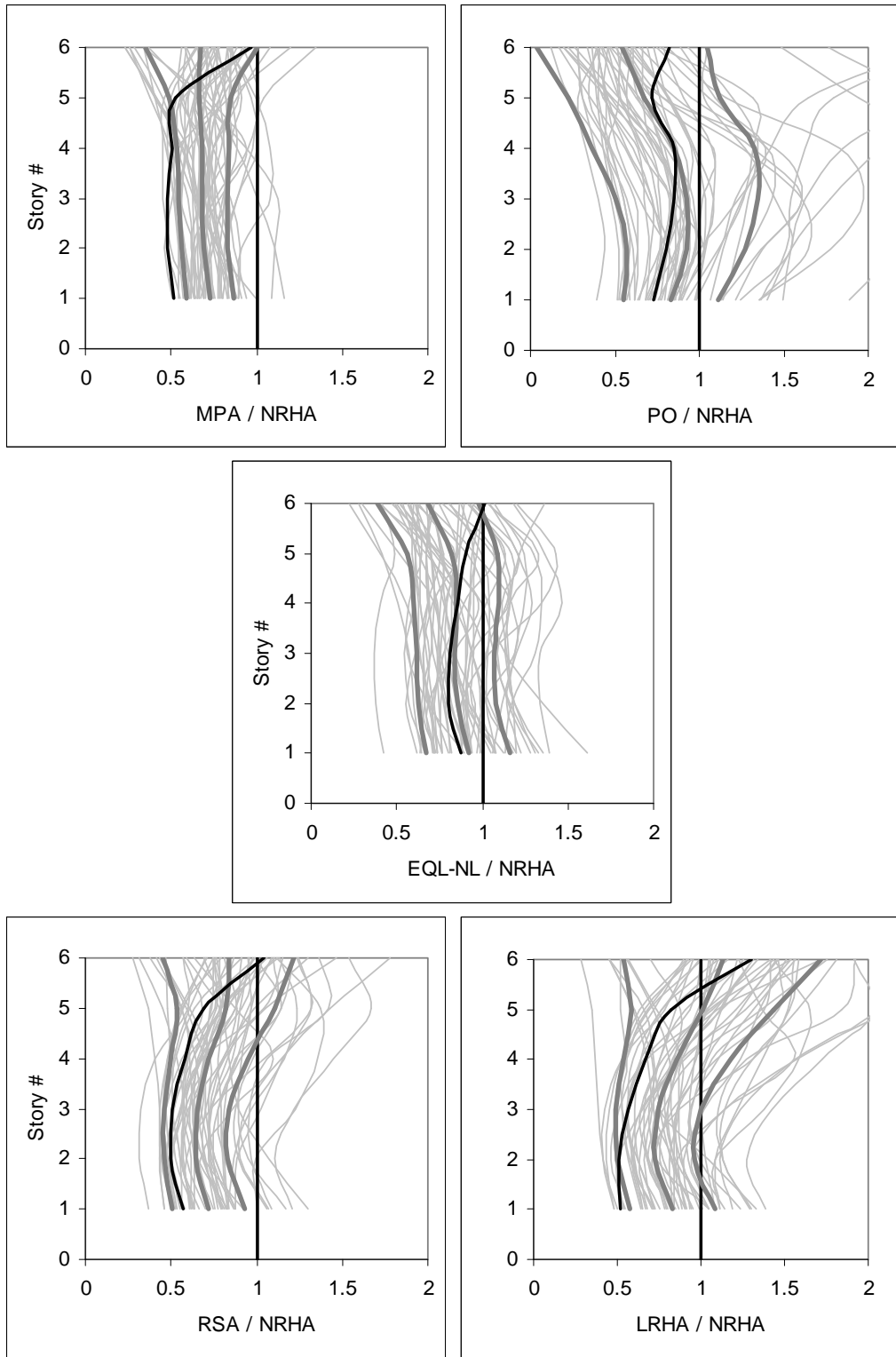


Figure 6.20 Beam chord rotations obtained from the approximate methods normalized with those obtained from NRHA at the stiff edge frame under pulse type ground motions

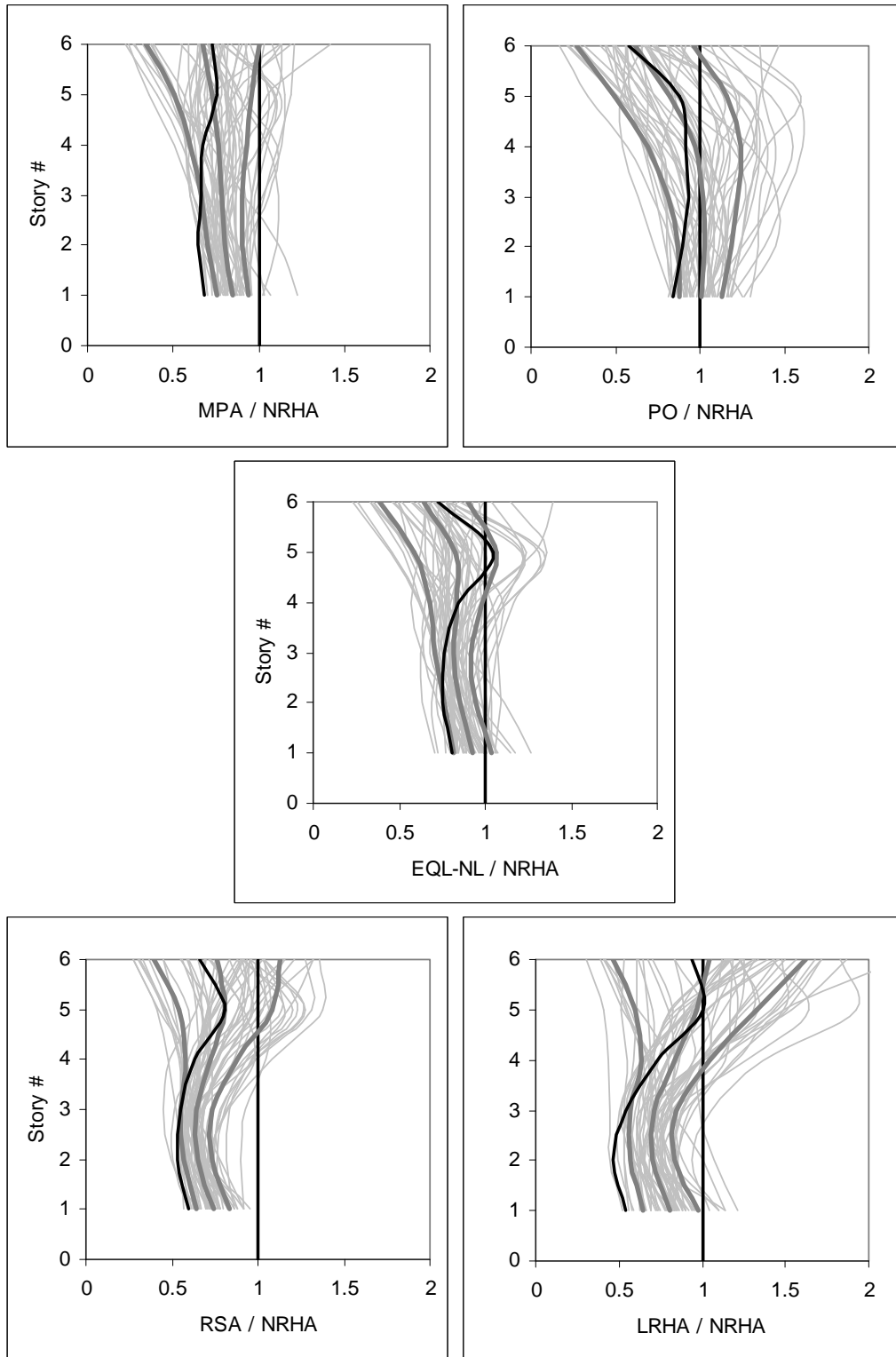


Figure 6.21 Beam chord rotations obtained from the approximate methods normalized with those obtained from NRHA at the inner frame close to the stiff edge under pulse type ground motions

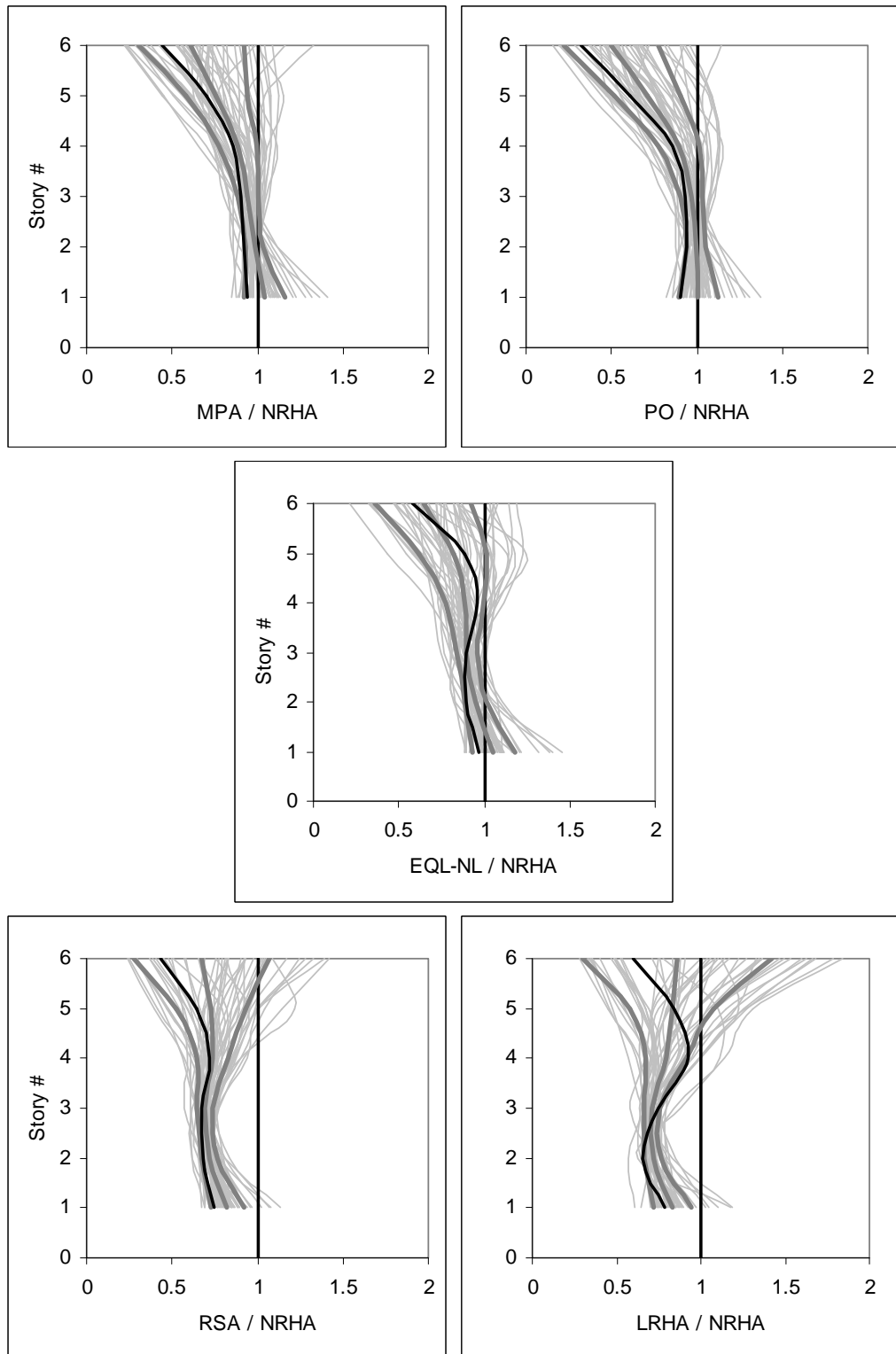


Figure 6.22 Beam chord rotations obtained from the approximate methods normalized with those obtained from NRHA at the inner frame close to the flexible edge under pulse type ground motions

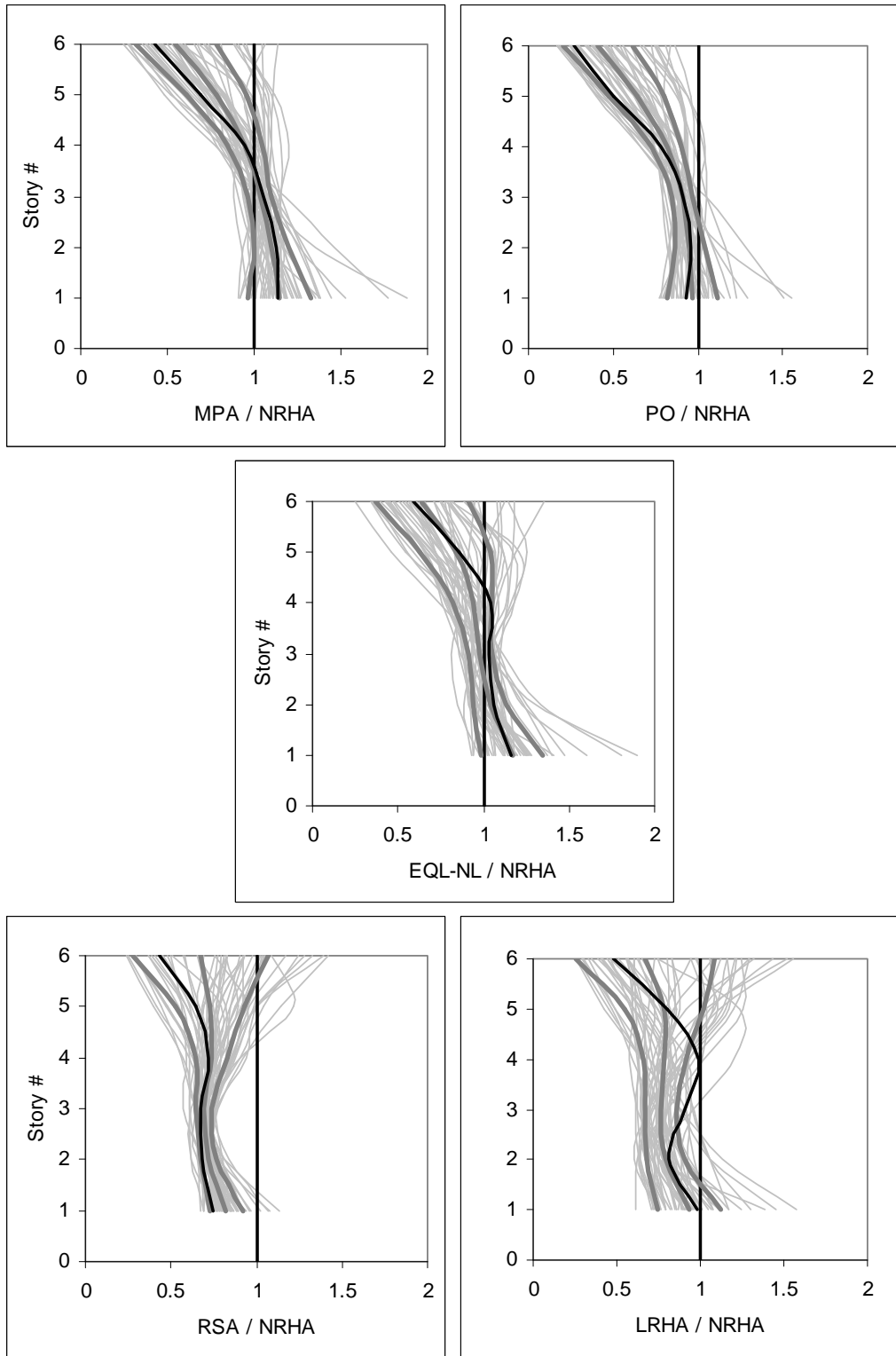


Figure 6.23 Beam chord rotations obtained from the approximate methods normalized with those obtained from NRHA at the flexible edge frame under pulse type ground motions

## b) Ordinary Ground Motions

Median of interstory drift ratios and beam chord rotations obtained from the employed analysis methods are plotted in Figures 6.24-6.27 for all of the frames of the case study building under ordinary ground motions. Beam chord rotations obtained from the approximate methods divided by those obtained from NRHA are plotted in Figures 6.28-6.31. Observations related to these figures are very similar to those noted from the pulse type ground motions.

- Equivalent linearization procedure is successful in improving the median predictions of RSA for all the frames. Improvement in the beam chord rotation estimations is more pronounced than the improvement in the interstory drift ratios. There is considerable improvement in the beam chord rotations of the flexible edge frame and the inner frame close to the flexible edge.
- Observing the dispersion in the beam chord rotations in Figures 6.28-6.31, it can be stated that EQL-NL results in similar values of scatter with RSA. Therefore EQL-NL reduces the errors of RSA since it improves the median predictions.
- Generally, RSA and LRHA underestimate the beam chord rotations and interstory drift ratios. LRHA overestimates the top two story responses. As can be seen from Figures 6.28-6.31, there are substantial differences between the beam chord rotation predictions of RSA and LRHA because of the differences in the consideration of torsional components of the modal forces.
- PO results in accurate predictions at the lower three stories of the frame at the inner frame close to the stiff edge, inner frame close to the flexible edge and the flexible edge frame. It underestimates the responses at the top three stories. Equivalent linearization procedure results in better predictions than PO at the top three stories of all frames. It also results in better beam chord rotation predictions at the lower three stories of the stiff edge frame. EQL-NL and PO results in similar errors in the beam chord rotation predictions at the

lower three stories of the flexible edge frame. PO results in more accurate predictions at the lower three stories of the inner frames (Figures 6.28-6.31).

- MPA underestimates the response at the stiff edge frame and the inner frame close to the stiff edge. It overestimates the response at the lower three stories of the flexible edge frame. MPA underestimates the beam chord rotations at all of the stories of the stiff edge frame and the inner frame close to stiff edge under nearly all of the ground motions (Figures 6.28 and 6.29). It overestimates the beam chord rotations at the lower two stories of the flexible edge frame under nearly all of the ground motions (Figure 6.31). Response predictions of MPA can be regarded as accurate at the inner frame close to the flexible edge where the torsion effect is smallest.
- Observing the results from both types of ground motions, it can be stated that MPA does not improve the predictions of PO for 3D buildings with unsymmetrical plans.
- Like the pulse type ground motions, equivalent linearization procedure results in more accurate response predictions with respect to MPA for ordinary ground motions.

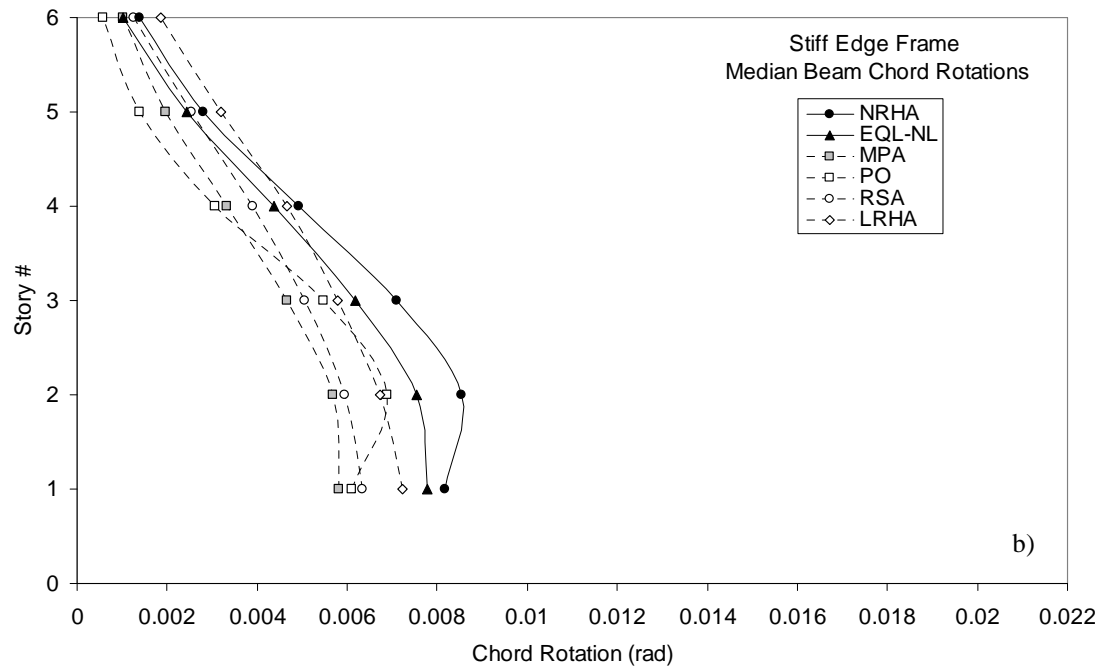
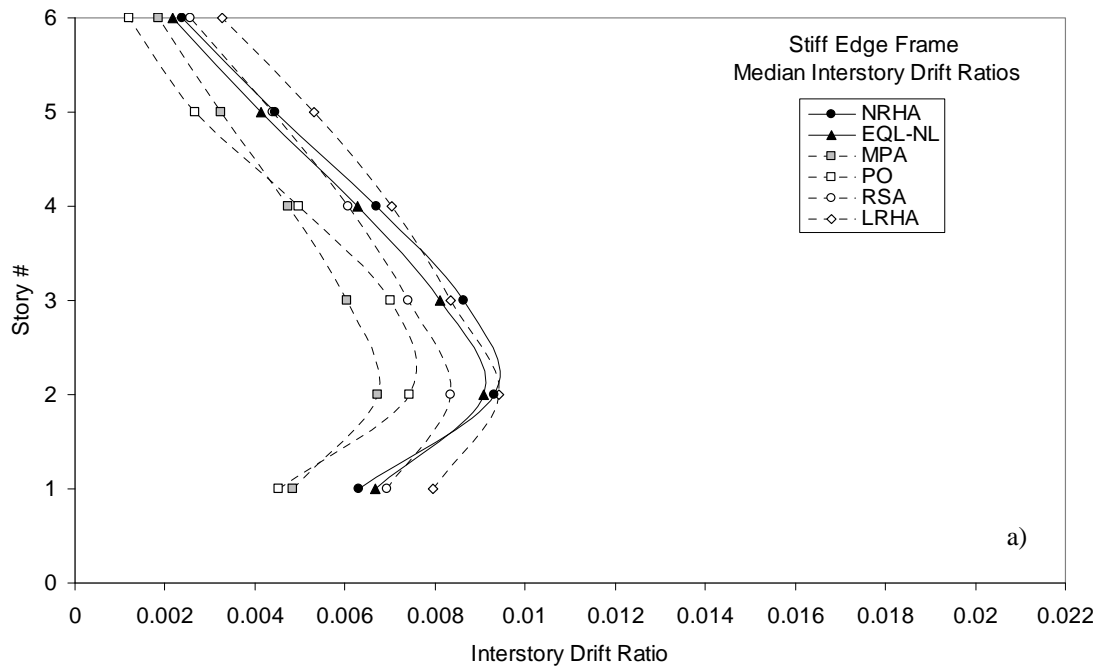


Figure 6.24 Median of a) interstory drift ratios, b) beam chord rotations at the stiff edge frame for ordinary ground motions

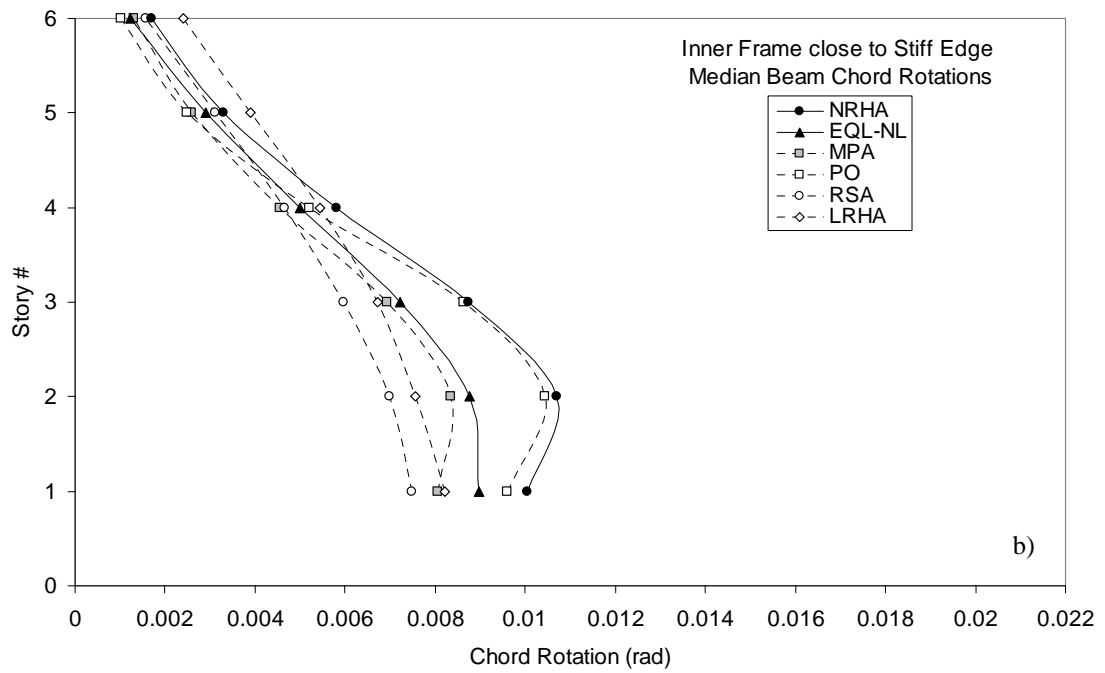
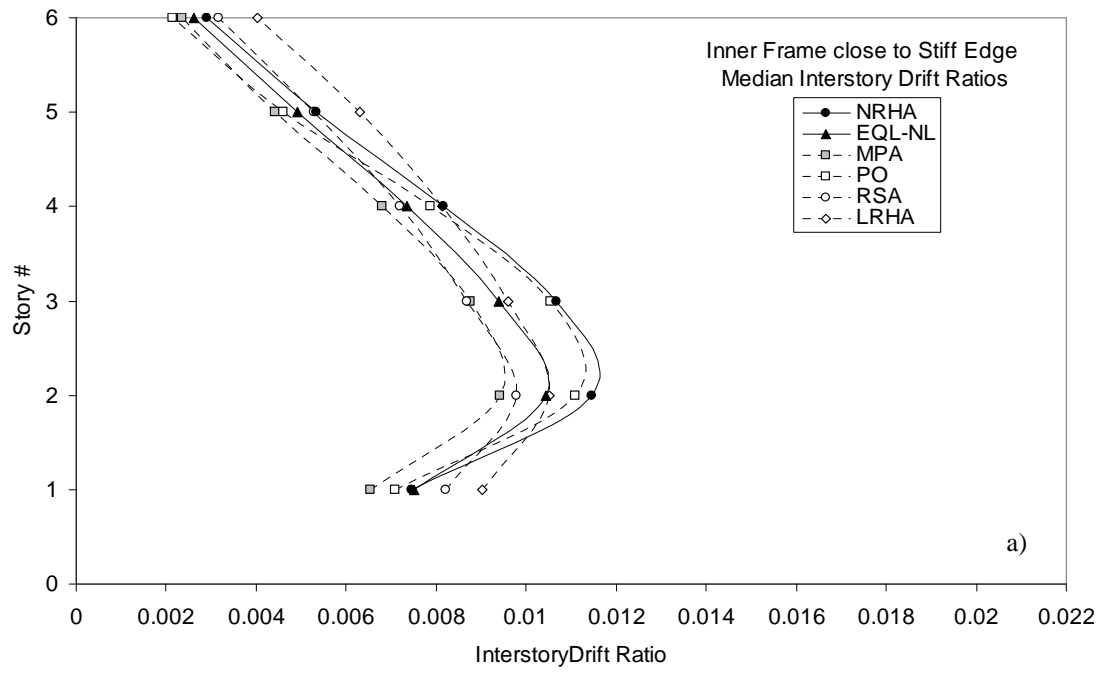


Figure 6.25 Median of a) interstory drift ratios, b) beam chord rotations at the inner frame close to the stiff edge for ordinary ground motions

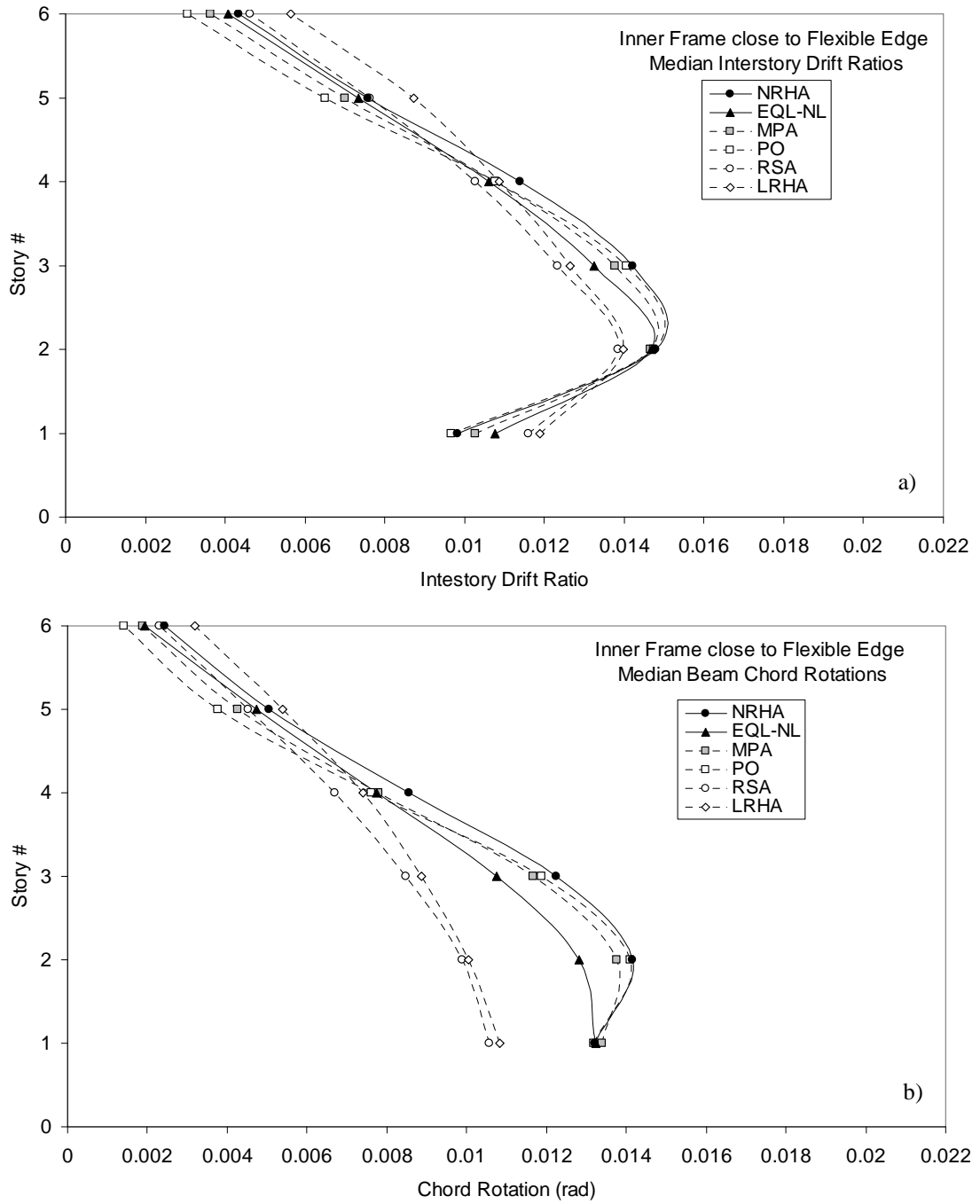


Figure 6.26 Median of a) interstory drift ratios, b) beam chord rotations at the inner frame close to the flexible edge for ordinary ground motions

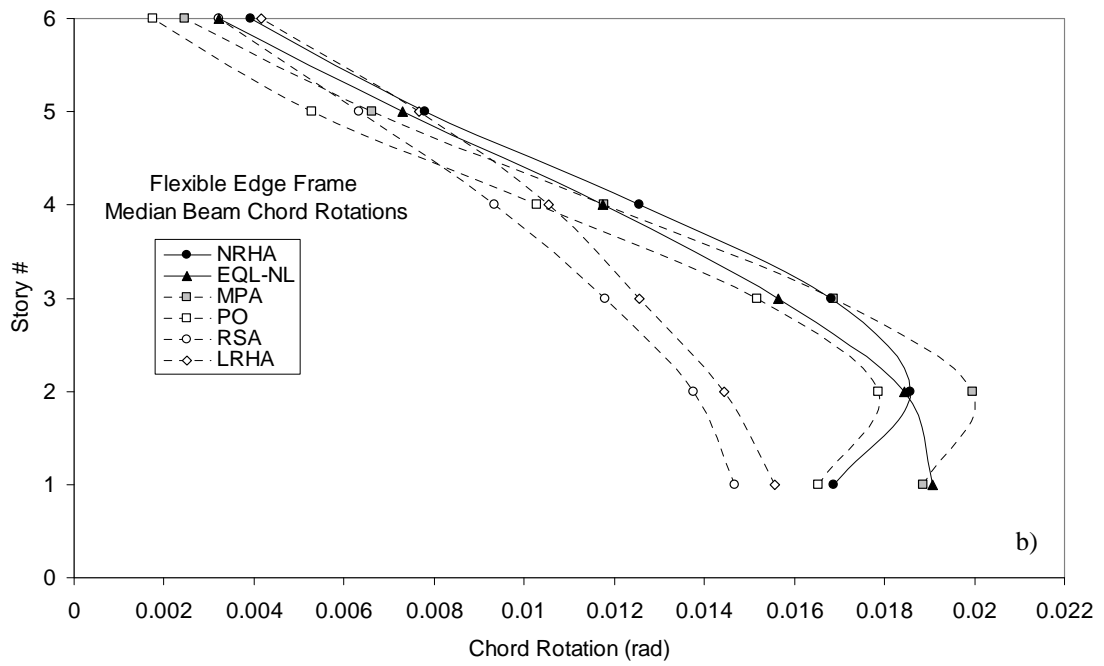
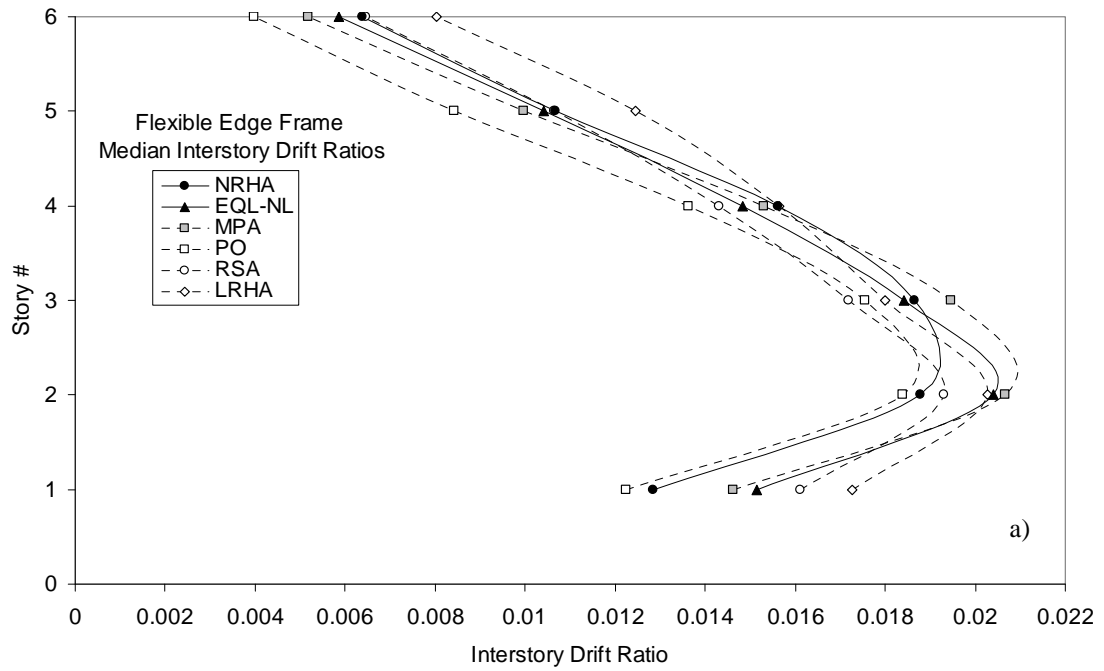


Figure 6.27 Median of a) interstory drift ratios, b) beam chord rotations at the flexible edge frame for ordinary ground motions

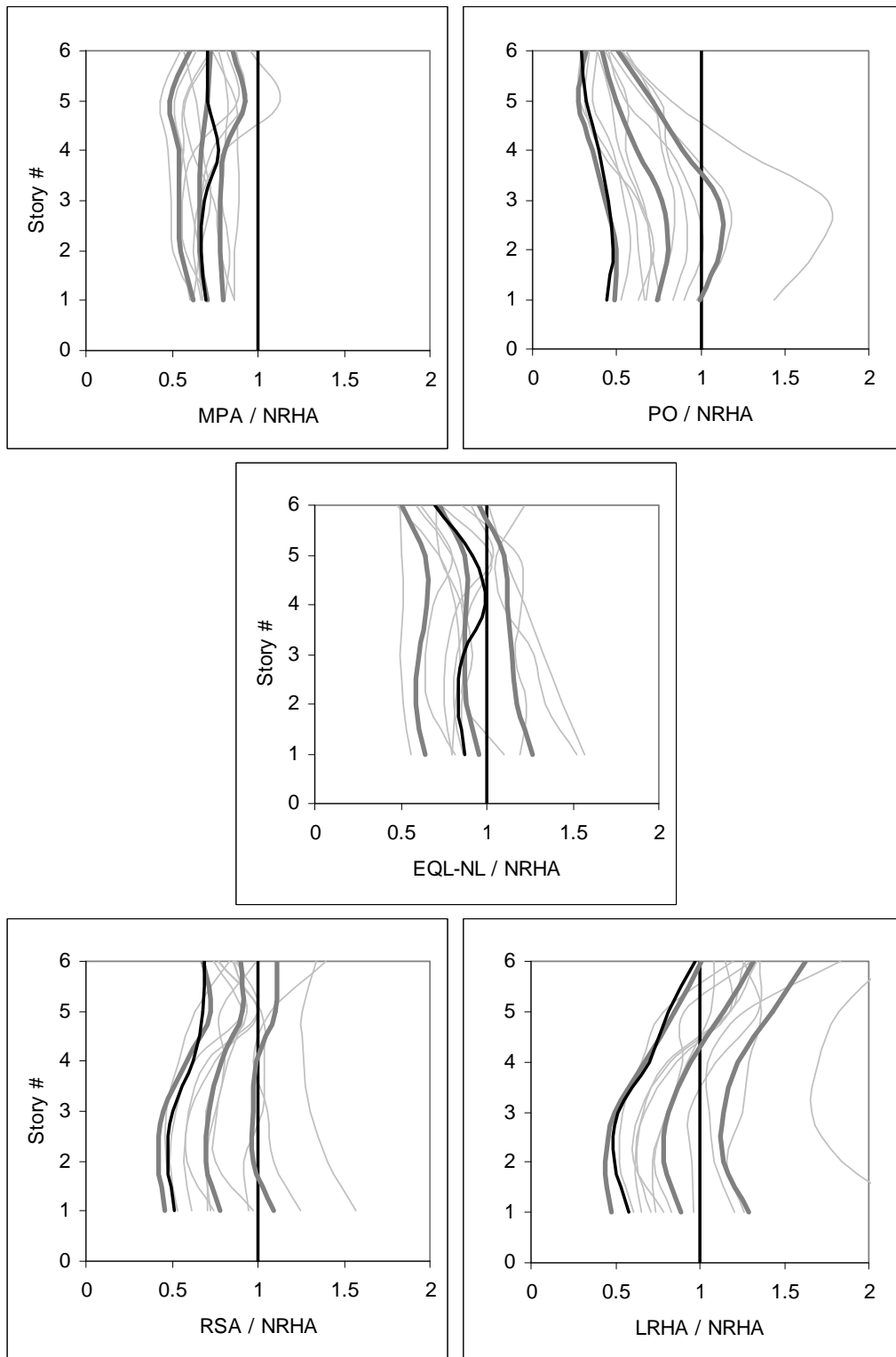


Figure 6.28 Beam chord rotations obtained from the approximate methods normalized with those obtained from NRHA at the stiff edge frame under ordinary ground motions

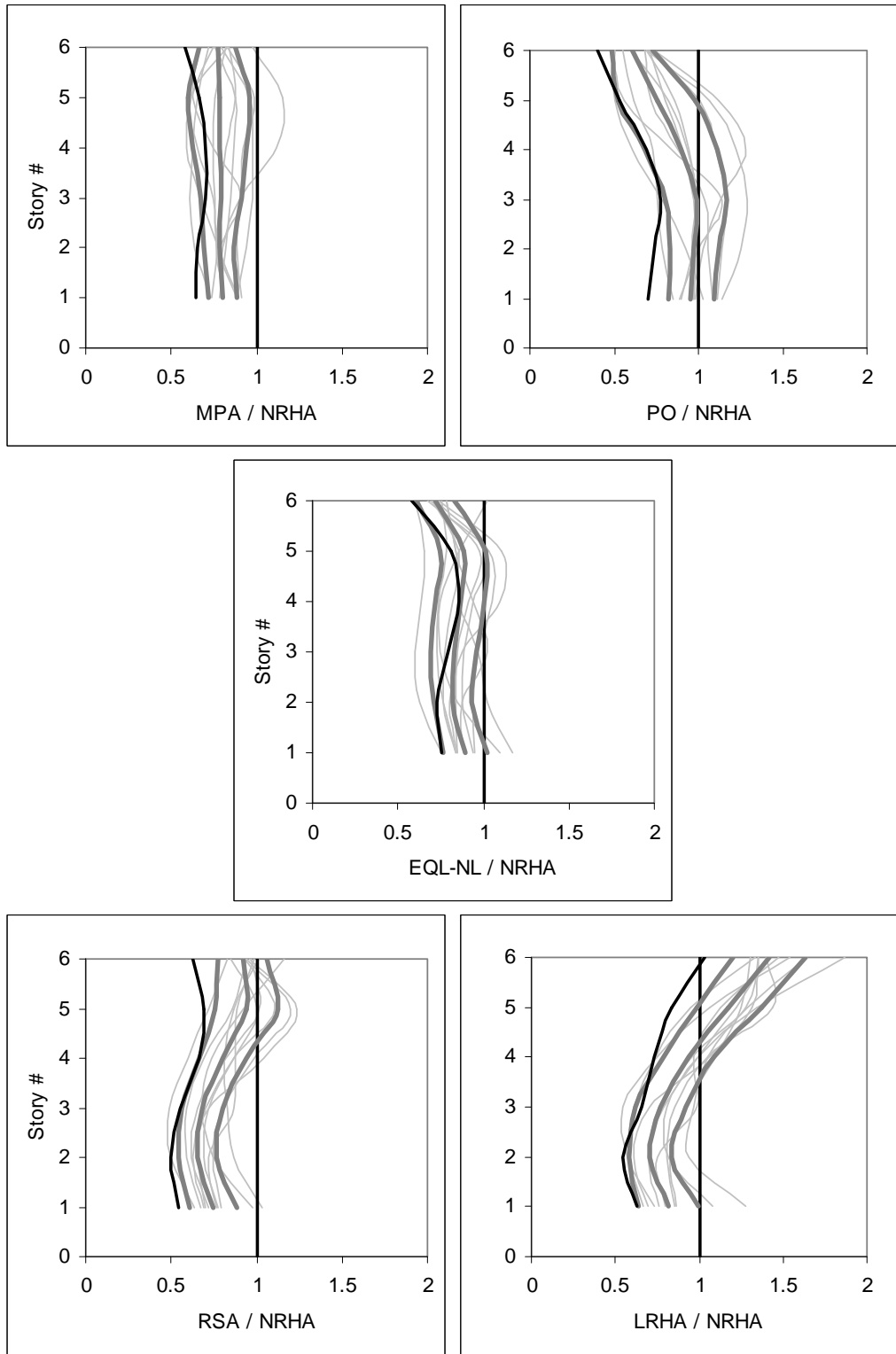


Figure 6.29 Beam chord rotations obtained from the approximate methods normalized with those obtained from NRHA at the inner frame close to stiff edge under ordinary ground motions

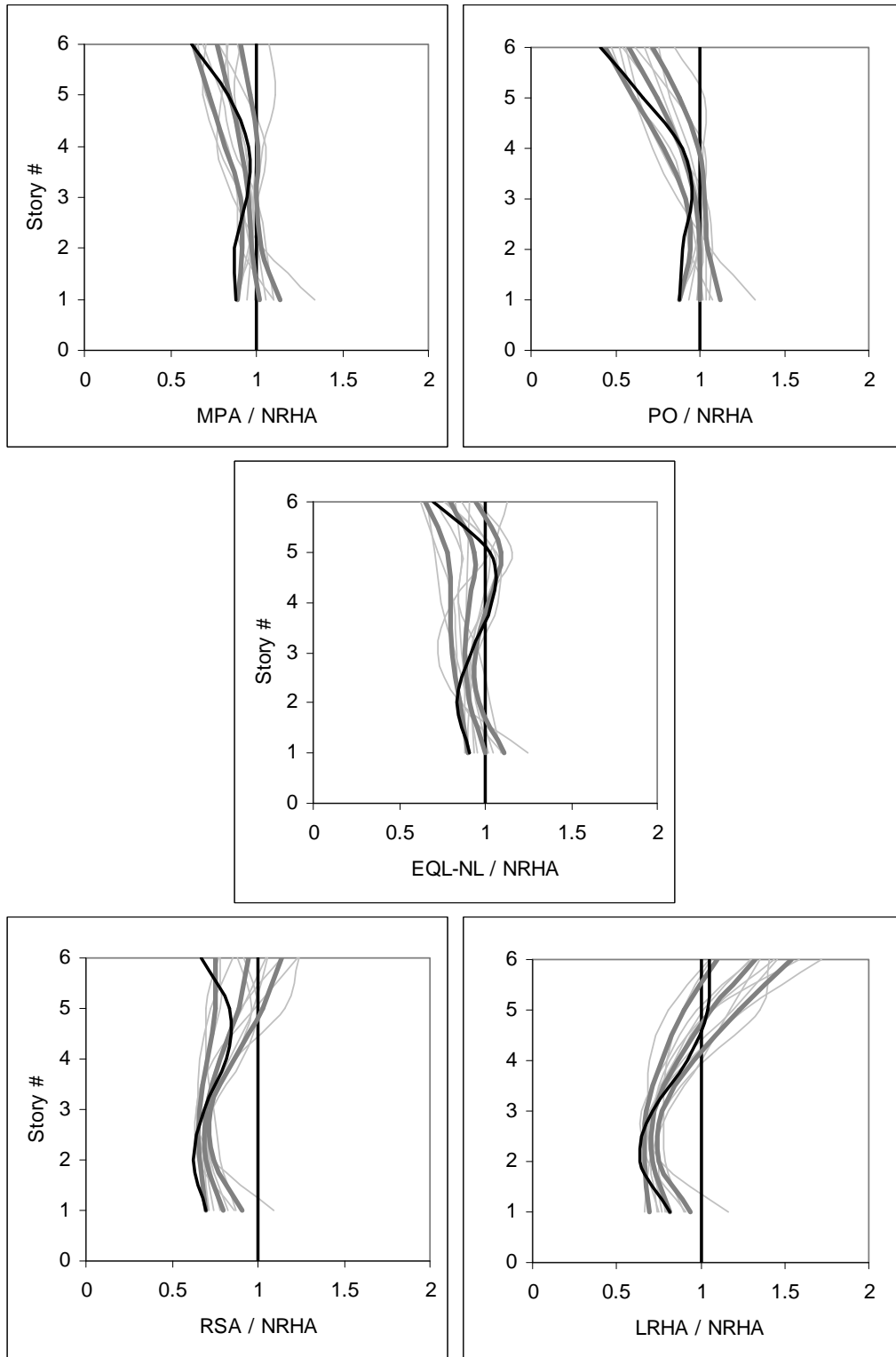


Figure 6.30 Beam chord rotations obtained from the approximate methods normalized with those obtained from NRHA at the inner frame close to flexible edge under ordinary ground motions

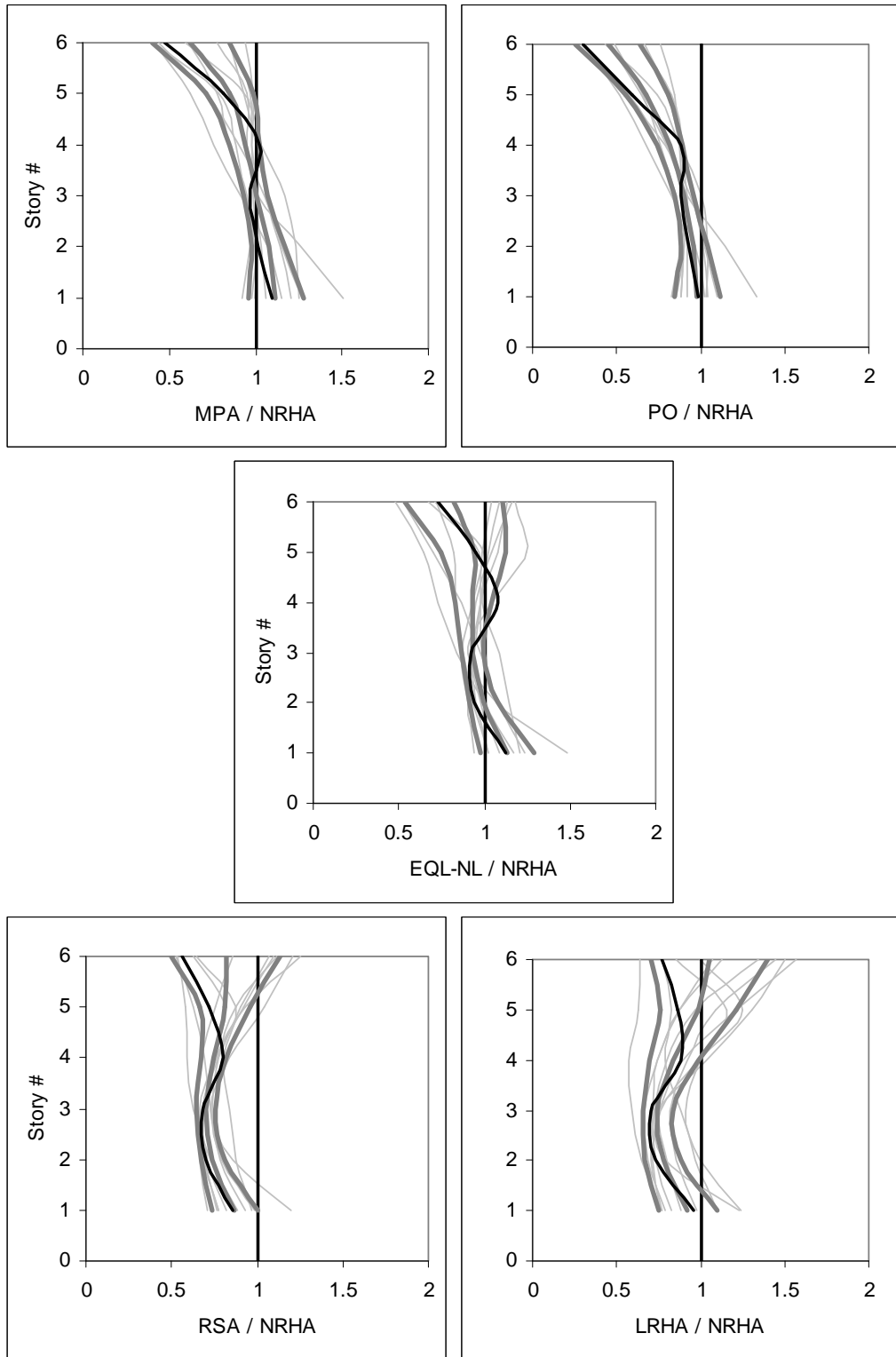


Figure 6.31 Beam chord rotations obtained from the approximate methods normalized with those obtained from NRHA at the flexible edge frame under ordinary ground motions

### 6.4.3 Response Prediction Under a Pulse Type Ground Motion

The proposed equivalent linearization procedure is evaluated in comparison with other analysis methods under a pulse type ground motion in this section. Each method is evaluated at the center of mass roof displacement determined by NRHA as in the case of the statistical evaluations presented previously.

The ground motion selected as a pulse type example is the one with the code SYL360 in Table 4.1. It is a strong ground motion recorded during 1994 Northridge earthquake with PGA, PGV and PGD of 0.843 g, 129.4 cm/sec and 31.9 cm respectively. Ground acceleration, velocity and displacement traces of this ground motion are presented in Figure 6.32. Existence of strong pulses can be identified from this figure. Pseudo acceleration and displacement response spectra of the ground motion are presented in Figure 6.33. First and second mode periods are also marked on these figures. The reason for selecting this ground motion is that it results in considerable amount of nonlinearity and torsional response.

Comparison of maximum story displacements, interstory drift ratios and beam chord rotations obtained from several analysis methods under the selected pulse type ground motion are presented in Figures 6.34-6.39. Following observations can be noted from these figures.

- Equivalent linearization procedure improves the predictions of RSA. Improvement is clearly observed in the beam chord rotations. Since the beam chord rotation is a better indicator of structural damage than interstory drift ratio and story displacement, accurate prediction of beam chord rotations is an achievement of the equivalent linearization procedure for assessment purposes.
- Increase in the beam chord rotations and interstory drift ratios at the top two stories of the flexible edge frame resembling the effect of higher modes is best captured by the equivalent linearization procedure among the considered approximate methods.
- LRHA and RSA result in substantially different interstory drift ratios and beam chord rotations at the flexible edge frame because of the differences in

the consideration of the torsional components of the modal force vectors as indicated previously.

- All of the methods underestimate the responses at the stiff edge, MPA resulting in the largest underestimations. MPA greatly underestimates the displacements, interstory drift ratios and beam chord rotations at the stiff edge frame and overestimates the displacements at the flexible edge frame. It also overestimates the interstory drift ratios and beam chord rotations at the lower three stories which was previously observed for the statistical results. This situation is because of the overestimation of torsion as explained previously.
- PO results in very accurate displacements at the flexible edge. It results in underestimations for the other cases.

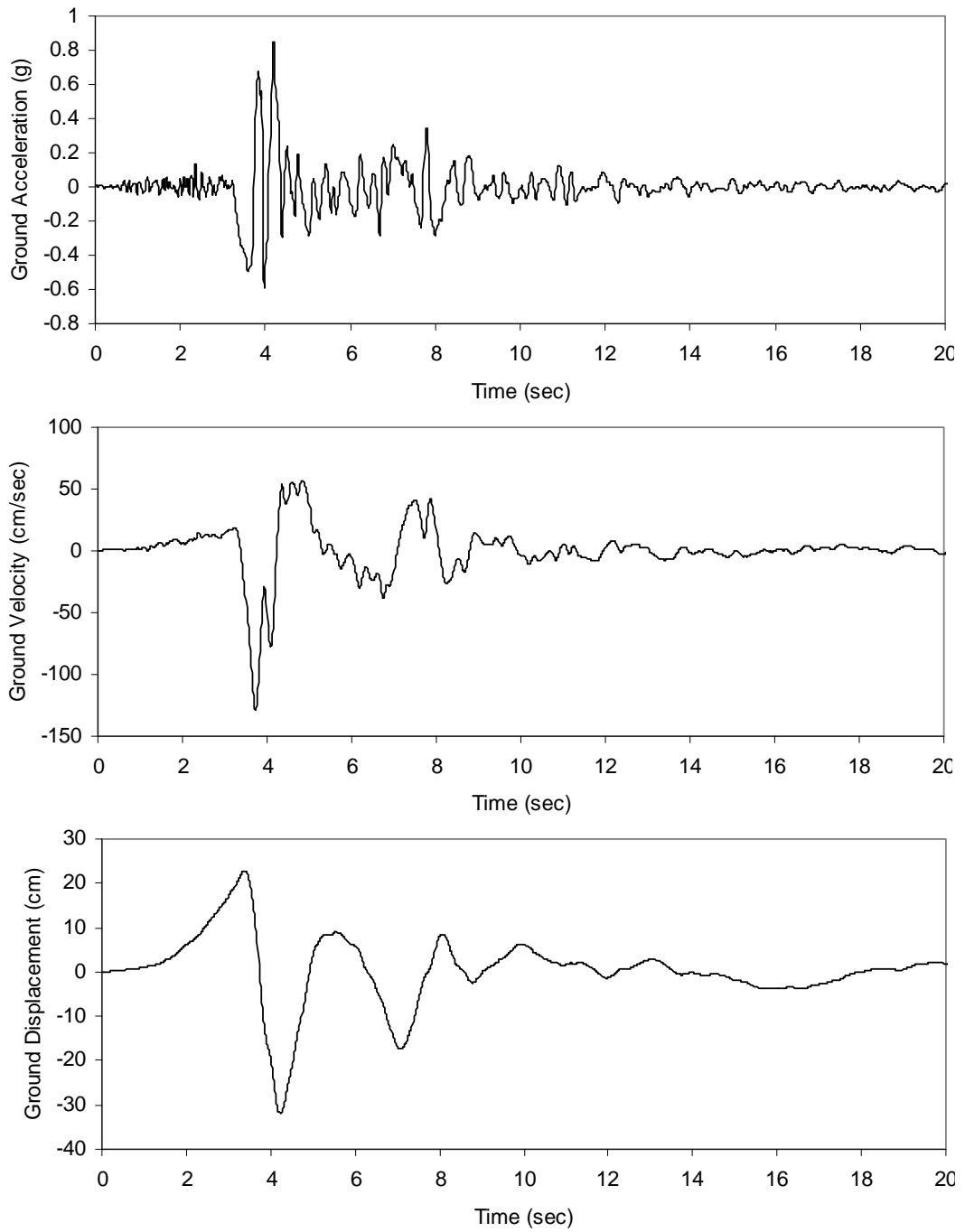


Figure 6.32 Ground acceleration, velocity and displacement traces for the ground motion SYL360

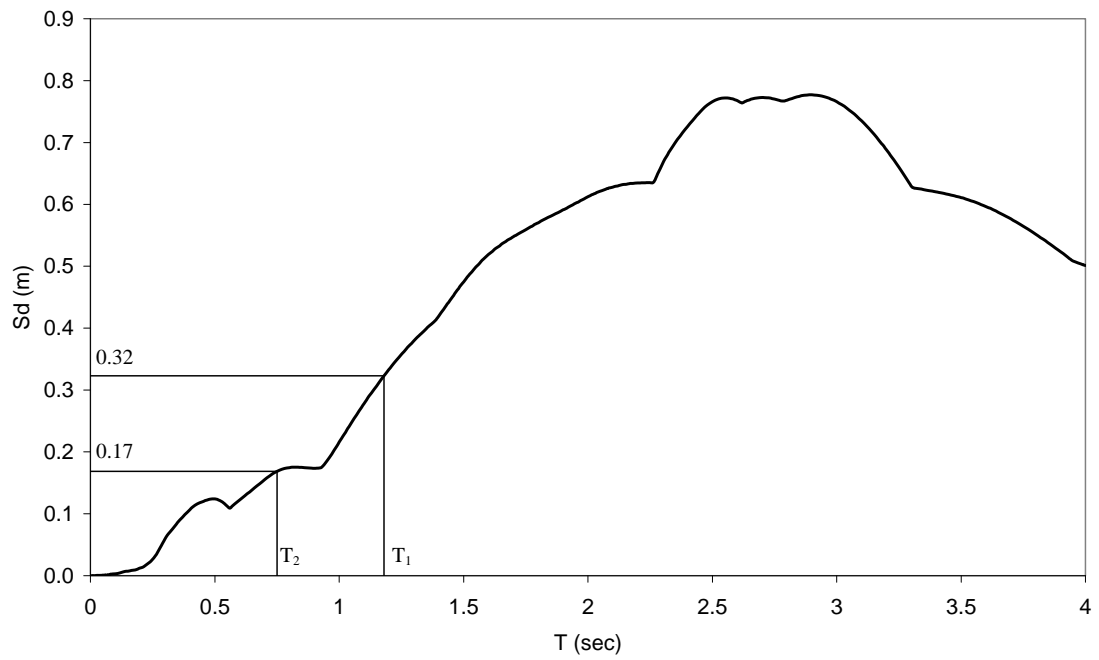
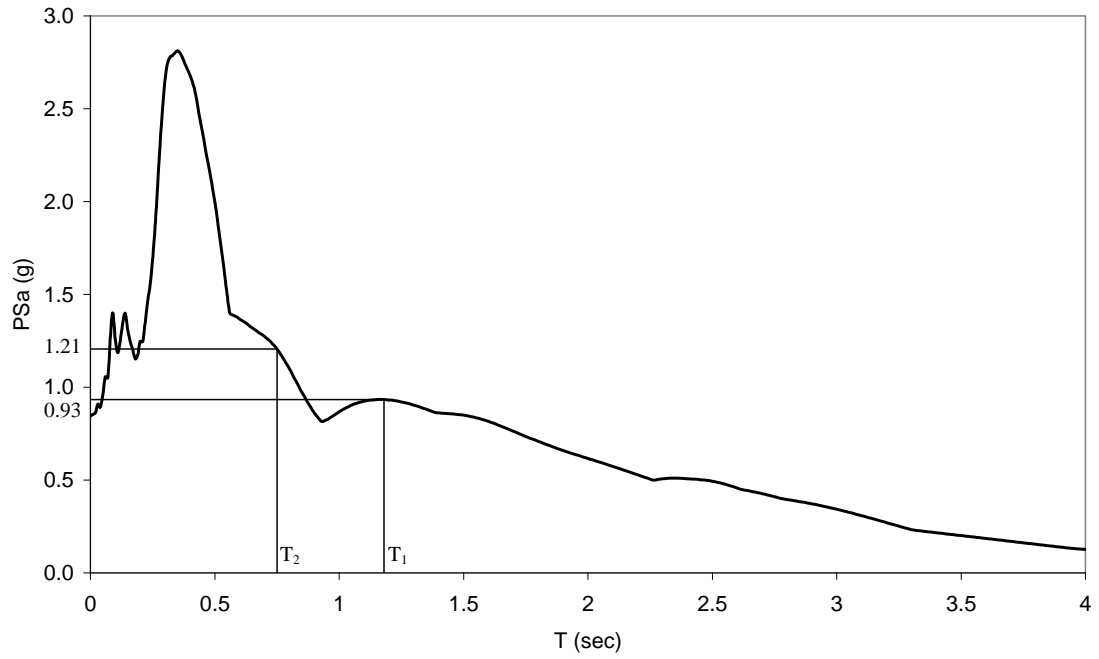


Figure 6.33 5% damped pseudo acceleration and displacement response spectra for the ground motion SYL360

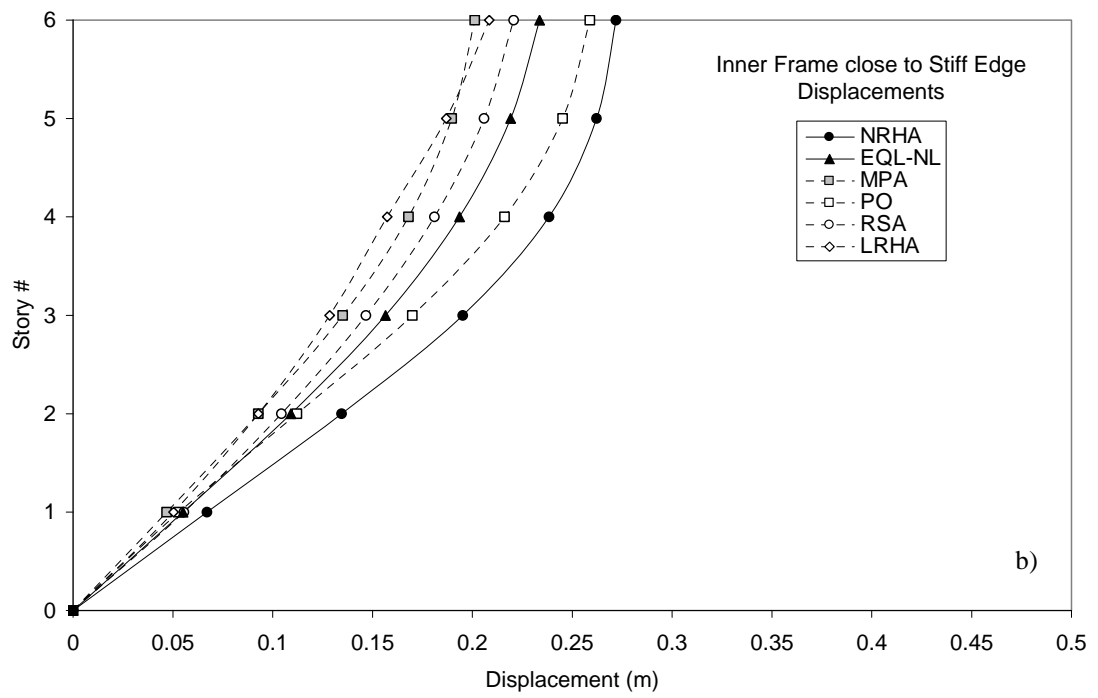
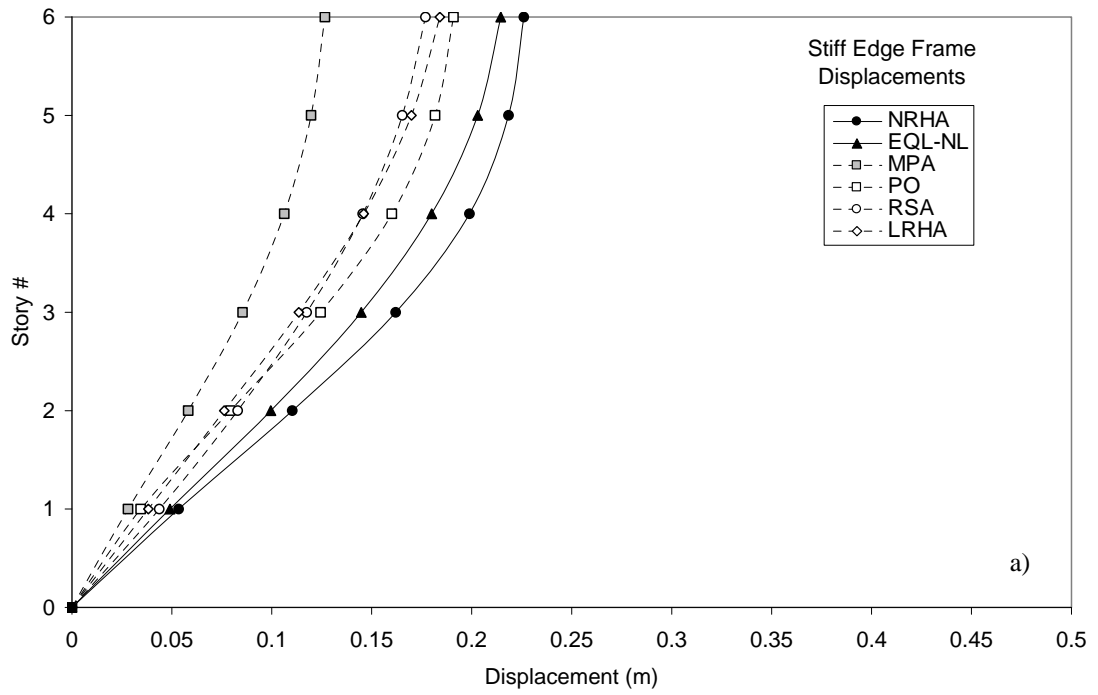


Figure 6.34 Comparison of maximum story displacements a) at the stiff edge frame, b) at the inner frame close to the stiff edge for the ground motion SYL360

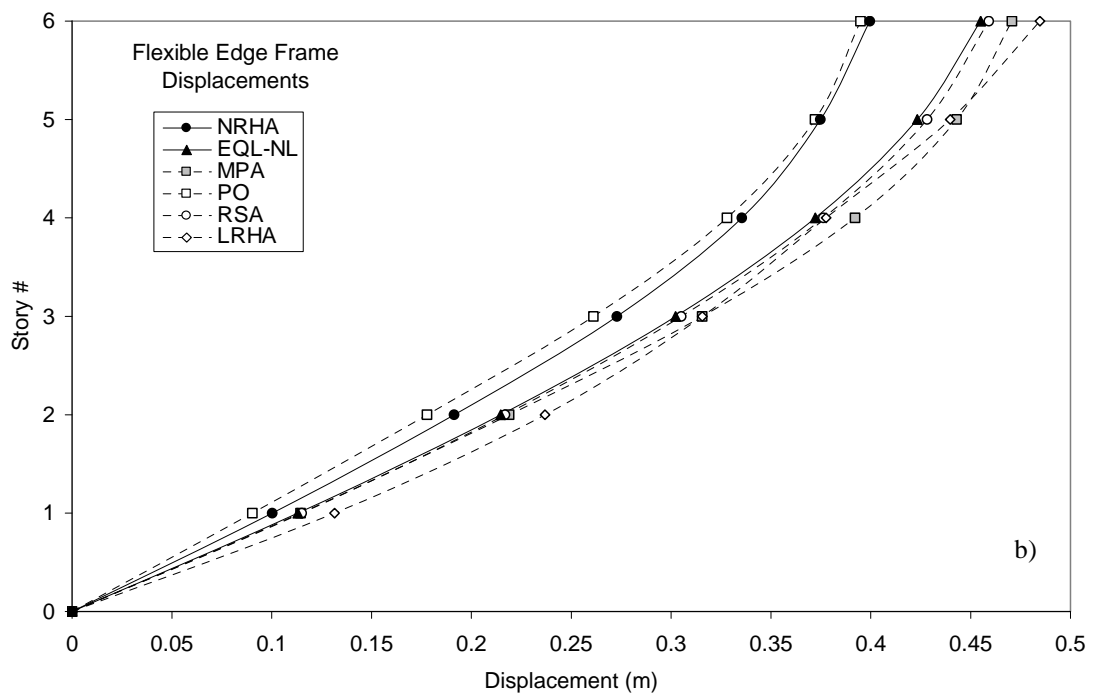
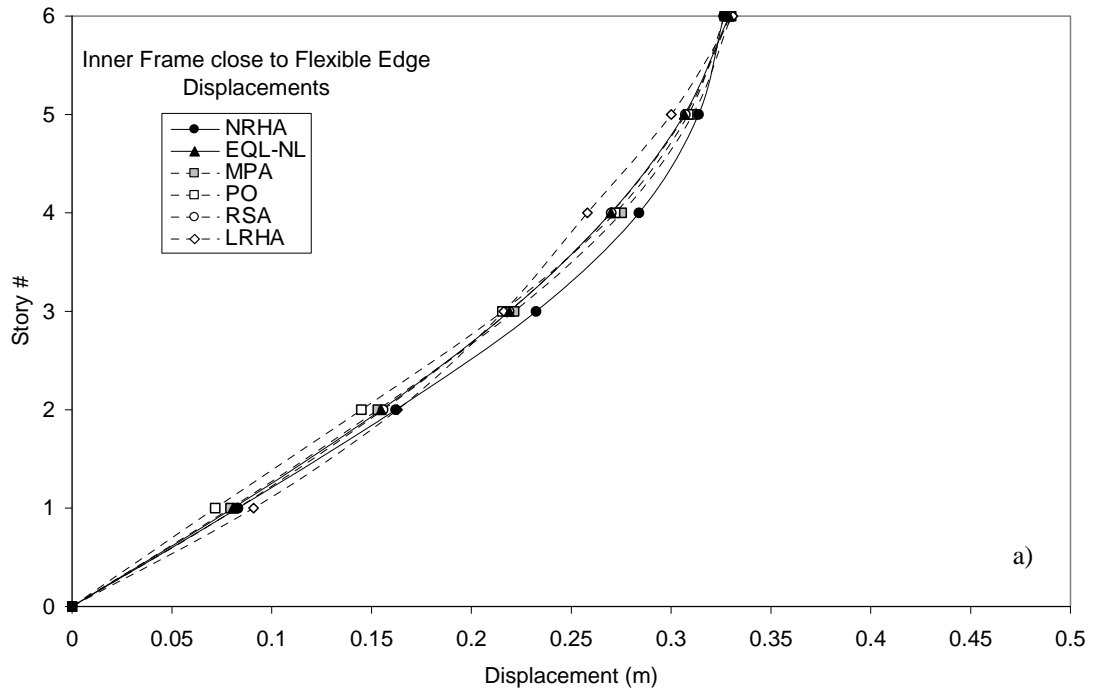


Figure 6.35 Comparison of maximum story displacements a) at the inner frame close to the flexible edge, b) at the flexible edge frame for the ground motion SYL360

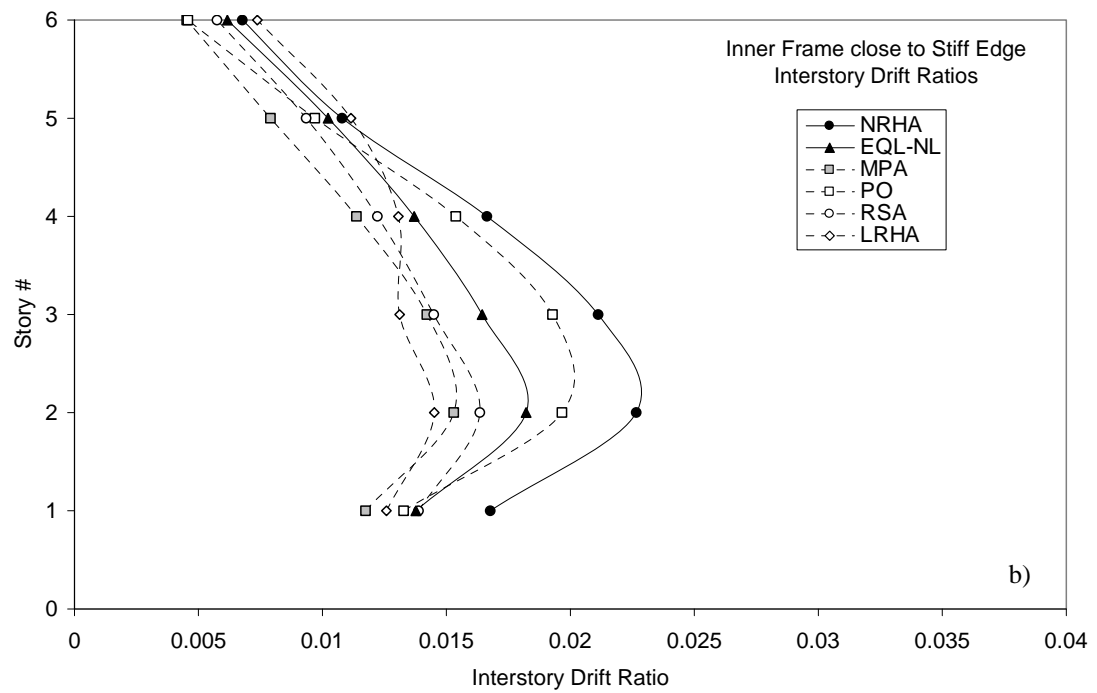
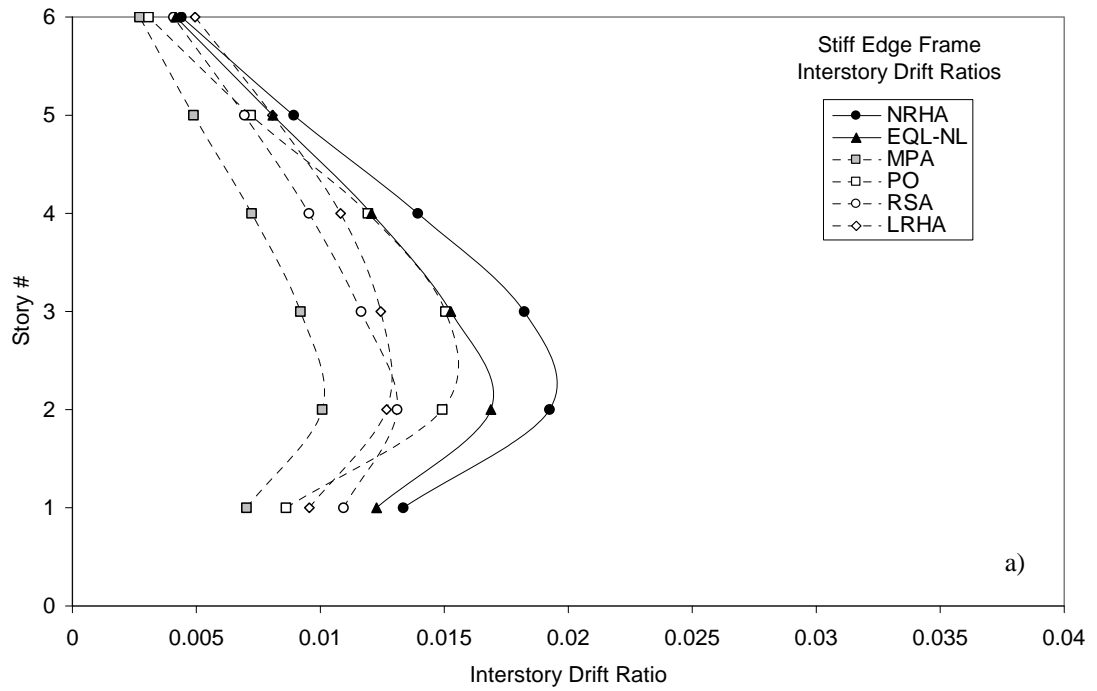


Figure 6.36 Comparison of maximum interstory drift ratios a) at the stiff edge frame, b) at the inner frame close to the stiff edge for the ground motion SYL360

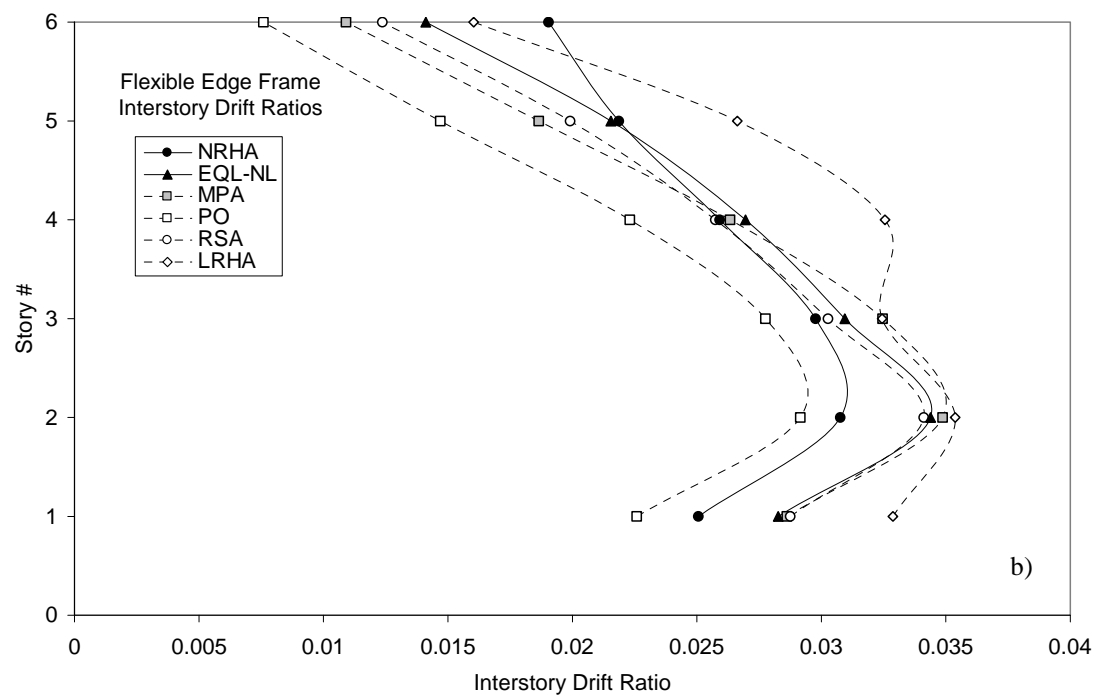
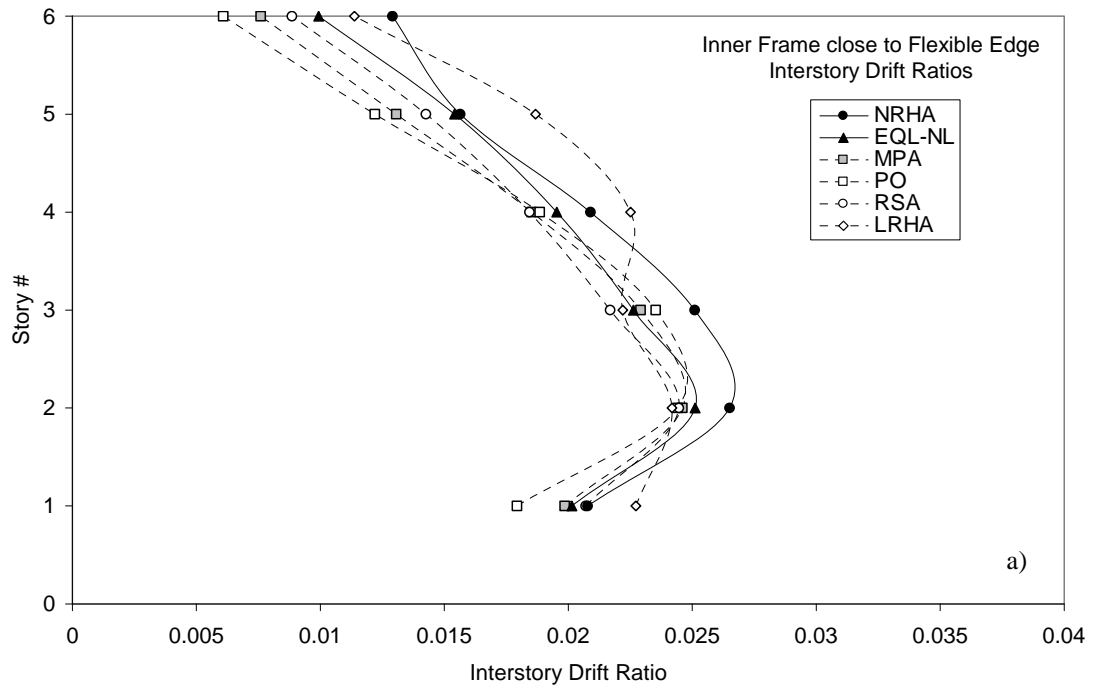


Figure 6.37 Comparison of maximum interstory drift ratios a) at the inner frame close to the flexible edge, b) at the flexible edge frame for the ground motion SYL360

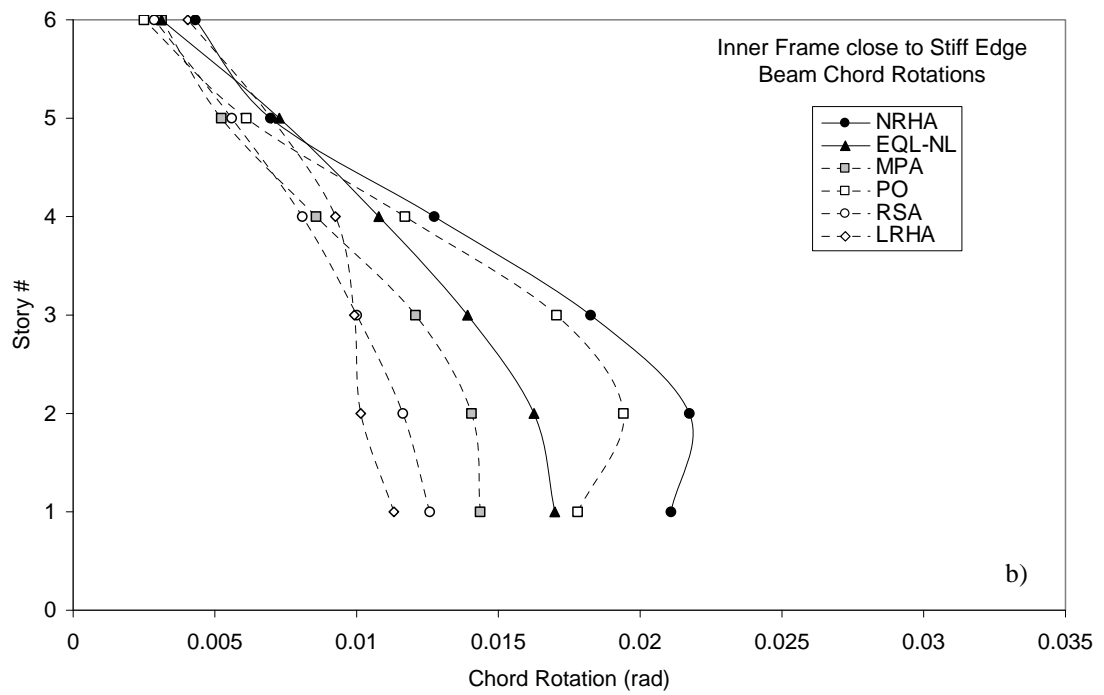
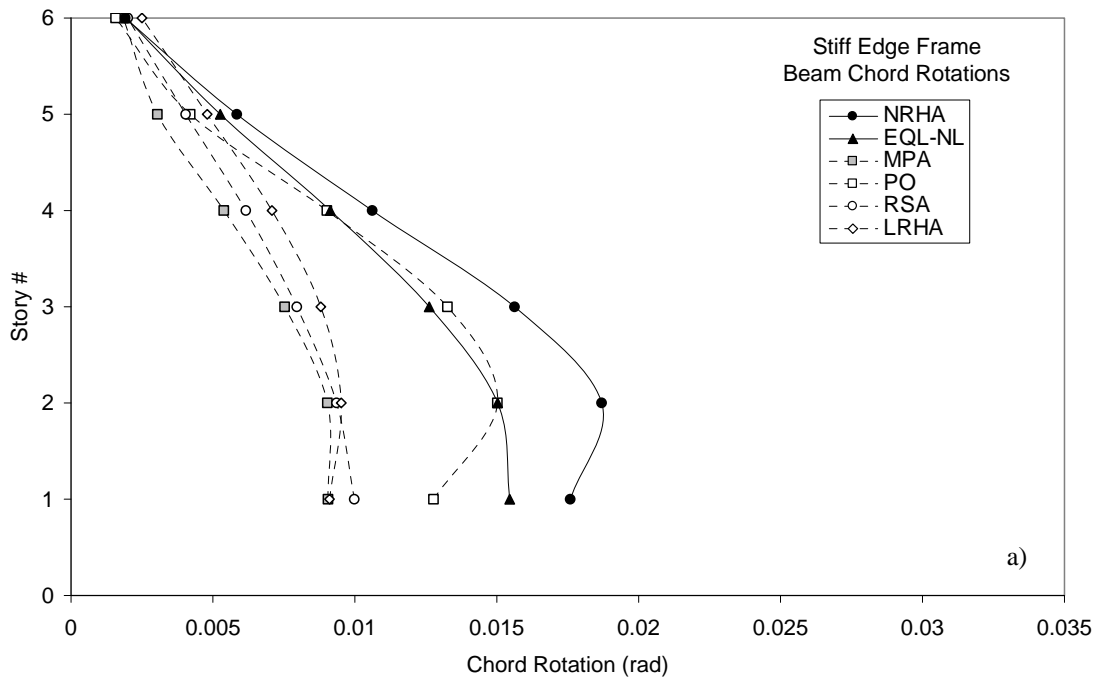


Figure 6.38 Comparison of maximum beam chord rotations a) at the stiff edge frame, b) at the inner frame close to the stiff edge for the ground motion SYL360

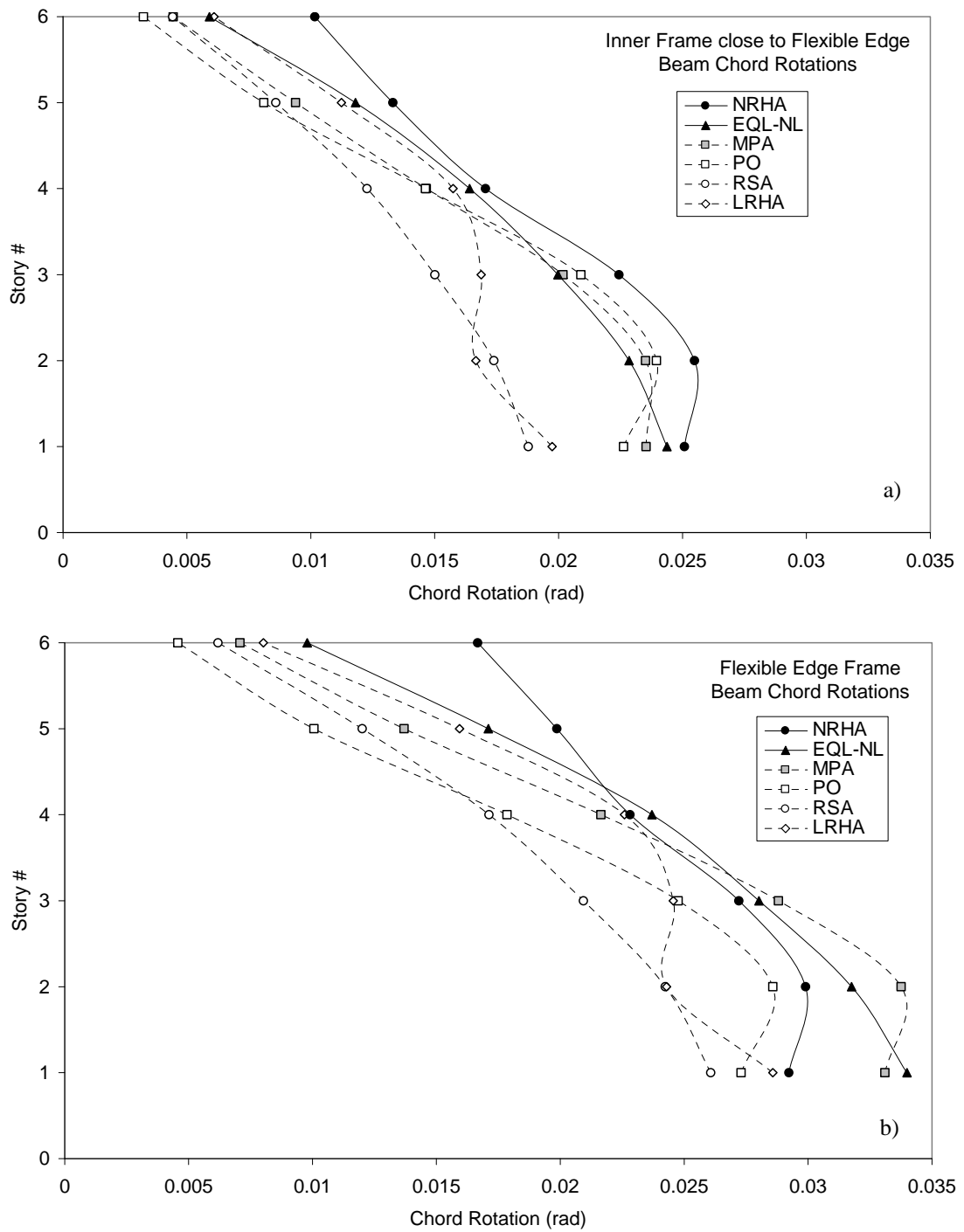


Figure 6.39 Comparison of maximum beam chord rotations a) at the inner frame close to flexible edge, b) at the flexible edge frame for the ground motion SYL360

#### 6.4.4 Response Prediction Under an Ordinary Ground Motion

The proposed equivalent linearization procedure is evaluated in comparison with other analysis methods under an ordinary ground motion in this section. Each method is evaluated at the roof displacement determined by NRHA.

The ground motion selected as the ordinary ground motion example is the one with the code ELC180 in Table 4.2. It is a strong ground motion recorded during 1940 Imperial Valley earthquake with PGA, PGV and PGD of 0.313 g, 29.8 cm/sec and 13.3 cm respectively. Ground acceleration, velocity and displacement traces of this ground motion are presented in Figure 6.40. Pseudo acceleration and displacement response spectra of the ground motion are presented in Figure 6.41. First and second mode periods are also marked on these figures. The reason for selecting this ground motion is that it is a well known ground motion covering a wide range of frequencies. It is scaled with two in order to induce inelasticity.

Comparison of maximum story displacements, interstory drift ratios and beam chord rotations obtained from the employed analysis methods under the selected pulse type ground motion are presented in Figures 6.42-6.47. Following observations are noted from these figures.

- Equivalent linearization procedure is successful in improving the predictions of RSA. Improvement is substantial for the beam chord rotations. It results in very accurate beam chord rotations and interstory drift ratios at the upper stories.
- Similar to the pulse type ground motion example, MPA severely underestimates the displacements, interstory drift ratios and beam chord rotations at the stiff edge frame. It results in accurate predictions at the flexible edge frame. PO also greatly underestimates the responses at the stiff edge frame. Underestimation in PO is greater than the underestimation in MPA. Because the second mode contribution increases the response values at the stiff edge in MPA, however this contribution is not sufficient to prevent the significant amount of underestimation.

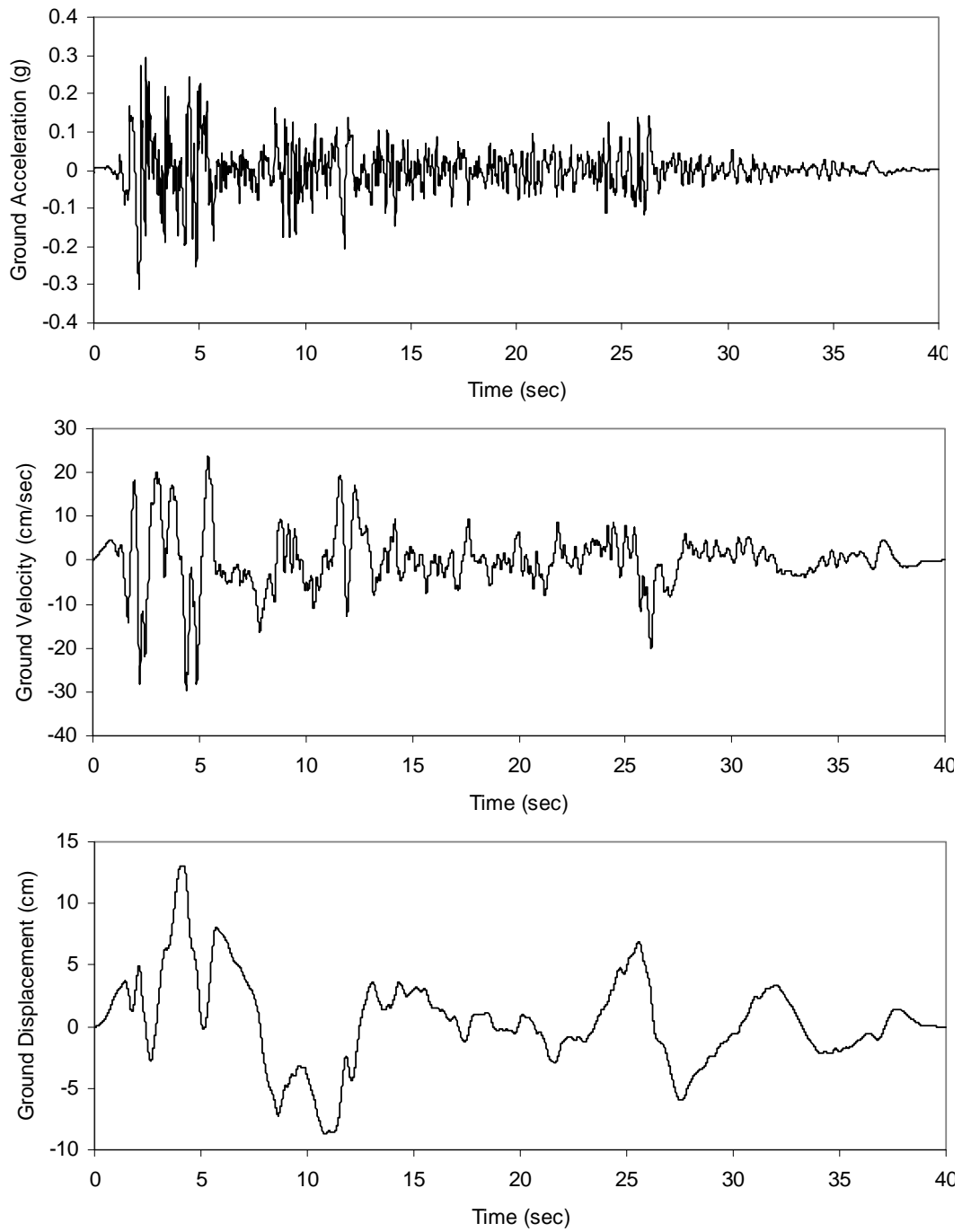


Figure 6.40 Ground acceleration, velocity and displacement traces for the ground motion ELC180

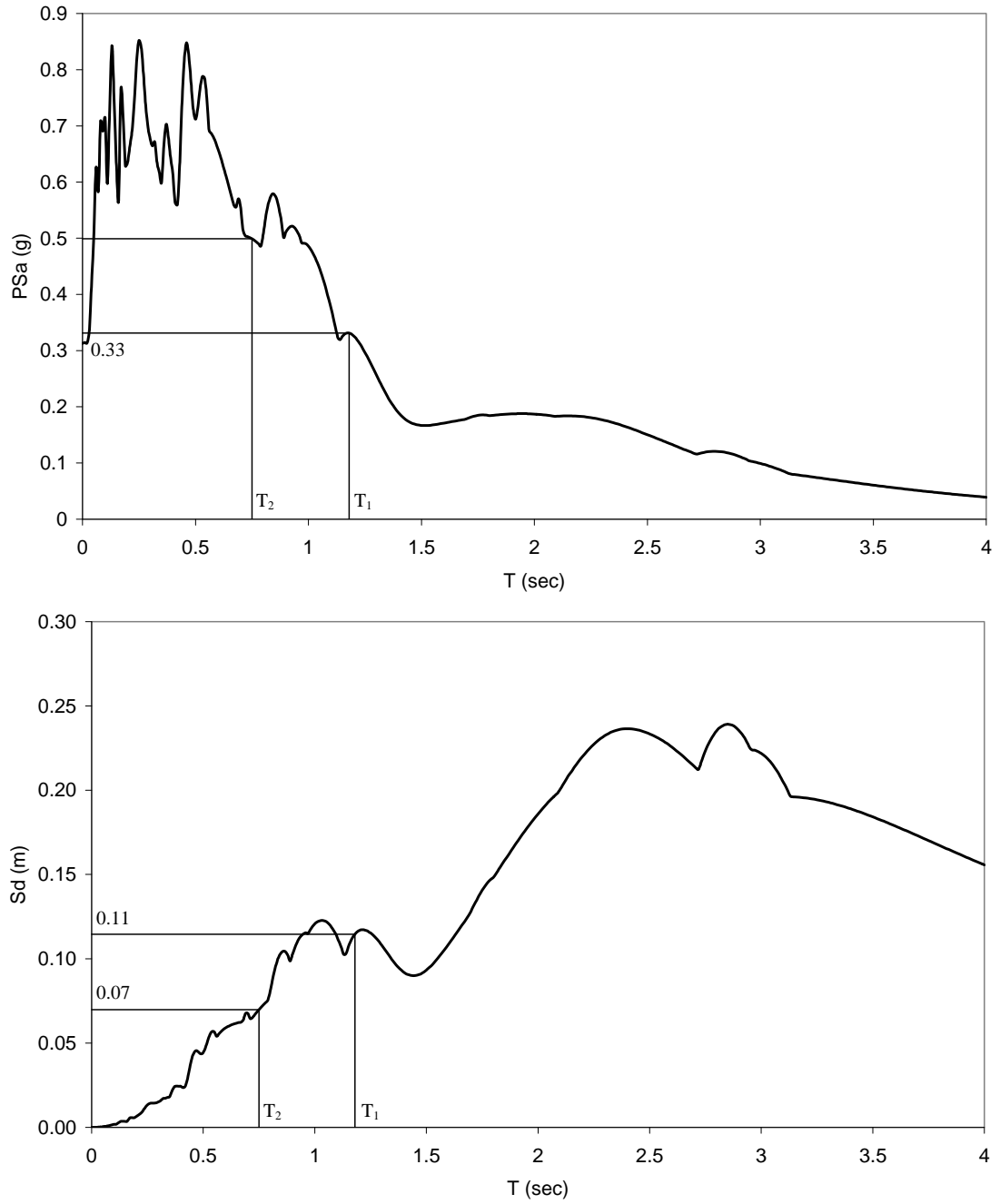


Figure 6.41 5% damped pseudo acceleration and displacement response spectra for the ground motion ELC180

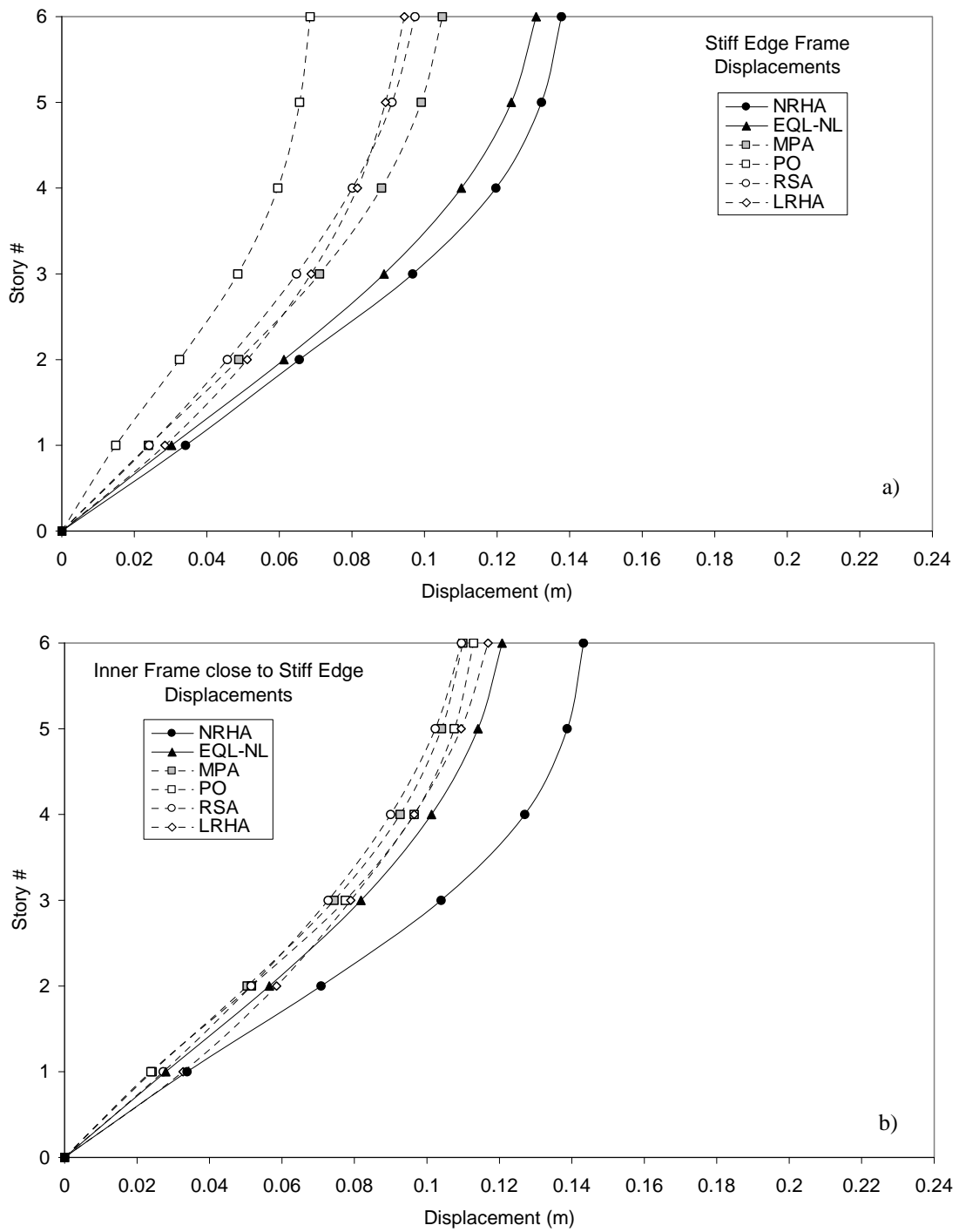


Figure 6.42 Comparison of maximum story displacements a) at the stiff edge frame, b) at the inner frame close to the stiff edge for the ground motion ELC180

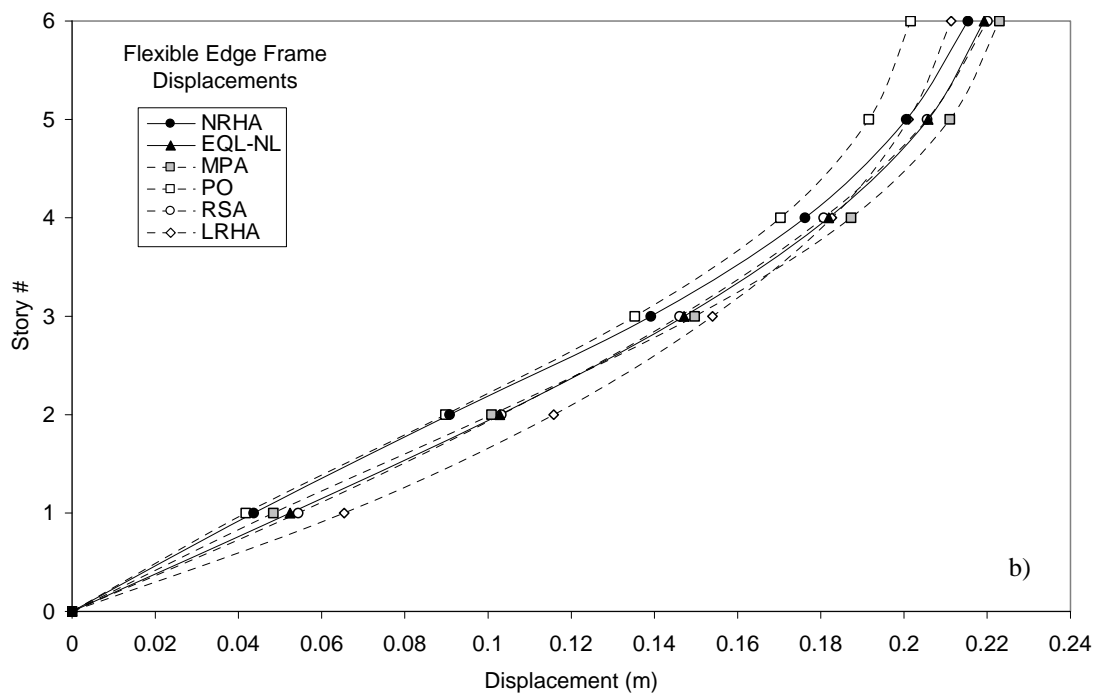
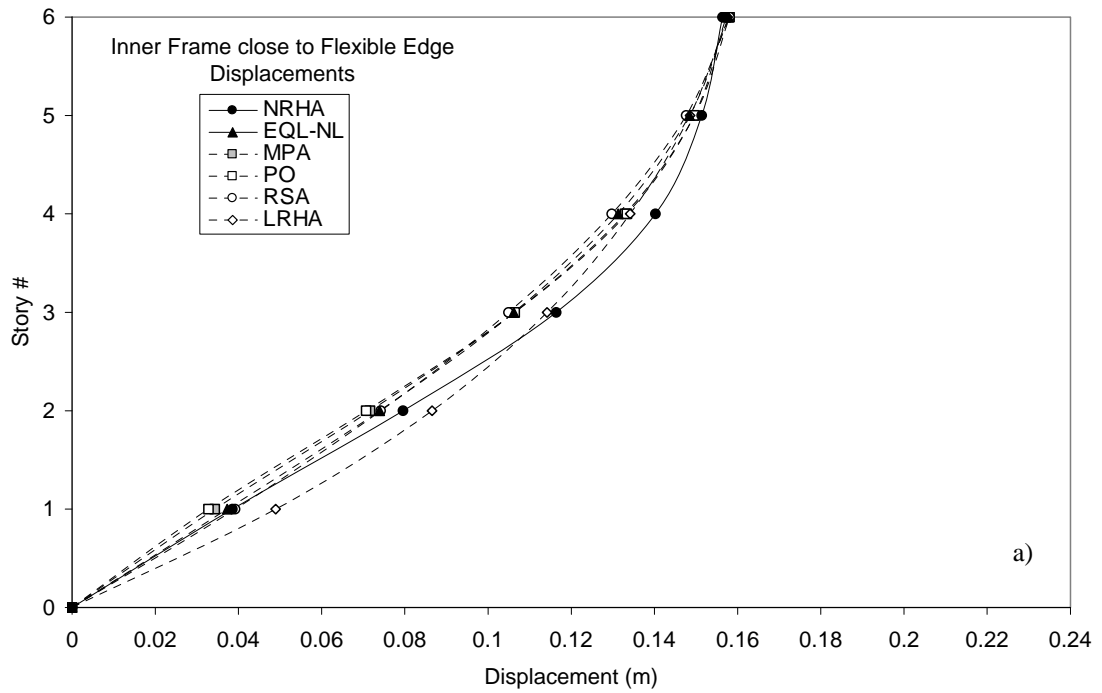


Figure 6.43 Comparison of maximum story displacements a) at the inner frame close to flexible edge, b) at the flexible edge frame for the ground motion ELC180

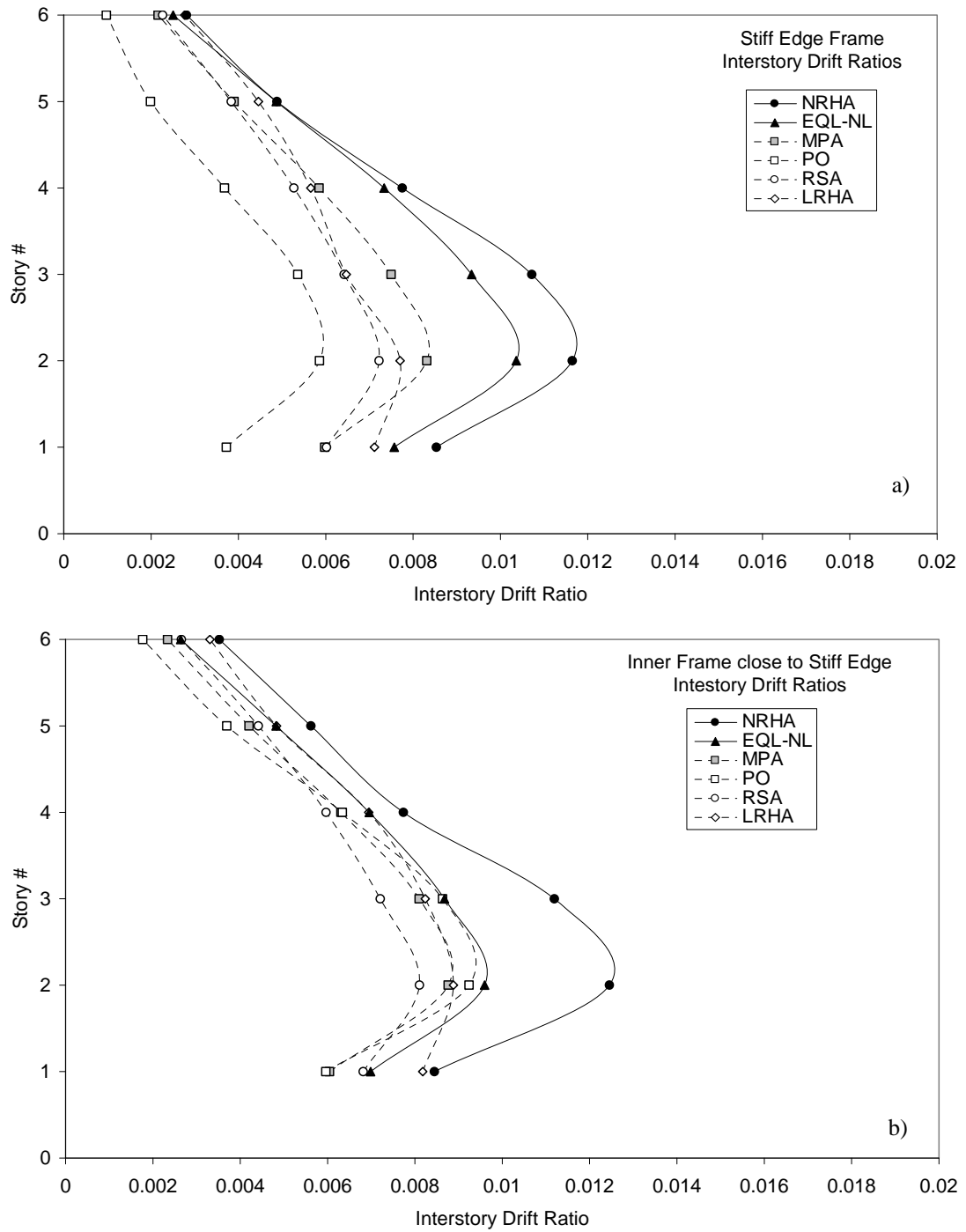


Figure 6.44 Comparison of maximum interstory drift ratios a) at the stiff edge frame, b) at the inner frame close to the stiff edge for the ground motion ELC180

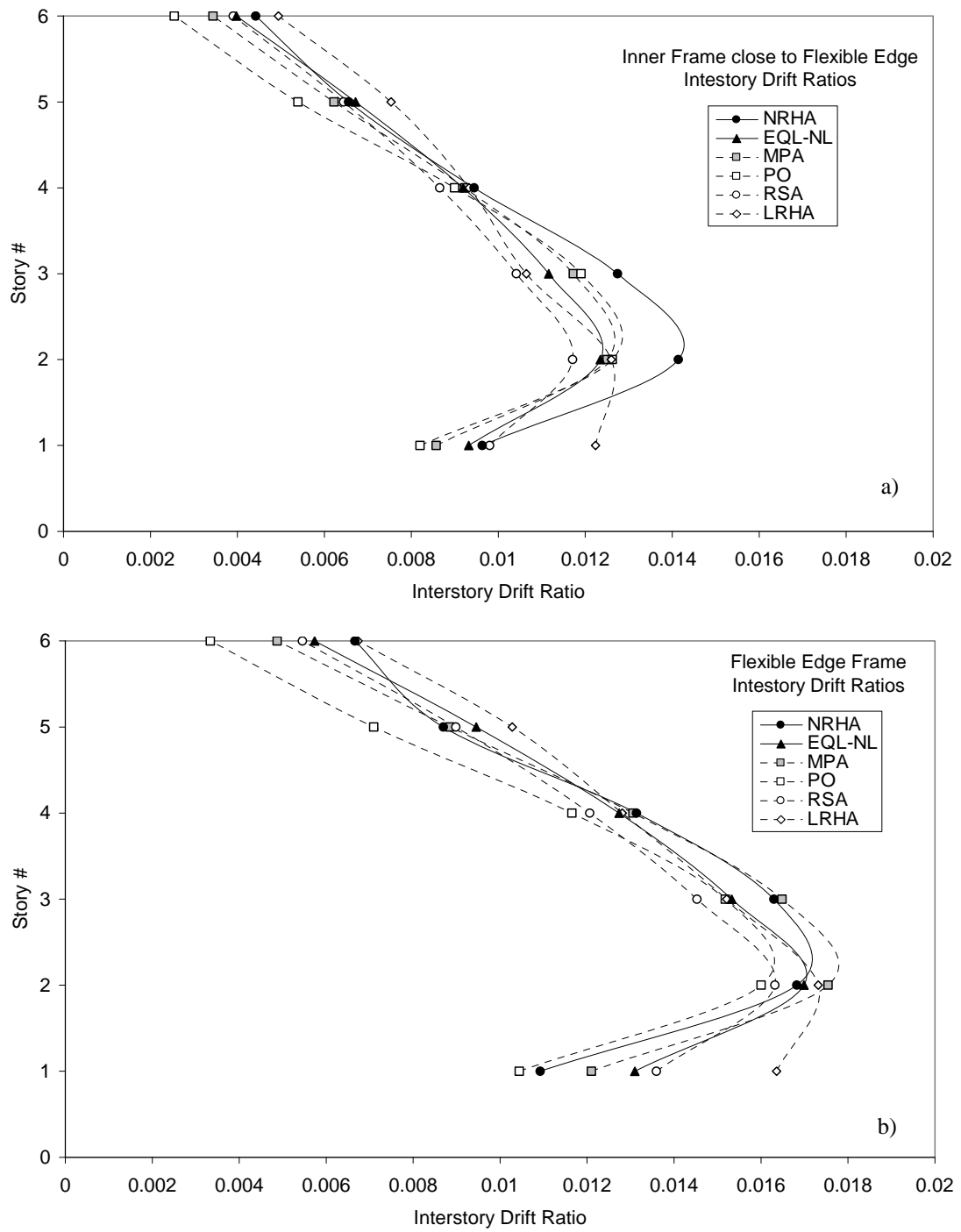


Figure 6.45 Comparison of maximum interstory drift ratios a) at the inner frame close to flexible edge, b) at the flexible edge frame for the ground motion ELC180

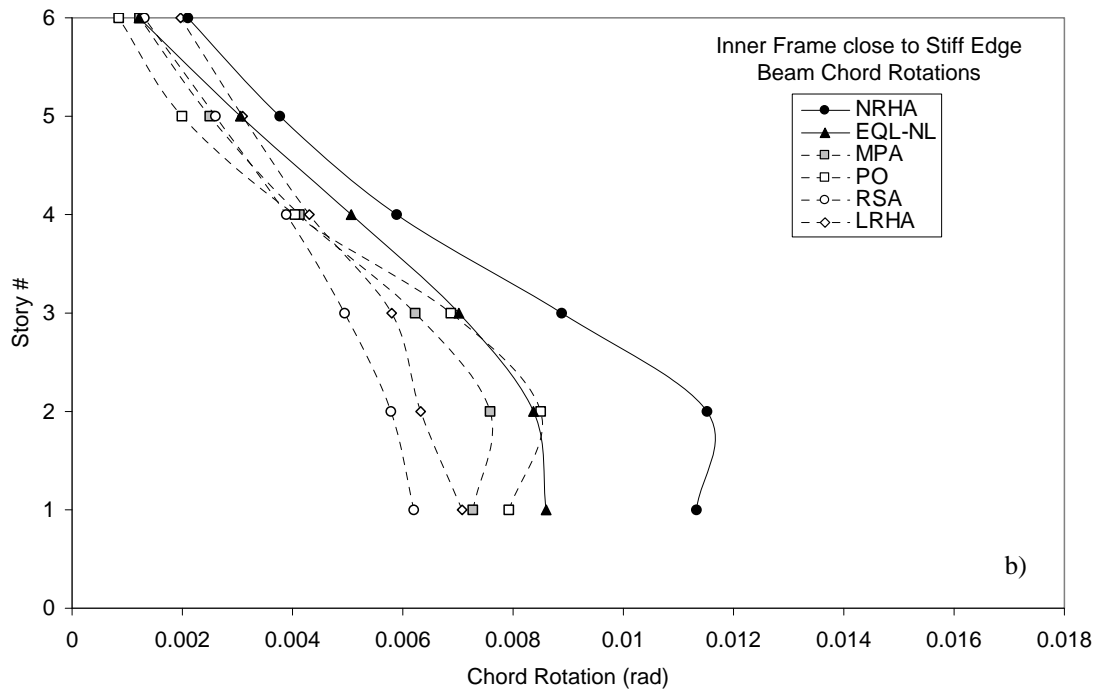
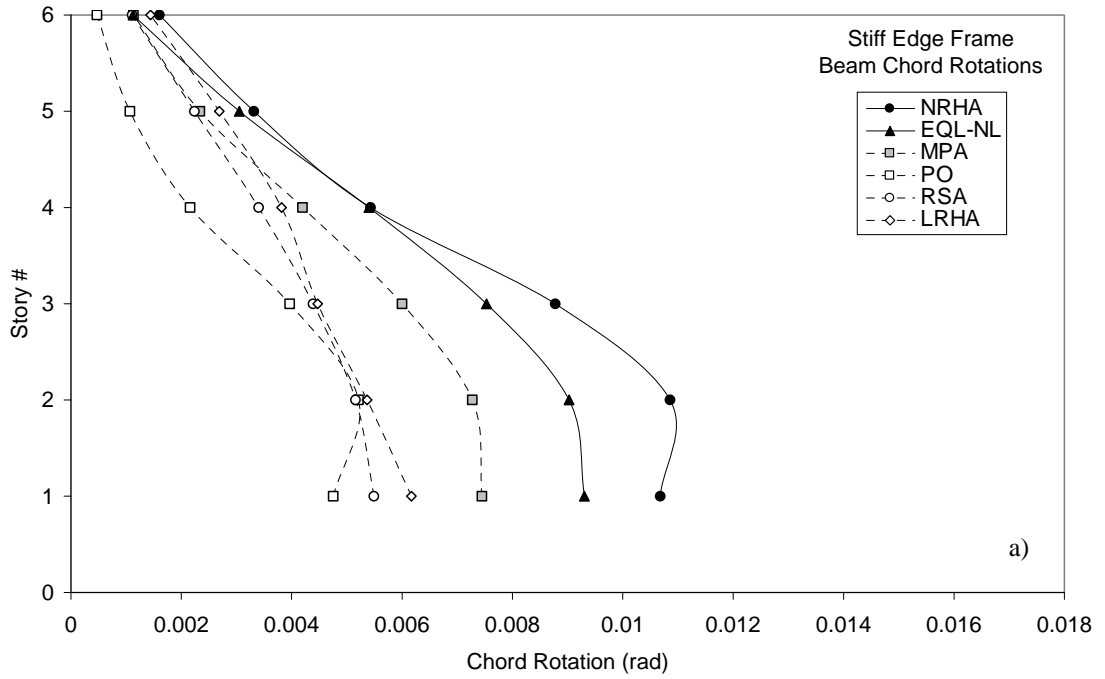


Figure 6.46 Comparison of maximum beam chord rotations a) at the stiff edge frame, b) at the inner frame close to the stiff edge for the ground motion ELC180

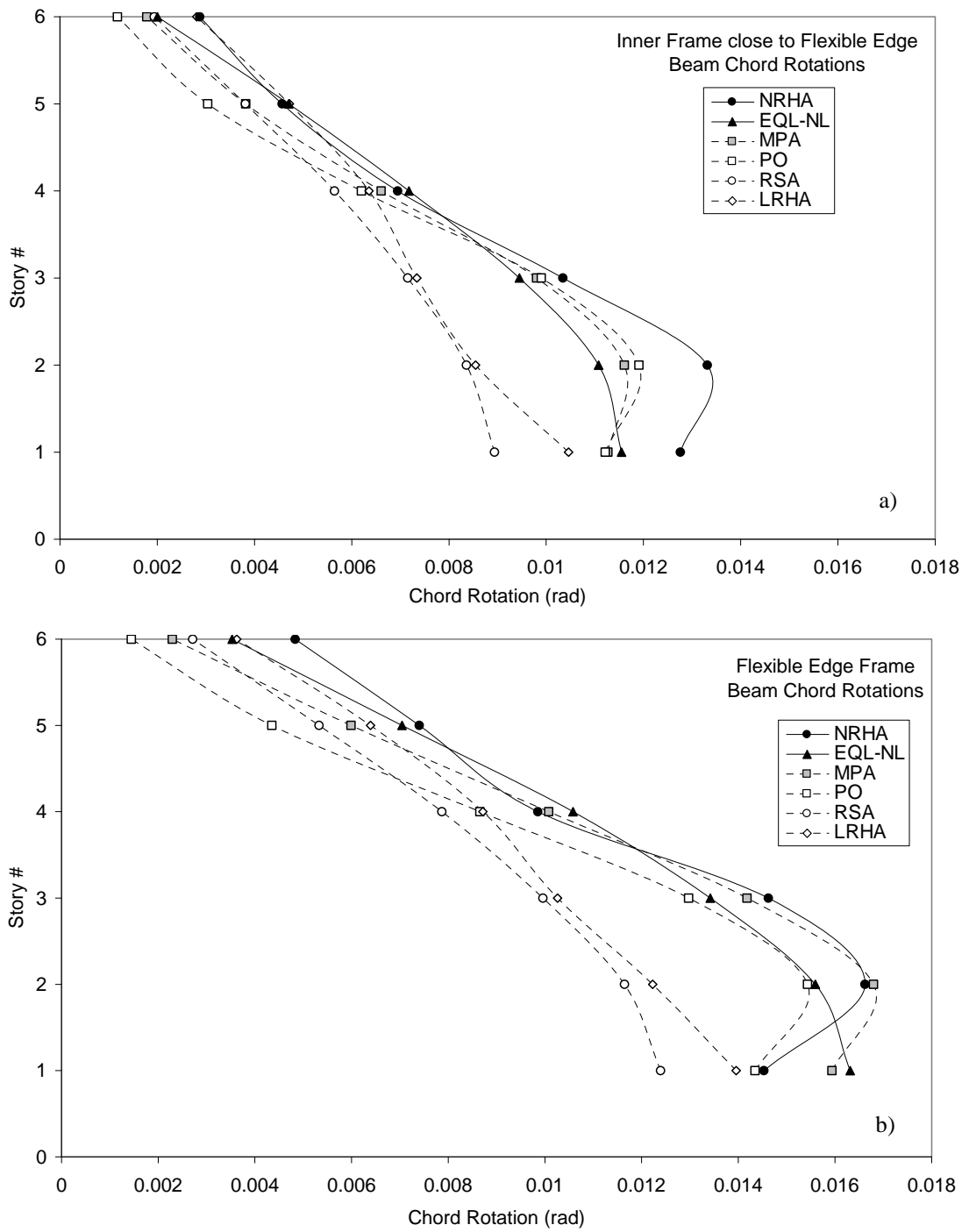


Figure 6.47 Comparison of maximum beam chord rotations a) at the inner frame close to flexible edge, b) at the flexible edge frame for the ground motion ELC180

## CHAPTER 7

### SUMMARY AND CONCLUSIONS

#### 7.1 Summary

An equivalent linearization procedure is developed herein as an approximate method for predicting the inelastic seismic displacement response of MDOF systems under earthquake excitations. The procedure mainly consists of reducing the stiffness of the structural members which are anticipated to respond in the inelastic range. Combined results of demand and capacity analyses are used for the construction of equivalent linear system with reduced stiffness. Different from similar studies in literature, equivalent damping is not explicitly employed in this study. Instead, predetermined spectral displacement demands are utilized in each mode of the equivalent linear system for the determination of global displacement demands. In the first variant of the equivalent linearization procedure (EQL-ED), spectral displacements of all the modes are determined by means of the equal displacement rule. In the second variant (EQL-NL), spectral displacement of only the first mode is determined by conducting nonlinear response history analysis of an equivalent SDOF system, different from EQL-ED. Modal response spectrum analysis of the equivalent linear system is then conducted by using the pseudo accelerations calculated from the spectral displacements, and the requested response parameters are obtained.

Equivalent linearization procedure with both variants for calculating demand (EQL-NL, EQL-ED) are applied on a twelve story reinforced concrete plane frame for which the higher mode effects are important, and a six story unsymmetrical-plan reinforced concrete space frame where torsion significantly effects the response. The predictions of the equivalent linearization procedure are compared with the nonlinear response history analysis (NRHA) results by utilizing 162 ground motions. Response predictions from two other approximate procedures, which are conventional pushover analysis according to FEMA-356 (PO-FEMA) and modal pushover analysis (MPA) are also presented. Modal pushover analysis results conducted by considering only the first mode (MPA-1) are also presented for the twelve story building. In addition, results of response spectrum analyses (RSA) and linear response history analyses (LRHA) are used for comparison purposes. Roof displacement demands and the local response parameters; namely, story displacements, interstory drift ratios and chord rotations are used in the comparisons.

## **7.2 Conclusions**

The following conclusions are reached according to the results obtained in this study.

- EQL-NL is very successful in predicting the roof displacement demands. It greatly improves the inaccurate predictions of RSA. The same conclusion is not valid for EQL-ED. Roof displacement predictions of EQL-ED are close to those of RSA, since same spectral displacements are employed in both of the methods and the modal participation factors for the equivalent linear and the original systems are similar. In this respect, it can be stated that EQL-NL is superior to EQL-ED.

- Regarding the differences in the roof displacement demand predictions of EQL-NL and EQL-ED, and the success of MPA in roof displacement predictions, it is clear that the improvement in roof displacement prediction is due to considering the inelastic response of SDOF systems instead of employing the equal displacement assumption.
- Displacement demands of pulse type ground motions are much greater than those demanded by ordinary ground motions. Considering that pulse type and ordinary ground motions possess similar PGA levels, it can be concluded that the pulses with high velocity peaks lead to the observed differences between the displacement demands of pulse type and ordinary ground motions.
- Artificial axial forces develop in the beams despite the imposition of diaphragm constraints when fiber sections are employed. Moment capacities of the beams increase due to these artificial axial forces. Accordingly, a building designed for beam yielding may result in a failure formation different than the intended if the design is based on a model without fiber sections. This is a critical issue for the nonlinear analysis of structures modeled by using fiber sections, therefore it should be further investigated.
- For the twelve story plane frame, equivalent linearization procedure significantly improves the inaccurate beam chord rotation and interstory drift ratio predictions of RSA. Errors are greatly reduced at the upper stories at which higher modes are effective on the response. Error of the equivalent linearization procedure is much smaller than that of the first mode pushover (MPA-1) at the upper stories. Generally, error of the equivalent linearization procedure is between the error of RSA and MPA, being closer to the error of MPA under pulse type ground motions where significant inelasticity develops. Error of the equivalent linearization procedure is generally smaller

than that of MPA for all the considered response parameters under ordinary ground motions which result in relatively smaller levels of inelasticity.

- Equivalent linearization procedure is also successful in predicting the beam chord rotations and interstory drift ratios of the six story building with unsymmetrical-plan. It improves the predictions of RSA. Improvement in the beam chord rotations is more pronounced than the improvement in the interstory drift ratios. There is considerable improvement in the beam chord rotations at the flexible edge frame and the inner frame close to the flexible edge where inelasticity is larger. Response predictions of the equivalent linearization procedure have similar accuracy with the response predictions of the conventional pushover analysis; in addition they are more accurate at the top stories where higher mode effects are important. Equivalent linearization procedure results in more accurate predictions of local response parameters with respect to MPA.
- Owing to the results obtained from the two case study buildings, it is observed that equivalent linearization procedure significantly improves the response predictions of the response spectrum analysis. It also results in predictions similar to or better than those obtained from the approximate methods which employ nonlinear analysis. Considering the conceptual simplicity of the procedure and the conventional analysis tools used in its application, it can be stated that the equivalent linearization procedure is a practically applicable method in the prediction of inelastic displacement response parameters with sufficient accuracy.
- According to the response predictions of MPA for the six story building, it can be stated that consideration of torques in the modal force vectors is a drawback of MPA for 3D buildings with unsymmetrical plans. MPA is successful in correcting the interstory drift ratios and beam chord rotations at the upper stories predicted by the first mode pushover analysis (MPA-1) for

the twelve story plane frame. However, it leads to inaccurate response predictions for the six story building because of the overestimation of torsion.

- Most of the improved pushover methods in literature are validated by using 2D models. It is essential that the accuracy of these methods should be assessed by using 3D models.

## REFERENCES

Akkar S. and Metin A., 2007, 'Assessment of Nonlinear Static Procedures in FEMA-440', Journal of Structural Engineering, ASCE, Volume 133, No. 9, pp. 1237-1246

Akkar S. and Miranda E., 2005, 'Statistical Evaluation of Approximate Methods for Estimating Maximum Deformation Demands on Existing Structures', Journal of Structural Engineering, ASCE, Volume 131, No. 1, pp.160-172.

Akkar S., Yazgan U. and Gülkan P., 2005, 'Drift Estimates in Frame Buildings Subjected to Near-Fault Ground Motions', Journal of Structural Engineering, ASCE, Volume 131, No. 7, pp. 1014-1024.

Alavi B. and Krawinkler H., 2001, 'Effects of Near-fault Ground Motions on Frame Structures', John A. Blume Earthquake Engineering Center, Report No. 138, Stanford University.

Alavi B. and Krawinkler H., 2004, 'Behaviour of Moment Resisting Frame Structures Subjected to Near-fault Ground Motions', Earthquake Engineering and Structural Dynamics, Volume 33, pp. 687-706.

Allahabadi R. 1987, 'Drain-2DX - Seismic Response and Damage Assessment for 2D structures', Ph.D. Thesis, University of California, Berkeley, California.

American Society of Civil Engineers (ASCE), 2000, 'Prestandard and Commentary for the Seismic Rehabilitation of Buildings', Report No. FEMA-356, Washington, D.C.

Ang A.H.S. and Tang W.H., 1975, 'Probability Concepts in Engineering Planning and Design, Volume I: Basic Principles', Wiley, New York, 409 pp.

Antoniou S. and Pinho R., 2004a, 'Advantages and Limitations of Adaptive and Non-Adaptive Force-Based Pushover Procedures', Journal of Earthquake Engineering, Volume 8, No. 4, pp. 497-522.

Antoniou S. and Pinho R., 2004b, 'Development and Verification of a Displacement-Based Adaptive Pushover Procedure', Journal of Earthquake Engineering, Volume 8, No. 5, pp. 643-661.

Applied Technology Council (ATC), 1978, 'Tentative Provisions for the Development of Seismic Regulations for Buildings', Report No. ATC-3, Washington D.C.

Applied Technology Council (ATC), 1996, 'Seismic Evaluation and Retrofit of Concrete Buildings', Report No. ATC-40, Volume 1-2, Redwood City, California.

Applied Technology Council (ATC), 1997, 'NEHRP Guidelines for the Seismic Rehabilitation of Buildings' Report No. FEMA-273, Washington, D.C.

Applied Technology Council (ATC), 2005, 'Improvement of Nonlinear Static Seismic Analysis Procedures', Report No. FEMA-440, Washington, D.C.

Aschheim M., Tjhinb T., Comartin C., Hamburger R. and Inel M., 2007, 'The Scaled Nonlinear Dynamic Procedure', Engineering Structures, Volume 29, No. 7, pp. 1422-1441.

Aydinoglu N.M., 2003, 'An Incremental Response Spectrum Analysis Procedure Based on Inelastic Spectral Displacements for Multi-Mode Seismic Performance Evaluation', Bulletin of Earthquake Engineering, Volume 1, pp.3-36.

Benjamin J.R. and Cornell C.A., 1970, 'Probability, Statistics, and Decision for Civil Engineers', McGraw-Hill, New York, 684 pp.

Bracci J. M., Kunnath S. K. and Reinhorn A. M., 1997, 'Seismic Performance and Retrofit Evaluation of Reinforced Concrete Structures', *Journal of Structural Engineering*, ASCE, Volume 123, No. 1, pp. 3-10.

Chintanapakdee C. and Chopra A.K., 2003, 'Evaluation of Modal Pushover Analysis Using Generic Frames', *Earthquake Engineering and Structural Dynamics*, Volume 32, pp. 417-442.

Chintanapakdee C. and Chopra A.K., 2004, 'Seismic Response of Vertically Irregular Frames: Response History and Modal Pushover Analyses', *Journal of Structural Engineering*, ASCE, Volume 130, No. 8, pp. 1177-1185.

Chopra A. K., 2001, 'Dynamics of Structures: Theory and Applications to Earthquake Engineering', 2nd Edition, Prentice Hall, Englewood Cliffs, N.J., 844 pp.

Chopra A.K. and Goel R.K., 2000, 'Evaluation of NSP to Estimate Seismic Deformation: SDF Systems', *Journal of Structural Engineering*, ASCE, Volume 126, No. 4, pp. 482-490.

Chopra A.K. and Goel R.K., 2002, 'A Modal Pushover Analysis Procedure for Estimating Seismic Demands for Buildings', *Earthquake Engineering and Structural Dynamics*, Volume 31, pp. 561-582.

Chopra A. K. and Goel R. K., 2004, 'A Modal Pushover Analysis Procedure to Estimate Seismic Demands for Unsymmetric-plan Buildings', *Earthquake Engineering and Structural Dynamics*, Volume 33, pp. 903-927.

Chopra A. K., Goel R. K., and Chintanapakdee C., 2004, 'Evaluation of a Modified MPA Procedure Assuming Higher Modes as Elastic to Estimate Seismic Demands', *Earthquake Spectra*, Volume 20, No. 3, pp. 757-778.

Comite Europeen de Normalisation, 2005, 'European Standard EN 1998-3:2005 Eurocode 8. Design of Structures for Earthquake Resistance—Part 3: Assessment and Retrofitting of Buildings', Brussels.

Cuesta I. and Aschheim M.A., 2001, 'Using Pulse R-factors to Estimate Structural Response to Earthquake Ground Motions', CD release 01-03, Mid-America Earthquake Center, Urbana, Illinois.

De Stefano M. and Pintucchi B., 2007, 'A Review of Research on Seismic Behaviour of Irregular Building Structures Since 2002', Bulletin of Earthquake Engineering, currently published online.

Der Kiureghian A., 1981, 'A Response Spectrum Method for Random Vibration Analysis of MDF Systems', Earthquake Engineering and Structural Dynamics, Volume 9, pp. 419-435.

Fajfar P., 2000, 'A Nonlinear Analysis Method for Performance-Based Seismic Design', Earthquake Spectra, Volume 16, No. 3, pp. 573-592.

Fajfar P. and Fischinger M., 1987, 'Nonlinear Seismic Analysis of RC Buildings: Implications of a Case Study', European Earthquake Engineering, Volume 1, pp. 31-43.

Fajfar P. and Gaspersic P., 1996, 'The N2 Method for the Seismic Damage Analysis of RC Buildings', Earthquake Engineering and Structural Dynamics, Volume 25, pp. 31-46.

Fajfar P., Marusic D. and Perus I., 2005, 'Torsional Effects in the Pushover-based Seismic Analysis of Buildings', Journal of Earthquake Engineering, Volume 9, pp. 831-854.

Fardis M.N. and Kosmopoulos A., 2007, 'Practical Implementation of Seismic Assessment Method in Eurocode 8 - Part 3, with Linear or Nonlinear Analysis and Deformation-Based Verification Using Empirical Chord Rotation Capacity Expressions', Invited Lecture, Proceedings of the Sixth National Conference on Earthquake Engineering, Istanbul, Turkey.

Freeman S.A., Nicoletti J.P. and Tyrell J.V., 1975, 'Evaluation of Existing Buildings for Seismic Risk - A Case Study of Puget Sound Naval Shipyard, Bremerton, Washington', Proceedings of the First U.S. National Conference on Earthquake Engineering, Berkeley, California.

Goel R.K. and Chopra A.K., 2004, 'Evaluation of Modal and FEMA Pushover Analyses: SAC buildings', *Earthquake Spectra*, Volume 20, pp. 225–254.

Grant D.N., Blandon C.A. and Priestley M.J.N., 2005, 'Modeling Inelastic Response in Direct Displacement-Based Design', Report No. 2005/03, IUSS Press, Pavia, Italy, 104 pp.

Gulkan P. and Sozen M.A., 1974, 'Inelastic Responses of Reinforced Concrete Structures to Earthquake Motions', *Journal of the American Concrete Institute*, Volume 71, pp. 604-610.

Gupta B. and Kunnath S. K., 2000, 'Adaptive Spectra-Based Pushover Procedure for Seismic Evaluation of Structures', *Earthquake Spectra*, Volume 16, No. 2, pp. 367-391.

Guyader A.C., 2003, 'A Statistical Approach to Equivalent Linearization with Application to Performance-Based Engineering', Ph.D. Thesis, California Institute of Technology, Pasadena, California.

Hilber H.M., Hughes T.J.R. and Taylor R.L., 1977, 'Improved Numerical Dissipation for Time Integration Algorithms in Structural Dynamics', *Earthquake Engineering and Structural Dynamics*, Volume 5, pp. 283-292.

Idriss I.M. and Seed H.B., 1968, 'Seismic Response of Horizontal Soil Layers', *Journal of the Soil Mechanics and Foundations Division, ASCE*, Volume 94, No. SM4, pp. 1003-1031.

Iwan W.D., 1980, 'Estimating Inelastic Response Spectra from Elastic Spectra', *Earthquake Engineering and Structural Dynamics*, Volume 8, pp. 375–388.

Iwan W.D. and Gates N.C., 1979, 'The Effective Period and Damping of a Class of Hysteretic Structures', *Earthquake Engineering and Structural Dynamics*, Volume 7, pp. 199-212.

Jacobsen L.S., 1930, 'Steady Forced Vibrations as Influenced by Damping', *Transactions ASME*, Volume 52, pp. 169–181.

Jacobsen L.S., 1960, 'Damping in Composite Structures', Proceedings of the 2WCEE, Volume 2, Tokyo and Kyoto, Japan, pp.1029-1044.

Jennings P.C., 1968, 'Equivalent Viscous Damping for Yielding Structures', Journal of Engineering Mechanics Division, ASCE, Volume 94, pp. 103-116.

Judi H.J., Davidson B. J. and Fenwick R. C., 2000, 'The Direct Displacement Based Design - A Damping Perspective', 12th World Conference on Earthquake Engineering, Auckland, New Zealand, Paper No. 0330.

Kalkan E. and Kunnath S.K., 2006, 'Adaptive Modal Combination Procedure For Nonlinear Static Analysis of Building Structures', ASCE, Journal of Structural Engineering, Volume 132, No. 11, pp. 1721-1731.

Kalkan E. and Kunnath S.K., 2006, 'Effects of Fling Step and Forward Directivity on Seismic Response of Buildings', Earthquake Spectra, Volume 22, No. 2, pp. 367-390.

Kent D.C. and Park R., 1971, 'Flexural Members with Confined Concrete', Journal of the Structural Division, ASCE Volume 97, No. ST7, pp. 1969-1990.

Kilar V. and Fajfar P., 1997, 'Simple Push-over Analysis of Asymmetric Buildings', Earthquake Engineering and Structural Dynamics, Volume 26, pp. 233-249.

Kosmopoulos A. and Fardis M.N., 2004, 'Seismic Testing of 3-storey Full-scale Torsionally Unbalanced RC Structure: Pretest Predictions, Design and Analysis of Retrofitting', Proceedings of 5th International PhD Symposium in Civil Engineering, Delft, The Netherlands, Balkema, Rotterdam, pp. 1115-1123.

Kosmopoulos A. and Fardis M.N., 2007, 'Estimation of Inelastic Seismic Deformations in Asymmetric Multistory RC Buildings', Earthquake Engineering and Structural Dynamics, Volume 36, No. 9, pp. 1209-1234.

Kowalsky M.J., 1994, 'Displacement-Based Design-A Methodology for Seismic Design Applied to RC Bridge Columns', Master's Thesis, University of California at San Diego, La Jolla, California.

Kowalsky M.J., Priestley M.J.N. and McRae G.A., 1994, 'Displacement Based Design of RC Bridge Columns', Proceedings of the Second International Workshop, New Zealand, pp. 145-169.

Krawinkler H. and Nassar A.A., 1992, 'Seismic Design Based on Ductility and Cumulative Damage Demands and Capacities', Nonlinear Seismic Analysis and Design of Reinforced Concrete Buildings, editors, Fajfar and Krawinkler, Elsevier Applied Science, New York.

Krawinkler H. and Seneviratna G.D.P.K., 1998, 'Pros and Cons of a Pushover Analysis of Seismic Performance Evaluation', Engineering Structures, Volume 20, pp. 452-464.

Mahaney J. A., Freeman S.A., Paret T.F. and Kehoe B.E., 1993, 'The Capacity Spectrum Method for Evaluating Structural Response During the Loma Prieta Earthquake', Proceedings of the 1993 National Earthquake Conference, Memphis, pp. 501-510.

MathWorks Inc., 2002, MATLAB - Version 6.5.

Mengi Y., McNiven H.D. and Tanrikulu A.K., 1992, 'Models for Nonlinear Earthquake Analysis of Brick Masonry Buildings', Report No: UCB/EERC - 92/03, Earthquake Engineering Research Center, University of California, Berkeley.

Ministry of Public Works and Settlement, 1998, 'Turkish Earthquake Code: Specifications for the Buildings to be Constructed in Disaster Areas', Ankara, Turkey.

Miranda E., 2000, 'Inelastic Displacement Ratios for Structures on Firm Sites', Journal of Structural Engineering, ASCE, Volume 126, pp. 1150-1159.

Miranda E., 2001, 'Estimation of Inelastic Deformation Demands of SDOF Systems', Journal of Structural Engineering, ASCE, Volume 127, pp. 1005-1012.

Miranda E., and Akkar S., 2002, 'Evaluation of Approximate Methods to Estimate Target Displacements in Nonlinear Static Procedures', Report No. PEER-2002/21; Proceedings of the 4th U.S.-Japan Workshop on Performance-Based Earthquake Engineering Methodology for Reinforced Concrete Building Structures, Pacific Earthquake Engineering Research Center, California, pp. 75–86.

Miranda E. and Bertero V.V., 1994, 'Evaluation of Strength Reduction Factors for Earthquake-Resistant Design', *Earthquake Spectra*, Volume 10, No. 2, pp. 357-379.

Miranda E. and Lin Y., 2004, 'Non-Iterative Equivalent Linear Method For Displacement-Based Design', 13WCEE, Paper No. 3422, Vancouver, B.C., Canada.

Miranda E. and Ruiz-Garcia J., 2002, 'Evaluation of Approximate Methods to Estimate Maximum Inelastic Displacement Demands', *Earthquake Engineering and Structural Dynamics*, Volume 31, No. 3, pp. 539-560.

Moehle J.P., 1984, 'Seismic Analysis of R/C Frame-Wall Structures', *Journal of Structural Engineering*, ASCE, Vol. 110, No. 11, pp. 2619-2634.

Moehle J.P. and Alarcon I.F., 1986, 'Seismic Analysis Methods For Irregular Buildings', *Journal of Structural Engineering*, ASCE, Vol. 112, No. 1, pp. 35-52.

Moghadam A.S. and Tso W-K., 1998, 'Pushover Analysis for Asymmetrical Multistorey Buildings', Proceedings of the 6th U.S. National Conference on Earthquake Engineering, EERI, Oakland, California.

Mwafy A.M., and Elnashai A.S., 2001, 'Static Pushover versus Dynamic Collapse Analysis of RC Buildings', *Engineering Structures*, Volume 23, pp. 407-424.

Negro P., Mola E., Molina J. and Magonette G., 2004, 'Full Scale Bi-directional PSD Testing of a Torsionally Unbalanced Three Storey Non-seismic RC Frame' 13WCEE, Paper No. 968, Vancouver, Canada.

New Zealand Society for Earthquake Engineering (NZSEE), 2003, 'Assessment and Improvement of the Structural Performance of Buildings in Earthquake', Study Group Draft, Hawke's Bay, New Zealand.

Newmark N.M., 1959, 'A Method of Computation for Structural Dynamics', Journal of Engineering Mechanics Division, ASCE, Volume 85, No. EM3, pp. 67-94

Newmark N.M. and Hall W.J., 1973, 'Procedures and Criteria for Earthquake Resistant Design, Building Practices for Disaster Mitigation', National Bureau of Standards, Building Science Series, No. 46, Vol. 1, Md.: 209-236.

Newmark N.M. and Hall W.J., 1982, 'Earthquake Spectra and Design', EERI Monograph Series, EERI, Oakland.

OpenSees, 2005, 'Open System for Earthquake Engineering Simulation', '<http://opensees.berkeley.edu>', last accessed date: February 11, 2008.

Panagiotakos T.B. and Fardis M.N., 1999, 'Estimation of Inelastic Deformation Demands in Multistorey R/C Frame Buildings', Earthquake Engineering and Structural Dynamics, Volume 28, No. 5, pp. 501-528.

Paret T.F., Sasaki K., Eilbeck D.H., and Freeman S.A., 1996, 'Approximate Inelastic Procedures to Identify Failure Mechanisms From Higher Mode Effect', 11th World Conference on Earthquake Engineering, Paper No. 966, Acapulco, Mexico

Powell G.H., 1993, 'Drain-2DX Element Description and User Guide For Element Type01, Type02, Type04, Type06, Type09 and Type15, Version 1.10', Report No. UCB/SEMM-93/18, Department of Civil Engineering, University of California, Berkeley, California.

Prakash V., Powell G.H. and Campbell S., 1993, 'Drain-2DX Base Program Description and User Guide, Version 1.10', Report No. UCB/SEMM-93/17, Department of Civil Engineering, University of California, Berkeley, California.

Priestley M.J.N., 2000, 'Performance-Based Seismic Design', Keynote Address, Proceedings of 12WCEE, Auckland, New Zealand.

Priestley M.J.N., 2003, 'Myths and Fallacies in Earthquake Engineering, Revisited', The Ninth Mallet Milne Lecture, IUSS Press, Pavia, Italy.

Priestley M.J.N., Calvi G.M. and Kowalsky M.J., 2007, 'Displacement-Based Seismic Design of Structures', IUSS Press, Pavia, Italy, 740 pp.

Rosenblueth E., 1951, 'A Basis for Aseismic Design', Ph.D. Thesis, University of Illinois, Urbana, Illinois.

Rosenblueth E. and Herrera I., 1964, 'On a Kind of Hysteretic Damping', Journal of Engineering Mechanics Division, ASCE, Volume 90, pp. 37-48.

Rutenberg A., 1998, 'EAEE Task Group (TG) 8: Behavior of Irregular and Complex Structures –State of the Art Report: Seismic Nonlinear Response of Code-Designed Asymmetric Structures', Proceedings of the 11th European Conference on Earthquake Engineering, Paris.

Rutenberg A., 2002, 'EAEE Task Group (TG) 8: Behaviour of Irregular and Complex Structures: Asymmetric structures - Progress since 1998', Proceedings of the 12th European Conference on Earthquake Engineering, London, UK, Paper No. 832.

Rutenberg A., Chandler A.M., Duan X.N. and Correnza J.C., 1995, 'Nonlinear Seismic Response of Asymmetric Structures: Bibliography', National Building Research Institute: Haifa.

Saiidi M. and Hudson K.E.Jr., 1982, 'Analytical Study of Irregular R/C Structures Subjected to In-Plane Earthquake Loads', College of Engineering, Report No. 59, University of Nevada, Reno.

Saiidi M. and Sözen M.A., 1981, 'Simple Nonlinear Seismic Analysis of R/C Structures', Journal of the Structural Division, ASCE, Vol. 107, No. ST5, pp. 937-952.

Sasaki F., Freeman S. and Paret T., 1998, 'Multi-Mode Pushover Procedure (MMP)-A Method to Identify the Effect of Higher Modes in a Pushover Analysis', Proceedings of the 6th U.S. National Conference on Earthquake Engineering, Seattle, CD-ROM, EERI, Oakland.

Schnabel P.B., Lysmer J. and Seed H.B., 1972, 'SHAKE: A Computer Program for Earthquake Response Analysis of Horizontally Layered Sites', Report No: UCB/EERC-72/12, Earthquake Engineering Research Center, University of California, Berkeley.

Seed H.B. and Idriss I.M., 1970, 'Soil Moduli and Damping Factors for Dynamic Response Analysis', Report No: UCB/EERC - 70/10, Earthquake Engineering Research Center, University of California, Berkeley.

Shibata A. and Sozen M.A., 1976, 'Substitute-Structure Method for Seismic Design in RC', Journal of the Structural Division, ASCE, Vol.102, pp. 1-17.

Turkish Standard Institute, 2000, 'TS-500 Requirements for Design and Construction of Reinforced Concrete Structures', Ankara, Turkey.

Vamvatsikos D. and Cornell C. A., 2002, 'Incremental Dynamic Analysis', Earthquake Engineering and Structural Dynamics, Volume 31, No. 3, pp. 491-514.

Veletsos A.S. and Newmark N.M., 'Effect of Inelastic Behavior on the Response of Simple Systems to Earthquake Motions', Proceedings of the 2nd World Conference on Earthquake Engineering, Volume 2, Japan, 1960, pp. 895-912.

Vidic T., Fajfar P. and Fischinger M., 1994, 'Consistent Inelastic Design Spectra: Strength and Displacement', Earthquake Engineering and Structural Dynamics, Volume 23, pp. 507-521.

## APPENDIX A

### STIFFNESS FORMULATION of DRAIN-2DX for “PLASTIC HINGE BEAM-COLUMN ELEMENT”

Lumped plasticity approach is utilized for “Plastic Hinge Beam-Column Element” in Drain-2DX. The software considers inelasticity only at the member ends due to flexure. Stiffness matrix of an element is updated at each step where yielding or unloading takes place. Modification of the stiffness matrix for the cases of yielding at one end, and yielding at both ends is briefly explained below.

The local stiffness matrix for a prismatic element with the degrees of freedom shown in Figure A.1 is presented in Figure A.2.

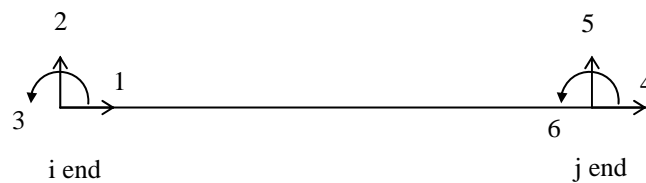


Figure A.1 Local degrees of freedom for a prismatic beam-column element

$$\begin{pmatrix} E \frac{A}{L} & 0 & 0 & -E \frac{A}{L} & 0 & 0 \\ 0 & 12E \frac{I}{L^3} & 6E \frac{I}{L^2} & 0 & -12E \frac{I}{L^3} & 6E \frac{I}{L^2} \\ 0 & 6E \frac{I}{L^2} & 4E \frac{I}{L} & 0 & -6E \frac{I}{L^2} & 2E \frac{I}{L} \\ -E \frac{A}{L} & 0 & 0 & E \frac{A}{L} & 0 & 0 \\ 0 & -12E \frac{I}{L^3} & -6E \frac{I}{L^2} & 0 & 12E \frac{I}{L^3} & -6E \frac{I}{L^2} \\ 0 & 6E \frac{I}{L^2} & 2E \frac{I}{L} & 0 & -6E \frac{I}{L^2} & 4E \frac{I}{L} \end{pmatrix}$$

Figure A.2 Local stiffness matrix for a prismatic beam-column element with the degrees of freedom shown in Figure A.1

Bilinear moment curvature relationship is employed at the member ends in “Plastic Hinge Beam-Column Element” (Figure A.3, Powell, 1993).

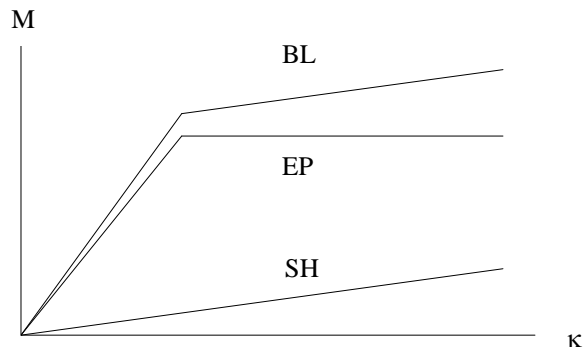


Figure A.3 Bilinear moment curvature relationship and decomposition into components

In Figure A.3, BL represents the bilinear moment curvature relation. At this stage, an assumption is made and the bilinear moment curvature relation is

decomposed into elastoplastic and strain hardening components designated with EP and SH. After flexural yielding occurs at an element end; stiffness matrix for component EP is reduced to a 5\*5 matrix using the information that the moment at the yielding end is zero. A row and column of zeros are added to the 5\*5 matrix for the yielding degree of freedom and modified 6\*6 matrix is obtained for component EP. The modified 6\*6 matrices for elements with only i end yielding and with only j end yielding are shown in Figures A.4a and A.4b respectively. For component SH, the 6\*6 local stiffness matrix in Figure A.2 is created using an EI value equal to the slope of line SH (this value is input to the program as strain hardening ratio). The flexural terms in the stiffness matrix of component SH is added to the stiffness matrix of component EP to calculate the local stiffness matrix of the yielding element.

If both ends of an element yield; the stiffness matrix for component EP is reduced to a 4\*4 matrix using the information that moments at both ends are equal to zero. Two rows and columns of zeros are added to the 4\*4 matrix to form the modified stiffness matrix. The stiffness matrix of the element becomes the stiffness matrix of a truss element, which is presented in Figure A.5. For component SH, the 6\*6 local stiffness matrix in Figure A.2 is created using an EI value equal to the slope of line SH. The flexural terms in the stiffness matrix of component SH is added to the stiffness matrix of component EP to calculate the local stiffness matrix of the yielding element.

$$\begin{matrix}
 \left( \begin{array}{cccccc}
 E \frac{A}{L} & 0 & 0 & -E \frac{A}{L} & 0 & 0 \\
 0 & 3 \cdot E \frac{I}{L^3} & 0 & 0 & -3 \cdot E \frac{I}{L^3} & 3 \cdot E \frac{I}{L^2} \\
 0 & 0 & 0 & 0 & 0 & 0 \\
 -E \frac{A}{L} & 0 & 0 & E \frac{A}{L} & 0 & 0 \\
 0 & -3 \cdot E \frac{I}{L^3} & 0 & 0 & 3 \cdot E \frac{I}{L^3} & -3 \cdot E \frac{I}{L^2} \\
 0 & 3 \cdot E \frac{I}{L^2} & 0 & 0 & -3 \cdot E \frac{I}{L^2} & 3 \cdot E \frac{I}{L}
 \end{array} \right) &
 \left( \begin{array}{cccccc}
 E \frac{A}{L} & 0 & 0 & -E \frac{A}{L} & 0 & 0 \\
 0 & 3 \cdot E \frac{I}{L^3} & 3 \cdot E \frac{I}{L^2} & 0 & -3 \cdot E \frac{I}{L^3} & 0 \\
 0 & 3 \cdot E \frac{I}{L^2} & 3 \cdot E \frac{I}{L} & 0 & -3 \cdot E \frac{I}{L^2} & 0 \\
 -E \frac{A}{L} & 0 & 0 & E \frac{A}{L} & 0 & 0 \\
 0 & -3 \cdot E \frac{I}{L^3} & -3 \cdot E \frac{I}{L^2} & 0 & 3 \cdot E \frac{I}{L^3} & 0 \\
 0 & 0 & 0 & 0 & 0 & 0
 \end{array} \right) \\
 \text{a)} & \text{b)}
 \end{matrix}$$

Figure A.4 Stiffness matrices for component EP of a “Plastic Hinge Beam-Column Element” for which yielding occurs a) at end i, b) at end j

$$\left( \begin{array}{cccccc}
 E \frac{A}{L} & 0 & 0 & -E \frac{A}{L} & 0 & 0 \\
 0 & 0 & 0 & 0 & 0 & 0 \\
 0 & 0 & 0 & 0 & 0 & 0 \\
 -E \frac{A}{L} & 0 & 0 & E \frac{A}{L} & 0 & 0 \\
 0 & 0 & 0 & 0 & 0 & 0 \\
 0 & 0 & 0 & 0 & 0 & 0
 \end{array} \right)$$

Figure A.5 Stiffness matrix for component EP of a “Plastic Hinge Beam-Column Element” both ends of which yield

## **CURRICULUM VITAE**

### **PERSONAL INFORMATION**

Name : Mehmet Selim GÜNAY  
Birth Date : 03/10/1978  
Birth Place : Ankara / TURKEY  
Citizenship : Republic of Turkey  
Phone : +90 (312) 2105408  
Fax : +90 (312) 2101193  
e-mail : selim\_gunay@yahoo.com

### **EDUCATION**

2003 - 2008 Ph.D., Civil Engineering, METU (CGPA: 4.00/4.00)  
2000 - 2003 MS, Civil Engineering, METU (CGPA: 3.64/4.00)  
1996 - 2000 BS, Civil Engineering, METU (CGPA: 3.60/4.00)  
1989 - 1996 Ankara Atatürk Anatolian High School

### **EMPLOYMENT RECORD**

2001 - 2008: Research Assistant, Graduate School of Natural and Applied Sciences,  
Pro-Ad Program, METU

### **COMPUTER SKILLS**

#### **Computer Programming Languages**

MATLAB, Mathcad, Fortran, Visual Basic

#### **Software Related to Earthquake Engineering and Structural Analysis**

SAP2000, OpenSees, Drain-2DX, SeismoStruct, SeismoSignal, Bispec, NONLIN

## **Other Software**

Microsoft Office Applications, AutoCAD

## **SCIENTIFIC PUBLICATIONS**

### **International Refereed Journals**

1. Sucuođlu H., Gr T., and **Gnay M.S.**, 2004, ‘Performance Based Seismic Rehabilitation of Damaged R/C Buildings’, Journal of Structural Engineering, Volume 130, No. 10, pp. 1475-1486.

### **Chapter in a Book**

1. **Gnay M.S.**, Sucuođlu H., 2005, ‘An Equivalent Linearization Procedure for Displacement-Based Seismic Assessment of Vulnerable RC Buildings’, Advances in Earthquake Engineering for Urban Risk Reduction, Editors G. zcebe, and S.T. Wasti, Kluwer.

### **International Conference Proceedings**

1. **Gnay M.S.**, Sucuođlu H., 2003, ‘Simplified Procedures For Seismic Assessment of Medium Rise Reinforced Concrete Building Structures’, Concrete Structures in Seismic Regions, FIB Symposium, 6-9 May, Athens, Greece, Paper No: 79.
2. **Gnay M.S.**, Sucuođlu H., 2004, ‘A Comparative Evaluation of Performance-Based Seismic Assessment Procedures’, 13th World Conference on Earthquake Engineering, 1-6 August, Vancouver, Canada, Paper No: 0453.
3. **Gnay M.S.**, Sucuođlu H., 2005, ‘Capacity-Based Equivalent Linear Modeling of the SPEAR Test Frame’, SPEAR International Workshop, Ispra, Italy.
4. **Gnay M.S.**, Sucuođlu H., 2006, ‘Capacity Control Method For Seismic Assessment of Low-to-Medium Rise Reinforced Concrete Buildings’, First European Conference on Earthquake Engineering and Seismology, 3-8 September, Geneva, Switzerland, Paper No: 1042.

### **National Conference Proceedings**

1. Sucuođlu H., **Gnay M.S.**, 2003, ‘Orta Ykseklikteki Betonarme Yapılar iin Basitleřtirilmiř Deprem Dayanımı Deđerlendirme Yntemleri’, Beřinci Ulusal Deprem Mhendisliđi Konferansı, İstanbul, Trkiye.